

DISS. ETH NO. 26932

***Controlled Radical Polymerization for Surface
Modification with Designed Polymer Architectures***

A thesis submitted to attain the degree of
DOCTOR OF SCIENCES of ETH ZURICH
(Dr. sc. ETH Zurich)

presented by
Wenqing Yan

M.Sc. in Polymer Science, University of Freiburg

born on 13.07.1991

citizen of China

accepted on the recommendation of
Prof. Nicholas D. Spencer, Examiner
Dr. Edmondo M. Benetti, Co-examiner
Prof. Harm-Anton Klok, Co-examiner

2020

" Die Wahrheit wird euch frei machen.

(The truth will set you free)

(真理让你们自由)"

Abstract

Surface-initiated controlled radical polymerizations (SI-CRPs) have progressively emerged as extremely versatile methods to generate polymer films with well-defined architectures and controlled physicochemical properties.

In this thesis, I especially focus on surface-initiated atom transfer radical polymerization (SI-ATRP), investigate its application to fabricate polymer brushes with different branched structures, and explore how this technique can be scaled up for the functionalization of large substrates, in the presence of oxygen, and employing biocompatible catalytic systems.

The fabrication of linear, graft copolymer and bottlebrush brushes was performed by employing multistep SI-ATRP. The synthesis of a library of different branched brush structures enabled me to precisely dissect the effect of brush branching on an array of technologically relevant physicochemical properties, including swelling, nanomechanical and nanotribological properties.

The mechanisms and applications of zerovalent metal (Cu^0 and Fe^0)-mediated SI-ATRP are subsequently introduced. Cu^0 SI-ATRP enables the rapid synthesis of compositionally different polymer brushes over extremely large areas, by employing microliter volumes of reaction mixtures, and without the need for inert atmosphere. The vertical distance between a Cu^0 -coated plate and an initiator-functionalized substrate determines polymer-grafting kinetics and the rate of oxygen consumption. The concentration of Cu^{II} species added in the polymerization solution strongly influences the growth of polymer brushes and their dispersity (D). Having achieved a comprehensive understanding of its mechanism, Cu^0 SI-ATRP was later on applied to fabricate biopassive and lubricious brushes from large flat surfaces, as well as from various organic supports, including cellulose fibers and elastomers.

Analogously to Cu^0 SI-ATRP, SI-ATRP mediated by Fe^0 -coated plates (Fe^0 SI-ATRP) enables the rapid growth of a wide range of polymer brushes under ambient conditions, utilizing either organic or aqueous reaction media. Due to its cytocompatibility, Fe^0 SI-ATRP could be applied *in situ* within cell cultures, enabling the growth of polymer brushes while cells are adhered to the substrates, substantially altering their affinity toward the functionalized surface, but without influencing their viability.

Finally, the mechanism and application of photoinduced SI-ATRP (SI-photoATRP) for the fabrication of thick polymer brushes are revealed. In particular, I investigated how the presence of a grafting surface affects those parameters that have already been identified as crucial for

photoATRP in solution. During SI-photoATRP, both the concentration of Cu^{II} species initially added to the reaction mixture, and the type of ligand are chiefly responsible for determining polymer-brush growth rate, and the degree of control over the polymerization process. These parameters additionally regulate the tolerance of the polymerization reaction toward oxygen as well as the temporal control over polymer-brush growth using UV light as a trigger.

Zusammenfassung

Oberflächeninitiierte kontrollierte radikalische Polymerisationen (SI-CRPs) haben sich als äusserst vielfältige Methoden etabliert um Polymerfilme auf Oberflächen wachsen zu lassen, die sich durch eine präzise Architektur und kontrollierte physikochemische Eigenschaften auszeichnen.

In dieser Arbeit, konzentriere ich mich insbesondere auf die oberflächeninitiierte radikalische Atomtransferpolymerisation (SI-ATRP), untersuche ihre Anwendung zur Herstellung von Polymerbürsten mit unterschiedlichen verzweigten Strukturen, und untersuche wie diese Technik für die Funktionalisierung großer Substrate skaliert werden kann – bei gleichzeitiger Anwesenheit von Sauerstoff und der Verwendung von biokompatiblen katalytischen Systemen.

Die Herstellung von Linear-, Pfropfcopolymer- und Flaschenbürstenbürsten wurde unter Verwendung von mehrstufiger SI-ATRP durchgeführt. Die Synthese einer Bibliothek verschiedener verzweigter Bürstenstrukturen ermöglichte es, den Effekt der Bürstenverzweigung auf eine Reihe technologisch relevanter physikalisch-chemischer Eigenschaften, einschließlich Quell-, nanomechanischer und nanotribologischer Eigenschaften, präzise zu analysieren.

Anschließend werden die Mechanismen und Anwendungen von durch nullwertiges Metall (Cu^0 und Fe^0) vermitteltem SI-ATRP vorgestellt. Cu^0 -SI-ATRP ermöglicht die schnelle Synthese von Polymerbürsten mit unterschiedlicher Zusammensetzung über extrem grosse Flächen bei Verwendung von minimalstem Volumen an Reaktionsmischungen und ohne die Notwendigkeit einer inerten Atmosphäre. Der vertikale Abstand zwischen einer Cu^0 -beschichteten Platte und einem initiatorfunktionalisierten Substrat bestimmt die Polymerpfropfkinetik und die Geschwindigkeit des Sauerstoffverbrauchs. Die Konzentration der Cu^{II} -Spezies, die der Polymerisationslösung zugesetzt wird, beeinflusst das Wachstum der Polymerbürsten und ihre Dispersität (D) stark. Nachdem ein umfassendes Verständnis über den Mechanismus der Cu^0 -SI-ATRP erreicht war, wurde sie später zur Herstellung von biopassiven und schmierfähigen Bürsten auf großen flachen Oberflächen sowie auf verschiedenen organischen Trägern, einschließlich Cellulosefasern und Elastomeren, eingesetzt.

Analog zu Cu^0 -SI-ATRP bewirkt SI-ATRP vermittelt durch Fe^0 -beschichtete Platten (Fe^0 -SI-ATRP) ein schnelles Wachstum einer Vielzahl von Polymerbürsten unter

Umgebungsbedingungen bei Verwendung von entweder organischen oder wässrigen Reaktionsmedien. Aufgrund seiner Zytokompatibilität kann Fe^0 SI-ATRP in Zellkulturen angewendet, wodurch das Wachstum von Polymerbürsten ermöglicht wird, während Zellen an den Substraten haften. Dadurch wird die Affinität der Zellen zur funktionalisierten Oberfläche wesentlich verändert, ohne ihre Lebensfähigkeit zu beeinflussen.

Schließlich werden der Mechanismus und die Anwendung von photoinduzierter SI-ATRP (SI-photoATRP) zur Herstellung von dicken Polymerbürsten untersucht. Insbesondere untersuche ich, wie sich das Vorhandensein einer Pfropfoberfläche auf die Parameter auswirkt, die bereits früher als entscheidend für photoATRP in Lösung identifiziert wurden. Während der SI-photoATRP sind die Konzentration der Cu^{II} -Spezies, die anfänglich dem Reaktionsgemisch zugesetzt wurde, und die Art des Liganden hauptsächlich für die Bestimmung der Wachstumsrate der Polymerbürste und den Grad der Kontrolle über den Polymerisationsprozess verantwortlich. Diese Parameter regulieren zusätzlich die Toleranz der Polymerisationsreaktion gegenüber Sauerstoff sowie die zeitliche Kontrolle des Polymerbürstenwachstums unter Verwendung von UV-Licht als Auslöser.

Table of Contents

| | |
|---|-----------|
| Abstract..... | 5 |
| 1. General Introduction..... | 1 |
| 1.1 Introduction..... | 2 |
| References..... | 4 |
| 2. Bioinert and Lubricious Surfaces by Macromolecular Design | 7 |
| 2.1 Introduction..... | 8 |
| 2.2 Modulation of Polymer-Brush Thickness and Grafting Density | 10 |
| 2.3 Mixed and Copolymer Brushes | 13 |
| 2.4 Branched and Crosslinked Polymer Brushes..... | 18 |
| 2.5 Polymer Brushes Presenting Cyclic and Loop Topologies | 23 |
| 2.6 Conclusions and Perspectives..... | 25 |
| References..... | 27 |
| 3. Oxygen-Tolerant Surface-Initiated Controlled Radical Polymerizations | 43 |
| 3.1 Introduction..... | 43 |
| 3.2 Metal-Free SI-ATRP | 45 |
| 3.3 SI PET RAFT | 47 |
| 3.4 Conclusions..... | 49 |
| Reference | 49 |
| 4. Brushes, Graft Copolymers, or Bottlebrushes? The Effect of Polymer Architecture on the Nano-tribological Properties of Grafted-from Assemblies..... | 52 |
| 4.1. Introduction..... | 53 |
| 4.2 Results and Discussion | 54 |
| 4.2.1 Synthesis, compositional and structural analysis | 54 |
| 4.2.2 Nanomorphology of PMMA _x -ran-PHEMATMS _y (PMPC) brushes | 64 |
| 4.2.3 Nanomechanical and nanotribological properties of PMMA _x -ran-PHEMATMS _y (PMPC) brushes..... | 66 |

| | |
|---|------------|
| 4.2.4 Comparison of linear PMPC brushes and PMMA ₇₅ -ran-PHEMATMS ₂₅ (PMPC)long graft-copolymer brushes..... | 70 |
| 4.3 Conclusions..... | 72 |
| 4.4 Materials and Methods | 73 |
| References..... | 77 |
| 5. Translating Surface-Initiated Atom Transfer Radical Polymerization into Technology: The Mechanism of Cu⁰-Mediated SI-ATRP under Environmental Conditions | 83 |
| 5.1 Introduction..... | 84 |
| 5.2 Results and Discussion | 85 |
| 5.2.1 Cu ⁰ -mediated SI-ATRP and its oxygen tolerance | 85 |
| 5.2.2 Effect of ligand (L), activators (CuBr/L), and deactivators (CuBr ₂ /L) | 87 |
| 5.2.3 Effect of alkyl halide initiator, the distance (d) and “polarity” of solvent..... | 89 |
| 5.3 Conclusions..... | 93 |
| 5.4 Materials and Methods | 93 |
| References..... | 96 |
| 6. Growing Polymer Brushes from a Variety of Substrates under Ambient Conditions by Cu⁰-Mediated Surface-Initiated ATRP | 102 |
| 6.1 Introduction..... | 103 |
| 6.2 Results and Discussion | 104 |
| 6.2.1 Mechanism of Cu ⁰ SI-ATRP in Deoxygenated Media..... | 104 |
| 6.2.2 Structure and Properties of PMPC Brushes Synthesized by Cu ⁰ SI-ATRP | 107 |
| 6.2.3 Functionalization of Large and Compositionally Different Substrates by Cu ⁰ SI-ATRP under Ambient Conditions..... | 110 |
| 6.3 Conclusions..... | 113 |
| 6.4 Materials and Methods | 114 |
| References..... | 117 |
| 7. Oxygen Tolerant and Cytocompatible Fe⁰-Mediated ATRP Enables the Controlled Growth of Polymer Brushes from Mammalian Cell Cultures | 123 |
| 7.1 Introduction..... | 124 |

| | |
|---|------------|
| 7.2 Results and Discussion | 124 |
| 7.2.1 Mechanism and kinetics of Fe ⁰ SI-ATRP..... | 124 |
| 7.2.2 Cytocompatibility toward mammalian cells..... | 129 |
| 7.3 Conclusions..... | 135 |
| 7.4 Materials and Methods | 135 |
| References..... | 139 |
| 8. Surface-Initiated Photoinduced ATRP: Mechanism, Oxygen Tolerance and Temporal Control during the Synthesis of Polymer Brushes | 143 |
| 8.1 Introduction..... | 144 |
| 8.2 Results and Discussion | 145 |
| 8.2.1 Effect of Ligand..... | 147 |
| 8.2.2 Effect of Catalyst Concentration | 149 |
| 8.2.3 Temporal Control of SI-photoATRP..... | 153 |
| 8.3 Conclusions..... | 156 |
| 8.4 Materials and Methods | 157 |
| References..... | 159 |
| 9. Conclusions | 166 |
| Acknowledgements | 168 |
| List of Publications | 169 |
| Curriculum Vitae | 171 |

Chapter 1

General Introduction

1.1 Introduction

Surface modification by polymer grafting has progressively been demonstrated as a convenient and highly flexible strategy to modify the physicochemical properties of a variety of compositionally different substrates. Besides their chemical composition, the architecture of surface-anchored polymers strongly influence the morphology of the subsequently obtained films, their swelling, nanomechanical, and nanotribological properties. These properties can be modulated through the introduction of cross-links^{1,2}, side chains^{3,4} or branchings⁵ along the grafted polymers, enabling the precise tuning of the above-mentioned characteristics.

Surface-initiated controlled radical polymerization (SI-CRP) represents a powerful approach to modify surfaces with thin polymer films in order to tailor their interfacial properties. During the past decade significant advances in the application of SI-CRPs have been achieved, especially applying this techniques from flat inorganic substrates, nanoparticles (NPs), natural or polymer fibers, mesoporous materials^{6, 7}, graphene⁸⁻¹⁰, and viruses¹¹. However, the translation of SI-CRP into technologically relevant surface modification processes remains limited, due to the need for an inert atmosphere and large amount of costly catalysts and ligands.

To overcome these drawbacks, oxygen-tolerant controlled radical polymerizations have emerged in the literature, where enzymes^{12, 13} or different reducing agents¹⁴ are employed to consume oxygen within the polymerization mixture. These methods enable polymerization to be performed under environmental conditions, providing a means to functionalize more complex systems, such as hydrogels^{15, 16}, proteins and antibodies¹⁷, and cell surfaces^{18, 19}, substantially broadening the applicability of SI-CRP in materials science.

In **Chapter 2**, recent progress in the macromolecular design of polymer-brush interfaces are presented. A particular emphasis is given to the effect of polymer topology, and how the structural properties of polymer-brush assemblies determine interfacial properties, including bioinertness and lubrication.

In **Chapter 3**, oxygen-tolerant, surface-initiated controlled radical polymerizations (SI-CRP) are reviewed. A special focus is given to the mechanisms of the different methods and how these can be applied to structure the surface of different materials.

In **Chapter 4**, I compare the properties of linear poly(2-methacryloyloxyethyl phosphorylcholine) (PMPC) brushes with those displayed by graft-copolymer and bottlebrush brushes, demonstrating that, besides their chemical composition, the architecture of PMPC

brushes strongly determines their morphological, nanomechanical and nanotribological characteristics.

In **Chapter 5**, I demonstrate that through a comprehensive analysis of its mechanism, Cu^0 -mediated, surface-initiated, atom-transfer radical polymerization (Cu^0 SI-ATRP) can be exploited to translate controlled/"living" polymerization into technologically relevant surface fabrication. In particular, I describe how Cu^0 SI-ATRP enables the highly controlled synthesis of compositionally different, thick brushes in short reaction times, over extremely large areas and without the need for degassing the monomer mixtures or carrying out the reaction in the presence of an inert atmosphere.

In **Chapter 6**, I show how Cu^0 SI-ATRP enables the rapid growth of biopassive and lubricious PMPC brushes, over very large and morphologically different substrates. Cu^0 SI-ATRP enables the fabrication of PMPC brushes presenting a broad range of thicknesses and tunable interfacial physicochemical properties on large flat substrates. In addition, the same process could be applied for the rapid and efficient modification of cellulose sheets and poly(butyl acrylate) (PBA)-based elastomers. These substrates are structurally similar to supports that are widely applied for the fabrication of medical devices, such as wound dressings and catheters, where the highly hydrophilic, biopassive and lubricious properties of PMPC brushes could substantially improve their performance when placed in contact with tissues and/or body fluids.

In **Chapter 7**, I systematically assess the application of Fe-based SI-ATRP for the controlled synthesis of a variety of polymer brushes either in organic or in aqueous media—a topic that has remained basically unexplored until now. In particular, I demonstrate that when this process is mediated by Fe^0 plates, it can be efficiently performed under ambient conditions and without the need for deoxygenation of the reaction mixtures.

Fe^0 -mediated SI-ATRP can additionally be performed within cell-culture media and in the presence of primary articular chondrocytes (ACs) that had been previously cultured on initiator-bearing substrates, generating brushes that lead to a marked shift in the interfacial properties of the supports, and a consequent modulation of their affinity towards cells.

In **Chapter 8**, I introduce surface-initiated photoinduced ATRP (SI-photoATRP) for the oxygen-tolerant modification of large inorganic substrates. During SI-photoATRP, the concentration of Cu^{II} species initially added to the reaction mixture as well as the type and amount of ligand determine polymer-brush growth rate and the degree of control over the polymerization. These parameters additionally regulate the tolerance of the polymerization toward oxygen, which has already been identified as crucial for photoATRP in solution.

Finally, in **Chapter 9**, I summarize the main findings reported in my PhD work and highlight possible further applications of the methods developed and reported in this thesis.

References

1. Li, A.; Benetti, E. M.; Tranchida, D.; Clasohm, J. N.; Schonherr, H.; Spencer, N. D., Surface-Grafted, Covalently Cross-Linked Hydrogel Brushes with Tunable Interfacial and Bulk Properties. *Macromolecules* **2011**, *44* (13), 5344-5351.
2. Kang, C. J.; Ramakrishna, S. N.; Nelson, A.; Cremmel, C. V. M.; Stein, H. V.; Spencer, N. D.; Isa, L.; Benetti, E. M., Ultrathin, freestanding, stimuli-responsive, porous membranes from polymer hydrogel-brushes. *Nanoscale* **2015**, *7* (30), 13017-13025.
3. Hucknall, A.; Rangarajan, S.; Chilkoti, A., In Pursuit of Zero: Polymer Brushes that Resist the Adsorption of Proteins. *Advanced Materials* **2009**, *21* (23), 2441-2446.
4. Divandari, M.; Dehghani, E. S.; Spencer, N. D.; Ramakrishna, S. N.; Benetti, E. M., Understanding the effect of hydrophobic protecting blocks on the stability and biopassivity of polymer brushes in aqueous environments: A Tiramisu for cell-culture applications. *Polymer* **2016**, *98*, 470-480.
5. Banquy, X.; Burdynska, J.; Lee, D. W.; Matyjaszewski, K.; Israelachvili, J., Bioinspired Bottle-Brush Polymer Exhibits Low Friction and Amontons-like Behavior. *Journal of the American Chemical Society* **2014**, *136* (17), 6199-6202.
6. Park, J. T.; Chi, W. S.; Roh, D. K.; Ahn, S. H.; Kim, J. H., Hybrid Templated Synthesis of Crack-Free, Organized Mesoporous TiO₂ Electrodes for High Efficiency Solid-State Dye-Sensitized Solar Cells. *Advanced Functional Materials* **2013**, *23* (1), 26-33.
7. Celikbicak, O.; Bayramoglu, G.; Yilmaz, M.; Ersoy, G.; Bicak, N.; Salih, B.; Arica, M. Y., Immobilization of laccase on hairy polymer grafted zeolite particles: Degradation of a model dye and product analysis with MALDI-ToF-MS. *Microporous and Mesoporous Materials* **2014**, *199*, 57-65.
8. Ye, Y. S.; Chen, Y. N.; Wang, J. S.; Rick, J.; Huang, Y. J.; Chang, F. C.; Hwang, B. J., Versatile Grafting Approaches to Functionalizing Individually Dispersed Graphene Nanosheets Using RAFT Polymerization and Click Chemistry. *Chemistry of Materials* **2012**, *24* (15), 2987-2997.

9. Ou, B. L.; Zhou, Z. H.; Liu, Q. Q.; Liao, B.; Yi, S. J.; Ou, Y. J.; Zhang, X.; Li, D. X., Covalent functionalization of graphene with poly(methyl methacrylate) by atom transfer radical polymerization at room temperature. *Polymer Chemistry* **2012**, *3* (10), 2768-2775.
10. Ren, L. L.; Huang, S.; Zhang, C.; Wang, R. Y.; Tjiu, W. W.; Liu, T. X., Functionalization of graphene and grafting of temperature-responsive surfaces from graphene by ATRP "on water". *Journal of Nanoparticle Research* **2012**, *14* (6).
11. Rosilo, H.; McKee, J. R.; Kontturi, E.; Koho, T.; Hytonen, V. P.; Ikkala, O.; Kostianen, M. A., Cationic polymer brush-modified cellulose nanocrystals for high-affinity virus binding. *Nanoscale* **2014**, *6* (20), 11871-11881.
12. Chapman, R.; Gormley, A. J.; Herpoldt, K. L.; Stevens, M. M., Highly Controlled Open Vessel RAFT Polymerizations by Enzyme Degassing. *Macromolecules* **2014**, *47* (24), 8541-8547.
13. Chapman, R.; Gormley, A. J.; Stenzel, M. H.; Stevens, M. M., Combinatorial Low-Volume Synthesis of Well-Defined Polymers by Enzyme Degassing. *Angewandte Chemie-International Edition* **2016**, *55* (14), 4500-4503.
14. Yeow, J.; Chapman, R.; Xu, J. T.; Boyer, C., Oxygen tolerant photopolymerization for ultralow volumes. *Polymer Chemistry* **2017**, *8* (34), 5012-5022.
15. Johnson, L. M.; DeForest, C. A.; Pendurti, A.; Anseth, K. S.; Bowman, C. N., Formation of Three-Dimensional Hydrogel Multilayers Using Enzyme-Mediated Redox Chain Initiation. *Acs Applied Materials & Interfaces* **2010**, *2* (7), 1963-1972.
16. Shenoy, R.; Bowman, C. N., Kinetics of interfacial radical polymerization initiated by a glucose-oxidase mediated redox system. *Biomaterials* **2012**, *33* (29), 6909-6914.
17. Hume, P. S.; Bowman, C. N.; Anseth, K. S., Functionalized PEG hydrogels through reactive dip-coating for the formation of immunoactive barriers. *Biomaterials* **2011**, *32* (26), 6204-6212.
18. Layadi, A.; Kessel, B.; Yan, W. Q.; Romio, M.; Spencer, N. D.; Zenobi-Wong, M.; Matyjaszewski, K.; Benetti, E. M., Oxygen Tolerant and Cytocompatible Iron(0)-Mediated ATRP Enables the Controlled Growth of Polymer Brushes from Mammalian Cell Cultures. *Journal of the American Chemical Society* **2020**, *142* (6), 3158-3164.
19. Johnson, L. M.; Fairbanks, B. D.; Anseth, K. S.; Bowman, C. N., Enzyme-Mediated Redox Initiation for Hydrogel Generation and Cellular Encapsulation. *Biomacromolecules* **2009**, *10* (11), 3114-3121.
20. Chen, M.; Briscoe, W. H.; Armes, S. P.; Klein, J., Lubrication at Physiological Pressures by Polyzwitterionic Brushes. *Science (New York, N.Y.)* **2009**, *323* (5922), 1698-1701.

21. Zhang, Z. Y.; Moxey, M.; Alswieleh, A.; Morse, A. J.; Lewis, A. L.; Geoghegan, M.; Leggett, G. J., Effect of Salt on Phosphorylcholine-based Zwitterionic Polymer Brushes. *Langmuir : the ACS journal of surfaces and colloids* **2016**, *32* (20), 5048-5057.

22. Zhang, Z. Y.; Morse, A. J.; Armes, S. P.; Lewis, A. L.; Geoghegan, M.; Leggett, G. J., Nanoscale Contact Mechanics of Biocompatible Polyzwitterionic Brushes. *Langmuir : the ACS journal of surfaces and colloids* **2013**, *29* (34), 10684-10692.

Chapter 2

Bioinert and Lubricious Surfaces by Macromolecular Design*

The modification of a variety of biomaterials and medical devices often encompasses the generation of biopassive and lubricious layers on their exposed surfaces. This is crucial when synthetic substrates are required to operate within physiological media without altering their interfacial composition, and when minimization of shear stress can prevent or reduce damage to the surrounding environment (e.g. in blood vessels). In many of these cases, hydrophilic polymer brushes assembled from surface-interacting polymer adsorbates, or directly grown by surface-initiated polymerizations (SIP) are chosen.

While growing efforts by polymer chemists have been focusing on varying the composition of polymer brushes in order to attain increasingly bioinert and lubricious surfaces, the precise modulation of polymer architecture has simultaneously allowed the tuning potential for the above-mentioned properties to be substantially broadened. This chapter concentrates on reviewing this latter strategy, comparatively analysing how polymer-brush parameters, such as molecular weight and grafting density, the application of block copolymers, the introduction of branching and crosslinks, or the variation of polymer topology beyond simple, linear chains all determine technologically relevant properties, such as biopassivity and lubrication.

* Part of this Chapter was published in *Langmuir*. **2019**, 35, 42, 13521-13535. Edmondo M. Benetti, Wenqing Yan, Shivaprakash N. Ramakrishna and Matteo Romio wrote the review together.

2.1 Introduction

The design of biomaterials, medical devices and sensors often encompasses surface-functionalization strategies that aim to impart well-defined interfacial physicochemical properties. These determine the way in which the functionalized materials interact with their application medium, and in most of the formulations, significantly influence their performance.

The assembly of functional polymers yielding “polymer brush” layers¹ or, alternatively, the growth of polymer brushes from pre-modified supports through surface-initiated polymerization (SIP)²⁻³ methods have emerged as the most versatile and efficient strategies to generate surfaces with tunable properties.

During the last decade, intensive efforts have been dedicated to establishing robust fabrication protocols for the generation of polymer brushes with precise architectures and well-defined compositions, especially concentrating on the influence of these two parameters on the biopassive and tribological properties of the obtained coatings.

The combination of high resistance towards nonspecific protein adsorption and lubrication is often highly required on the exposed surface of biomaterials. On the one hand, hampering the formation of a protein layer can help prevent microbial contamination, or an adverse immune response towards a synthetic construct when this is applied within physiological environments.⁴⁻⁷ On the other hand, the presence of a lubricious coating increases the comfort and prevents cell damage when a modified device is placed in contact with tissues, such as in the case of contact lenses or catheters.⁸⁻¹⁰

A large number of hydrophilic polymers forming dense brush assemblies on surfaces can meet these needs due to the interplay between enthalpic and entropic effects. These are respectively determined by the association of water molecules within the brush structure, and the distinctive, stretched conformation characterizing densely grafted chains.¹¹⁻¹⁴ Hence, dense and hydrated polymer brushes efficiently prevent nonspecific adhesion of biomolecules (and larger biomolecular entities), due to their unfavourable de-hydration and the loss of conformational entropy involved when biomolecules adhere to the surface.^{4, 11-14}

In addition, the interplay between high water content and the osmotic pressure generated within the brush provides fluid lubrication and load-bearing capacity, substantially reducing friction when a shearing countersurface is applied (Figure 1).¹⁵⁻¹⁹

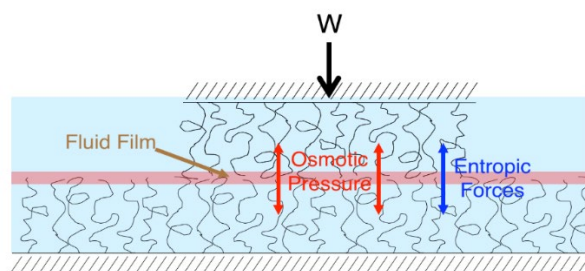


Figure 1. The lubricity of polymer brushes is due to a combination of osmotic pressure within the brush and the resistance to interpenetration of the two brushes due to entropic effects²⁰.

The design principle for biopassive and lubricious polymer brushes has primarily relied on a careful tuning of polymer composition, which allows one to enhance the hydration capacity of the assemblies while minimizing the presence of chemical functionalities that could trigger specific or nonspecific interactions with the surrounding biological environment. Through this strategy, in addition to poly(ethylene glycol) (PEG)^{13, 21-23} and its derivatives, several other polymers have been introduced as starting materials for fabricating brushes with improved antifouling properties and enhanced lubricity. These included polyzwitterions,²⁴⁻²⁷ poly(acrylamide)s and poly(methacrylamide)s,²⁸⁻³² poly(2-alkyl-2-oxazoline)s (PAOXAs)³³⁻³⁴ and very recently, poly(2-alkyl-2-oxazine)s (PAOZIs).³⁵

However, besides their composition, polymer architecture (*i.e.* branching or topology) and structural properties (*i.e.* grafting density and/or thickness) represent additional parameters strongly affecting the physicochemical properties of brush assemblies, consequently determining their resistance towards biological contamination, as well as their nanotribological properties.

In this chapter, we summarize our recent efforts in the macromolecular design of polymer-brush interfaces, especially focusing on how polymer topology and the structural properties of assemblies can be varied in order to modulate technologically relevant interfacial properties of the generated surfaces. In particular, we concentrate on bioinertness of polymer brushes, interpreted as protein and cell repellence, as well as the lubrication properties of the grafted films.

While additionally reporting the most prominent, recent works by others, in which polymer structure-brush properties relationships have been dissected, the main objective of this review is to derive from experimental works some general design principles, which for a given chemistry would enable the independent tuning of highly technologically relevant properties of polymer brushes, such as biopassivity and lubrication. Although we are aware that a comprehensive theoretical description of the brush structural parameters regulating these

properties has been derived from several fundamental works, including simulations,^{14-17, 36-42}, the focus of this chapter is rather on those studies that, through experiments, could rationalize the choices of determining parameters for such interfacial properties of polymer brushes.

2.2 Modulation of Polymer-Brush Thickness and Grafting Density

The independent variation of the structural properties of homopolymer brushes represents a powerful tool to modulate both their interaction with biological environments, as well as to tune their lubrication properties. The main structural variables that can be readily adjusted in order to vary these characteristics are the molecular weight of the brushes, which directly correlates to brush thickness, and their grafting density (σ).^{43-44, 14-16}

It is important to emphasize that the nonspecific adhesion of proteins can provide an indirect indication about the way polymer-brush interfaces would interact with larger biological objects, such as cells or bacteria, since these processes are mediated by initial protein adsorption.^{13-14, 41-42, 45} Nevertheless, enhancing resistance towards protein adsorption to a generalized antifouling behavior might be not valid for several systems.

The values of σ mainly determine the primary adsorption of proteins on polymer brushes, *i.e.* the unspecific interaction between the biomolecules and the underlying substrate.^{14, 41-42} A variation of grafted-polymer coverage thus regulates the extent of protein intercalation within the brush assembly, with low- σ brushes enabling significant surface contamination, especially by small, globular proteins such as albumin (Figure 2).

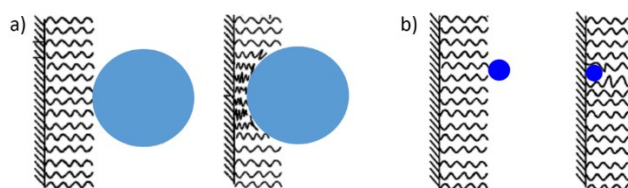


Figure 2. Large proteins can adsorb the outer edge on polymer brushes via secondary adsorption (a). In contrast, small proteins can intercalate within the brush structure undergoing primary adsorption (b)¹⁴.

In contrast, tuning of brush thickness, which for a given σ is directly correlated to the molecular weight of the grafted polymer, determines secondary protein adsorption.^{14, 41-42} This phenomenon arises from long-range interactions between biomolecules approaching the brush-medium interface and the underlying substrate, and it can be efficiently hindered when brush thickness is finely adjusted, for instance by fabricating brushes via surface-initiated controlled

radical polymerization (SI-CRP).² Hence, the fabrication of sufficiently thick and densely grafted brushes can assure an efficient and durable resistance towards nonspecific protein contamination.

When, in addition to biopassivity, high lubricity is sought, the composition of polymer brushes, *i.e.* their hydrophilic character, should be carefully considered while tuning the structural properties of the grafted assemblies. Friction progressively decreases with increasing brush thickness in the case of highly hydrophilic brushes, such as those based on polyzwitterions, due to the increment in the amount of water associated to the grafts with increasing molecular weight (Figure 3).⁴⁶⁻⁴⁹

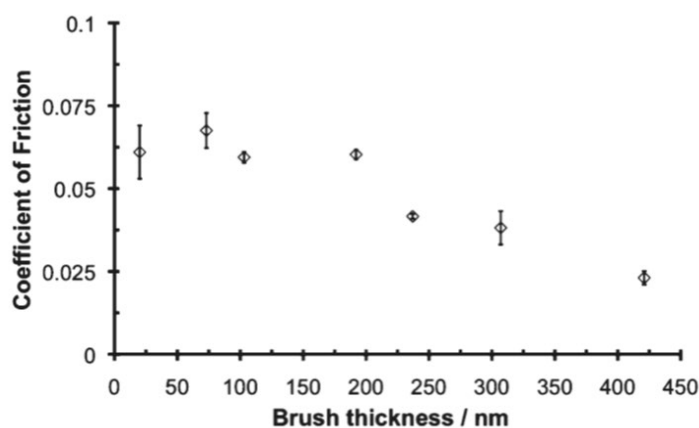


Figure 3. The coefficient of friction (μ) obtained by lateral force microscopy on poly[2-(methacryloyloxy)ethylphosphorylcholine] (PMPC) brushes was shown to decrease with increasing brush thickness ⁴⁹.

In contrast, brushes presenting an amphiphilic character, especially those based on poly(ethylene glycol) (PEG) and its derivatives, often showed the opposite behavior. This is the case for poly[(oligoethylene glycol)methacrylate] (POEGMA) brushes synthesized by surface-initiated atom-transfer radical polymerization (SI-ATRP), which present an amphiphilic character in water, and showed a progressive increment in friction with increasing brush thickness when analyzed by lateral force microscopy (LFM) (Figure 4).⁵⁰ This phenomenon was ascribed to the increment in mechanical-energy dissipation that arises while shearing progressively thicker POEGMA brushes, which contain just a limited amount of solvent within their structure, and display adhesive hydrophobic interactions towards the atomic force microscopy (AFM) colloidal probe.

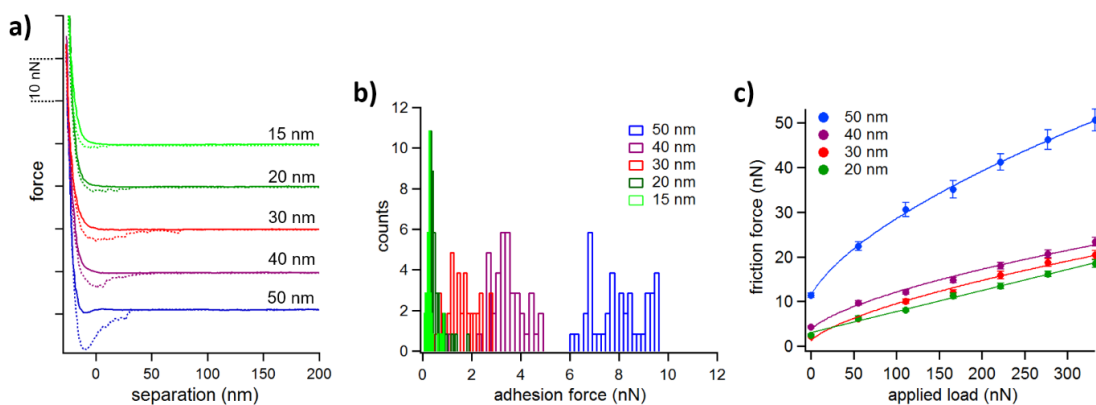


Figure 4. (a) Force-vs-separation (FS) profiles recorded on POEGMA brushes presenting different dry thicknesses (indicated in black along each FS profile). (b) Adhesion was shown to increase with brush thickness due to hydrophobic interactions between the silica-based AFM colloidal probe and POEGMA brushes. (c) Friction-vs-applied load profiles (F_fL) recorded by LFM highlighted how mechanical energy dissipation increased with increasing brush thickness, leading to a simultaneous increment in friction⁵⁰.

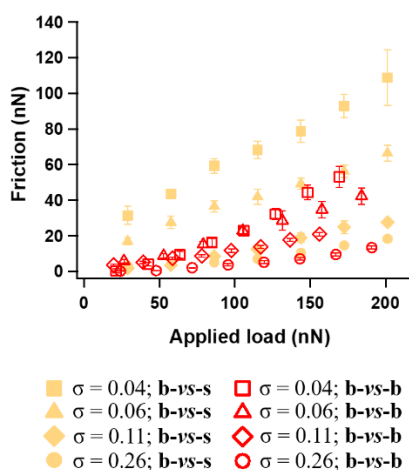


Figure 5. Friction-vs-applied load (F_fL) profiles recorded by LFM on poly(2-ethyl-2-oxazoline) (PEOXA) brushes presenting different values of σ . A reduction in friction was observed by increasing σ both when PEOXA brushes were sheared against a bare, silica-based colloidal AFM probe (b-vs-s), and when an identical brush was applied as countersurface (b-vs-b)⁵².

Similar results were recorded while studying the nanotribological properties of poly(N-isopropyl acrylamide) (PMIPAM) brushes below and above their lower critical solution temperature (LCST).⁵¹ Below LCST, highly swollen PNIPAM brushes were characterized by an increment in lubricity with increasing thickness, due to the higher content of fluid lubricant incorporated within thicker brushes. In contrast, above LCST, PNIPAM brushes are poorly hydrated and friction increases with thickness, due to the increase in dissipative forces as a shearing AFM probe is applied.

Differently from what has been observed while varying brush thickness, a variation of σ produced a similar effect on the nanotribological properties of hydrophilic and amphiphilic brushes. On both these types of assemblies, an increase in surface coverage of grafted chains was mirrored by a concomitant reduction in friction. Generally, denser brushes displayed an augmented load-bearing capacity, due to the higher osmotic pressure generated within their structure with respect to that exerted by their more loosely grafted counterparts.⁵²⁻⁵³ In addition, when polymer brushes are sheared against structurally identical brush-functionalized surfaces, an increment in grafting density translated into a reduction of interpenetration between opposing brushes,^{16, 54} leading to a diminution of dissipative collisions between sheared chains, and a simultaneous decrease in the resulting friction (Figure 5).^{52, 55-56}

2.3 Mixed and Copolymer Brushes

The fabrication of polymer brushes that include compositionally diverse homopolymer, random or block copolymer grafts enables the biopassive and nanotribological properties of the generated surfaces to be precisely tuned.

Following the seminal works by Stamm and Minko, where the morphological and interfacial physicochemical properties of mixed brushes in response to selective solvents were thoroughly investigated,⁵⁷⁻⁶² increasing efforts have been subsequently dedicated to synthesizing structurally similar assemblies capable of shifting their affinity towards proteins and/or their nanotribological properties.

Mixed brushes featuring tunable biopassivity were successfully synthesized following a general design principle, where two chemically different grafts are sequentially grafted to a functional surface,⁶¹ or consecutively grown by SI-CRP from initiator-bearing substrates.⁶³⁻⁷⁰ In most of these cases, mixed brushes comprised a biopassive component intercalated with an additional graft-type capable of changing its swelling properties or charge density in response to a variation in temperature, pH or ionic strength.

In the exemplary cases of ionizable poly(acrylic acid) or poly(methacrylic acid) (PAA and PMAA, respectively) grafts mixed with PEG⁷¹⁻⁷² or poly(2-methyl-2-oxazoline) (PMOXA)⁷³⁻⁷⁴ analogues, pH and ionic strength could be varied in order to modulate the exposure of the non-ionic and biopassive components at the interface, finally enabling the capture and successive release of proteins from the surrounding medium.

Through this strategy, and via the fine adjustment of molecular weight and relative content of PEG grafts within PAA/PEG mixed brushes, the selective and reversible physisorption of

defined biomolecules from mixtures of different protein types could be additionally accomplished.⁷⁵

Alternatively, by combining thermoresponsive poly(N-isopropylacrylamide) (PNIPAM) grafts with PAA analogues, switching of the affinity towards proteins could be triggered by varying the temperature of the medium, and it could further amplified by tuning of the relative content of each component at the surface.⁷⁶

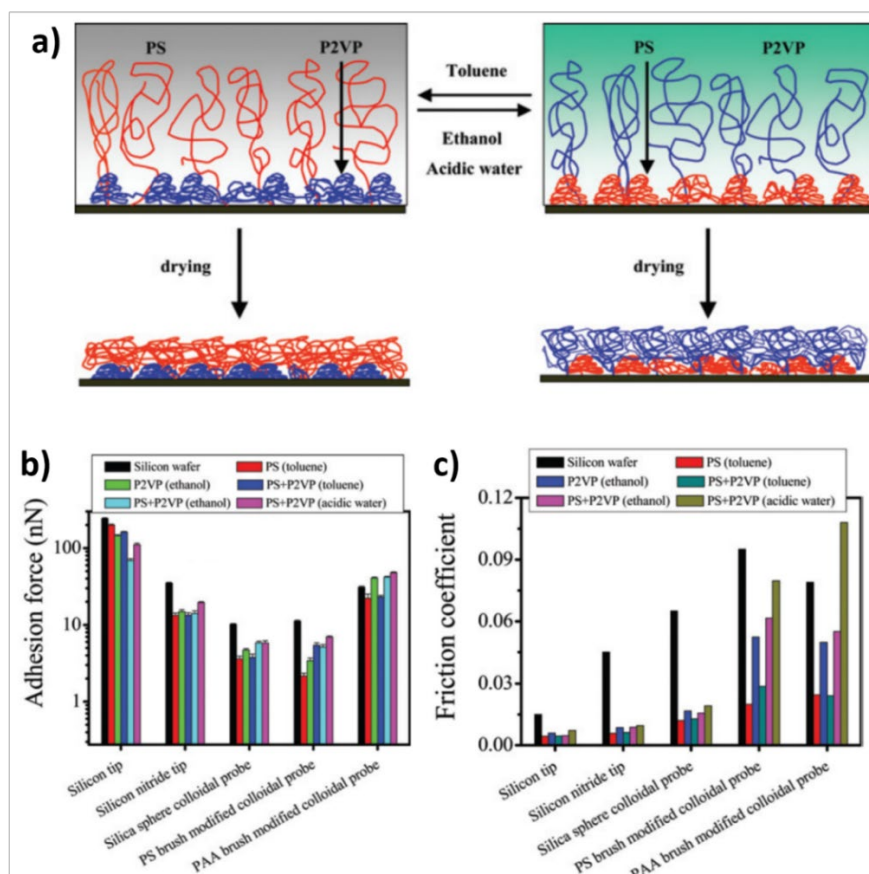


Figure 6. (a) The interfacial morphology of polystyrene (PS)-poly(2-vinylpyridine) (P2VP) mixed brushes was modulated by treating them with selective solvents. In this way, and by simultaneously varying the composition of the brush grafted on the AFM colloidal probe, both adhesive properties (b) and friction (c) could be tuned.⁸⁴

Switching of bioadhesion on polymer brushes could be also accomplished by synthesizing random copolymer grafts that incorporate different relative contents of amphiphilic, hydrophobic and charged co-monomers. Similarly to the case of mixed brushes, where the overall composition of the assemblies was tuned in order to amplify switching of properties, a careful adjustment of the relative content of each co-monomer was exploited to enhance the variation of interfacial properties of the generated brush in response to a temperature change, efficiently shifting the character of the surface from bio-repellent to bio-adhesive. This strategy

was successfully exploited by Okano et al. in order to stimulate the adhesion of different cells and subsequently release them following proliferation, yielding freestanding cell sheets, or to trigger attachment and release from the surface of a particular cell type from mixtures.⁷⁷⁻⁸³

Mixed brushes featuring two immiscible polymer grafts that can be selectively swollen in different solvent environments were additionally applied to modulate adhesion and friction at surfaces. In particular, grafted assemblies including polystyrene (PS) and poly(2-vinylpyridine) (P2VP) could significantly vary their morphology and interfacial composition in response to the exposure to selective solvents (toluene and ethanol/water) (Figure 6a).⁸⁴ In this way, adhesive and lubrication properties could be shifted by an order of magnitude, and further tuned as a function of the composition of the probe used as countersurface for the adhesion/friction force measurements (Figure 6b and 6c).

A significant alteration of the interfacial physicochemical properties of polymer brushes could be accomplished by mixing two non-ionic grafts that are both soluble in water, such as PEG and PMOXA or poly(2-ethyl-2-oxazoline) (PEOXA).⁸⁵ Surface dilution of a grafted component with a compositionally different analogue led to an increment in the hydration of the entire assembly, with a consequent improvement in its resistance towards protein contamination. Moreover, in combination with the increased brush swelling achieved through mixing, the inclusion of PEG grafts that are characterized by a low glass-transition temperature (T_g) within PMOXA and PEOXA brushes (with $T_g \geq 70^\circ\text{C}$) significantly reduced friction with respect to that measured on the corresponding homopolymer brushes, especially when relatively high pressures were applied (Figure 7).³⁵

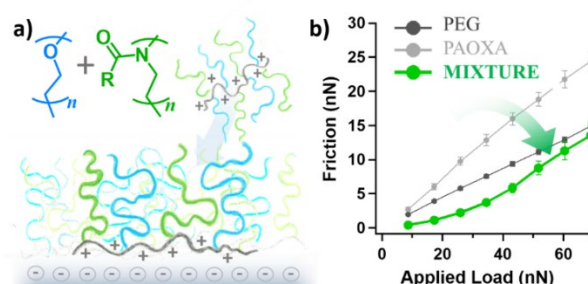


Figure 7. Mixed brushes featuring PEG and PAOXA grafts (a) showed improved lubricity when compared to PEG- and PAOXA-based single-component brushes (b)⁸⁵.

Besides studying the properties of grafts presenting two or more components mixed on the same substrate, the immiscibility between chemically diverse homopolymer brushes grafted from different surfaces allowed de Beer et al. to substantially hinder brush interpenetration when these two assemblies are sheared one against each other.³⁶ The consequent reduction of

dissipative forces between opposing grafts sliding in opposite directions^{17-18, 37} generated a substantial reduction in the coefficient of friction (μ) if compared to that measured by shearing identical, interpenetrating brushes.

It is also important to emphasize that a comparable suppression of brush interdigitation, with a concurrent improvement in lubricity, could be potentially accomplished by substituting one of the two countersurfaces with a responsive brush capable of varying its swelling and conformation in response to a physical stimulus, such as a shift in pH or temperature.^{37, 86}

An alternative approach for broadening the functional character of polymer brushes and expanding their physicochemical properties has encompassed the application of (multi)block copolymer grafts, typically synthesized by sequential SI-CRP methods.²

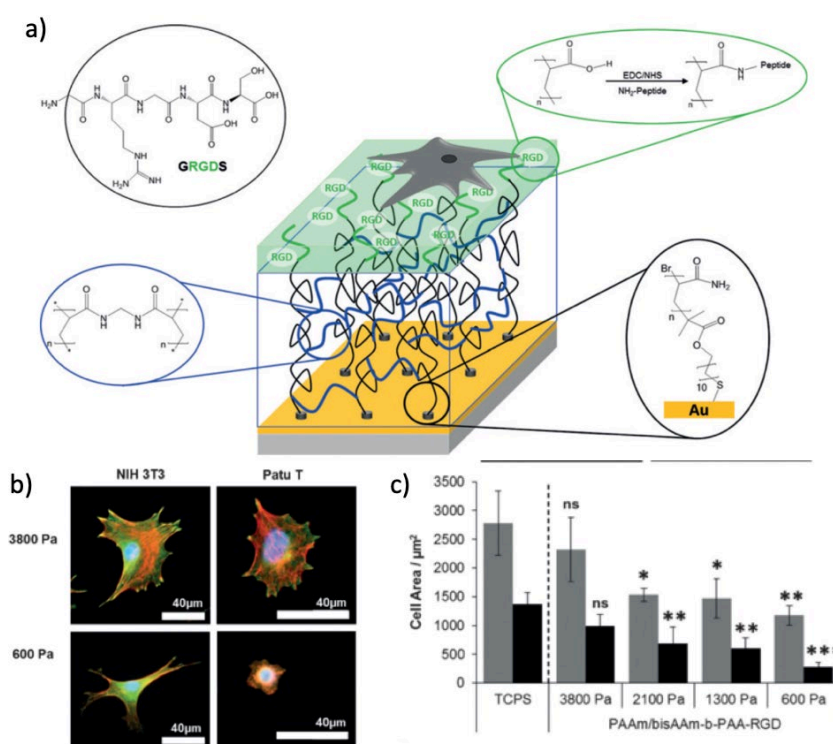


Figure 8. (a) Block copolymer brushes featuring a substrate bound, crosslinked PAAm brush hydrogel with variable stiffness, and an interfacial PAA brush functionalized with peptide-based cues were applied to study the attachment of different cell types and their cytoskeleton organization (b,c)⁹⁹.

Especially in the designing of biointerfaces, hierarchical brush structures including a substrate-bound, biopassive block, and functional/bioactive interfacial segments have been applied for regulating the adhesion of cells and bacteria. This general design enabled the fabrication of coatings capable of repelling bacteria, as well as displaying bactericidal properties.⁸⁷⁻⁸⁸ Similar block-copolymer brushes have been applied to functionalize the surface of biosensors, where just one brush block can selectively bind analytes from solution.⁸⁹⁻⁹²

Alternatively, functional block copolymer brushes have been exploited to trigger the adhesion of cells and simultaneously modulate their response.⁹³⁻⁹⁷ Generally, within these brush formulations one or more brush segments feature a biopassive character, although their tunable physical properties are exploited to regulate the behavior of cells, whose attachment to the surface is stimulated by the presence of functional cues on the other blocks.

Block-copolymer brushes characterized by an alternation of biopassive and cell-adhesive blocks were applied to modulate the surface exposure of covalently bound peptides, which were “buried” by interfacial brush segments of different molecular weights,⁹³⁻⁹⁴ and whose presentation at the interface could be altered when the bioinert segments feature temperature-dependent swelling properties.⁹⁸

Following this strategy, the morphology of adhering cells and their attachment on the brush interface could be precisely adjusted, suggesting possible strategies to influence cell’s behavior (proliferation and/or differentiation) on biomaterials previously modified with different brush architectures.

The influence of the physicochemical properties of cell-adhesive brush films on the adhesion of different cell types could be dissected by designing block-copolymer brushes including a substrate-bound brush block with variable degree of crosslinking and an interfacial linear brush decorated with cell-adhesive cues.⁹⁹ In particular, Schönherr et al. demonstrated how the nanomechanical properties of polyacrylamide (PAAm) brushes could be precisely varied by tuning of the relative concentration of acrylamide/bisacrylamide during SI-ATRP (Figure 8a). Simultaneously, an interfacial brush based on PAA functionalized with arginine-glycine-aspartic acid (RGD)-containing peptides guaranteed a comparable cell-adhesive character to the exposed surface. In this way, the effect of underlying brush stiffness on the behavior of both fibroblasts and cancer cells could be addressed independently of the morphology and composition of the interface (Figures 8b and 8c).

In addition to the fabrication of protein- or cell-responsive surfaces, block-copolymer brushes including a hydrophobic, substrate-bound block and hydrophilic interfacial segments were applied in order to increase the long-term stability of polymer-brush coatings within particularly aggressive media, such as cell culture solutions or salty water, and to preserve their distinctive interfacial properties, otherwise undergoing a progressive alteration during brush degradation.

For instance, the resistance of poly(sulfobetaine methacrylamide) (PSBMAM)¹⁰⁰ and poly(2-methacryloyloxyethyl phosphorylcholine) (PMPC) brushes¹⁰¹ towards hydrolytic degradation and degrafting could be significantly improved by including hydrophobic brush

blocks as protective layers bound to the underlying substrates. The presence of either PMMA, polystyrene (PS) or poly(glycidyl methacrylate) (PGMA) segments, all of which formed a collapsed, substrate-bound layer, preserved the structural integrity of the highly swollen PSBMAm and PMPC grafts at the interface, maintaining their attractive biopassive and lubrication properties (Figure 9).¹⁰¹

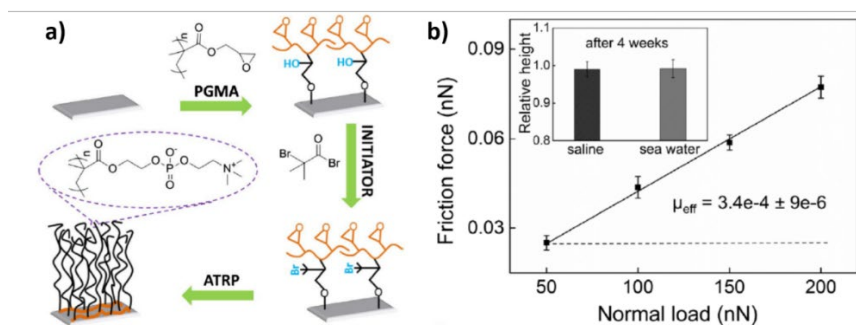


Figure 9. PMPC brushes grafted by SI-ATRP from initiator-bearing PGMA underlayers (a) preserve their structural properties even after 4 weeks of incubation in salty water, and maintain their lubricious character, as evidenced by LFM measurements (b) ¹⁰¹.

In a similar way, the stability of PMAA¹⁰² and poly[(oligoethylene glycol)methacrylate] (POEGMA)¹⁰³ brushes was significantly improved by the presence of substrate-bound PMMA blocks, which protected the underlying initiator functions from hydrolysis. Especially POEGMA-b-PMMA block copolymer brushes showed comparable biopassive properties and lubricity with respect to POEGMA homopolymer analogues, whereas the hydrophobic PMMA underlayer improved the structural stability of the entire films by several days under cell culture media at 37°C.¹⁰³

2.4 Branched and Crosslinked Polymer Brushes

Polymer adsorbates featuring a branched architecture were applied to generate biopassive, brush-like assemblies on a variety of inorganic and organic substrates. The most prominent examples included hyperbranched polyglycerol (hPG)¹⁰⁴⁻¹⁰⁵ and PEG adsorbates.¹⁰⁶⁻¹⁰⁸

Assemblies featuring hPG dendrons and dendrimers showed excellent resistance towards the unspecific surface contamination by proteins, cells and bacteria, often surpassing the antifouling properties displayed by linear polyglycerol brushes, and in several cases matching those showed by densely grafted PEG analogues.¹⁰⁹⁻¹¹²

Dendronized PEG adsorbates assembled on TiO₂ surfaces via catechol-based anchors formed brushes that were less hydrated and more rigid (less viscoelastic) with respect to their

linear PEG counterparts (Figure 10).¹⁰⁷ However, dendronized PEG brushes showed a resistance towards the adsorption of undiluted full human serum (FHS) comparable to that showed by highly swollen linear PEG assemblies. These results suggested that hydration might not represent a strict determinant for biopassivity in the case of brushes presenting an hyperbranched structure, which could thus compensate their reduced swelling with a concomitant increment in surface passivation.

The biopassive properties displayed by grafted-from polymer brushes featuring side chains with different degrees of branching further highlighted the effect of brush architecture on its resistance towards unspecific biological contamination. In particular, the groups of Haag and Huck compared the antifouling properties of glycerol-containing linear polymethacrylate brushes synthesized by SI-ATRP with those displayed by analogous grafts featuring linear, first- and second-generation dendritic polyglycerol side chains.¹¹³ From this comparative analysis, brushes including branched side chains were characterized by excellent biopassivity within FHS and undiluted blood plasma, with first-generation polyglycerol-bearing brushes outperforming all the other tested coatings.

In addition to branching, an alternative approach to modulate both biopassivity and lubrication properties relied on the introduction of covalent or physical crosslinks between surface-grafted chains.

Brush-hydrogels of diverse compositions and including different concentrations of crosslinks could be easily synthesized by SI-ATRP, mixing mono and bi-functional monomers within the polymerization mixture.¹¹⁴⁻¹¹⁸ Due to the intrinsic architecture of polymer brushes, which are characterized by polymer grafts immobilized by one chain end to the same substrate, the introduction of even a relatively low concentration of crosslinker, or a slight variation in its content, translated into a significant shift of the interfacial physicochemical properties of the resulting films.

For instance, crosslinking poly(hydroxyethyl methacrylate) (PHEMA) brushes with ~ 1 mol% of di(ethylene glycol) dimethacrylate (DEGDMA) reduced by nearly 20% the swelling ratio of the brushes, and significantly reduced their conformational freedom.¹¹⁹ These changes in brush structure and properties eventually led to a twofold increment in the amount of proteins physisorbed on brush-hydrogels from full human serum, when compared to that recorded on the corresponding linear PHEMA brushes presenting comparable dry thickness (Figure 11a).

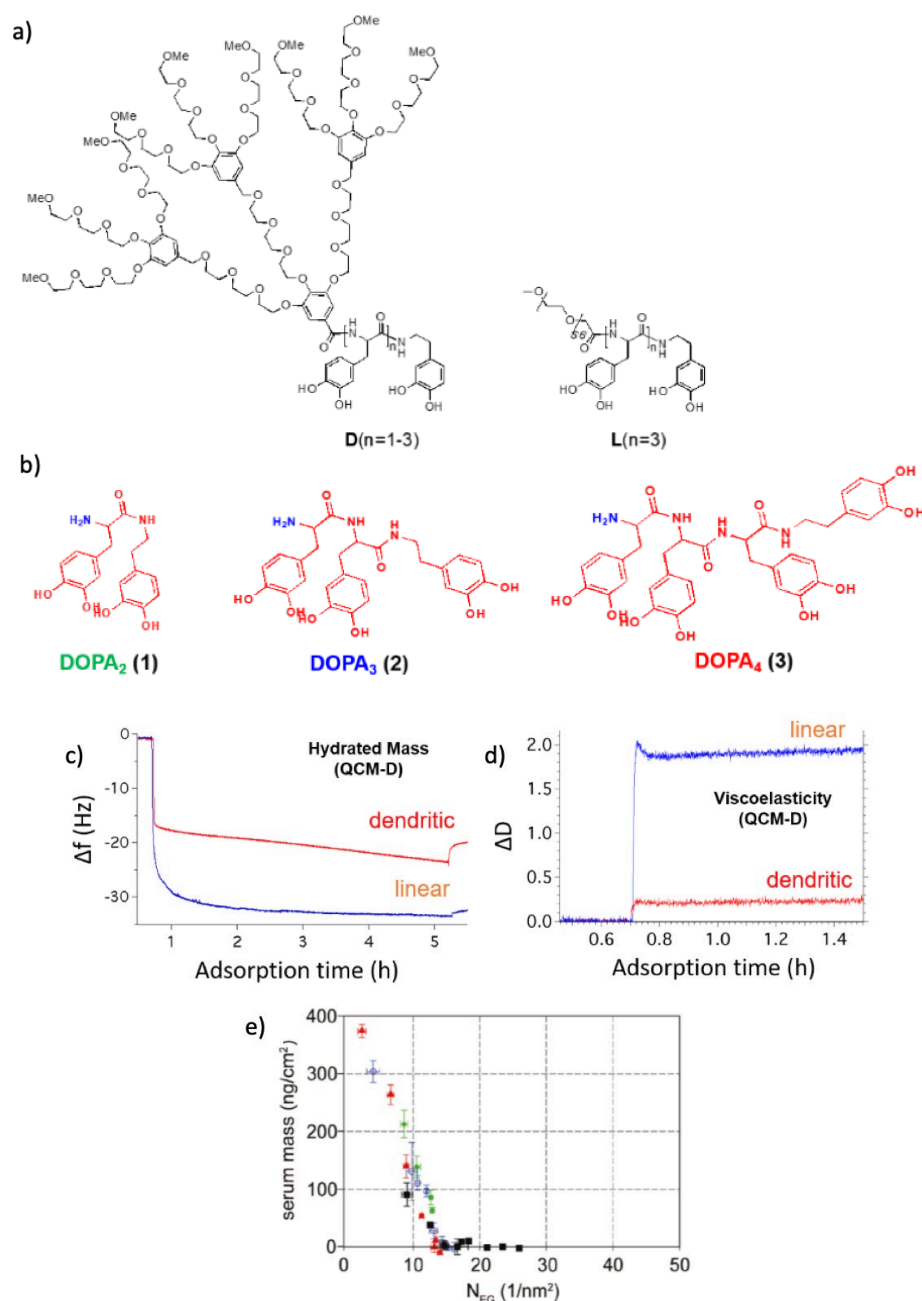


Figure 10. Dendronized PEG adsorbates (a) presenting multi-catechol anchors (b) formed brushes on TiO_2 surfaces that featured lower swelling compared to linear PEG analogues (c) and higher rigidity (d), as measured by monitoring frequency (Δf) and dissipation (ΔD) shifts with quartz crystal microbalance with dissipation (QCM-D). However, both linear and dendronized PEG brushes showed a comparable biopassivity when exposed to full human serum (e), as recorded by variable angle spectroscopic ellipsometry (VASE) on assemblies featuring different polymer surface coverages (expressed as number of ethylene glycol units, NEG, per nm^2)¹⁰⁷.

Interestingly, the substitution of DEGDMA with an equimolar amount of longer, tetra(ethylene glycol)dimethacrylate (TEGDMA) reduced the loss of biopassive properties observed on PHEMA-DEGDMA brush-hydrogels, presumably due to the increment in the overall content of water-associating ethylene glycol units within the films.

Irrespective of their composition, the introduction of covalent crosslinks between grafts and the simultaneous decrease in the content of fluid lubricant within the films caused a significant increase in friction. As an example, the coefficient of friction (μ) measured in water by lateral force microscopy (LFM) on PHEMA brushes increased from 0.49 to 0.67 and 0.76 when the grafted chains were crosslinked by 1 and 2 mol% of DEGDMA, respectively (Figure 11b and 11c).¹²⁰

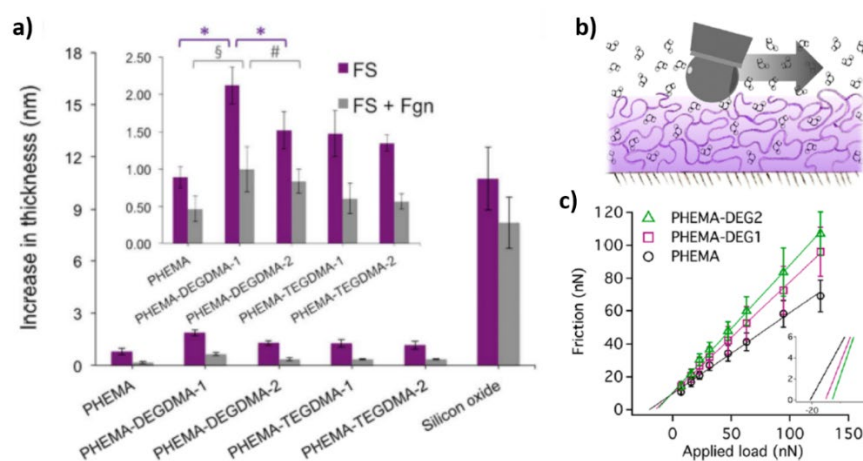


Figure 11. Adsorbed protein thickness on the different PHEMA brushes and brush-hydrogels measured by VASE following 90 minutes of incubation in FHS (violet bars) and FHS with added fibrinogen (Fgn) (gray bars). * indicates a statistically significant difference analyzed by ANOVA test $P < 0.0001$, § refers to $P < 0.001$, and # indicates $P < 0.05$. Reproduced from Dehghani, E. S.; Spencer, N. D.; Ramakrishna, S. N.; Benetti, E. M., Crosslinking Polymer Brushes with Ethylene Glycol-Containing Segments: Influence on Physicochemical and Antifouling Properties. *Langmuir* **2016**, 32 (40), 10317-10327, Copyright 2016 American Chemical Society. The values of μ recorded on PHEMA brushes and brush hydrogels by LFM (b) could be precisely modulated by varying the content of DEGDMA crosslinker between 1 and 2 mol%¹²⁰.

A more pronounced reduction in lubricity was observed in the case of more hydrophilic polymer grafts,^{30, 121-122} such as polyacrylamide (PAAm) brushes synthesized by surface-initiated photoiniferter-mediated polymerization (SI-PIMP),¹²³⁻¹²⁴ and crosslinked by 0.1-5 mol% of bisacrylamide (bisAAM).^{30, 122} In particular, PAAm brush-hydrogels presenting 5 mol% of bisAAM showed a tenfold decrease in swelling properties in water, and a concomitant increment in μ by more than an order of magnitude.

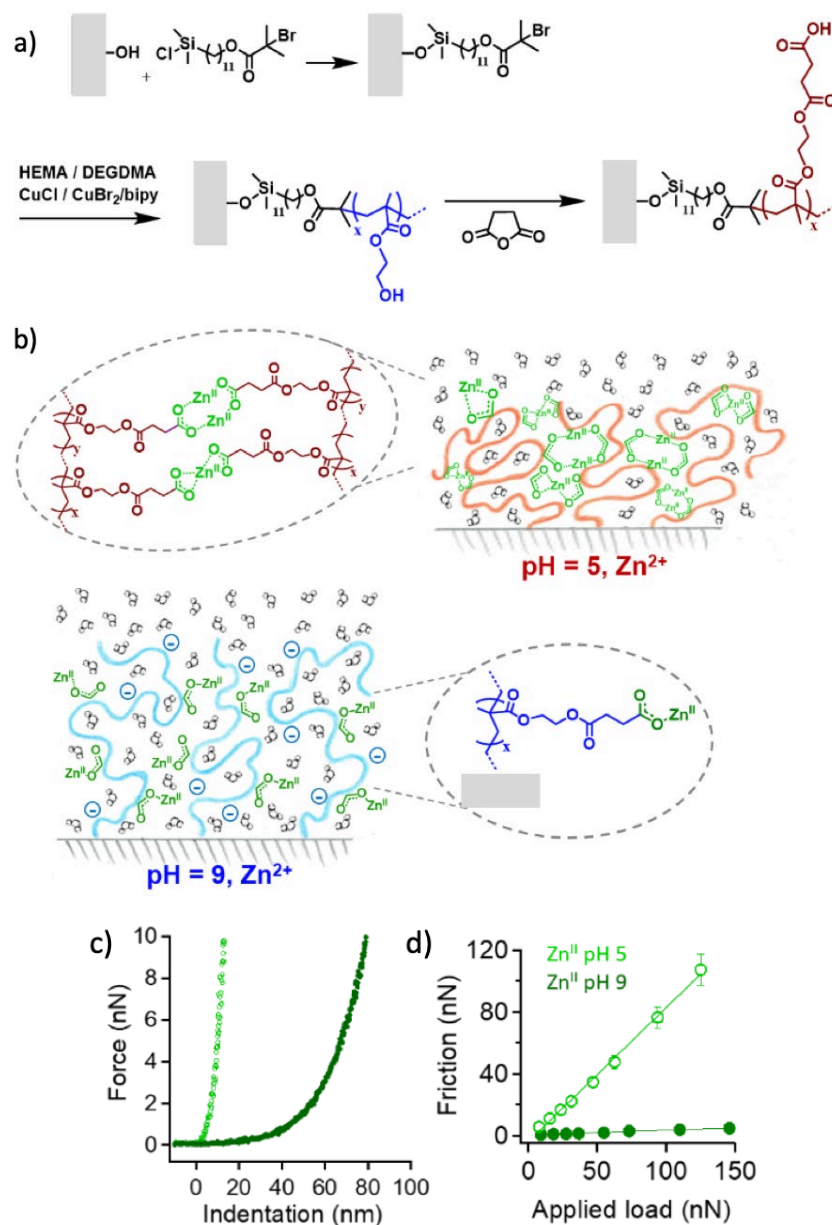


Figure 12. PHEMA-SA brushes were synthesized by SI-ATRP followed by derivatization with succinic anhydride (a). When PHEMA-SA brushes were treated with 10 mM Zn²⁺ solution at pH 5, bridging and chelating complexes were formed, while in 10 mM Zn²⁺ at pH 9 brush networks presenting monodentate conjugates were obtained (b). Force-vs-indentation (FI) and F_L profiles recorded by AFM on PHEMA-SA-Zn^{II} brushes highlight how the swelling and lubrication properties were determined by the formation of different types of crosslinks between the PHEMA-SA grafts ¹²⁶.

Besides the fabrication of covalent brush networks, the designing of polymer brushes that could be reversibly crosslinked through the formation of organometallic complexes between linear grafts, enabled the fabrication of surfaces presenting switchable swelling and nanotribological properties.¹²⁵⁻¹²⁷ In the chemically simplest case, linear PHEMA brushes bearing succinic acid-based side chains (PHEMA-SA) could be reversibly crosslinked by treatment with divalent metal ions, such as Zn^{II} and Ca^{II} (Figure 12a).¹²⁶ Tuning of the pH

during the formation of the polymer-metal complexes enabled the synthesis of either mono- or bidentate bridges between the grafts (Figure 12b), generating brush networks with pronounced differences in swelling and lubrication properties (Figure 12c and 12d). Brush networks including Zn^{II} ions thus showed a reversible shift in μ from 0.8, when more strongly crosslinked dehydrated structures were formed via bidentate complexes, to 0.03 in the case of more compliant and swollen networks based on monodentate bridges (Figure 12d).

2.5 Polymer Brushes Presenting Cyclic and Loop Topologies

Recent studies from our group have highlighted that shifting the topology of polymer brushes from simple, linear chain to their cyclic counterparts, while keeping their composition and molecular weight constant, determined a pronounced alteration of biopassivity and lubrication.^{52-53, 55, 128-133}

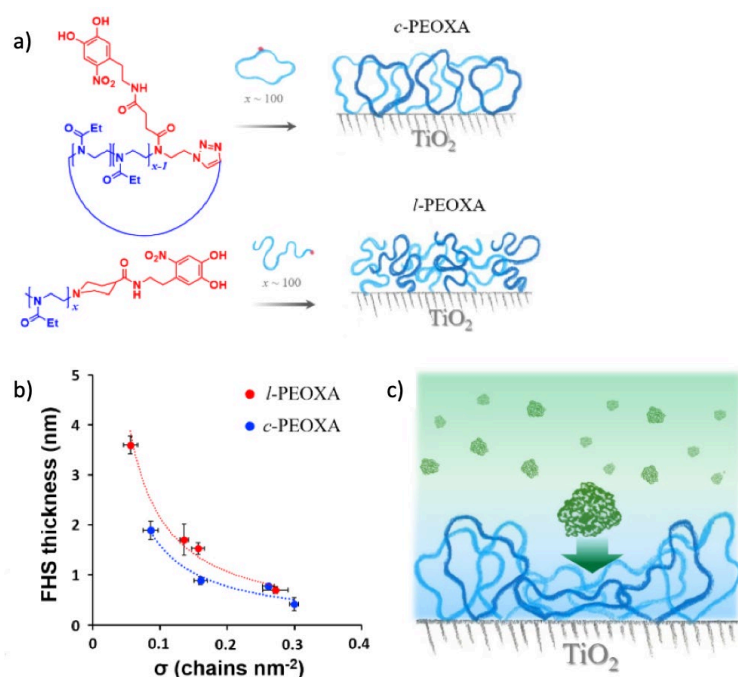


Figure 13. (a) Linear and cyclic PEOXA adsorbates featuring catechol anchors assemble on TiO_2 surfaces yielding topologically different PEOXA brushes (indicated as c -PEOXA and l -PEOXA, respectively). (b) c -PEOXA brushes showed an improved biopassivity towards FHS across a wide range of grafting densities with respect to l -PEOXA analogues. (c) The increased resistance towards unspecific protein contamination by cyclic brushes is ascribed to the additional steric barrier provided by the cyclic topology of the grafts⁵².

Due to their more compact molecular dimensions,¹³⁴⁻¹³⁷ cyclic polymer adsorbates assembling on inorganic and organic substrates tend to generate much denser brushes with

respect to their linear analogues, providing an exceptional steric stabilization to the functionalized surfaces. This “topological effect” translates into films that show an enhanced resistance towards biological contamination due to the exceptional osmotic pressure rising from dense cyclic brushes, as was demonstrated for PEOXA and PMOXA assemblies on TiO_2 ,^{52-53, 55, 132-133} and SiO_x surfaces.¹²⁸

It is important to emphasize that the steric constraints introduced during cyclization of polymer adsorbates provide an additional barrier towards nonspecific interaction with adsorbing biomolecules, leading to a slight but significant improvement in biopassivity for cyclic brushes across a wide range of surface densities, when compared to structurally and chemically identical linear analogues (Figure 13).^{52, 55}

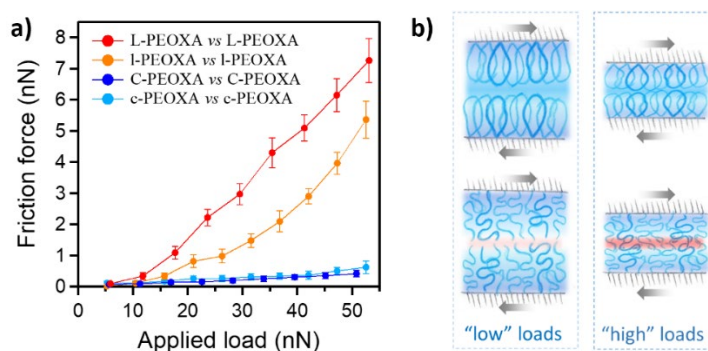


Figure 14. (a) F_L profiles recorded by LFM while shearing PEOXA brushes against topologically identical brush-bearing countersurfaces (b). In (a), the F_L profiles for 10 and 5 kDa linear PEOXA brushes (L and l-PEOXA, respectively) are compared to those recorded while shearing cyclic PEOXA brushes of 10 and 5 kDa (C- and c-PEOXA, respectively)⁵³.

The absence of interfacial chain ends, which is intrinsic in the cyclic topology, additionally hinders brush interpenetration when opposing assemblies are compressed and sheared against each other,^{18-19, 138-139} providing to cyclic brushes a superlubricious character.^{52, 132-133} As a result of the combined effects of suppression of dissipative forces between cyclic-brush countersurfaces, and increased steric stabilization of the underlying substrates, which leads to an improved load-bearing capacity, even amphiphilic cyclic PEOXA brushes in water provide values of μ as low as 10^{-3} , nearly reaching the lubricity typically displayed by highly hydrophilic polyzwitterionic-based linear analogues (Figure 14).²⁶

The unique biopassivity and lubricity of polymer brushes displayed by cyclic macromolecules triggered their application on supports where both these properties are highly required, such as in the case of the articular cartilage. Especially during degenerative syndromes that alter the content of natural biolubricants present in the synovial fluid,¹⁴⁰⁻¹⁴⁴ as

in the case of osteoarthritis (OA), tissue-adhesive graft-copolymers¹⁴⁵ forming a cyclic brush layer on the exposed collagenous surface of cartilage were demonstrated to re-establish its lubrication properties, and protect it from the enzymatic degradation connected to OA progression.¹²⁹

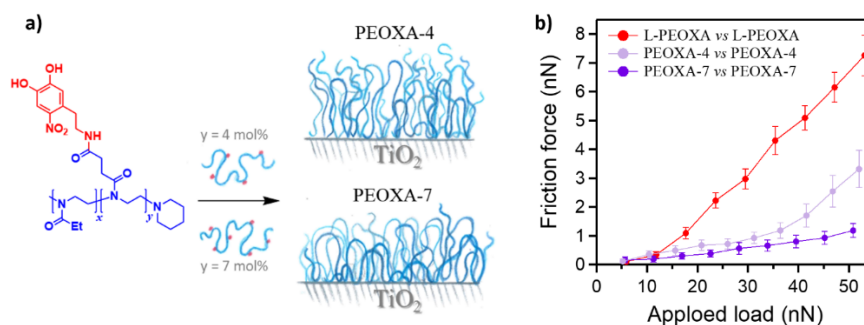


Figure 15. (a) PEOXA brushes featuring a mixture of loops and linear tails are assembled on TiO₂ surfaces from random PEOXA copolymers including 4 and 7 mol% of catechol-bearing co-monomers (indicated as PEOXA-4 and PEOXA-7, respectively). In (b) F_fL profiles for linear PEOXA brushes of 10 kDa (L-PEOXA) are compared to those recorded on PEOXA-4 and PEOXA-7⁵³.

Biopassive and nanotribological characteristics similar to those displayed by cyclic brushes could be observed on “loop”-forming grafts, usually assembled on surfaces from telechelic polymer-based or multifunctional copolymer adsorbates.^{53, 146-155} Interestingly, even a relatively low surface concentration of residual linear chain ends exposed at the interface was identified as a factor strongly influencing the lubricious character of loop brushes, while increasing the loops-to-linear “tails” ratio was accompanied by a progressive improvement of both biopassivity and lubrication, gradually approximating the interfacial properties of cyclic brushes (Figure 15).⁵³

2.6 Conclusions and Perspectives

During the last decade of research, increasing efforts have been spent in designing polymer interfaces on solid surfaces with molecular precision, in order to modulate interfacial physicochemical properties that are fundamental in the fabrication, modification and performance of devices, ranging from sensors to tissue engineering supports. The reduction of unspecific biological contamination and lubrication have represented two of the most required properties, especially when synthetic materials are expected to integrate within physiological media without altering their interfacial composition, and if a minimization of the mechanical stress towards the surrounding environment is sought when shear is applied.

In order to meet these needs, the composition of polymer-brush-based coatings has been progressively optimized in order to reach full biopassivity within highly contaminating media, such as blood and serum, reduce polymer degradation even after long incubation times, and simultaneously increment lubricity. While attaining increasingly bioinert and lubricious surfaces has encompassed the application of highly hydrated polymer brushes, for instance featuring polyzwitterions,¹⁵⁶ the modulation of polymer-brush architecture has concomitantly emerged as an additional method to broaden the tuning potential for the above-mentioned properties.

In particular, while keeping the composition of a polymer assembly constant, the translation of topology effects under the confinement of a grafting surface has enabled us to significantly alter interfacial physicochemical properties that determine the performance of polymer brushes within physiological environments.

We have demonstrated that the application of branched or looped polymer architectures substantially altered steric stabilization and viscoelasticity of brush assemblies, providing a more efficient barrier towards unspecific contamination by biomolecules, and suggesting new approaches for suppressing mechanical energy dissipation under shear, and reduce friction.

The introduction of covalent or physical crosslinks between grafts, yielding brush gels or hydrogels, enabled the nanomechanical and nanotribological properties of the obtained films to be precisely tuned, and provided a tool to modulate their swelling properties.

Alternatively, the application of block copolymer and mixed brushes enlarged the tuning potential for interfacial composition, and allowed one to generate assemblies that can vary their nanomorphology in response to selective solvent environments, often improving the structural stability of the entire coating within aggressive media.

Despite the wealth of possibilities in the molecular structuring of polymer brushes, even the most sophisticated polymer architectures have been always characterized by a constant or “quenched” structure, which enabled just limited conformational transitions in response to *e.g.* a variation of temperature or solvent quality. Hence, it has become progressively evident that one of the next challenges that will involve polymer and materials chemists will deal with the realization of soft-matter interfaces characterized by a “dynamic” architecture, which can remodel itself via topological transformations of its macromolecular constituents,¹⁵⁷⁻¹⁵⁸ in this way modulating surface interaction with the surrounding medium.

Simultaneously, a growing need for controlled SI-CRP processes, compatible with ambient conditions, and scalable to large and morphologically different substrates has emerged. Following closely the development of oxygen-tolerant reversible deactivation radical

polymerization (RDRP) processes in solution,¹⁵⁹ several methods enabling the living growth of polymer brushes in the presence of oxygen, and which are applicable on extremely large substrates while using just microliter-volumes of reaction mixtures were proposed.¹⁶⁰⁻¹⁶⁶

Collectively, all these ongoing and future challenges involve experts from different fields of chemistry, physics and materials science, who are concentrating not only on defining new chemistries for the fabrication of polymeric biointerfaces, but also developing coating processes, and establishing robust analytical methods for dissecting interfacial properties.

References

1. Zdyrko, B.; Luzinov, I., Polymer Brushes by the "Grafting to" Method. *Macromol. Rapid Commun.* **2011**, *32* (12), 859-869.
2. Zoppe, J. O.; Ataman, N. C.; Mocny, P.; Wang, J.; Moraes, J.; Klok, H. A., Surface-Initiated Controlled Radical Polymerization: State-of-the-Art, Opportunities, and Challenges in Surface and Interface Engineering with Polymer Brushes. *Chem. Rev.* **2017**, *117* (5), 4667-4667.
3. Krishnamoorthy, M.; Hakobyan, S.; Ramstedt, M.; Gautrot, J. E., Surface-Initiated Polymer Brushes in the Biomedical Field: Applications in Membrane Science, Biosensing, Cell Culture, Regenerative Medicine and Antibacterial Coatings. *Chem. Rev.* **2014**, *114* (21), 10976-11026.
4. Banerjee, I.; Pangule, R. C.; Kane, R. S., Antifouling Coatings: Recent Developments in the Design of Surfaces That Prevent Fouling by Proteins, Bacteria, and Marine Organisms. *Adv. Mater.* **2011**, *23* (6), 690-718.
5. Raynor, J. E.; Capadona, J. R.; Collard, D. M.; Petrie, T. A.; García, A. s. J., Polymer brushes and self-assembled monolayers: Versatile platforms to control cell adhesion to biomaterials. *Biointerphases* **2009**, *4*, FA3.
6. Moroni, L.; Gunnewiek, M. K.; Benetti, E. M., Polymer brush coatings regulating cell behavior: Passive interfaces turn into active. *Acta Biomater.* **2014**, *10* (6), 2367-2378.
7. Hadjesfandiari, N.; Yu, K.; Mei, Y.; Kizhakkedathu, J. N., Polymer brush-based approaches for the development of infection-resistant surfaces. *J. Mater. Chem. B* **2014**, *2* (31), 4968-4978.
8. Yu, K.; Lo, J. C. Y.; Yan, M.; Yang, X. Q.; Brooks, D. E.; Hancock, R. E. W.; Lange, D.; Kizhakkedathu, J. N., Anti-adhesive antimicrobial peptide coating prevents catheter associated infection in a mouse urinary infection model. *Biomaterials* **2017**, *116*, 69-81.

9. Bozukova, D.; Pagnouille, C.; De Pauw-Gillet, M. C.; Desbief, S.; Lazzaroni, R.; Ruth, N.; Jerome, R.; Jerome, C., Improved performances of intraocular lenses by poly(ethylene glycol) chemical coatings. *Biomacromolecules* **2007**, *8* (8), 2379-2387.
10. Gensheimer, W. G.; Kleinman, D. M.; Gonzalez, M. O.; Sobti, D.; Cooper, E. R.; Smits, G.; Loxley, A.; Mitchnick, M.; Aquavella, J. V., Novel Formulation of Glycerin 1% Artificial Tears Extends Tear Film Break-Up Time Compared with Systane Lubricant Eye Drops. *J. Ocul. Pharmacol. Th.* **2012**, *28* (5), 473-478.
11. Yoshikawa, C.; Goto, A.; Tsujii, Y.; Fukuda, T.; Kimura, T.; Yamamoto, K.; Kishida, A., Protein repellency of well-defined, concentrated poly(2-hydroxyethyl methacrylate) brushes by the size-exclusion effect. *Macromolecules* **2006**, *39* (6), 2284-2290.
12. Hamilton-Brown, P.; Gengebach, T.; Griesser, H. J.; Meagher, L., End Terminal, Poly(ethylene oxide) Graft Layers: Surface Forces and Protein Adsorption. *Langmuir* **2009**, *25* (16), 9149-9156.
13. Leckband, D.; Sheth, S.; Halperin, A., Grafted poly(ethylene oxide) brushes as nonfouling surface coatings. *J. Biomat. Sci. Polym. Ed.* **1999**, *10* (10), 1125-1147.
14. Halperin, A., Polymer brushes that resist adsorption of model proteins: Design parameters. *Langmuir* **1999**, *15* (7), 2525-2533.
15. Grest, G. S., Normal and shear forces between polymer brushes. *Adv. Polym. Sci.* **1999**, *138*, 149-183.
16. Grest, G. S., Interfacial sliding of polymer brushes: A molecular dynamics simulation. *Phys. Rev. Lett.* **1996**, *76* (26), 4979-4982.
17. Klein, J., Shear, friction, and lubrication forces between polymer-bearing surfaces. *Annu. Rev. Mater. Sci.* **1996**, *26*, 581-612.
18. Klein, J.; Kumacheva, E.; Mahalu, D.; Perahia, D.; Fetters, L. J., Reduction of Frictional Forces between Solid-Surfaces Bearing Polymer Brushes. *Nature* **1994**, *370* (6491), 634-636.
19. Klein, J.; Kamiyama, Y.; Yoshizawa, H.; Israelachvili, J. N.; Fredrickson, G. H.; Pincus, P.; Fetters, L. J., Lubrication Forces between Surfaces Bearing Polymer Brushes. *Macromolecules* **1993**, *26* (21), 5552-5560.
20. Benetti, E. M.; Spencer, N. D., Using Polymers to Impart Lubricity and Biopassivity to Surfaces: Are These Properties Linked? *Helv. Chim. Acta* **2019**, *102* (5).
21. Lee, S.; Spencer, N. D., Aqueous lubrication of polymers: Influence of surface modification. *Tribol. Int.* **2005**, *38* (11-12), 922-930.

22. Yan, X.; Perry, S. S.; Spencer, N. D.; Pasche, S.; De Paul, S. M.; Textor, M.; Lim, M. S., Reduction of Friction at Oxide Interfaces upon Polymer Adsorption from Aqueous Solutions. *Langmuir* **2004**, *20* (2), 423-428.
23. Lee, S.; Muller, M.; Ratoi-Salagean, M.; Voros, J.; Pasche, S.; De Paul, S. M.; Spikes, H. A.; Textor, M.; Spencer, N. D., Boundary lubrication of oxide surfaces by Poly(L-lysine)-g-poly(ethylene glycol) (PLL-g-PEG) in aqueous media. *Tribol. Lett.* **2003**, *15* (3), 231-239.
24. Ishihara, K., Highly lubricated polymer interfaces for advanced artificial hip joints through biomimetic design. *Polym. J.* **2015**, *47* (9), 585-597.
25. Kitano, K.; Inoue, Y.; Matsuno, R.; Takai, M.; Ishihara, K., Nanoscale evaluation of lubricity on well-defined polymer brush surfaces using QCM-D and AFM. *Colloid Surf. B* **2009**, *74* (1), 350-357.
26. Chen, M.; Briscoe, W. H.; Armes, S. P.; Klein, J., Lubrication at Physiological Pressures by Polyzwitterionic Brushes. *Science* **2009**, *323* (5922), 1698-1701.
27. Zhang, Z.; Chao, T.; Chen, S. F.; Jiang, S. Y., Superlow fouling sulfobetaine and carboxybetaine polymers on glass slides. *Langmuir* **2006**, *22* (24), 10072-10077.
28. Liu, Q. S.; Singh, A.; Lalani, R.; Liu, L. Y., Ultralow Fouling Polyacrylamide on Gold Surfaces via Surface-Initiated Atom Transfer Radical Polymerization. *Biomacromolecules* **2012**, *13* (4), 1086-1092.
29. Cringus-Fundeanu, I.; Luijten, J.; van der Mei, H. C.; Busscher, H. J.; Schouten, A. J., Synthesis and Characterization of Surface-Grafted Polyacrylamide Brushes and Their Inhibition of Microbial Adhesion. *Langmuir* **2007**, *23* (9), 5120-5126.
30. Li, A.; Benetti, E. M.; Tranchida, D.; Clasohm, J. N.; Schonherr, H.; Spencer, N. D., Surface-Grafted, Covalently Cross-Linked Hydrogel Brushes with Tunable Interfacial and Bulk Properties. *Macromolecules* **2011**, *44* (13), 5344-5351.
31. Rodriguez-Emmenegger, C.; Brynda, E.; Riedel, T.; Houska, M.; Subr, V.; Alles, A. B.; Hasan, E.; Gautrot, J. E.; Huck, W. T. S., Polymer Brushes Showing Non-Fouling in Blood Plasma Challenge the Currently Accepted Design of Protein Resistant Surfaces. *Macromol. Rapid Commun.* **2011**, *32* (13), 952-957.
32. Zhao, C.; Zheng, J., Synthesis and Characterization of Poly(N-hydroxyethylacrylamide) for Long-Term Antifouling Ability. *Biomacromolecules* **2011**, *12* (11), 4071-4079.
33. Morgese, G.; Benetti, E. M., Polyoxazoline biointerfaces by surface grafting. *Eur. Polym. J.* **2017**, *88*, 470-485.

34. Tauhardt, L.; Kempe, K.; Gottschaldt, M.; Schubert, U. S., Poly(2-oxazoline) functionalized surfaces: from modification to application. *Chem. Soc. Rev.* **2013**, *42* (20), 7998-8011.
35. Morgese, G.; Verbraeken, B.; Ramakrishna, S. N.; Gombert, Y.; Cavalli, E.; Rosenboom, J. G.; Zenobi-Wong, M.; Spencer, N. D.; Hoogenboom, R.; Benetti, E. M., Chemical Design of Non-Ionic Polymer Brushes as Biointerfaces: Poly(2-oxazine)s Outperform Both Poly(2-oxazoline)s and PEG. *Angew. Chem. Int. Edit.* **2018**, *57* (36), 11667-11672.
36. de Beer, S.; Kutnyanszky, E.; Schon, P. M.; Vancso, G. J.; Muser, M. H., Solvent-induced immiscibility of polymer brushes eliminates dissipation channels. *Nat. Commun.* **2014**, *5*, 3781.
37. de Beer, S., Switchable Friction Using Contacts of Stimulus-Responsive and Nonresponding Swollen Polymer Brushes. *Langmuir* **2014**, *30* (27), 8085-8090.
38. Kreer, T.; Muser, M. H.; Binder, K.; Klein, J., Frictional drag mechanisms between polymer-bearing surfaces. *Langmuir* **2001**, *17* (25), 7804-7813.
39. Neelov, I. M.; Borisov, O. V.; Binder, K., Shear deformation of two interpenetrating polymer brushes: Stochastic dynamics simulation. *J. Chem. Phys.* **1998**, *108* (16), 6973-6988.
40. Zhulina, E. B.; Leermakers, F. A. M.; Borisov, O. V., Brushes of Cycled Macromolecules: Structure and Lubricating Properties. *Macromolecules* **2016**, *49* (22), 8758-8767.
41. Halperin, A.; Kroger, M., Theoretical considerations on mechanisms of harvesting cells cultured on thermoresponsive polymer brushes. *Biomaterials* **2012**, *33* (20), 4975-4987.
42. Halperin, A.; Kröger, M., Collapse of Thermoresponsive Brushes and the Tuning of Protein Adsorption. *Macromolecules* **2011**, *44*, 6986-7005.
43. de Gennes, P. G., *Scaling Concepts in Polymer Physics*. Ithaca, NY, 1979.
44. de Gennes, P. G. Polymers at an interface: a simplified view. *Adv. Colloid Interface Sci.* 1987, *27* (3-4), 189-209.
45. Takahashi, H.; Nakayama, M.; Yamato, M.; Okano, T., Controlled Chain Length and Graft Density of Thermoresponsive Polymer Brushes for Optimizing Cell Sheet Harvest. *Biomacromolecules* **2010**, *11* (8), 1991-1999.
46. Kobayashi, M.; Terayama, Y.; Hosaka, N.; Kaido, M.; Suzuki, A.; Yamada, N.; Torikai, N.; Ishihara, K.; Takahara, A., Friction behavior of high-density poly(2-methacryloyloxyethyl phosphorylcholine) brush in aqueous media. *Soft Matter* **2007**, *3* (6), 740-746.

47. Zhang, Z. Y.; Moxey, M.; Alswieleh, A.; Morse, A. J.; Lewis, A. L.; Geoghegan, M.; Leggett, G. J., Effect of Salt on Phosphorylcholine-based Zwitterionic Polymer Brushes. *Langmuir* **2016**, *32* (20), 5048-5057.
48. Zhang, Z. Y.; Morse, A. J.; Armes, S. P.; Lewis, A. L.; Geoghegan, M.; Leggett, G. J., Nanoscale Contact Mechanics of Biocompatible Polyzwitterionic Brushes. *Langmuir* **2013**, *29* (34), 10684-10692.
49. Zhang, Z. Y.; Morse, A. J.; Armes, S. P.; Lewis, A. L.; Geoghegan, M.; Leggett, G. J., Effect of Brush Thickness and Solvent Composition on the Friction Force Response of Poly(2-(methacryloyloxy)ethylphosphorylcholine) Brushes. *Langmuir* **2011**, *27* (6), 2514-2521.
50. Gunnewiek, M. K.; Ramakrishna, S. N.; di Luca, A.; Vancso, G. J.; Moroni, L.; Benetti, E. M., Stem-Cell Clinging by a Thread: AFM Measure of Polymer-Brush Lateral Deformation. *Adv. Mater. Interfaces* **2016**, *3* (3), 1500456.
51. Ramakrishna, S. N.; Cirelli, M.; Divandari, M.; Benetti, E. M., Effects of Lateral Deformation by Thermoresponsive Polymer Brushes on the Measured Friction Forces. *Langmuir* **2017**, *33* (17), 4164-4171.
52. Divandari, M.; Trachsel, L.; Yan, W. Q.; Rosenboom, J. G.; Spencer, N. D.; Zenobi-Wong, M.; Morgese, G.; Ramakrishna, S. N.; Benetti, E. M., Surface Density Variation within Cyclic Polymer Brushes Reveals Topology Effects on Their Nanotribological and Biopassive Properties. *ACS Macro Lett.* **2018**, *7* (12), 1455-1460.
53. Divandari, M.; Morgese, G.; Trachsel, L.; Romio, M.; Dehghani, E. S.; Rosenboom, J. G.; Paradisi, C.; Zenobi-Wong, M.; Ramakrishna, S. N.; Benetti, E. M., Topology Effects on the Structural and Physicochemical Properties of Polymer Brushes. *Macromolecules* **2017**, *50* (19), 7760-7769.
54. Nomura, A.; Okayasu, K.; Ohno, K.; Fukuda, T.; Tsujii, Y., Lubrication Mechanism of Concentrated Polymer Brushes in Solvents: Effect of Solvent Quality and Thereby Swelling State. *Macromolecules* **2011**, *44* (12), 5013-5019.
55. Divandari, M.; Morgese, G.; Ramakrishna, S. N.; Benetti, E. M., Surface-grafted assemblies of cyclic polymers: Shifting between high friction and extreme lubricity. *Eur. Polym. J.* **2019**, *110*, 301-306.
56. Perry, S. S.; Yan, X. P.; Limpoco, F. T.; Lee, S.; Muller, M.; Spencer, N. D., Tribological Properties of Poly(L-lysine)-graft-poly(ethylene glycol) Films: Influence of Polymer Architecture and Adsorbed Conformation. *ACS Appl. Mater. Interfaces* **2009**, *1* (6), 1224-1230.

57. Motornov, M.; Sheparovych, R.; Katz, E.; Minko, S., Chemical gating with nanostructured responsive polymer brushes: Mixed brush versus homopolymer brush. *ACS Nano* **2008**, *2* (1), 41-52.
58. Usov, D.; Gruzdev, V.; Nitschke, M.; Stamm, M.; Hoy, O.; Luzinov, I.; Tokarev, I.; Minko, S., Three-dimensional analysis of switching mechanism of mixed polymer brushes. *Macromolecules* **2007**, *40* (24), 8774-8783.
59. Santer, S.; Kopyshov, A.; Yang, H. K.; Ruhe, J., Local composition of nanophase-separated mixed polymer brushes. *Macromolecules* **2006**, *39* (8), 3056-3064.
60. Ionov, L.; Houbenov, N.; Sidorenko, A.; Stamm, M.; Luzinov, I.; Minko, S., Inverse and reversible switching gradient surfaces from mixed polyelectrolyte brushes. *Langmuir* **2004**, *20* (23), 9916-9919.
61. Houbenov, N.; Minko, S.; Stamm, M., Mixed polyelectrolyte brush from oppositely charged polymers for switching of surface charge and composition in aqueous environment. *Macromolecules* **2003**, *36* (16), 5897-5901.
62. Minko, S.; Muller, M.; Usov, D.; Scholl, A.; Froeck, C.; Stamm, M., Lateral versus perpendicular segregation in mixed polymer brushes. *Phys. Rev. Lett.* **2002**, *88* (3).
63. Li, D. J.; Sheng, X.; Zhao, B., Environmentally responsive "Hairy" nanoparticles: Mixed homopolymer brushes on silica nanoparticles synthesized by living radical polymerization techniques. *J. Am. Chem. Soc.* **2005**, *127* (17), 6248-6256.
64. Zhao, B.; He, T., Synthesis of well-defined mixed poly(methyl methacrylate)/polystyrene brushes from an asymmetric difunctional initiator-terminated self-assembled monolayer. *Macromolecules* **2003**, *36* (23), 8599-8602.
65. Bao, C. H.; Tang, S. D.; Wright, R. A. E.; Tang, P.; Qiu, F.; Zhu, L.; Zhao, B., Effect of Molecular Weight on Lateral Microphase Separation of Mixed Homopolymer Brushes Grafted on Silica Particles. *Macromolecules* **2014**, *47* (19), 6824-6835.
66. Calabrese, D. R.; Ditter, D.; Liedel, C.; Blumfield, A.; Zentel, R.; Ober, C. K., Design, Synthesis, and Use of Y-Shaped ATRP/NMP Surface Tethered Initiator. *ACS Macro Lett.* **2015**, *4* (6), 606-610.
67. Julthongpiput, D.; Lin, Y. H.; Teng, J.; Zubarev, E. R.; Tsukruk, V. V., Y-shaped polymer brushes: Nanoscale switchable surfaces. *Langmuir* **2003**, *19* (19), 7832-7836.
68. Sui, X. F.; Zapotoczny, S.; Benetti, E. M.; Memesa, M.; Hempenius, M. A.; Vancso, G. J., Grafting mixed responsive brushes of poly(N-isopropylacrylamide) and poly(methacrylic acid) from gold by selective initiation. *Polym. Chem.* **2011**, *2* (4), 879-884.

69. Zhang, S. X.; Liu, W. Y.; Dong, Y. S.; Wei, T.; Wu, Z. Q.; Chen, H., Design, Synthesis, and Application of a Difunctional Y-Shaped Surface-Tethered Photoinitiator. *Langmuir* **2019**, *35* (9), 3470-3478.
70. Ionov, L.; Minko, S., Mixed Polymer Brushes with Locking Switching. *ACS Appl. Mater. Interfaces* **2012**, *4* (1), 483-489.
71. Delcroix, M. F.; Laurent, S.; Huet, G. L.; Dupont-Gillain, C. C., Protein adsorption can be reversibly switched on and off on mixed PEO/PAA brushes. *Acta Biomater.* **2015**, *11*, 68-79.
72. Bratek-Skicki, A.; Eloy, P.; Morga, M.; Dupont-Gillain, C., Reversible Protein Adsorption on Mixed PEO/PAA Polymer Brushes: Role of Ionic Strength and PEO Content. *Langmuir* **2018**, *34* (9), 3037-3048.
73. Mumtaz, F.; Chen, C. S.; Zhu, H. K.; Pan, C.; Wang, Y. M., Controlled protein adsorption on PMOXA/PAA based coatings by thermally induced immobilization. *Appl. Surf. Sci.* **2018**, *439*, 148-159.
74. Pan, C.; Liu, X. R.; Gong, K.; Mumtaz, F.; Wang, Y. M., Dopamine assisted PMOXA/PAA brushes for their switchable protein adsorption/desorption. *J. Mater. Chem. B* **2018**, *6* (4), 556-567.
75. Bratek-Skicki, A.; Cristaudo, V.; Savocco, J.; Nootens, S.; Morsomme, P.; Delcorte, A.; Dupont-Gillain, C., Mixed Polymer Brushes for the Selective Capture and Release of Proteins. *Biomacromolecules* **2019**, *20* (2), 778-789.
76. Psarra, E.; Konig, U.; Ueda, Y.; Bellmann, C.; Janke, A.; Bittrich, E.; Eichhorn, K. J.; Uhlmann, P., Nanostructured Biointerfaces: Nanoarchitectonics of Thermoresponsive Polymer Brushes Impact Protein Adsorption and Cell Adhesion. *ACS Appl. Mater. Interfaces* **2015**, *7* (23), 12516-12529.
77. Nagase, K.; Hatakeyama, Y.; Shimizu, T.; Matsuura, K.; Yamato, M.; Takeda, N.; Okano, T., Thermoresponsive Cationic Copolymer Brushes for Mesenchymal Stem Cell Separation. *Biomacromolecules* **2015**, *16* (2), 532-540.
78. Nagase, K.; Hatakeyama, Y.; Shimizu, T.; Matsuura, K.; Yamato, M.; Takeda, N.; Okano, T., Hydrophobized Thermoresponsive Copolymer Brushes for Cell Separation by Multistep Temperature Change. *Biomacromolecules* **2013**, *14* (10), 3423-3433.
79. Arisaka, Y.; Kobayashi, J.; Yamato, M.; Akiyama, Y.; Okano, T., Switching of cell growth/detachment on heparin-functionalized thermoresponsive surface for rapid cell sheet fabrication and manipulation. *Biomaterials* **2013**, *34* (17), 4214-4222.

80. Nagase, K.; Mukae, N.; Kikuchi, A.; Okano, T., Thermally Modulated Retention of Lymphocytes on Polymer-Brush-Grafted Glass Beads. *Macromol. Biosci.* **2012**, *12* (3), 333-340.
81. Nagase, K.; Kimura, A.; Shimizu, T.; Matsuura, K.; Yamato, M.; Takeda, N.; Okano, T., Dynamically cell separating thermo-functional biointerfaces with densely packed polymer brushes. *J. Mater. Chem.* **2012**, *22* (37), 19514-19522.
82. Takahashi, H.; Nakayama, M.; Itoga, K.; Yamato, M.; Okano, T., Micropatterned Thermoresponsive Polymer Brush Surfaces for Fabricating Cell Sheets with Well-Controlled Orientational Structures. *Biomacromolecules* **2011**, *12* (5), 1414-1418.
83. Nagase, K.; Watanabe, M.; Kikuchi, A.; Yamato, M.; Okano, T., Thermo-Responsive Polymer Brushes as Intelligent Biointerfaces: Preparation via ATRP and Characterization. *Macromol. Biosci.* **2011**, *11* (3), 400-409.
84. Vyas, M. K.; Schneider, K.; Nandan, B.; Stamm, M., Switching of friction by binary polymer brushes. *Soft Matter* **2008**, *4* (5), 1024-1032.
85. Morgese, G.; Gombert, Y.; Ramakrishna, S. N.; Benetti, E. M., Mixing Poly(ethylene glycol) and Poly(2-alkyl-2-oxazoline)s Enhances Hydration and Viscoelasticity of Polymer Brushes and Determines Their Nanotribological and Antifouling Properties. *ACS Appl. Mater. Interfaces* **2018**, *10* (48), 41839-41848.
86. Nordgren, N.; Rutland, M. W., Tunable Nanolubrication between Dual-Responsive Polyionic Grafts. *Nano Lett.* **2009**, *9* (8), 2984-2990.
87. Wang, X. H.; Yan, S. J.; Song, L. J.; Shi, H. C.; Yang, H. W.; Luan, S. F.; Huang, Y. B.; Yin, J. H.; Khan, A. F.; Zhao, J., Temperature-Responsive Hierarchical Polymer Brushes Switching from Bactericidal to Cell Repellency. *ACS Appl. Mater. Interfaces* **2017**, *9* (46), 40930-40939.
88. Ye, G.; Lee, J. H.; Perreault, F.; Elimelech, M., Controlled Architecture of Dual-Functional Block Copolymer Brushes on Thin-Film Composite Membranes for Integrated "Defending" and "Attacking" Strategies against Biofouling. *ACS Appl. Mater. Interfaces* **2015**, *7* (41), 23069-23079.
89. de los Santos Pereira, A.; Kostina, N. Y.; Bruns, M.; Rodriguez-Emmenegger, C.; Barner-Kowollik, C., Phototriggered Functionalization of Hierarchically Structured Polymer Brushes. *Langmuir* **2015**, *31* (21), 5899-5907.
90. de los Santos Pereira, A.; Riedel, T.; Brynda, E.; Rodriguez-Emmenegger, C., Hierarchical antifouling brushes for biosensing applications. *Sens. Actuator B-Chem.* **2014**, *202*, 1313-1321.

91. Fortin, N.; Klok, H. A., Glucose Monitoring Using a Polymer Brush Modified Polypropylene Hollow Fiber-based Hydraulic Flow Sensor. *ACS Appl. Mater. Interfaces* **2015**, *7* (8), 4631-4640.
92. Badoux, M.; Billing, M.; Klok, H. A., Polymer brush interfaces for protein biosensing prepared by surface-initiated controlled radical polymerization. *Polym. Chem.* **2019**.
93. Navarro, M.; Benetti, E. M.; Zapotoczny, S.; Planell, J. A.; Vancso, G. J., Buried, covalently attached RGD peptide motifs in poly(methacrylic acid) brush layers: The effect of brush structure on cell adhesion. *Langmuir* **2008**, *24* (19), 10996-11002.
94. Desseaux, S.; Klok, H. A., Fibroblast adhesion on ECM-derived peptide modified poly(2-hydroxyethyl methacrylate) brushes: Ligand co-presentation and 3D-localization. *Biomaterials* **2015**, *44*, 24-35.
95. Desseaux, S.; Klok, H.-A., Temperature-controlled masking/unmasking of cell-adhesive cues with poly(ethylene glycol) methacrylate based brushes. *Biomacromolecules* **2014**, *15*, 3859-65.
96. Paripovic, D.; Hall-Bozic, H.; Klok, H. A., Osteoconductive surfaces generated from peptide functionalized poly(2-hydroxyethyl methacrylate-co-2-(methacryloyloxy)ethyl phosphate) brushes. *J. Mater. Chem.* **2012**, *22* (37), 19570-19578.
97. Dou, X. Q.; Li, P.; Jiang, S. Y.; Bayat, H.; Schonherr, H., Bioinspired Hierarchically Structured Surfaces for Efficient Capture and Release of Circulating Tumor Cells. *ACS Appl. Mater. Interfaces* **2017**, *9* (10), 8508-8518.
98. Desseaux, S.; Klok, H. A., Temperature-Controlled Masking/Unmasking of Cell-Adhesive Cues with Poly(ethylene glycol) Methacrylate Based Brushes. *Biomacromolecules* **2014**, *15* (10), 3859-3865.
99. Lilge, I.; Schonherr, H., Block Copolymer Brushes for Completely Decoupled Control of Determinants of Cell-Surface Interactions. *Angew. Chem. Int. Edit.* **2016**, *55* (42), 13114-13117.
100. Quintana, R.; Gosa, M.; Janczewski, D.; Kutnyanszky, E.; Vancso, G. J., Enhanced Stability of Low Fouling Zwitterionic Polymer Brushes in Seawater with Diblock Architecture. *Langmuir* **2013**, *29* (34), 10859-10867.
101. Yu, Y. L.; Vancso, G. J.; de Beer, S., Substantially enhanced stability against degrafting of zwitterionic PMPC brushes by utilizing PGMA-linked initiators. *Eur. Polym. J.* **2017**, *89*, 221-229.

102. Paripovic, D.; Klok, H.-A., Improving the Stability in Aqueous Media of Polymer Brushes Grafted from Silicon Oxide Substrates by Surface-Initiated Atom Transfer Radical Polymerization. *Macromol. Chem. Phys.* **2011**, *212* (9), 950-958.

103. Divandari, M.; Dehghani, E. S.; Spencer, N. D.; Ramakrishna, S. N.; Benetti, E. M., Understanding the effect of hydrophobic protecting blocks on the stability and biopassivity of polymer brushes in aqueous environments: A Tiramisù for cell-culture applications. *Polymer* **2016**, *98*, 470-480.

104. Wyszogrodzka, M.; Haag, R., Synthesis and Characterization of Glycerol Dendrons, Self-Assembled Monolayers on Gold: A Detailed Study of Their Protein Resistance. *Biomacromolecules* **2009**, *10* (5), 1043-1054.

105. Wyszogrodzka, M.; Haag, R., Study of Single Protein Adsorption onto Monoamino Oligoglycerol Derivatives: A Structure-Activity Relationship. *Langmuir* **2009**, *25* (10), 5703-5712.

106. Rud, O. V.; Polotsky, A. A.; Gillich, T.; Borisov, O. V.; Leermakers, F. A. M.; Textor, M.; Birshtein, T. M., Dendritic Spherical Polymer Brushes: Theory and Self-Consistent Field Modeling. *Macromolecules* **2013**, *46* (11), 4651-4662.

107. Gillich, T.; Benetti, E. M.; Rakhmatullina, E.; Konradi, R.; Li, W.; Zhang, A.; Schlüter, A. D.; Textor, M., Self-Assembly of Focal Point Oligo-catechol Ethylene Glycol Dendrons on Titanium Oxide Surfaces: Adsorption Kinetics, Surface Characterization, and Nonfouling Properties. *J. Am. Chem. Soc.* **2011**, *133* (28), 10940-10950.

108. Gillich, T.; Acikgöz, C.; Isa, L.; Schlüter, A. D.; Spencer, N. D.; Textor, M., PEG-Stabilized Core-Shell Nanoparticles: Impact of Linear versus Dendritic Polymer Shell Architecture on Colloidal Properties and the Reversibility of Temperature-Induced Aggregation. *ACS Nano* **2012**, *7* (1), 316-329.

109. Lukowiak, M. C.; Wettmarshausen, S.; Hidde, G.; Landsberger, P.; Boenke, V.; Rodenacker, K.; Braun, U.; Friedrich, J. F.; Gorbushina, A. A.; Haag, R., Polyglycerol coated polypropylene surfaces for protein and bacteria resistance. *Polym. Chem.* **2015**, *6* (8), 1350-1359.

110. Wei, Q.; Krysiak, S.; Achazi, K.; Becherer, T.; Noeske, P. L. M.; Paulus, F.; Liebe, H.; Grunwald, I.; Dervede, J.; Hartwig, A.; Hugel, T.; Haag, R., Multivalent anchored and crosslinked hyperbranched polyglycerol monolayers as antifouling coating for titanium oxide surfaces. *Colloid Surf. B* **2014**, *122*, 684-692.

111. Weinhart, M.; Becherer, T.; Schnurbusch, N.; Schwibbert, K.; Kunte, H. J.; Haag, R., Linear and Hyperbranched Polyglycerol Derivatives as Excellent Bioinert Glass Coating Materials. *Adv. Eng. Mater.* **2011**, *13* (12), B501-B510.
112. Calderon, M.; Quadir, M. A.; Sharma, S. K.; Haag, R., Dendritic Polyglycerols for Biomedical Applications. *Adv. Mater.* **2010**, *22* (2), 190-218.
113. Gunkel, G.; Weinhart, M.; Becherer, T.; Haag, R.; Huck, W. T. S., Effect of Polymer Brush Architecture on Antibiofouling Properties. *Biomacromolecules* **2011**, *12* (11), 4169-4172.
114. Costantini, F.; Benetti, E. M.; Tiggelaar, R. M.; Gardeniers, H. J. G. E.; Reinhoudt, D. N.; Huskens, J.; Vancso, G. J.; Verboom, W., A Brush-Gel/Metal-Nanoparticle Hybrid Film as an Efficient Supported Catalyst in Glass Microreactors. *Chem. Eur. J* **2010**, *16* (41), 12406-12411.
115. Benetti, E. M.; Sui, X. F.; Zapotoczny, S.; Vancso, G. J., Surface-Grafted Gel-Brush/Metal Nanoparticle Hybrids. *Adv. Funct. Mater.* **2010**, *20* (6), 939-944.
116. Ramakrishna, S. N.; Cirelli, M.; Kooij, E. S.; Klein Gunnewiek, M.; Benetti, E. M., Amplified Responsiveness of Multilayered Polymer Grafts: Synergy between Brushes and Hydrogels. *Macromolecules* **2015**, *48*, 7106-7116.
117. Kang, C. J.; Ramakrishna, S. N.; Nelson, A.; Cremmel, C. V. M.; Stein, H. V.; Spencer, N. D.; Isa, L.; Benetti, E. M., Ultrathin, freestanding, stimuli-responsive, porous membranes from polymer hydrogel-brushes. *Nanoscale* **2015**, *7* (30), 13017-13025.
118. Benetti, E. M.; Chung, H. J.; Vancso, G. J., pH Responsive Polymeric Brush Nanostructures: Preparation and Characterization by Scanning Probe Oxidation and Surface Initiated Polymerization. *Macromol. Rapid Commun.* **2009**, *30* (6), 411-417.
119. Dehghani, E. S.; Spencer, N. D.; Ramakrishna, S. N.; Benetti, E. M., Crosslinking Polymer Brushes with Ethylene Glycol-Containing Segments: Influence on Physicochemical and Antifouling Properties. *Langmuir* **2016**, *32* (40), 10317-10327.
120. Dehghani, E. S.; Ramakrishna, S. N.; Spencer, N. D.; Benetti, E. M., Controlled Crosslinking Is a Tool To Precisely Modulate the Nanomechanical and Nanotribological Properties of Polymer Brushes. *Macromolecules* **2017**, *50* (7), 2932-2941.
121. Iuster, N.; Tairy, O.; Driver, M. J.; Armes, S. P.; Klein, J., Cross-Linking Highly Lubricious Phosphocholinated Polymer Brushes: Effect on Surface Interactions and Frictional Behavior. *Macromolecules* **2017**, *50* (18), 7361-7371.

122. Li, A.; Ramakrishna Shivaprakash, N.; Nalam Prathima, C.; Benetti Edmondo, M.; Spencer Nicholas, D., Stratified Polymer Grafts: Synthesis and Characterization of Layered 'Brush' and 'Gel' Structures. *Adv. Mater. Interfaces* **2014**, *1* (1), 1300007.
123. Benetti, E. M.; Zapotoczny, S.; Vancso, J., Tunable thermoresponsive polymeric platforms on gold by "photoiniferter"-based surface grafting. *Adv. Mater.* **2007**, *19* (2), 268-271.
124. Benetti, E. M.; Reimhult, E.; de Bruin, J.; Zapotoczny, S.; Textor, M.; Vancso, G. J., Poly(methacrylic acid) Grafts Grown from Designer Surfaces: The Effect of Initiator Coverage on Polymerization Kinetics, Morphology, and Properties. *Macromolecules* **2009**, *42* (5), 1640-1647.
125. Loveless, D. M.; Abu-Lail, N. I.; Kaholek, M.; Zauscher, S.; Craig, S. L., Reversibly cross-linked surface-grafted polymer brushes. *Angew. Chem. Int. Edit.* **2006**, *45* (46), 7812-7814.
126. Dehghani, E. S.; Naik, V. V.; Mandal, J.; Spencer, N. D.; Benetti, E. M., Physical Networks of Metal-Ion-Containing Polymer Brushes Show Fully Tunable Swelling, Nanomechanical and Nanotribological Properties. *Macromolecules* **2017**, *50* (6), 2495-2503.
127. Yu, J.; Jackson, N. E.; Xu, X.; Morgenstern, Y.; Kaufman, Y.; Ruths, M.; de Pablo, J. J.; Tirrell, M., Multivalent counterions diminish the lubricity of polyelectrolyte brushes. *Science* **2018**, *360* (6396), 1434-+.
128. Yan, W. Q.; Divandari, M.; Rosenboom, J. G.; Ramakrishna, S. N.; Trachsel, L.; Spencer, N. D.; Morgese, G.; Benetti, E. M., Design and characterization of ultrastable, biopassive and lubricious cyclic poly(2-alkyl-2-oxazoline) brushes. *Polym Chem.* **2018**, *9* (19), 2580-2589..
129. Morgese, G.; Cavalli, E.; Rosenboom, J. G.; Zenobi-Wong, M.; Benetti, E. M., Cyclic Polymer Grafts That Lubricate and Protect Damaged Cartilage. *Angew. Chem. Int. Edit.* **2018**, *57* (6), 1621-1626.
130. Morgese, G.; Shaghasemi, B. S.; Causin, V.; Zenobi-Wong, M.; Ramakrishna, S. N.; Reimhult, E.; Benetti, E. M., Next-Generation Polymer Shells for Inorganic Nanoparticles are Highly Compact, Ultra-Dense, and Long-Lasting Cyclic Brushes. *Angew. Chem. Int. Edit.* **2017**, *56* (16), 4507-4511.
131. Benetti, E. M.; Divandari, M.; Ramakrishna, S. N.; Morgese, G.; Yan, W. Q.; Trachsel, L., Loops and Cycles at Surfaces: The Unique Properties of Topological Polymer Brushes. *Chem. Eur. J.* **2017**, *23* (51), 12433-12442.

132. Morgese, G.; Trachsel, M.; Romio, M.; Divandari, M.; Ramakrishna, S. N.; Benetti, E. M., Topological Polymer Chemistry Enters Surface Science: Linear versus Cyclic Polymer Brushes. *Angew. Chem. Int. Edit.* **2016**, *55*, 15583–15588
133. Ramakrishna, S. N.; Morgese, G.; Zenobi-Wong, M.; Benetti, E. M., Comblike Polymers with Topologically Different Side Chains for Surface Modification: Assembly Process and Interfacial Physicochemical Properties. *Macromolecules* **2019**, *52* (4), 1632-1641.
134. Yamamoto, T.; Tezuka, Y., Cyclic polymers revealing topology effects upon self-assemblies, dynamics and responses. *Soft Matter* **2015**, *11* (38), 7458-7468.
135. Satokawa, Y.; Shikata, T.; Tanaka, F.; Qiu, X. P.; Winnik, F. M., Hydration and Dynamic Behavior of a Cyclic Poly(N-isopropylacrylamide) in Aqueous Solution: Effects of the Polymer Chain Topology. *Macromolecules* **2009**, *42* (4), 1400-1403.
136. Xu, J.; Ye, J.; Liu, S. Y., Synthesis of well-defined cyclic poly(N-isopropylacrylamide) via click chemistry and its unique thermal phase transition behavior. *Macromolecules* **2007**, *40* (25), 9103-9110.
137. Hadziioannou, G.; Cotts, P. M.; Tenbrinke, G.; Han, C. C.; Lutz, P.; Strazielle, C.; Rempp, P.; Kovacs, A. J., Thermodynamic and Hydrodynamic Properties of Dilute-Solutions of Cyclic and Linear Polystyrenes. *Macromolecules* **1987**, *20* (3), 493-497.
138. Erbas, A.; Paturej, J., Friction between ring polymer brushes. *Soft Matter* **2015**, *11* (16), 3139-3148.
139. Eiser, E.; Klein, J.; Witten, T. A.; Fetters, L. J., Shear of telechelic brushes. *Phys. Rev. Lett.* **1999**, *82* (25), 5076-5079.
140. Jahn, S.; Seror, J.; Klein, J., Lubrication of Articular Cartilage. *Annu. Rev. Biomed. Eng.* **2016**, *18*, 235-258.
141. Bonnevie, E. D.; Galesso, D.; Secchieri, C.; Cohen, I.; Bonassar, L. J., Elastoviscous Transitions of Articular Cartilage Reveal a Mechanism of Synergy between Lubricin and Hyaluronic Acid. *PLoS One* **2015**, *10* (11).
142. Seror, J.; Merkher, Y.; Kampf, N.; Collinson, L.; Day, A. J.; Maroudas, A.; Klein, J., Normal and Shear Interactions between Hyaluronan-Aggregan Complexes Mimicking Possible Boundary Lubricants in Articular Cartilage in Synovial Joints. *Biomacromolecules* **2012**, *13* (11), 3823-3832.
143. Seror, J.; Merkher, Y.; Kampf, N.; Collinson, L.; Day, A. J.; Maroudas, A.; Klein, J., Articular Cartilage Proteoglycans As Boundary Lubricants: Structure and Frictional Interaction of Surface-Attached Hyaluronan and Hyaluronan-Aggregan Complexes. *Biomacromolecules* **2011**, *12* (10), 3432-3443.

144. Schmidt, T. A.; Gastelum, N. S.; Nguyen, Q. T.; Schumacher, B. L.; Sah, R. L., Boundary lubrication of articular cartilage - Role of synovial fluid constituents. *Arthritis Rheumatol.* **2007**, *56* (3), 882-891.
145. Morgese, G.; Cavalli, E.; Muller, M.; Zenobi-Wong, M.; Benetti, E. M., Nanoassemblies of Tissue-Reactive, Polyoxazoline Graft-Copolymers Restore the Lubrication Properties of Degraded Cartilage. *ACS Nano* **2017**, *11* (3), 2794-2804.
146. Kang, T.; Banquy, X.; Heo, J. H.; Lim, C. N.; Lynd, N. A.; Lundberg, P.; Oh, D. X.; Lee, H. K.; Hong, Y. K.; Hwang, D. S.; Waite, J. H.; Israelachvili, J. N.; Hawker, C. J., Mussel-Inspired Anchoring of Polymer Loops That Provide Superior Surface Lubrication and Antifouling Properties. *ACS Nano* **2016**, *10* (1), 930-937.
147. Li, L.; Yan, B.; Zhang, L.; Tian, Y.; Zeng, H. B., Mussel-inspired antifouling coatings bearing polymer loops. *Chem. Commun.* **2015**, *51* (87), 15780-15783.
148. Patton, D.; Knoll, W.; Advincula, R. C., Polymer Loops vs. Brushes on Surfaces: Adsorption, Kinetics, and Viscoelastic Behavior of alpha,omega-Thiol Telechelics on Gold. *Macromol. Chem. Phys.* **2011**, *212* (5), 485-497.
149. Ashcraft, E.; Ji, H. N.; Mays, J.; Dadmun, M., Grafting Polymer Loops onto Functionalized Nanotubes: Monitoring Grafting and Loop Formation. *Macromol. Chem. Phys.* **2011**, *212* (5), 465-477.
150. Huang, Z. Y.; Ji, H. N.; Mays, J.; Dadmun, M.; Smith, G.; Bedrov, D.; Zhang, Y., Polymer Loop Formation on a Functionalized Hard Surface: Quantitative Insight by Comparison of Experimental and Monte Carlo Simulation Results. *Langmuir* **2010**, *26* (1), 202-209.
151. Huang, Z.; Alonzo, J.; Liu, M.; Ji, H.; Yin, F.; Smith, G. D.; Mays, J. W.; Kilbey, S. M.; Dadmun, M. D., Impact of solvent quality on the density profiles of looped triblock copolymer brushes by neutron reflectivity measurements. *Macromolecules* **2008**, *41* (5), 1745-1752.
152. Alonzo, J.; Huang, Z. Y.; Liu, M.; Mays, J. W.; Toomey, R. G.; Dadmun, M. D.; Kilbey, S. M., Looped polymer brushes formed by self-assembly of poly(2-vinylpyridine)-polystyrene-poly(2-vinylpyridine) triblock copolymers at the solid-fluid interface. Kinetics of preferential adsorption. *Macromolecules* **2006**, *39* (24), 8434-8439.
153. Du, Y. Q.; Jin, J.; Liang, H. J.; Jiang, W., Structural and Physicochemical Properties and Biocompatibility of Linear and Looped Polymer-Capped Gold Nanoparticles. *Langmuir* **2019**, *35* (25), 8316-8324.

154. Han, Y. Y.; Ma, J. N.; Hu, Y.; Jin, J.; Jiang, W., Effect of End-Grafted Polymer Conformation on Protein Resistance. *Langmuir* **2018**, *34* (5), 2073-2080.
155. Zhou, T.; Qi, H.; Han, L.; Barbash, D.; Li, C. Y., Towards controlled polymer brushes via a self-assembly-assisted-grafting-to approach. *Nat. Commun.* **2016**, *7*, 11119.
156. Jiang, S. Y.; Cao, Z. Q., Ultralow-Fouling, Functionalizable, and Hydrolyzable Zwitterionic Materials and Their Derivatives for Biological Applications. *Adv. Mater.* **2010**, *22* (9), 920-932.
157. Sun, H.; Kabb, C. P.; Dai, Y. Q.; Hill, M. R.; Ghiviriga, I.; Bapat, A. P.; Sumerlin, B. S., Macromolecular metamorphosis via stimulus-induced transformations of polymer architecture. *Nat. Chem.* **2017**, *9* (8), 817-823.
158. Aoki, D.; Aibara, G.; Uchida, S.; Takata, T., A Rational Entry to Cyclic Polymers via Selective Cyclization by Self-Assembly and Topology Transformation of Linear Polymers. *J. Am. Chem. Soc.* **2017**, *139* (20), 6791-6794.
159. Yeow, J.; Chapman, R.; Gormley, A. J.; Boyer, C., Up in the air: oxygen tolerance in controlled/living radical polymerisation. *Chem. Soc. Rev.* **2018**, *47* (12), 4357-4387.
160. Zhang, T.; Du, Y.; Muller, F.; Amin, I.; Jordan, R., Surface-initiated Cu(0) mediated controlled radical polymerization (SI-CuCRP) using a copper plate. *Polym. Chem.* **2015**, *6* (14), 2726-2733.
161. Zhang, T.; Du, Y.; Kalbacova, J.; Schubel, R.; Rodriguez, R. D.; Chen, T.; Zahn, D. R. T.; Jordan, R., Wafer-scale synthesis of defined polymer brushes under ambient conditions. *Polym. Chem.* **2015**, *6* (47), 8176-8183.
162. Dehghani, E. S.; Du, Y.; Zhang, T.; Ramakrishna, S. N.; Spencer, N. D.; Jordan, R.; Benetti, E. M., Fabrication and Interfacial Properties of Polymer Brush Gradients by Surface-Initiated Cu(0)-Mediated Controlled Radical Polymerization. *Macromolecules* **2017**, *50* (6), 2436-2446.
163. Narupai, B.; Page, Z. A.; Treat, N. J.; McGrath, A. J.; Pester, C. W.; Discekici, E. H.; Dolinski, N. D.; Meyers, G. F.; de Alaniz, J. R.; Hawker, C. J., Simultaneous Preparation of Multiple Polymer Brushes under Ambient Conditions using Microliter Volumes. *Angew. Chem. Int. Edit.* **2018**, *57* (41), 13433-13438.
164. Fantin, M.; Ramakrishna, S. N.; Yan, J. J.; Yan, W. Q.; Divandari, M.; Spencer, N. D.; Matyjaszewski, K.; Benetti, E. M., The Role of Cu-0 in Surface-Initiated Atom Transfer Radical Polymerization: Tuning Catalyst Dissolution for Tailoring Polymer Interfaces. *Macromolecules* **2018**, *51* (17), 6825-6835.

165. Li, M.; Fromel, M.; Ranaweera, D.; Rocha, S.; Boyer, C.; Pester, C. W., SI-PET-RAFT: Surface-Initiated Photoinduced Electron Transfer-Reversible Addition–Fragmentation Chain Transfer Polymerization. *ACS Macro Lett.* **2019**, *8*, 374-380.

166. Yan, W. Q.; Fantin, M.; Spencer, N. D.; Matyjaszewski, K.; Benetti, E. M., Translating Surface-Initiated Atom Transfer Radical Polymerization into Technology: The Mechanism of Cu⁰-Mediated SI-ATRP under Environmental Conditions. *ACS Macro Lett.* **2019**, *8*, 865-870.

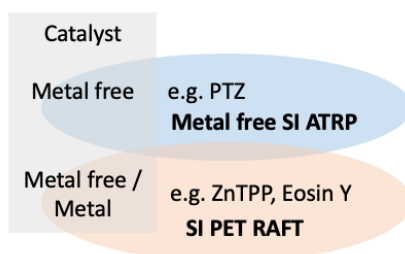
Chapter 3

Oxygen-Tolerant Surface-Initiated Controlled Radical Polymerizations

Surface-initiated controlled radical polymerizations (SI-CRP) enable the controlled fabrication of compositionally different, structured polymer films. Tolerance toward oxygen can be introduced into a SI-CRP method by including oxygen scavengers or reducing agents, such as photoredox catalysts or zerovalent metals. In this chapter, we summarize two types of oxygen-tolerant SI-CRP methods, metal-free, surface-initiated atom-transfer radical polymerization (metal-free SI ATRP) and surface-initiated photo-induced electron transfer, reversible addition-fragmentation chain-transfer polymerization (SI-PET-RAFT). I specifically compare the differences in mechanisms and catalytic systems, and highlight how these methods were recently applied to the generation of structurally complex polymer interfaces.

3.1 Introduction

The need for fabricating thin polymeric films under completely ambient conditions has driven increasing interest in the development and application of oxygen-tolerant, surface-initiated controlled radical polymerization (SI-CRP). In addition to traditional controlled-radical-polymerization (CRP) techniques, such as reversible addition-fragmentation chain transfer (RAFT) polymerization, atom-transfer radical polymerization (ATRP) and related techniques, which have already been extensively used to polymerize a broad range of monomers with intricate structures and multiple functionalities, there has been a recent effort towards more straightforward, environmentally benign and user-friendly, oxygen-tolerant, surface-initiated, controlled-radical-polymerization methods. Specifically, by using an oxygen scavenger, e.g. photocatalyst or zerovalent metals, the formation of peroxy radicals and hydroperoxides can be substantially prevented, and consequently the livingness of propagating radicals and hence the chain-end functionality are retained.



Scheme 1. Overview of oxygen-tolerant controlled radical polymerization methods featuring different catalysts.

Two different oxygen-tolerant SI-CRP approaches are summarized in Scheme 1. Hawker et al developed metal-free, surface-initiated, atom-transfer radical polymerization (metal-free SI ATRP)^{1,2}. In this technique, an organic catalyst is required e.g. 10-phenylphenothiazine (PTH), which has an excited-state reduction potential on par with the metal catalyst Ir(ppy)₃. The mechanism involves stable radical cation species formed after the reduction of the alkyl bromide-based initiator groups, an excited state reduction potential and a stable cation species, which is formed after the reduction of alkyl bromide³. Boyer and coworkers have introduced surface-initiated photo-induced electron transfer, reversible addition-fragmentation chain-transfer polymerization (SI-PET-RAFT)⁴⁻⁶—a process that relies on the visible-light activation of transition-metal-based or organic photoredox catalysts, resulting in electron or energy transfer between the electron-deficient catalyst and the RAFT chain-transfer agent, which serves as a sacrificial electron donor.

These oxygen-tolerant SI-CRP techniques are capable of being performed under environmental conditions, without the need for removal of oxygen by inert gas sparging or

freeze-pump-thaw cycles, and for some of them just ppm levels of catalysts are required. These new techniques open new avenues for further research, especially in synthesizing combinatorial arrays of polymers with unprecedented control over chain-end functionality, architecture, molar mass, and dispersity. In this section, these versatile methods and mechanisms for oxygen-tolerant SI CRP will be discussed and reviewed.

3.2 Metal-Free SI-ATRP

The technical difficulties in separating metallic residues as well as the intolerance toward oxygen have limited the applicability of SI-ATRP in technologically relevant surface fabrications. However, these intrinsic drawbacks can be circumvented. Metal-free SI-ATRP encompasses the use of a photo-catalyst, which enables the efficient fabrication of large-area patterned polymer films on commercial silicon wafers², as well as the synthesis of well-defined polymeric hybrids on silica nanoparticles^{13, 14}, and block-copolymer architectures². These studies are introducing new possibilities for further studies in oxygen-tolerant polymerization processes. This mainly results from the dual-action nature of Ph-PTH as both oxygen scavenger and catalyst.

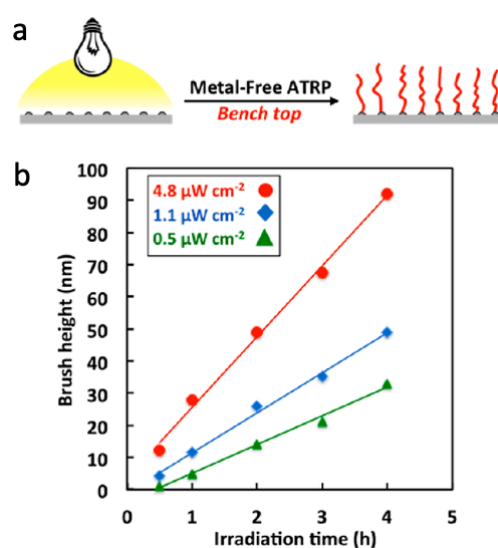


Figure 1. a. Scheme of metal-free ATRP. b. Brush-growth kinetics at different light intensities in the benchtop chamber².

With the smart use of glass coverslips, metal-free benchtop setups were used to conduct surface-initiated ATRP (Figure 1a). Upon excitation with light, a propagating radical could be generated via the reduction of an alkyl bromide-based initiator, as well as deactivating catalysts. Irradiation intensities were investigated as a key factor affecting the reaction kinetics (Figure

1b)². Apart from irradiation intensity, using certain type of surface-tethered initiators has been identified as an effective way to enhance initiation efficiency in metal-free SI-ATRP.

Matyjaszewski and colleagues have sought to enhance the initiation efficiency of metal-free SI-ATRP from silica nanoparticles ¹³ (Figure 2b), while manipulating the activation-deactivation equilibrium between propagating radicals and dormant species in ATRP, which determines the reaction rate and grafting density as well as the degree of end-group retention. In conventional metal-complex-mediated ATRP, transition-metal catalysts activate the dormant species to generate radicals, and the metal in its high oxidation state acts as a deactivator to generate dormant species. The probability of each growing chain propagating can be adjusted by this approach, the aim being to maintain the overall radical concentration, thereby reducing termination reactions e.g. chain-chain coupling. In metal-free ATRP, on the other hand, the mechanism underlying the activation/deactivation cycles relies on a photoactive catalyst such as the inexpensive photoexcited 10-phenylphenothiazine (PhPTZ) (Figures 2 a and b), which plays the role of the Cu(I) and Cu(II) species in conventional ATRP, serving as the activator and the resulting radical cation serving as the deactivator.

The activation rate in metal-free SI-ATRP is influenced by both the chemical composition of the tethered initiators as well as the catalyst concentrations (Figure 2a). Ethyl 2-bromoisobutyrate-based (BiBSiCl) and ethyl 2-bromo-2-phenylacetate-based (BPASiCl) initiators, incorporating silane functions, were tethered to silica nanoparticles (NPs) to assess the overall polymerization rate. The reaction kinetics of grafted-polymer formation from BiBSiCl was slower than the same reaction initiated from BPASiCl, which is related to the activation rate constants¹⁵. Moreover, the higher the catalyst concentration, the higher was the initiation efficiency.

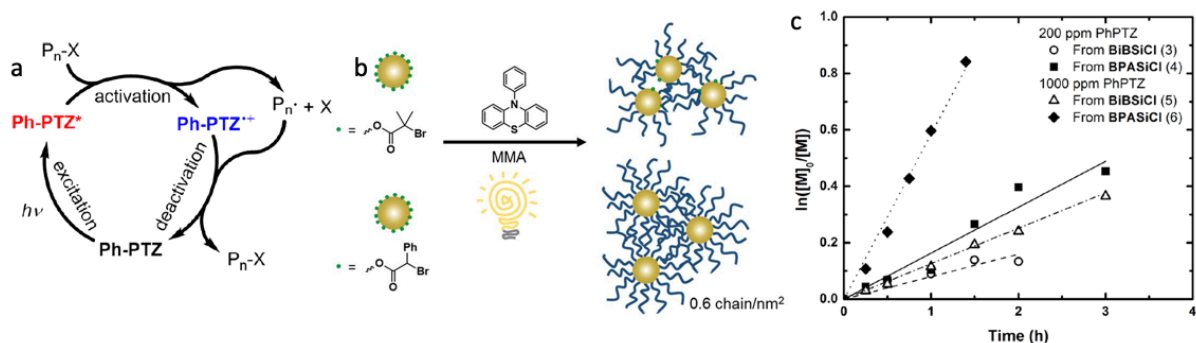


Figure 2. a. Proposed mechanism of activation/deactivation cycles for metal-free ATRP from silica NPs catalyzed by PhPTZ. b. Preparation of polymer-inorganic hybrid materials via metal-free SI-ATRP with 10-phenylphenothiazine (PhPTZ) as the photocatalyst and 2-bromo-2-phenylacetate initiator tethered to silica surfaces. c. Semilogarithmic kinetic plots of metal-free SI-ATRP from 16 nm silica

nanoparticles functionalized with BiBSiCl (200 ppm PhPTZ: open circle, dashed line; 1000 ppm PhPTZ: open triangle, dash-dotted line) or BPASiCl (200 ppm PhPTZ: solid square, solid line; 1000 ppm PhPTZ: solid diamond, dotted line). The solid line in molecular weight evolution is the theoretical value calculated from the target degree of polymerization¹³.

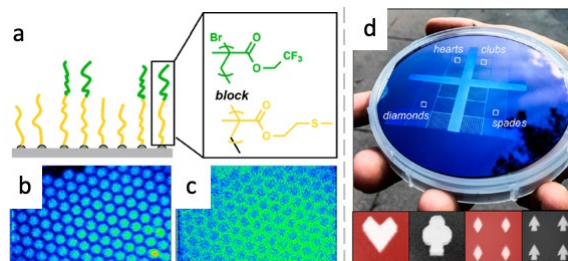


Figure 3. a. Schematic of PMTEMA-*b*-PTFEMA patterned surfaces. b-c. Dynamic secondary ion mass spectroscopy (SIMS) image of the patterned fluorine signal from PTFEMA (b) and sulfur signal from PMTEMA (c). d. Implementation of the discretionary patterning by performing Metal-free SI-ATRP on commercial 4-inch silicon wafers using light and a binary photomask. The scale bars are 200 μm ².

To broaden the potential applications of metal-free SI-ATRP, more efforts were dedicated to the fabrication of PMMA-*b*-PTFEMA copolymer brushes and well-defined polymer-brush patterning² (Figure 3). These studies demonstrated that multiblock copolymers can be easily synthesized by metal-free SI-ATRP, and spatially selective initiation enabled the fabrication of structured polymer films.

3.3 SI-PET-RAFT

Development of surface-initiated photo-induced electron transfer, reversible addition-fragmentation chain-transfer polymerization has further enhanced the capabilities of SI-CRP. In this process, both metal-based and metal-free organic photoredox catalysts can participate in the activation of chain-transfer agent (CTA) by means of an electron-transfer process⁴⁻⁶. The CTA serves both to initiate every polymer chain in solution and as a sacrificial electron donor. This has led to further applications in the large-scale, commercial utilization potential, thanks to its compatibility toward different types of monomers¹⁶ and solvents¹⁷.

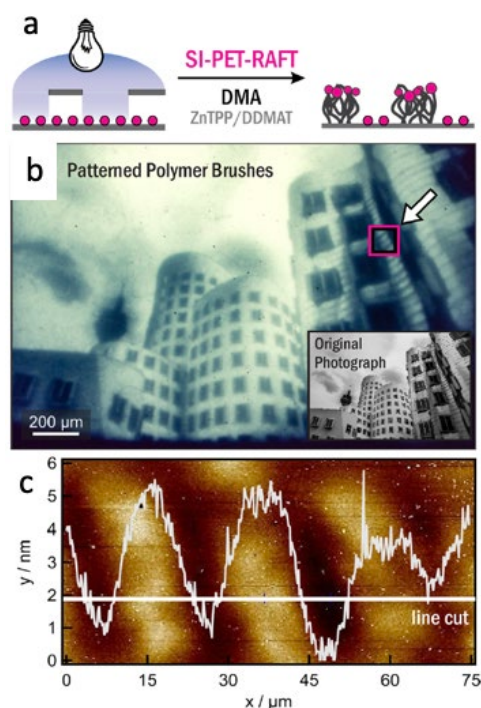


Figure 4. a. Schematic of the fabrication of patterned polymer coatings using SI-PET-RAFT from CTA-functionalized substrates. b. Images of patterned *l*-p(DMA) brushes (light) on silica surface caught by optical microscopy. c. Micromorphology and line profile of brush area in b ⁴.

Applying spatial control over the polymerization kinetics by means of a difference in photon flux, Boyer and collaborators have successfully fabricated 3D patterns of polymer brushes from SiO₂ surfaces by performing oxygen-tolerant SI-PET-RAFT under ambient conditions⁴ (Figure 4). In these experiments, metal-based catalyst zinc tetraphenylporphyrin (ZnTPP) and CTA 2-(dodecylthiocarbonothioylthio)-2-methylpropionic acid (DDMAT) were used.

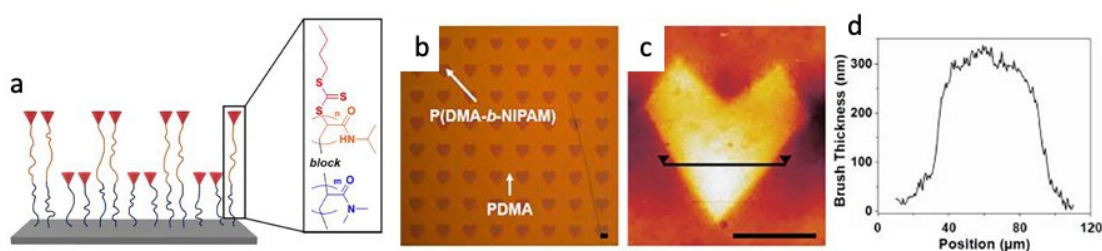


Figure 5. a. Scheme of diblock patterning of polymer brushes via two-step SI-PET-RAFT. b. Optical micrograph of patterned diblock copolymer brushes. c. AFM of a heart-shaped pattern shows a contrast between the P(DMA-*b*-NIPAM) pattern and the initial PDMA layer. scale bars are 50 μm. d. Height profile along marked line in c ⁵.

Taking advantage of the unique features of SI-PET-RAFT, the block copolymers were efficiently synthesized via two-step SI-PET-RAFT⁵. The ability for re-initiation indicates the livingness of the chain ends.

3.4 Conclusions

In summary, interest in oxygen-tolerant SI-CRP methods have been recently rising, with the aim of fabricating structured polymer films without the need for deoxygenation.

Metal-free SI-ATRP utilizes an inexpensive organic phenothiazine-based photocatalyst, which can reduce the alkyl bromide initiator and subsequently form a stable radical cation. The design of the metal-free catalytic systems helps to avoid the release of environmentally hazardous metal ions. This involves its applications in areas such as marine antifouling coatings, microelectronics and biomaterials.

In SI-PET-RAFT, visible light activates the catalysts, which can be transition-metal-based or metal-free organic photoredox catalysts. This leads to electron or energy transfer between the RAFT chain-transfer agent and catalyst. SI-PET-RAFT makes it possible to fabricate the coating of organic materials in a broad range of solvents under ambient conditions.

The development of oxygen-tolerant SI-CRP techniques opens more possibilities for the translation of CRP methods into technologically relevant surface-functionalization methods.

Reference

1. Discekici, E. H.; Anastasaki, A.; de Alaniz, J. R.; Hawker, C. J., Evolution and Future Directions of Metal-Free Atom Transfer Radical Polymerization. *Macromolecules* **2018**, *51* (19), 7421-7434.
2. Discekici, E. H.; Pester, C. W.; Treat, N. J.; Lawrence, I.; Mattson, K. M.; Narupai, B.; Toumayan, E. P.; Luo, Y. D.; McGrath, A. J.; Clark, P. G.; de Alaniz, J. R.; Hawker, C. J., Simple Benchtop Approach to Polymer Brush Nanostructures Using Visible-Light-Mediated Metal-Free Atom Transfer Radical Polymerization. *Acs Macro Letters* **2016**, *5* (2), 258-262.
3. Treat, N. J.; Sprafke, H.; Kramer, J. W.; Clark, P. G.; Barton, B. E.; de Alaniz, J. R.; Fors, B. P.; Hawker, C. J., Metal-Free Atom Transfer Radical Polymerization. *Journal of the American Chemical Society* **2014**, *136* (45), 16096-16101.
4. Li, M. X.; Fromel, M.; Ranaweera, D.; Rocha, S.; Boyer, C.; Pester, C. W., SI-PET-RAFT: Surface-Initiated Photoinduced Electron Transfer-Reversible Addition-Fragmentation Chain Transfer Polymerization. *Acs Macro Letters* **2019**, *8* (4), 374-380.

5. Seo, S. E.; Discekici, E. H.; Zhang, Y. Y.; Bates, C. M.; Hawker, C. J., Surface-initiated PET-RAFT polymerization under metal-free and ambient conditions using enzyme degassing. *Journal of Polymer Science* **2020**, *58* (1), 70-76.
6. Watanabe, A.; Niu, J.; Lunn, D. J.; Lawrence, J.; Knight, A. S.; Zhang, M. W.; Hawker, C. J., PET-RAFT as a facile strategy for preparing functional lipid-polymer conjugates. *Journal of Polymer Science Part a-Polymer Chemistry* **2018**, *56* (12), 1259-1268.
7. Pintauer, T.; Matyjaszewski, K., Atom transfer radical addition and polymerization reactions catalyzed by ppm amounts of copper complexes. *Chemical Society reviews* **2008**, *37* (6), 1087-1097.
8. Fantin, M.; Ramakrishna, S. N.; Yan, J. J.; Yan, W. Q.; Divandari, M.; Spencer, N. D.; Matyjaszewski, K.; Benetti, E. M., The Role of Cu(0) in Surface-Initiated Atom Transfer Radical Polymerization: Tuning Catalyst Dissolution for Tailoring Polymer Interfaces. *Macromolecules* **2018**, *51* (17), 6825-6835.
9. Zhang, T.; Du, Y. H.; Kalbacova, J.; Schubel, R.; Rodriguez, R. D.; Chen, T.; Zahn, D. R. T.; Jordan, R., Wafer-scale synthesis of defined polymer brushes under ambient conditions. *Polymer Chemistry* **2015**, *6* (47), 8176-8183.
10. Zhang, T.; Du, Y. H.; Muller, F.; Amin, I.; Jordan, R., Surface-initiated Cu(0) mediated controlled radical polymerization (SI-CuCRP) using a copper plate. *Polymer Chemistry* **2015**, *6* (14), 2726-2733.
11. Zhang, T.; Benetti, E. M.; Jordan, R., Surface-Initiated Cu(0)-Mediated CRP for the Rapid and Controlled Synthesis of Quasi-3D Structured Polymer Brushes. *Acs Macro Letters* **2019**, *8* (2), 145-153.
12. Layadi, A.; Kessel, B.; Yan, W. Q.; Romio, M.; Spencer, N. D.; Zenobi-Wong, M.; Matyjaszewski, K.; Benetti, E. M., Oxygen Tolerant and Cytocompatible Iron(0)-Mediated ATRP Enables the Controlled Growth of Polymer Brushes from Mammalian Cell Cultures. *Journal of the American Chemical Society* **2020**, *142* (6), 3158-3164.
13. Yan, J. J.; Pan, X. C.; Schmitt, M.; Wang, Z. Y.; Bockstaller, M. R.; Matyjaszewski, K., Enhancing Initiation Efficiency in Metal-Free Surface-Initiated Atom Transfer Radical Polymerization (SI-ATRP). *Acs Macro Letters* **2016**, *5* (6), 661-665.
14. Ma, L.; Li, N.; Zhu, J.; Chen, X. D., Visible Light-Induced Metal Free Surface Initiated Atom Transfer Radical Polymerization of Methyl Methacrylate on SBA-15. *Polymers* **2017**, *9* (2).
15. Tang, W.; Matyjaszewski, K., Effects of initiator structure on activation rate constants in ATRP. *Macromolecules* **2007**, *40* (6), 1858-1863.

16. McCormack, C. L.; Lowe, A. B., Aqueous RAFT polymerization: Recent developments in synthesis of functional water-soluble (Co)polymers with controlled structures. *Accounts of Chemical Research* **2004**, *37* (5), 312-325.
17. Schneiderman, D. K.; Ting, J. M.; Purchel, A. A.; Miranda, R.; Tirrell, M. V.; Reineke, T. M.; Rowan, S. J., Open-to-Air RAFT Polymerization in Complex Solvents: From Whisky to Fermentation Broth. *Acs Macro Letters* **2018**, *7* (4), 406-411.
18. Matyjaszewski, K.; Coca, S.; Gaynor, S. G.; Wei, M. L.; Woodworth, B. E., Zerovalent metals in controlled "living" radical polymerization. *Macromolecules* **1997**, *30* (23), 7348-7350.
19. Dadashi-Silab, S.; Matyjaszewski, K., Temporal Control in Atom Transfer Radical Polymerization Using Zerovalent Metals. *Macromolecules* **2018**, *51* (11), 4250-4258.
20. Yan, W. Q.; Fantin, M.; Ramakrishna, S.; Spencer, N. D.; Matyjaszewski, K.; Benetti, E. M., Growing Polymer Brushes from a Variety of Substrates under Ambient Conditions by Cu-0-Mediated Surface-Initiated ATRP. *Acs Applied Materials & Interfaces* **2019**, *11* (30), 27470-27477.
21. Yan, W. Q.; Fantin, M.; Spencer, N. D.; Matyjaszewski, K.; Benetti, E. M., Translating Surface-Initiated Atom Transfer Radical Polymerization into Technology: The Mechanism of Cu-0-Mediated SI-ATRP under Environmental Conditions. *Acs Macro Letters* **2019**, *8* (7), 865-870.

Chapter 4

Brushes, Graft Copolymers, or Bottlebrushes? The Effect of Polymer Architecture on the Nanotribological Properties of Grafted-from Assemblies *

Surface-grafted polyzwitterions (PZW) have gained a foothold in the design of synthetic materials that closely mimic the lubricious properties of articular joints in mammals. Besides their chemical composition, the architecture of PZW brushes strongly determines their morphological, nanomechanical and nanotribological characteristics. This emerges while comparing the properties of linear poly(2-methacryloyloxyethyl phosphorylcholine) (PMPC) brushes with those displayed by graft-copolymer and bottlebrush brushes, either featuring a low or a high content of PMPC side chains.

Surface-initiated atom transfer polymerization (SI-ATRP) enabled the synthesis of different branched brush architectures from multifunctional macroinitiators via multiple grafting steps, and allowed us to modulate their structure by tuning the polymerization conditions.

At relatively low grafting densities (σ), long PMPC side segments extend at the interface of bottlebrush and graft-copolymer brushes, providing both morphology and lubrication properties comparable to those shown by loosely grafted, linear PMPC brushes.

When $\sigma > 0.1$ chains nm^{-2} the effect of the branched-polymer-brush architecture on the nanotribological properties of the films became evident. Linear PMPC brushes showed the lowest friction among the studied brush structures, with a coefficient of friction (μ) that reached 10^{-4} , as measured by atomic force microscopy (AFM). Bottlebrush brushes showed comparatively higher friction, although the high content of hydrophilic PMPC side chains along their backbone substantially improved lubrication compared to that displayed by the more sparsely substituted graft-copolymer brushes.

* Edmondo M Benetti and Nicholas D Spencer supervised this project. Wenqing Yan and Shivaprakash N Ramakrishna performed experimental work. All the authors wrote the paper. Part of this Chapter was published in *Langmuir*. 2019. 35, 35, 11255-11264.

4.1. Introduction

The unique lubricious characteristics provided to surfaces by polymer “brushes” have increasingly attracted the attention of materials scientists over the past two decades. The mechanism underlying the reduction of friction when brushes are sheared in a good solvent under an applied normal load relies on the osmotic pressure exerted by their densely chain-end grafted polymer components, which sterically stabilizes the surface and generates a highly lubricating fluid film at the interface.¹⁻⁷

In the area of aqueous lubrication, highly hydrophilic⁸⁻¹² and ionic polymers³⁻⁵ have been identified as suitable constituents for brush assemblies aimed to reduce friction. Among these, the most lubricious brush formulations have involved polyzwitterions (PZW), and these have displayed coefficients of friction (μ) as low as 10^{-4} , under applied pressures analogous to those typically exerted within the articular joints of mammals.¹³⁻¹⁸

Thanks to their highly lubricious properties, coupled with an intrinsic inertness towards biological contamination,¹⁸⁻²⁰ PZW brushes have been applied on a variety of surfaces, mainly in the form of linear “grafted-from” brushes,²¹⁻²⁷ and have been synthesized by means of surface-initiated controlled radical polymerizations (SI-CRP) from initiator-modified substrates. In addition to being prepared as linear brushes grafted from surfaces, PZWs have been included as side segments within highly branched copolymer formulations, yielding surface modifiers featuring a molecular brush or bottlebrush structure.²⁸⁻²⁹ These high-molar-mass copolymer species mimic the highly branched molecular architecture that is characteristic of biomacromolecules responsible of physiological lubrication,³⁰⁻³⁵ and were designed to adsorb on model inorganic surfaces, exposing their PZW-based molecular brush structure at the interface, in order to confer lubricity and simultaneously prevent fouling by proteins and cells.

Despite the wealth of studies focusing on the application and characterization of linear PZW brushes as well as branched macromolecules including PZW segments, a systematic and comprehensive analysis of how the brush structure determines the interfacial physicochemical properties and nanotribological characteristics of surface-grafted PZW-containing films is currently lacking. More specifically, it has yet to be clarified what effects the presence and density of branching along surface-grafted macromolecules might have in regulating morphology, steric stabilization and friction of brush assemblies.

In order to determine which polymer-brush architecture is more suitable for reducing friction on surfaces, we have exploited surface-initiated, atom-transfer radical polymerization

(SI-ATRP)³⁶⁻³⁹ to design linear and branched PZW brushes, investigating their interfacial physicochemical properties by a variety of surface-analytical approaches, and probing the effects of brush structure on lubrication properties by means of lateral force microscopy (LFM).⁴⁰⁻⁴¹

Linear poly(2-methacryloyloxyethyl phosphorylcholine) (PMPC) brushes, graft-copolymer brushes including 25 mol% of PMPC side chains along polymethacrylate “backbones”, and bottlebrush brushes featuring 85 mol% of PMPC side segments were synthesized by SI-ATRP following single or multiple grafting steps (Scheme 1). Within all the structurally different films, brush density was systematically varied by dilution of ATRP initiator functions within silane-based monolayers,⁴²⁻⁴⁴ yielding a library of grafted-polymer architectures in which the degree of branching and surface coverage were varied, and the influence of these parameters on interfacial properties could be assessed.

Both the overall composition and the grafting density of highly lubricating PMPC chains emerge as key factors regulating the lubrication properties of brush films, while the simplest grafted-polymer design, featuring densely crowded, linear PMPC brushes demonstrates the highest efficiency in reducing friction. From a more fundamental point of view, this study expands our existing knowledge on the relationship between brush structure and interfacial properties, especially regarding nanomechanics and nanotribology, which are highly relevant characteristics in the formulation of coatings for biomaterials and lubricious interfaces.

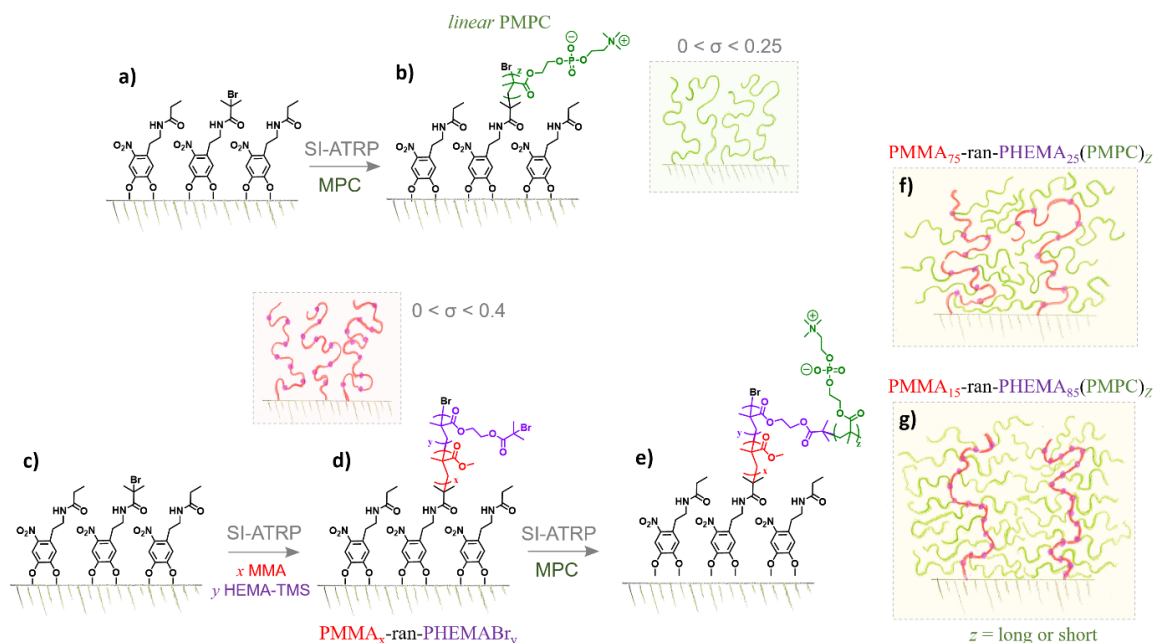
4.2 Results and Discussion

4.2.1 Synthesis, compositional and structural analysis

Linear PMPC brushes and branched brushes presenting different surface densities were synthesized from substrates featuring various coverages of ATRP initiators. These were obtained starting from monolayers of nitrodopamine (ND) assembled on TiO₂ surfaces,⁴⁵ followed by reaction with mixtures of propionyl bromide (PB), which forms inert ethyl amide functions at the surface, and α -bromoisobutyryl bromide (BiBB), which generates alkyl halide moieties, functioning as initiators for ATRP (Scheme 1a).

Fine adjustment of the concentration of PB and BiBB in solution enabled the fabrication of monolayers with a relative coverage of ATRP initiator functions varying from 1 to 100 mol%.⁴⁶

We first investigated the fabrication and interfacial properties of linear PMPC brushes, and later used the results as a reference for comparing the characteristics of branched polymer brushes featuring PMPC side chains.



Scheme 1. Linear PMPC brushes are fabricated by SI-ATRP from catechol-based mixed SAMs on TiO_2 surfaces (a,b), yielding films with different values of σ . From similar, initiating SAMs, graft-copolymer and bottlebrush brushes were synthesized by multiple SI-ATRP steps. Multifunctional initiator grafts with general formula $\text{PMMA}_x\text{-ran-PHEMA}Br_y$ were initially synthesized by SI-ATRP of MMA/HEMATMS mixtures, followed by introduction of Br-isobutyrate functions (c,d). Subsequent grafting of PMPC by a further SI-ATRP step generated $\text{PMMA}_{75}\text{-ran-PHEMA}_{25}(\text{PMPC})_z$ graft-copolymer brushes and $\text{PMMA}_{15}\text{-ran-PHEMA}_{85}(\text{PMPC})_z$ bottlebrush brushes (e-g).

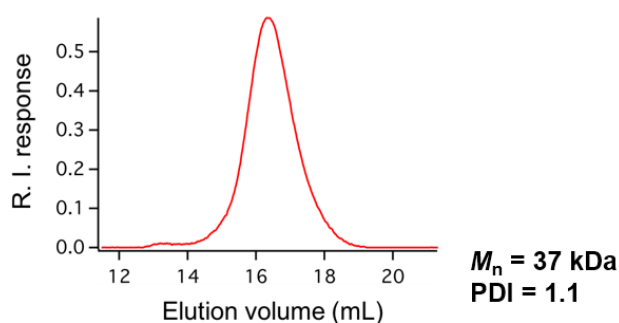


Figure 1. SEC elugram of PMPC synthesized by sacrificial initiator in solution.

Size-exclusion chromatography (SEC) provided a M_n of 37 kDa and PDI of 1.1 (Figure 1). The measured molecular weight was used to estimate the grafting density (σ) of PMPC brushes, according to $\sigma = \rho T_{\text{dry}} N_A M_n^{-1}$, where ρ is the density of the polymer (1.30 g cm^{-3}), T_{dry} is the dry thickness (measured by VASE), N_A is Avogadro's number, and M_n is the molecular weight

measured by SEC. FTIR spectroscopy confirmed the composition of PMPC brushes (Figure 2).

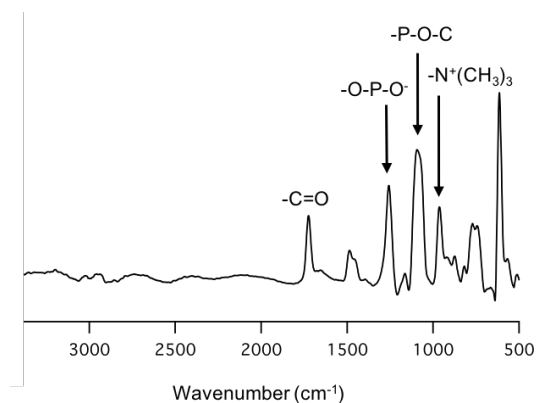


Figure 2. FTIR spectrum recorded on PMPC brushes synthesized by SI-ATRP. The signals centered at 1730 cm^{-1} (C=O stretching), 1240 cm^{-1} (-O-P-O-), 1080 cm^{-1} (-P-O-C), and 970 cm^{-1} (-N⁺(CH₃)₃) are characteristic of the repeating unit of PMPC.

Linear PMPC brushes presenting a broad range of grafting densities (σ) were synthesized by SI-ATRP from mixed monolayers of ATRP initiators. In particular, by maintaining a constant polymerization time (and thus a comparable molecular weight of the obtained grafts) while varying the initiator coverage at the surface, the values of σ could be varied between 0.01 and 0.38 chains nm⁻², corresponding to brush dry thicknesses (T_{dry}) spanning from a few nm to ~ 20 nm, respectively (as measured by VASE and reported in Figure 3b and Table 1). Simultaneous solution ATRP performed from “sacrificial” initiator in solution provided PMPC with M_n of 37 kDa and PDI of 1.1 (Figure 1), parameters which were used to estimate the structural properties of the surface-grafted films.

Table 1. Values of σ for PMPC brushes.

| | | | | | |
|--|---------------|-------------|---------------|----------------|----------------|
| Dry thickness [nm] | 0.5 ± 0.1 | 1 ± 0.2 | 5.7 ± 0.3 | 10.3 ± 0.3 | 17.7 ± 0.4 |
| Grafting density (σ) [chains nm ⁻²] | 0.01 | 0.02 | 0.12 | 0.21 | 0.38 |

AFM was subsequently employed to evaluate the nanomorphology of linear PMPC brushes immersed in aqueous medium and their nanomechanical properties, while lateral force microscopy (LFM) was applied to investigate how the progressive variation of σ determined the nanotribological properties of the films.^{41, 47}

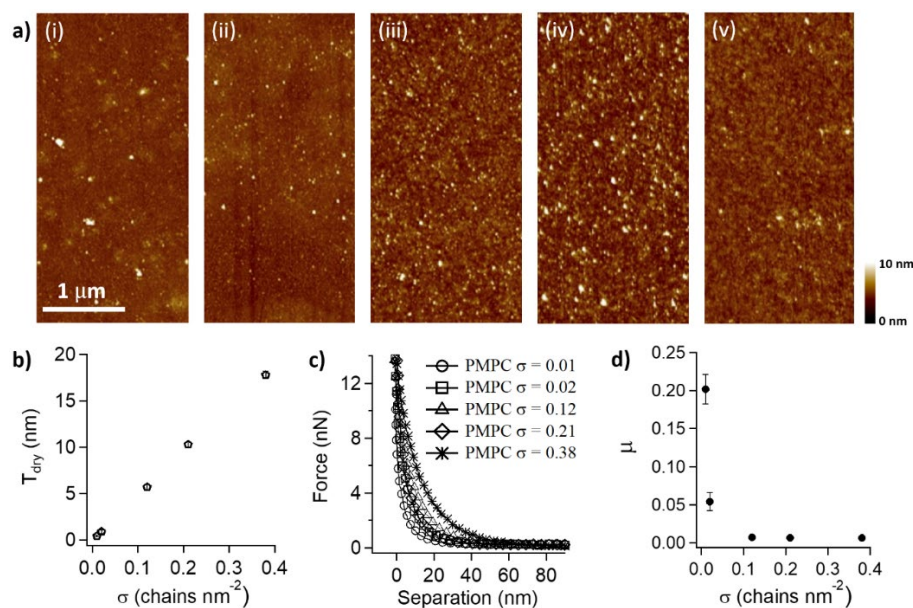


Figure 3. (a) Peakforce AFM height micrographs recorded in (4-(2-hydroxyethyl)-1-piperazineethanesulfonic acid) (HEPES) solution (pH = 7.4) on linear PMPC brushes presenting different values of σ : (i) 0.01, (ii) 0.02, (iii) 0.09, (iv) 0.16 and (v) 0.23 chains nm^{-2} . (b) Variation of T_{dry} (measured by VASE) as a function of σ . (c) Force-separation profiles recorded by AFM in HEPES solution on linear PMPC brushes featuring different grafting densities. (d) Variation of μ (measured by LFM) as a function of grafting density of linear PMPC brushes.

PMPC brushes with different values of σ all showed a uniform coverage across the substrates (Figure 3a), although a textured nanomorphology progressively developed with increasing σ , demonstrating the gradual transition from more loosely grafted chains coiling down onto the substrate and appearing as a smooth polymer layer, to bundles of denser grafts stretching out towards the interface.⁴⁴

The steric stabilization provided by PMPC brushes at the surface was strongly dependent on their grafting density. As demonstrated by comparing force-vs-separation profiles (FS) recorded by AFM (Experimental Section), the interaction between the approaching colloidal probe and the structurally different brushes was progressively more repulsive following the increment in σ (Figure 3c).⁴⁸ Simultaneously, the amount of water within the linear brushes, measured as the “swelling ratio” between their wet and dry thickness (T_{wet} and T_{dry} , respectively), gradually decreased (Figure 4 and Table 2), illustrating how densely assembled grafts can incorporate a lower amount of solvent in their swollen state, compared to more sparsely grafted chains.⁴⁷

The nanotribological properties of PMPC brushes were also found to be markedly dependent on their grafting density. As highlighted by comparing friction-force-vs-applied-load profiles (FiL) obtained by LFM (Figure 3c), friction progressively decreased with

increasing σ , the recorded coefficient of friction (μ) reaching values < 0.001 for brush coverages > 0.1 chains nm^{-2} .

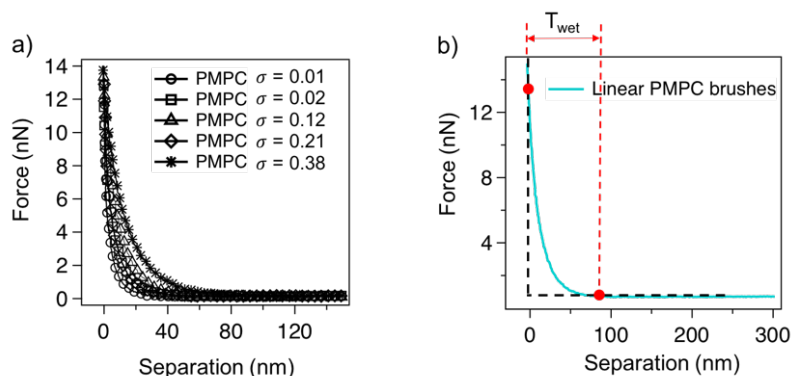


Figure 4. (a) FS profiles recorded on PMPC brushes presenting different σ in HEPES solution ($\text{pH} = 7.4$). (b) The swollen thickness (T_{wet}) of PMPC brushes was estimated from FS profiles. Namely, T_{wet} was estimated as the distance between the brush-AFM probe contact point, i.e. the point where the approaching FS curve separate from the horizontal line, and the point where the PMPC brush is fully compressed, i.e. where the approaching FS curve approximates a vertical line.

Table 2. Values of T_{dry} and T_{wet} of PMPC brushes presenting different σ , respectively measured by VASE and estimated by AFM from FS profiles.

| | | | | | |
|---|---------------|-------------|---------------|----------------|----------------|
| T_{dry} [nm] | 0.5 ± 0.1 | 1 ± 0.2 | 5.7 ± 0.3 | 10.3 ± 0.3 | 17.7 ± 0.4 |
| T_{wet} [nm] | 13 ± 0.5 | 16 ± 3 | 31 ± 8 | 37 ± 5 | 50 ± 4 |
| Grafting density [chains nm^{-2}] | 0.01 | 0.02 | 0.12 | 0.21 | 0.38 |

This result agrees well with previous studies of the lubricating properties of PMPC brushes,^{14, 16-17} and confirms how the increase in osmotic pressure accompanying the increment in brush density translates into an enhancement of its lubricious character.⁴⁸⁻⁴⁹

The interfacial properties of linear PMPC brushes were subsequently compared to those measured for branched brushes featuring different concentrations and lengths of PMPC segments (Scheme 1).

Multifunctional macro-initiators were initially grafted from mixed monolayers of ATRP initiators previously deposited on TiO_2 surfaces (Scheme 1c-d). Poly(methyl methacrylate)-ran-poly[2-(trimethylsilyloxy)ethyl methacrylate] ($\text{PMMA}_x\text{-ran-PHEMATMS}_y$) brushes including 25 and 85 mol% of HEMATMS units (referred to as $\text{PMMA}_{75}\text{-ran-PHEMATMS}_{25}$ and $\text{PMMA}_{15}\text{-ran-PHEMATMS}_{85}$, respectively) were grafted by SI-ATRP, yielding grafts with M_w of 34 and 72 kDa, corresponding to a DP of ~ 270 and ~ 380 , and PDI of 1.35 and 1.33, respectively (measured on polymers obtained by the use of sacrificial initiator in solution, as described in Figure 5).

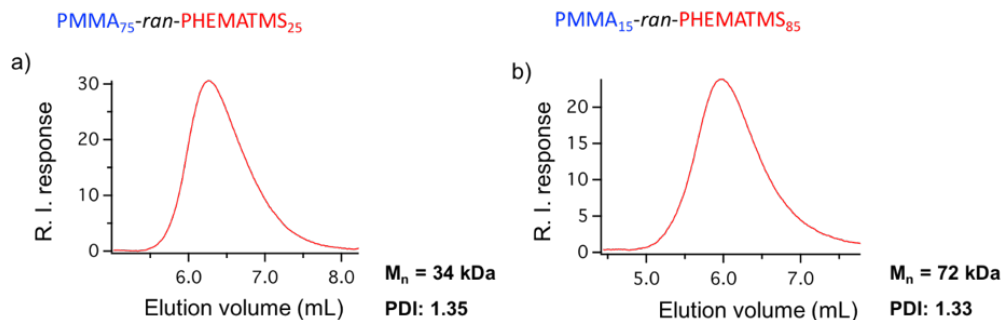


Figure 5. SEC elution profiles of (a) $PMMA_{75}$ -ran- $PHEMATMS_{25}$ and (b) $PMMA_{15}$ -ran- $PHEMATMS_{85}$ synthesized from sacrificial initiators in solution during SI-ATRP. The number average molecular weights M_n and polydispersity of the copolymers are indicated as insets, and they were used to estimate the values of σ of the corresponding brushes.

The polymer synthesized in solution was characterized by 1H NMR, in order to precisely estimate the relative content of the two co-monomers (Figure 6). Size-exclusion chromatography provided $M_n = 34$ kDa and a $PDI = 1.35$ (Figure 5). These parameters were used to estimate the values of σ for $PMMA_{75}$ -ran- $PHEMATMS_{25}$ brushes, according to $\sigma = \rho T_{dry} N_A M_n^{-1}$.

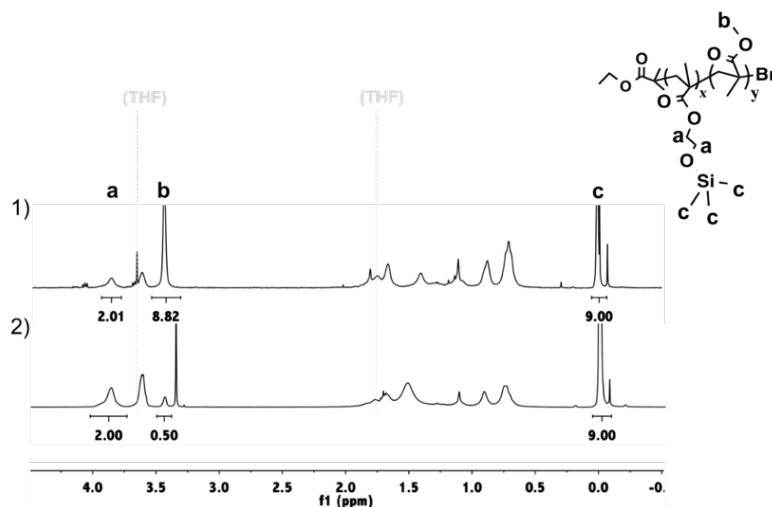


Figure 6. 1H -NMR spectra (500 MHz) of $PMMA_{75}$ -ran- $PHEMATMS_{25}$ (1) and $PMMA_{15}$ -ran- $PHEMATMS_{85}$ (2) synthesized from sacrificial initiators in solution during SI-ATRP.

Tuning of the ATRP-initiator coverage at the surface generated brushes with values of σ ranging from 0.02 to 0.38 chains nm^{-2} , for $PMMA_{75}$ -ran- $PHEMATMS_{25}$, and from 0.01 to 0.34 chains nm^{-2} , in the case of $PMMA_{15}$ -ran- $PHEMATMS_{85}$.

The different $PMMA_x$ -ran- $PHEMATMS_y$ brushes were subsequently converted into α -bromoisobutyrate-functionalized grafts (yielding $PMMA_x$ -ran- $PHEMATMS_yBr$) by removal of the

TMS groups along the chains and subsequent reaction of deprotected hydroxyl functions with BiBB.

Table 3. Dry thickness (T_{dry}) measured by VASE of graft-copolymer brushes presenting different values of σ following each SI-ATRP step.

| σ (chains nm ⁻²) | 0.02 | 0.04 | 0.1 | 0.15 | 0.38 |
|---|------------|------------|------------|------------|------------|
| PMMA₇₅-ran-PHEMATMS₂₅ (nm) | 1.7 ± 0.2 | 2.8 ± 0.3 | 5.8 ± 0.4 | 8.3 ± 0.3 | 21.5 ± 1.2 |
| PMMA₇₅-ran-PHEMABr₂₅ (nm) | 1.4 ± 0.2 | 2.5 ± 0.3 | 5.3 ± 0.2 | 7.9 ± 0.4 | 19.1 ± 0.5 |
| PMMA₇₅-ran-PHEMATMS₂₅(PMPC)_{long} (nm) | 12.2 ± 0.9 | 14.5 ± 0.5 | 26.5 ± 1.6 | 29.4 ± 1.3 | 64.3 ± 2.5 |

Table 4. Dry thickness (T_{dry}) measured by VASE of graft-copolymer brushes presenting different values of σ following each SI-ATRP step.

| $\sigma_{surface}$ (chains nm ⁻²) | 0.02 | 0.04 | 0.1 | 0.15 | 0.38 |
|--|-----------|-----------|-----------|------------|------------|
| PMMA₇₅-ran-PHEMATMS₂₅ (nm) | 1.2 ± 0.2 | 2.2 ± 0.3 | 6.0 ± 0.6 | 10.3 ± 0.4 | 24.2 ± 0.5 |
| PMMA₇₅-ran-PHEMABr₂₅ (nm) | 1.2 ± 0.1 | 2.0 ± 0.1 | 5.6 ± 0.1 | 8.9 ± 0.3 | 19.6 ± 0.3 |
| PMMA₇₅-ran-PHEMATMS₂₅(PMPC)_{short} (nm) | 1.5 ± 0.2 | 2.4 ± 0.2 | 7.2 ± 0.2 | 10.7 ± 0.3 | 21.5 ± 0.5 |

Table 5. Dry thickness (T_{dry}) measured by VASE of bottlebrush brushes presenting different values of σ following each SI-ATRP step.

| σ (chains nm ⁻²) | 0.01 | 0.02 | 0.08 | 0.24 | 0.34 |
|---|------------|------------|------------|------------|------------|
| PMMA₁₅-ran-PHEMATMS₈₅ (nm) | 1.5 ± 0.4 | 2.4 ± 0.3 | 9.2 ± 1.0 | 27.3 ± 2.2 | 38.6 ± 3.5 |
| PMMA₁₅-ran-PHEMABr₈₅ (nm) | 1.4 ± 0.3 | 2.3 ± 0.5 | 8.7 ± 0.7 | 25.0 ± 1.9 | 35.4 ± 2.5 |
| PMMA₁₅-ran-PHEMATMS₈₅(PMPC)_{long} (nm) | 11.6 ± 1.3 | 11.7 ± 2.5 | 26.8 ± 3.1 | 68.4 ± 3.7 | 98.8 ± 4.6 |

Table 6. Dry thickness (T_{dry}) measured by VASE of bottlebrush brushes presenting different values of σ following each SI-ATRP step.

| σ (chains nm ⁻²) | 0.01 | 0.02 | 0.08 | 0.24 | 0.34 |
|--|-----------|-----------|-----------|------------|------------|
| PMMA₁₅-ran-PHEMATMS₈₅ (nm) | 1.3 ± 0.1 | 2.9 ± 0.2 | 7.2 ± 0.4 | 12.4 ± 0.3 | 16.5 ± 0.7 |
| PMMA₁₅-ran-PHEMABr₈₅ (nm) | 1.2 ± 0.2 | 2.6 ± 0.3 | 6.3 ± 0.3 | 10.6 ± 0.4 | 15.8 ± 0.8 |
| PMMA₁₅-ran-PHEMATMS₈₅(PMPC)_{short} (nm) | 3.5 ± 0.2 | 6.2 ± 0.6 | 8.9 ± 0.3 | 14.8 ± 1.1 | 18.7 ± 0.2 |

The introduction of Br-isobutyrate functions along the brush structures was confirmed by Fourier-transform infrared spectroscopy (FTIR) and VASE, as shown in Table 3-6 and Figure 7-8.

From these multifunctional macro-initiator brushes, grafting of PMPC side chains was carried out through an additional SI-ATRP step, employing two different concentrations of Cu^{II}-based deactivator and thus generating a library of branched brushes, featuring: i) a

different surface coverage, ii) two different densities of side chains along the macro-initiator grafts, determined by the relative content of HEMABr units, and iii) two different lengths of side chains, which were controlled by varying the deactivator concentration (and thus the rate of MPC polymerization) during the second ATRP step (Scheme 1e-g).

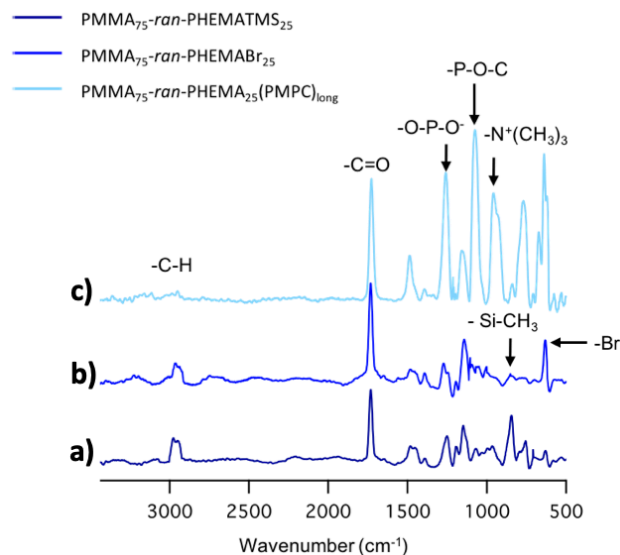


Figure 7. FTIR spectra of $PMMA_{75}\text{-ran-PHEMATMS}_{25}$ (a), $PMMA_{75}\text{-ran-PHEMABr}_{25}$ (b) and $PMMA_{75}\text{-ran-PHEMA}_{25}(\text{PMPC})_{\text{long}}$ (c) brushes synthesized by sequential SI-ATRP from initiator-modified TiO_2 substrates. The appearance of the signal at 638 cm^{-1} in (b), corresponding to C-Br stretching, and the simultaneous disappearance of the signal centered at 850 cm^{-1} in (a), corresponding to $-\text{Si-CH}_3$, indicate the successful introduction of ATRP initiator functions along $PMMA_{75}\text{-ran-PHEMABr}_{25}$ brushes. In (c), the appearance of the signals at 1240 cm^{-1} ($-\text{O-P-O-}$), 1080 cm^{-1} ($-\text{P-O-C}$), and 970 cm^{-1} ($-\text{N}^+(\text{CH}_3)_3$) confirmed the successful grafting of PMPC side chains, yielding $PMMA_{75}\text{-ran-PHEMA}_{25}(\text{PMPC})_{\text{long}}$ graft-copolymer brushes.

Generally, $PMMA_{75}\text{-ran-PHEMABr}_{25}$ generated brushes with a relatively low content of branching, and thus were classified as $PMMA_{75}\text{-ran-PHEMA}_{25}(\text{PMPC})$ graft-copolymer brushes. In contrast, brushes featuring a high content of PMPC side chains were obtained by ATRP of MPC from $PMMA_{15}\text{-ran-PHEMABr}_{85}$, yielding $PMMA_{15}\text{-ran-PHEMA}_{85}(\text{PMPC})$ bottlebrush brushes.

Tuning of the polymerization rate during the growth of PMPC side chains generated graft copolymer and bottlebrush brushes alternatively presenting “long” and “short” side chains, (which were thus designated as $PMMA_{75}\text{-ran-PHEMA}_{25}(\text{PMPC})_{\text{long}}$ and $PMMA_{75}\text{-ran-PHEMA}_{25}(\text{PMPC})_{\text{short}}$, $PMMA_{15}\text{-ran-PHEMA}_{85}(\text{PMPC})_{\text{long}}$ and $PMMA_{15}\text{-ran-PHEMA}_{85}(\text{PMPC})_{\text{short}}$, respectively). It is important to emphasize that the molecular weight of PMPC side chains synthesized during the second SI-ATRP step was not only determined by the composition of the polymerization mixture (i.e. the relative content of externally added

Cu^{II}), but it was additionally strongly dependent on the surface density of PMMA_x-ran-PHEMABr_y multifunctional initiator brushes (Scheme 2). This latter parameter regulated the steric hindrance between side chains growing from neighbouring multifunctional initiator grafts (*vide infra*).

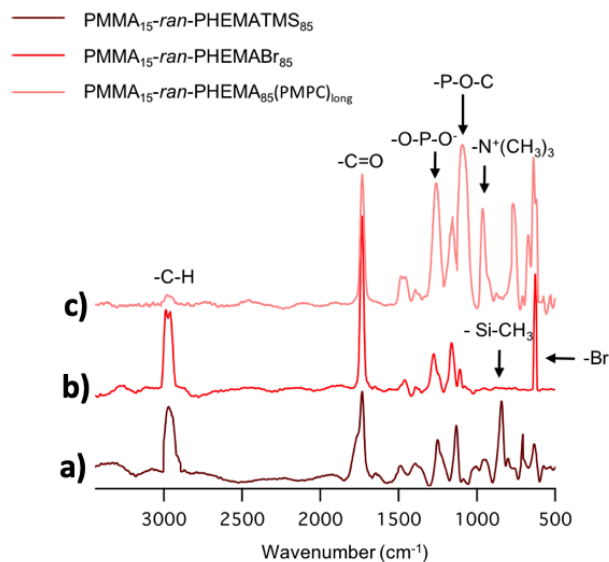
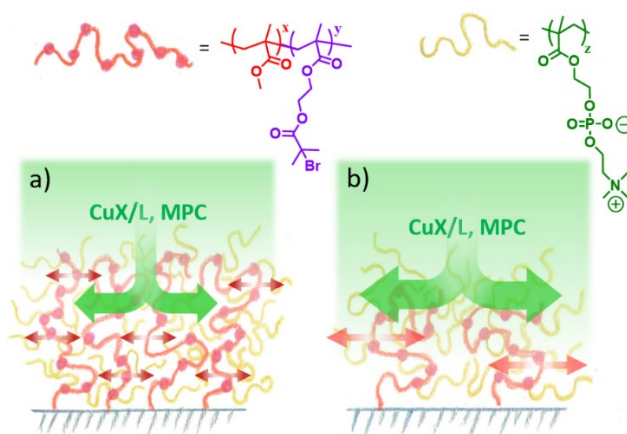


Figure 8. FTIR spectra of PMMA₁₅-ran-PHEMATMS₈₅ (a), PMMA₁₅-ran-PHEMABr₈₅ (b) and PMMA₁₅-ran-PHEMA₈₅(PMPC)_{long} (c) brushes synthesized by sequential SI-ATRP from initiator-modified TiO₂ substrates. The appearance of the signal at 638 cm⁻¹ in (b), corresponding to C-Br stretching, and the simultaneous disappearance of the signal centered at 850 cm⁻¹ in (a), corresponding to -Si-CH₃, indicate the successful introduction of ATRP initiator functions along PMMA₁₅-ran-PHEMABr₈₅ brushes. In (c), the appearance of the signals at 1240 cm⁻¹ (-O-P-O-), 1080 cm⁻¹ (-P-O-C), and 970 cm⁻¹ (-N⁺(CH₃)₃) confirmed the successful grafting of PMPC side chains, yielding PMMA₁₅-ran-PHEMA₈₅(PMPC)_{long} bottlebrush brushes.



Scheme 2. The growth of PMPC side chains from PMMA_x-ran-PHEMABr_y multifunctional initiator brushes can be modulated by varying the polymerization conditions but it is additionally determined by the density of the precursor brushes. This parameter, influences the steric hindrance between neighbouring grafts, which affect the formation of the branched brush architecture.

Although the simultaneous ATRP performed in solution from sacrificial initiator provided M_n of 30 and 7 kDa, when $[Cu^{II}]$ was 4 and 7 mM, respectively, we believe that these values only represent an accurate estimate in the case of sufficiently spaced multifunctional initiators (i.e. for $\sigma < 0.05$ chains nm^{-2}), where the limited inter-chain hindrance more closely reproduces their reactivity in solution (Scheme 2b). We thus prefer to maintain a more general identification for the side PMPC chain-lengths as relatively “long” or “short”.

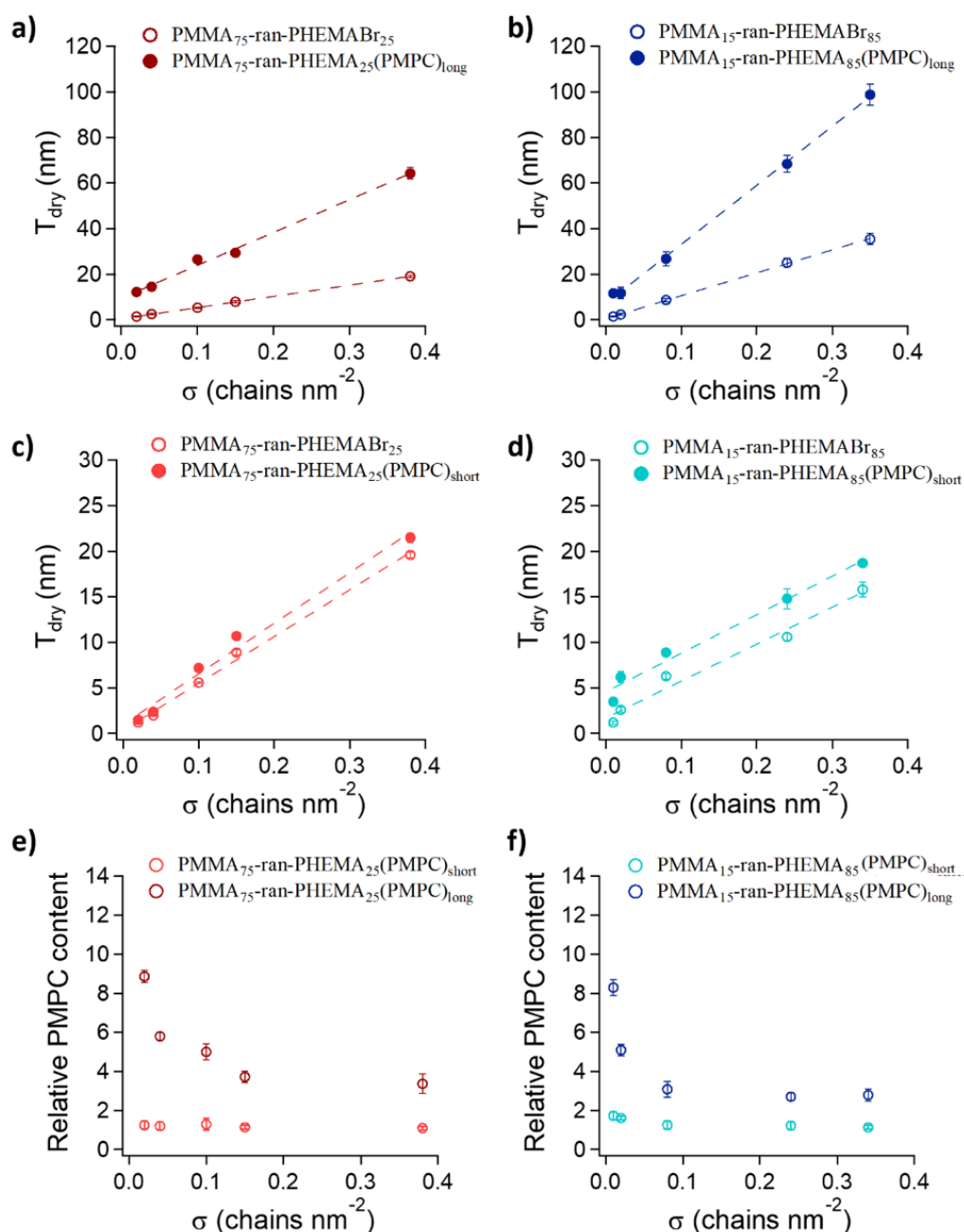


Figure 9. Increment of T_{dry} (VASE) following grafting of PMPC side chains. Graft copolymer brushes with relatively long (a) and short (c) PMPC side chains. Bottlebrush brushes with long (b) and short (d) PMPC side chains. The relative content of PMPC was expressed as $[T_{dry}(PMMA_x\text{-ran-}$

$PHEMA_y(PMPC) - T_{dry}(PMMA_x\text{-ran-PHEMABr}_y)] / T_{dry}(PMMA_x\text{-ran-PHEMABr}_y)$ and it is reported in the case of graft-copolymer (e) and bottlebrush brushes (f).

The successful growth of PMPC segments from $PMMA_x\text{-ran-PHEMABr}_y$ was confirmed by a concomitant increment in dry thickness across the entire range of σ (Table 3-6), as well as by FTIR (Figure 7-8). The amount of PMPC grafted from $PMMA_x\text{-ran-PHEMABr}_y$ macro-initiator brushes was expressed as relative PMPC content, which is the ratio between the dry thickness values recorded following PMPC grafting, and those measured on the initial, multifunctional initiator brush films (Figure 9).

When longer PMPC side chains were grafted, the values of T_{dry} significantly increased, especially from $PMMA_x\text{-ran-PHEMABr}_y$ brushes with $\sigma < 0.1$ chains nm^{-2} (Figure 9a-b and 9e-f), where the increment in brush thickness was more marked. For a given polymerization time, sparsely grafted $PMMA_x\text{-ran-PHEMABr}_y$ chains enable a more efficient grafting of PMPC side segments due to the reduced steric hindrance encountered during their surface-confined growth. In contrast, PMPC-grafting during the second SI-ATRP step was more sterically demanding, for both $PMMA_{15}\text{-ran-PHEMABr}_{85}$ and $PMMA_{85}\text{-ran-PHEMABr}_{15}$ brushes featuring $\sigma > 0.1$ chains nm^{-2} , and the relative PMPC content did not exceed 4 (Figure 9e-f).

When relatively short PMPC side chains were grafted from $PMMA_{15}\text{-ran-PHEMABr}_{85}$ and $PMMA_{75}\text{-ran-PHEMABr}_{25}$ films, graft-copolymer and bottlebrush brushes featuring a nearly constant relative PMPC content < 2 were obtained for all values of σ .

4.2.2 Nanomorphology of $PMMA_x\text{-ran-PHEMATMS}_y(\text{PMPC})$ brushes

Peakforce AFM was subsequently employed to investigate the nanomorphology of the different brush architectures. As reported in Figure 10a and 10c, $PMMA_{75}\text{-ran-PHEMA}_{25}(\text{PMPC})_{\text{short}}$ and $PMMA_{15}\text{-ran-PHEMA}_{85}(\text{PMPC})_{\text{short}}$ featuring $\sigma = 0.04$ and 0.02 chains nm^{-2} , respectively, showed a multitude of features covering the surface, corresponding to branched grafts. These became denser when σ was increased to 0.15 and 0.25 chains nm^{-2} (Figure 10b and 10d), respectively for $PMMA_{75}\text{-ran-PHEMA}_{25}(\text{PMPC})_{\text{short}}$ and $PMMA_{15}\text{-ran-PHEMA}_{85}(\text{PMPC})_{\text{short}}$.

Both at relatively low and high values of σ , $PMMA_{75}\text{-ran-PHEMA}_{25}(\text{PMPC})_{\text{short}}$ graft-copolymer brushes showed higher root mean square (RMS) roughness with respect to that measured on $PMMA_{15}\text{-ran-PHEMA}_{85}(\text{PMPC})_{\text{short}}$ bottlebrush brushes.

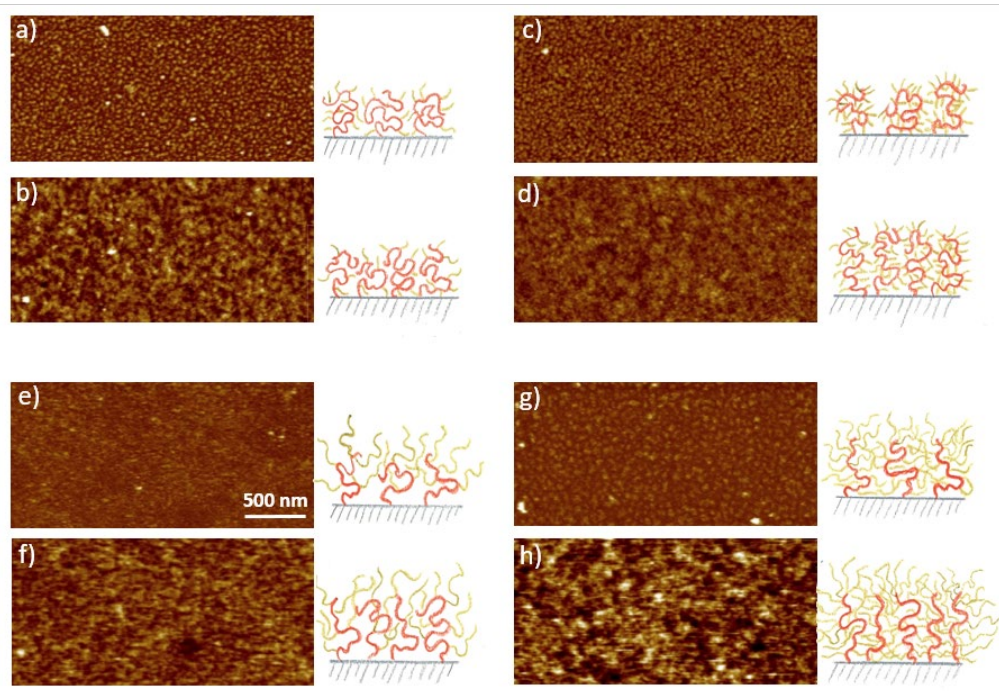


Figure 10. Peakforce AFM height micrographs recorded in HEPES solution on PMMA₇₅-ran-PHEMA₂₅(PMPC)_{short} graft-copolymer brushes with $\sigma = 0.04$ and 0.15 chains nm^{-2} (a, b); PMMA₁₅-ran-PHEMA₈₅(PMPC)_{short} bottlebrush brushes with $\sigma = 0.02$ and 0.25 chains nm^{-2} (c, d); PMMA₇₅-ran-PHEMA₂₅(PMPC)_{long} graft-copolymer brushes with $\sigma = 0.04$ and 0.15 chains nm^{-2} (e, f); PMMA₁₅-ran-PHEMA₈₅(PMPC)_{long} bottlebrush brushes with $\sigma = 0.02$ and 0.25 chains nm^{-2} (g, h).

In particular, RMS roughness values for for PMMA₇₅-ran-PHEMA₂₅(PMPC)_{short} was 2.7 ± 0.2 nm and 3.4 ± 0.6 nm, at 0.04 and 0.15 chains nm^{-2} , respectively, while PMMA₁₅-ran-PHEMA₈₅(PMPC)_{short} showed RMS roughness values of 1.8 ± 0.3 nm and 2.2 ± 0.5 nm, respectively at 0.02 and 0.25 chains nm^{-2} . The observed morphological differences between graft-copolymer and bottlebrush brushes could be explained by taking into consideration how the concentration of PMPC side chains determined the conformation of PMMA_x-ran-PHEMA_y(PMPC) branched brushes immobilized on the surface. Graft-copolymer brushes only show limited stretching from the substrate, implying a “collapsed” conformation that leads to rougher nanomorphologies. In contrast, the higher concentration of PMPC side segments induces a more marked expansion for the bottlebrush brushes, generating assemblies exposing a more uniform and swollen interface.

The nanomorphology of PMMA_x-ran-PHEMA_y(PMPC) brushes incorporating longer PMPC side chains could also be correlated with their molecular conformation.

PMMA₇₅-ran-PHEMA₂₅(PMPC)_{long} graft-copolymer brushes with a $\sigma = 0.04$ and 0.15 chains nm^{-2} were both characterized by a highly swollen polymer interface (RMS roughness = 1.2 ± 0.2 nm, and 4.1 ± 0.7 nm, respectively) (Figure 10e-f), which was presumably mainly

constituted by long, hydrophilic PMPC chains extending from the more hydrophobic and sparsely substituted PMMA₇₅-ran-PHEMA₂₅ backbones.

In contrast, PMMA₁₅-ran-PHEMA₈₅(PMPC)_{long} bottlebrush brushes still showed a structured nanomorphology, both at relatively low and high σ (RMS roughness = 1.5 ± 0.2 nm, and 7.1 ± 1.2 nm, respectively), where the densely substituted grafts stretch out from the underlying substrate and present a conformation that can be clearly resolved by AFM (Figure 10g-h).

4.2.3 Nanomechanical and nanotribological properties of PMMA_x-ran-PHEMATMS_y(PMPC) brushes

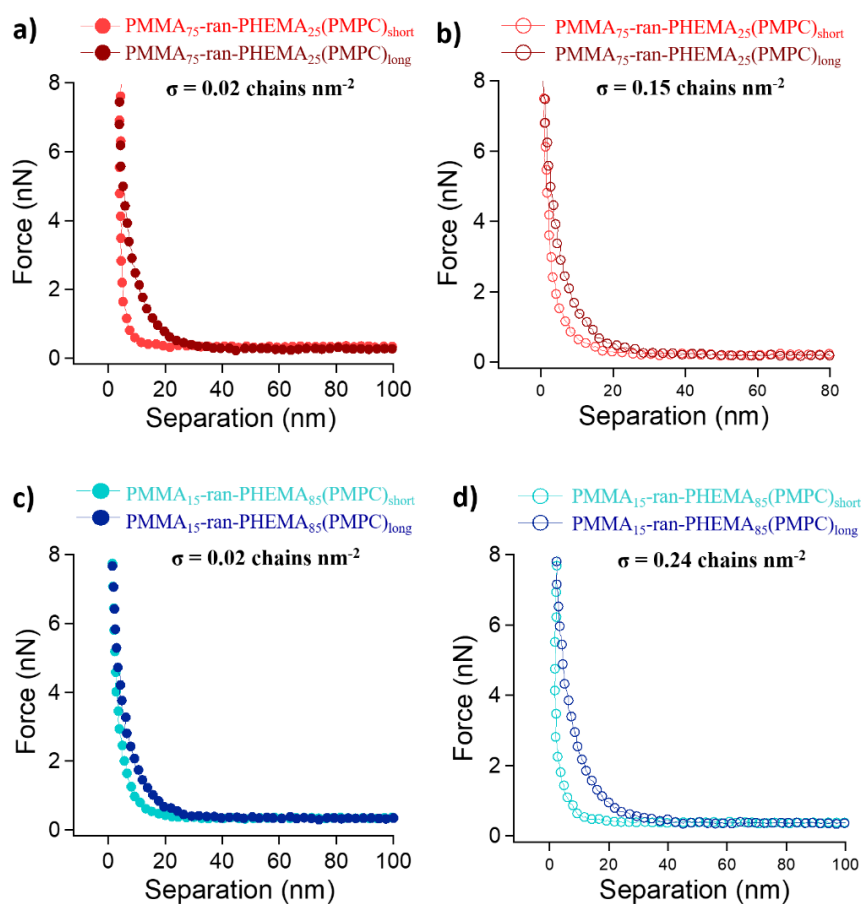


Figure 11. Approaching FS profiles recorded by AFM on PMMA_x-ran-PHEMATMS_y(PMPC) brushes presenting different branched architectures and grafting densities, immersed in HEPES solution.

The different morphologies and swelling properties of the branched-brush architectures were additionally highlighted by analysing the FS profiles recorded by AFM (Figure 11). Both in the cases of graft-copolymer and bottlebrush brushes, the increment in PMPC side-chain length was mirrored by a general increase in the values of separation at which repulsive

interactions are recorded. This phenomenon was due to the higher swollen thickness and increased steric stabilization by branched brushes presenting long PMPC segments, when compared to short-side chain-bearing analogues. No adhesion forces were recorded on the studied films (Figure 12), demonstrating that the content of highly hydrophilic PMPC at the film interface was in all cases sufficient to mask the rather hydrophobic brush backbones.

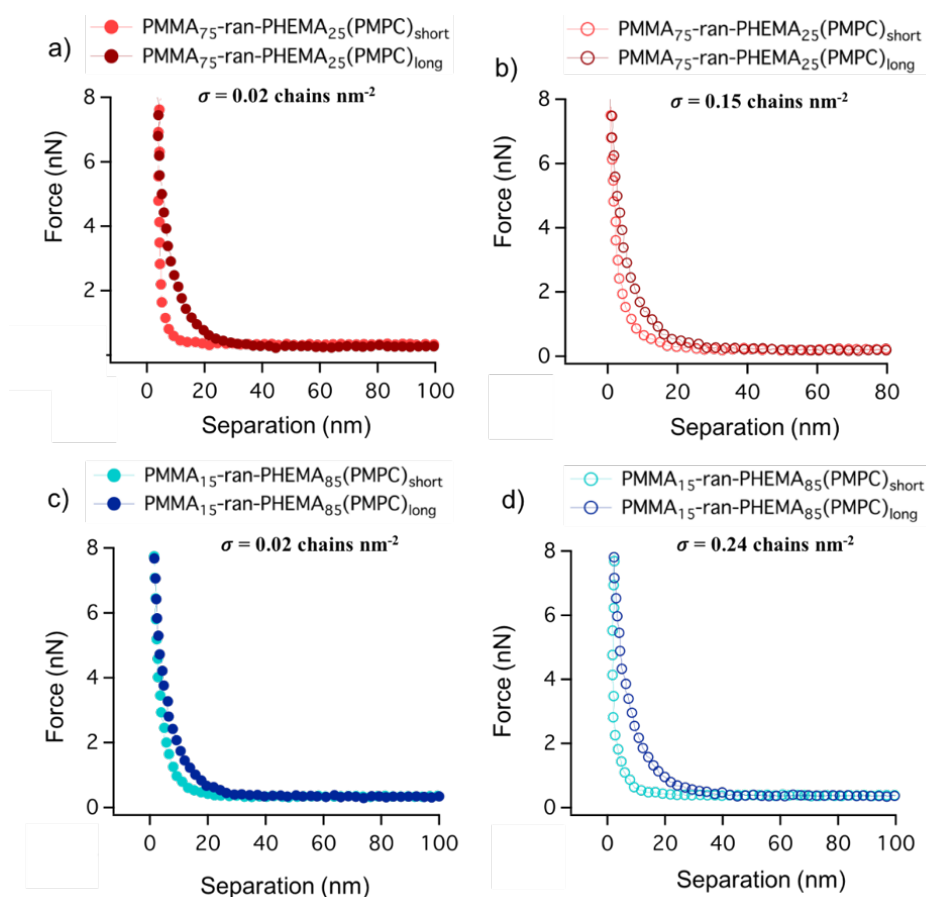


Figure 12. FS retraction profiles recorded in HEPES solution by AFM on $PMMA_x$ -ran- $PHEMA_y$ (PMPC) brushes presenting different branched architectures and grafting densities.

Having established how polymer architecture determined the interfacial physicochemical properties and morphology of branched brushes, we subsequently analysed their nanotribological properties by LFM.

As highlighted in Figure 13a-b, where F_L profiles recorded on the different brush types are compared, graft-copolymer and bottlebrush brushes presenting relatively short side PMPC chains generally showed significantly higher friction compared to analogous branched brushes featuring longer side segments.

The presence of longer, highly lubricating PMPC chains was thus identified as a prerequisite to attain low friction when the branched-brush surfaces are sheared against the AFM colloidal probe.

The contribution of PMPC could be further demonstrated by comparing the lubricating properties of PMMA₇₅-ran-PHEMA₂₅(PMPC) graft-copolymer brushes containing long PMPC segments and different surface coverages. In Figure 13c the F_L profiles recorded on PMMA₇₅-ran-PHEMA₂₅(PMPC)_{long} graft-copolymer brushes with different σ values are reported, while the resulting values of μ as a function of σ and the relative amount of PMPC within the films are plotted in Figure 13d.

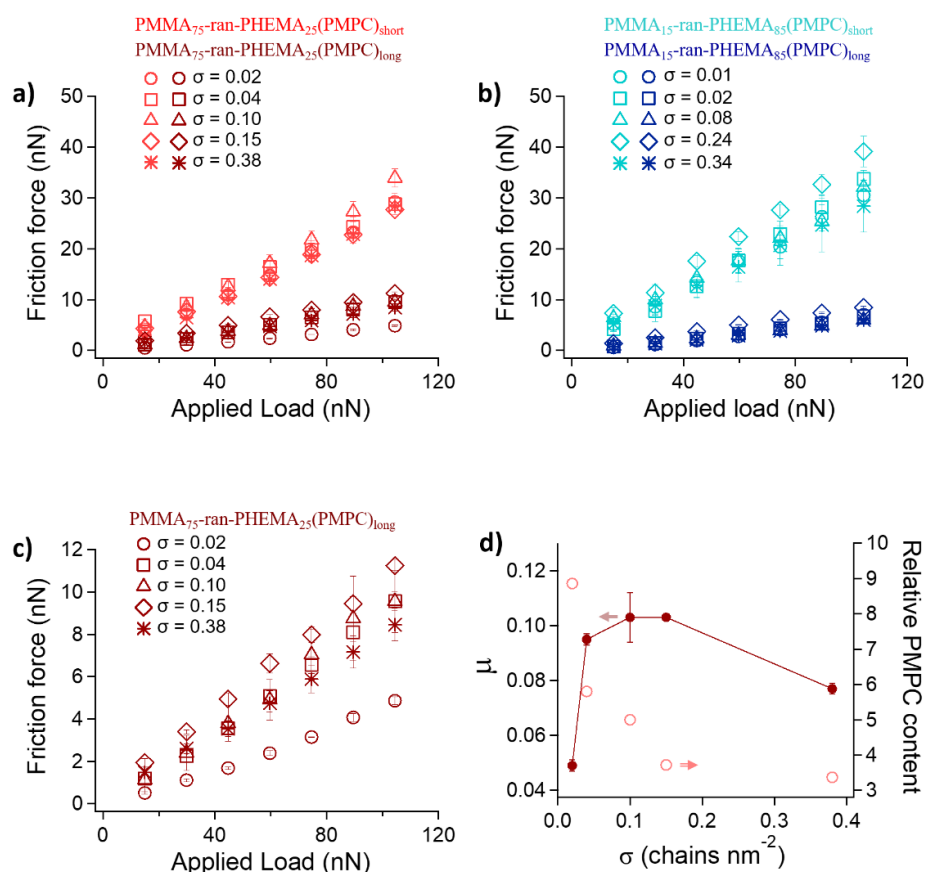


Figure 13. F_L profiles recorded by LFM on graft-copolymer brushes (a) and bottlebrush brushes (b). A detailed comparison of the F_L profiles recorded on graft-copolymer brushes with long PMPC side chains featuring different surface coverages is reported in (c). Variation of μ as a function of σ and the relative PMPC content for graft-copolymer brushes featuring long PMPC side chains (d).

The most lubricious graft-copolymer brushes showed a $\mu = 0.05$, and corresponded to those with the lowest value of σ , from which the highest amount of PMPC could be grafted following the second SI-ATRP step. The decrease in the relative amount of PMPC within the graft-copolymer brushes, which followed the simultaneous increment in σ , was accompanied by an increase in friction, with μ reaching a nearly constant value ~ 0.1 on PMMA₇₅-ran-PHEMA₂₅(PMPC)_{long} with σ included between 0.04 and 0.15 chains nm⁻².

Interestingly, a slight but significant decrease in friction was observed on dense graft-copolymer brushes ($\sigma = 0.38$ chains nm⁻²), which presented a μ of 0.08, demonstrating how the

enhancement of the osmotic barrier exerted by branched brushes with high surface coverage could partially compensate for the lower content of PMPC in determining their lubrication properties.

It is also important to mention that the nanotribological properties of graft-copolymer and bottlebrush brushes could be additionally influenced by the formation of crosslinks generated through radical recombination between propagating side PMPC chains. In particular, the formation of a covalent network would lead to an increment in friction, and a simultaneous decrease in brush swelling.¹⁰ Although crosslinking between grafts and its effect on their interfacial properties cannot be completely ruled out, this phenomenon would be likely to become more evident by increasing the density of macroinitiators at the surface, i.e. by incrementing the probability for neighbouring grafts to irreversibly recombine. However, our results showed that crowding of branched chains at the surface rather led to an enhancement of lubricity and steric stabilization (highlighted by recording FS profiles), suggesting how possible crosslinking reactions, even if they occurred to a significant extent, did not represent the main determinant for the interfacial physicochemical properties of the films.

A comparative analysis of the recorded values of μ as a function of σ for all the different films studied further enabled us to gain a general view of the influence of brush architecture on nanotribological properties (Figure 14).

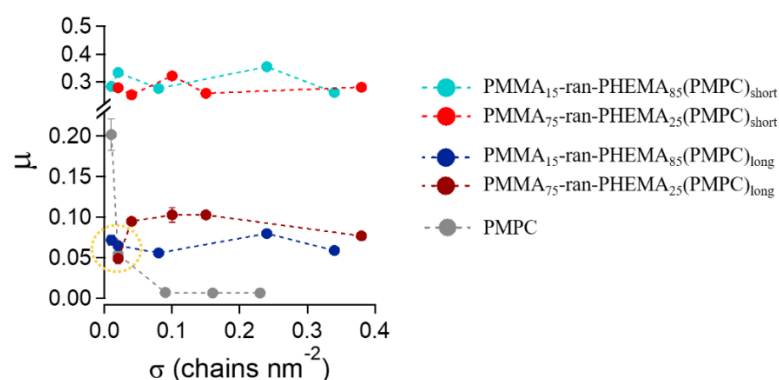


Figure 14. Variation of μ as a function of σ for the different brush architectures studied.

Remarkably, at relatively low surface coverages, linear, graft-copolymer and bottlebrush brushes showed very similar values of μ , while at higher grafting densities the effect of brush architecture led to a different nanotribological behavior among the studied films.

The lubricious character of branched brushes with $0.01 < \sigma < 0.04$ chains nm⁻² thus seemed mainly due to the highly swollen, linear PMPC chains extending from the surface and constituting a swollen polymer interface that is morphologically similar to that generated by loosely grafted linear PMPC brushes.

4.2.4 Comparison of linear PMPC brushes and PMMA₇₅-ran-PHEMATMS₂₅(PMPC)_{long} graft-copolymer brushes

The low-surface-coverage graft-copolymer brushes featuring PMPC side chains of relatively high molecular weight might be expected to adopt a conformation in which the sparsely substituted, hydrophobic backbones tend to shrink towards the underlying substrates, whilst the long PMPC segments stretch towards the interface.^{9, 50} In this configuration, the interface of the films would be mainly constituted of linear PMPC chains and provide surface properties analogous to those displayed by surface-grafted PMPC brushes. This view could be confirmed when the nanomorphology, steric stabilization and nanotribological properties of PMMA₇₅-ran-PHEMA₂₅(PMPC)_{long} graft-copolymer were compared with those PMPC brushes with $\sigma = 0.02$ chains nm⁻² (Figure 15).

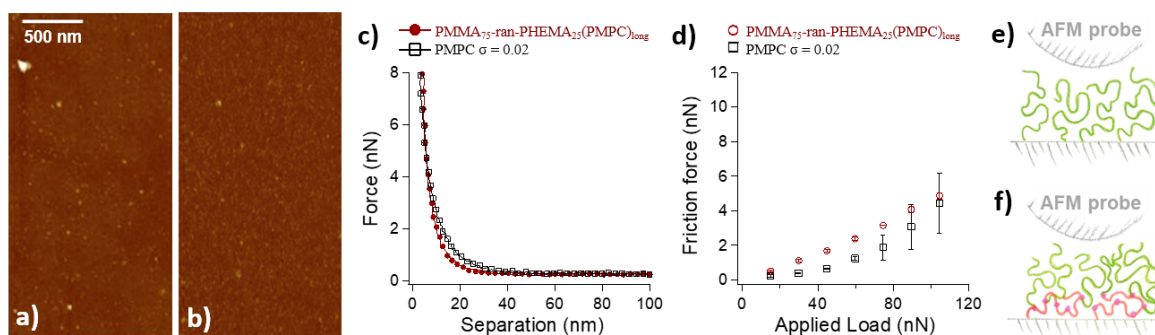


Figure 15. Peakforce AFM height micrographs recorded in HEPES solution on linear PMPC brushes (a) and PMMA₇₅-ran-PHEMA₂₅(PMPC)_{long} graft-copolymer brushes (b) with $\sigma = 0.02$ chains nm⁻². Approaching FS profiles recorded by AFM in HEPES solution on the same brush films (c). F_fL profiles recorded in HEPES solution by LFM on the two different brush structures (d). Schematics depicting the proposed morphology of linear PMPC brushes (e) and graft copolymer brushes (f) immersed in the aqueous medium.

As illustrated in Figure 15a-b, both graft-copolymer and linear brushes formed a uniform and swollen polymer interface, characteristic of assemblies of PMPC chains making up the exposed surface of the films. Moreover, the FS curves recorded on these two brush types demonstrated a very similar repulsive behavior towards the compressing AFM probe and comparable swelling, while their F_fL profiles showed an analogous lubricious character under shear.

The conformation of graft-copolymer brushes with a low σ is thus reminiscent of that assumed by structurally similar graft-copolymer-based adsorbates featuring a surface-interacting backbone and hydrophilic side chains, deposited on flat substrates from highly diluted solutions (Figure 15f).⁵¹⁻⁵² As previously reported in several experimental studies, these

copolymer species can be used to fabricate linear-polymer-brush interfaces when their backbones have sufficient affinity towards the substrate. In particular, graft-copolymers including a long side chain every 3-4 monomer units lie down on the substrate via their surface-interacting backbone, while their side segments stretch out to form a linear brush. A transition from a lying-down to a standing-up conformation can be attained via molecular-crowding effects, if the solution concentration of graft-copolymer adsorbates near the surface is increased above a certain threshold.^{50, 53-54}

In a similar way, when graft-copolymers are synthesized by grafting-from, and thus they are immobilized onto a surface via one chain end on their backbone, their conformation depends on surface crowding. For relatively low values of σ , and when the copolymer backbone presents sufficient affinity towards the underlying surface (as in the case of PMMA-based backbones and alkyl-carboxylate-bearing monolayers immersed in the aqueous medium) the branched macromolecules tend to lie down at the substrate, exposing their hydrophilic side chains and forming a linear brush at the interface.

From the general comparison of the nanotribological properties among the different brush architectures studied, the unique lubricity of linear PMPC brushes becomes especially clear, in particular when $\sigma \geq 0.1$ chains nm^{-2} . As showed in Figure 14, linear brushes always presented the most lubricious surfaces, the μ values measured on them being five times lower than those recorded on bottlebrush brushes, and nearly an order of magnitude lower than those characteristic of graft-copolymer films.

The surface concentration of highly hydrated PMPC segments emerged as a critical parameter regulating the lubricious character of graft-copolymer and bottlebrush brushes featuring relatively long side chains. In particular, this study revealed that graft-copolymer brushes present an insufficient concentration of PMPC segments to form a densely grafted and hydrated polymer interface capable of generating very low values of μ . In contrast, the high degree of substitution characteristic of bottlebrush brushes guarantees enough coverage of PMPC chains to attain values of μ as low as 0.05. Nevertheless, the lubricity of dense, linear PMPC brushes was in all cases superior.

This result agrees well to the nanotribological behavior of non-ionic polymer brushes featuring different architectures. In particular, by comparing the results of several distinct studies focusing on the nanotribological properties of compositionally similar but structurally diverse brushes, linear poly(ethylene glycol) (PEG) grafts^{9, 12, 50, 55-57} showed a significantly more pronounced lubricity when compared to that observed on bottlebrush brushes featuring PEG side chains.^{41, 47, 49}

Hence, although synthetic bottlebrushes, which mimic the structure of natural lubricating macromolecules such as lubricin,³¹⁻³³ have been identified in several studies as being extremely effective boundary lubricants,^{28,29} once covalently grafted onto surfaces they do not necessarily reduce friction as efficiently as the simplest linear brushes.

4.3 Conclusions

A comparison of the morphological, nanomechanical and nanotribological characteristics of linear PMPC brushes with those of graft-copolymer and bottlebrush brushes featuring PMPC side chains illustrates the relationship between polymer architecture and interfacial properties within grafted-from polymer assemblies.

SI-ATRP enabled the synthesis of a variety of branched brush architectures through multiple polymerization steps, including graft-copolymer brushes, with a relatively low concentration of side chains, and densely substituted bottlebrush brushes. For graft-copolymer, bottlebrush and linear brushes, the surface coverage was varied by diluting ATRP initiator functions within catechol-based monolayers assembled on TiO₂.

The length of the PMPC side chains on both graft-copolymer and bottlebrush brushes could be tuned by varying the polymerization conditions, and was additionally dependent on the surface grafting density of multifunctional macroinitiator brushes, a parameter that determined the steric hindrance encountered by the side segments during their growth.

Under the appropriate conditions, long PMPC side segments could be synthesized from loosely grafted macroinitiators, forming graft-copolymer and bottlebrush brushes mainly featuring linear PMPC chains at the interface. As a consequence, the interfacial physicochemical properties of these films were analogous to those displayed by low-density linear PMPC brushes.

The relative content of PMPC grafted from macroinitiator brushes decreased following the increment in their surface density, in a similar way for graft-copolymer and the more substituted bottlebrush brushes, due to crowding effects during the confined polymerization. Simultaneously, for $\sigma > 0.1$ chains nm⁻² the effect of branched-polymer-brush architecture on the nanotribological properties of the films clearly emerged. At relatively high surface coverages, linear PMPC brushes demonstrated the most lubricious films, reaching values of μ that approximated 10⁻⁴. Bottlebrush brushes showed comparatively higher friction, although the high concentration of hydrophilic PMPC side chains along each surface-grafted backbone

provided a significant improvement in lubrication with respect to the more sparsely substituted graft-copolymer-brush counterparts.

Overall, this study highlights how the relative content and density of hydrophilic polymer grafts chiefly determine the interfacial properties of linear and branched brushes. In the latter case, these two parameters can be adjusted by varying the side-chain concentration along the brush backbones. However, the simplest, linear brush design proved to be the most effective in reducing friction, reaching values of μ comparable to those observed within physiological lubricating systems, such as the articular cartilage of mammals.

4.4 Materials and Methods

Materials

Dopamine hydrochloride (Sigma-Aldrich), sodium nitrate (Sigma-Aldrich), sulfuric acid (Sigma-Aldrich), dichloromethane 99.8% extra dry (DCM; Acros organics), 2-bromoisobutyryl bromide (BiBB; Sigma-Aldrich), Propionyl bromide (PB; abcr GmbH), triethylamine (Sigma-Aldrich), 2-Methacryloyloxyethyl phosphorylcholine (MPC, 97%, Aldrich). 2,2'-bipyridyl (bipy, 99%, Aldrich), 4,4'-Dinonyl-2,2'-dipyridyl (dNbipy, 97%, Aldrich), potassium fluoride (KF, 99%, spray-dried, Aldrich), tetrabutylammonium fluoride (TBAF, 1M solution in THF, Aldrich) and tributyltin hydride (97%, Aldrich) were used without any additional purification, methyl methacrylate (MMA, 99%, Aldrich) and 2-(trimethylsilyloxy)ethyl methacrylate (HEMA-TMS, Scientific Polymer Products, Inc.) were passed through an alumina column to remove hydroquinone inhibitors prior to use, copper(I) Bromide (CuBr, Sigma-Aldrich) was purified by stirring in glacial acetic acid overnight, it was subsequently filtered and washed with methanol and diethyl ether. Nitrodopamine (ND) was synthesized according to the literature procedure.⁵⁸⁻⁵⁹ All the solvents were used as received.

Deposition of initiators on TiO₂

Silicon wafers (P/B<100), Si-Mat Silicon Wafers, Germany) were coated with 17 nm of TiO₂ by reactive magnetron sputtering (PSI Villigen, Switzerland). The TiO₂-coated substrates were subsequently cut into 1.5 × 1 cm² samples and sonicated twice for 10 min in toluene, twice for 10 min in isopropanol, and finally treated with UV-ozone for 30 min. ND assemblies were deposited by incubating the substrates overnight in a 0.05 M ND aqueous solution. Self-assembled monolayers (SAMs) featuring a different coverage of ATRP initiator were formed by incubating ND-functionalized TiO₂ substrates in 0.12 M mixed solutions of 2-bromoisobutyryl bromide (BiBB) and propionyl bromide (PB), and 0.12 M triethylamine. The

relative concentration of BiBB within the mixtures was varied, obtaining 1 mol%, 10 mol%, 40 mol%, 70 mol% and 100 mol% of initiator functions at the surface.

Synthesis of Linear PMPC brushes

A solution containing 16 mL of methanol, MPC (5g, 16.7 mmol, 1M) and bipy (114.6 mg, 0.73 mmol, 46 mM) was deoxygenated by bubbling Ar for 30 minutes. Later on, this was transferred to a flask containing CuBr (42 mg, 0.29 mmol, 18.3 mM) and CuBr₂ (16.4 mg, 0.07 mmol, 4.6 mM), which was kept under Ar. Following the formation of the Cu complex, the solution was transferred via a deoxygenated syringe into a flask containing the ATRP initiator-bearing substrates, and EBiB (5 μ L, 0.034 mmol) was added as sacrificial solution initiator. After 30 minutes of reaction, the samples were taken out and rinsed with water and ethanol thoroughly. The solution was collected, and PMPC was obtained by re-precipitation in cold THF.

Synthesis of PMMA_x-ran-PHEMATMS_y brushes

PMMA_x-ran-PHEMATMS_y brushes featuring different relative concentration of MMA and HEMATMS were grafted from initiator-modified TiO₂ surfaces by SI-ATRP. The synthesis of PMMA₇₅-ran-PHEMATMS₂₅ brushes is hereby exemplarily reported. HEMATMS (9 mL, 0.04 mol), MMA (18 mL, 0.16 mol), dNbipy (0.183 g, 0.45 mmol) and anisole (15 mL) were mixed in a 100 mL flask and deoxygenated by Ar bubbling for 30 minutes. The solution was subsequently transferred via a deoxygenated syringe to a flask containing CuBr (25.8 mg, 0.18 mmol) and CuBr₂ (9.69 mg, 0.043 mmol), which was kept under Ar. Sacrificial initiator EBiB (30 μ L, 0.2 mmol) was added to the reaction mixture just before this was transferred to the flask containing initiator-modified substrates. The reaction was conducted at 80°C and after the desired time the samples were taken out and rinsed with chloroform thoroughly.

PMMA₁₅-ran-PHEMATMS₈₅ brushes are synthesized through a similar procedure but using a different relative concentration of MMA and HEMATMS. Namely, the following reaction mixture was applied: HEMATMS (36 mL, 0.16 mol), MMA (4.5 mL, 0.04 mol), dNbipy (0.255 g, 0.62 mmol), anisole (18 mL), CuBr (36 mg, 0.25 mmol) and CuBr₂ (14 mg, 0.06 mmol). The copolymer synthesized by sacrificial initiator in solution was characterized by ¹HNMR (Figure 6) and SEC (Figure 5), providing M_n = 72 kDa and PDI = 1.33.

Synthesis of PMMA_x-ran-PHEMABr_y brushes

The procedure for the synthesis of PMMA₇₅-ran-PHEMABr₂₅ brushes is exemplarily reported. Substrates bearing PMMA₇₅-ran-PHEMATMS₂₅ brushes were placed in a flask containing a 0.05 M solution of 2,6-di-tert-butylphenol and KF in 10 mL of dry THF, the flask was flushed with Ar before adding 10 mL dry THF. The reaction flask was later on put in an

ice bath and 0.05 mL of a 1 M solution of tetrabutylammonium fluoride in THF was added. After this, 0.62 mL of 2-bromoisobutyryl bromide (5 mmol) were added dropwise to the mixture and the reaction was carried out overnight. The successful deprotection of HEMATMS functions along PMMA_x-ran-PHEMATMS_y brushes and the incorporation of ATRP initiator moieties was confirmed by FTIR and VASE (Figure 7-8 and Table 3-6).

Synthesis of PMMA_x-ran-PHEMA_y(PMPC)_z brushes

The synthesis of PMMA₇₅-ran-PHEMA₂₅(PMPC)_{long} graft-copolymer brushes is exemplarily reported. A solution containing 16 mL of methanol, MPC (5g, 16.7 mmol, 1M), bipy (114.6 mg, 0.73 mmol, 46 mM), and CuBr₂ (16.4 mg, 0.07 mmol, 4.6 mM) was deoxygenated by bubbling Ar for 30 min. After that, CuBr (42 mg, 0.29 mmol, 18.3 mM) was added and the reaction mixture was subsequently transferred to a flask containing PMMA₇₅-ran-PHEMABr₂₅ brush-bearing TiO₂ substrates. After 30 min of reaction, the samples were taken out, copiously rinsed with water and ethanol and finally dried under a stream of N₂.

The length of PMPC side chains was controlled by varying the amount CuBr₂-based deactivator during grafting. This was set to 20 and 30 mol% with respect to CuBr, respectively for “long” and “short” PMPC side chains.

Nuclear magnetic resonance (¹H-NMR)

¹H-NMR spectra were recorded on a Bruker Avance III 500 MHz spectrometer at room temperature using D₂O or CDCl₃ as solvents.

Size exclusion chromatography (SEC)

The values of M_n and M_w of PMPC samples were determined using an Agilent 1100 size exclusion chromatography (SEC) unit equipped with two PFG linear M columns (PSS) connected in series with an Agilent 1100 VWD/UV detector operated at 290 nm, a DAWN HELEOS 8 multi-angle laser-light-scattering (MALS) detector (Wyatt Technology Europe) followed by an Optilab T-rEX RI detector from Wyatt. Samples were eluted in hexafluoroisopropanol (HFIP) with 0.02 M K-TFAc at 1 mL min⁻¹ at room temperature. The values of M_n and M_w of PMMA_x-ran-PHEMATMS_y were obtained using a Malvern Viskotek PL- GPC 220 equipped with a 2 × PL-Gel Mix-B columns, and with refractive index (RI), viscosity and light scattering (LS; 15° angle) detectors. The samples were eluted using DMF with LiBr (1 g L⁻¹) at a rate of 1 mL min⁻¹, and at a temperature of 45°C.

Variable angle spectroscopic ellipsometry (VASE)

The values of dry thickness of the different brush films (T_{dry}) were measured using a M-2000F Woollam variable angle spectroscopic ellipsometer (J.A. Woollam Co. U.S.). The values of Ψ and Δ were acquired as a function of wavelength (350-800 nm) using focusing

lenses at 70° from the surface normal. Fitting of the raw data was performed based on a four-layers model, using bulk dielectric functions for Si, SiO₂ and TiO₂. The polymer brush layers were analyzed on the basis of the Cauchy model: $n = A + B \lambda^{-2}$, where n is the refractive index, λ is the wavelength and A and B were assumed to be 1.45 and 0.01, respectively, as values for transparent organic films.

Atomic force microscopy (AFM)

Force-vs-separation (FS) analysis and lateral force microscopy (LFM) on the different brush films was performed using a MFP3D AFM (Asylum Research, Oxford Instruments, Santa Barbara, USA) under 10 mM of 4-(2-hydroxyethyl)-1-piperazine-1-ethane-sulfonic acid (HEPES) buffer (pH = 7.4). The normal (K_N) and torsional spring (K_T) constants of tipless cantilevers (CSC38-A, Mikromasch, Bulgaria) were measured by the thermal-noise⁶⁰ and Sader's⁶¹ method, respectively, resulting $K_N = 0.259 \text{ N m}^{-1}$ and $K_T = 4.1\text{E}^{-9} \text{ N m}$. Silica microspheres (EKA Chemicals AM, Kormasil) having a diameter of 22 μm were glued to the end of the calibrated cantilevers by a home-built micromanipulator, using an epoxy glue (Araldite® Standard). The calibration of the friction force was carried out by using the "wall method", which was described by Cannara et al.⁶² The cantilevers were cleaned by UV-ozone treatment for 30 min prior to the measurements.

Friction values were obtained by averaging 10 "friction loops" recorded on each brush surface over three different positions for each sample. The friction loops were acquired by laterally scanning over a line on each brush film at a given applied normal load. A scanning distance of 1.5 μm and a scanning rate of 1 Hz were applied during the measurements. The values of coefficient of friction (μ) were obtained from the slope of the recorded friction force-vs-applied load (F_f/L) profiles, assuming the Amonton's law of friction: $F_f = \mu L$.

The nanomechanical properties of the different brush films were analyzed by recording approximately 20 FS profiles over three different positions on each sample. A Z-piezo distance of 500 nm and a ramping rate of 1 Hz was used to acquire the FS profiles.

The nanomorphology of the brush films in dry and under aqueous media was investigated by using a Dimension Icon AFM (Bruker Corporation). For imaging in dry conditions, tapping mode was used by selecting a cantilever having a nominal spring constant of 26 N m^{-1} (OMCL-AC240TS-R3, Olympus). For the imaging in liquid, cantilevers having a nominal spring constant 0.7 N m^{-1} (Scanasyt-Fluid+, Bruker AFM Probes) were used in PeakForce Tapping mode.

References

1. Klein, J.; Kamiyama, Y.; Yoshizawa, H.; Israelachvili, J. N.; Fredrickson, G. H.; Pincus, P.; Fetters, L. J., Lubrication Forces between Surfaces Bearing Polymer Brushes. *Macromolecules* 1993, 26 (21), 5552-5560.
2. Klein, J., Shear, friction, and lubrication forces between polymer-bearing surfaces. *Annu. Rev. Mater. Sci.* 1996, 26, 581-612.
3. Klein, J.; Kumacheva, E.; Mahalu, D.; Perahia, D.; Fetters, L. J., Reduction of Frictional Forces between Solid-Surfaces Bearing Polymer Brushes. *Nature* 1994, 370 (6491), 634-636.
4. Briscoe, W. H.; Titmuss, S.; Tiberg, F.; Thomas, R. K.; McGillivray, D. J.; Klein, J., Boundary lubrication under water. *Nature* 2006, 444 (7116), 191-194.
5. Raviv, U.; Giasson, S.; Kampf, N.; Gohy, J. F.; Jerome, R.; Klein, J., Lubrication by charged polymers. *Nature* 2003, 425 (6954), 163-165.
6. Grest, G. S., Normal and shear forces between polymer brushes. *Adv. Polym. Sci.* 1999, 138, 149-183.
7. Grest, G. S., Interfacial sliding of polymer brushes: A molecular dynamics simulation. *Phys Rev Lett* 1996, 76 (26), 4979-4982.
8. Lee, S.; Spencer, N. D., Materials science - Sweet, hairy, soft, and slippery. *Science* 2008, 319 (5863), 575-576.
9. Morgese, G.; Verbraeken, B.; Ramakrishna, S. N.; Gombert, Y.; Cavalli, E.; Rosenboom, J. G.; Zenobi-Wong, M.; Spencer, N. D.; Hoogenboom, R.; Benetti, E. M., Chemical Design of Non-Ionic Polymer Brushes as Biointerfaces: Poly(2-oxazine)s Outperform Both Poly(2-oxazoline)s and PEG. *Angew. Chem. Int. Edit.* 2018, 57 (36), 11667-11672.
10. Li, A.; Benetti, E. M.; Tranchida, D.; Clasohm, J. N.; Schonherr, H.; Spencer, N. D., Surface-Grafted, Covalently Cross-Linked Hydrogel Brushes with Tunable Interfacial and Bulk Properties. *Macromolecules* 2011, 44 (13), 5344-5351.
11. Perry, S. S.; Yan, X. P.; Limpoco, F. T.; Lee, S.; Muller, M.; Spencer, N. D., Tribological Properties of Poly(L-lysine)-graft-poly(ethylene glycol) Films: Influence of Polymer Architecture and Adsorbed Conformation. *ACS Appl. Mater. Interfaces* 2009, 1 (6), 1224-1230.

12. Lee, S.; Muller, M.; Ratoi-Salagean, M.; Voros, J.; Pasche, S.; De Paul, S. M.; Spikes, H. A.; Textor, M.; Spencer, N. D., Boundary lubrication of oxide surfaces by Poly(L-lysine)-g-poly(ethylene glycol) (PLL-g-PEG) in aqueous media. *Tribol. Lett.* 2003, 15 (3), 231-239.
13. Ishihara, K.; Ueda, T.; Nakabayashi, N., Preparation of Phospholipid Polymers and Their Properties as Polymer Hydrogel Membranes. *Polym. J.* 1990, 22 (5), 355-360.
14. Chen, M.; Briscoe, W. H.; Armes, S. P.; Klein, J., Lubrication at Physiological Pressures by Polyzwitterionic Brushes. *Science* 2009, 323 (5922), 1698-1701.
15. Zhang, Z. Y.; Moxey, M.; Alswieleh, A.; Morse, A. J.; Lewis, A. L.; Geoghegan, M.; Leggett, G. J., Effect of Salt on Phosphorylcholine-based Zwitterionic Polymer Brushes. *Langmuir* 2016, 32 (20), 5048-5057.
16. Zhang, Z. Y.; Morse, A. J.; Armes, S. P.; Lewis, A. L.; Geoghegan, M.; Leggett, G. J., Nanoscale Contact Mechanics of Biocompatible Polyzwitterionic Brushes. *Langmuir* 2013, 29 (34), 10684-10692.
17. Zhang, Z. Y.; Morse, A. J.; Armes, S. P.; Lewis, A. L.; Geoghegan, M.; Leggett, G. J., Effect of Brush Thickness and Solvent Composition on the Friction Force Response of Poly(2-(methacryloyloxy)ethylphosphorylcholine) Brushes. *Langmuir* 2011, 27 (6), 2514-2521.
18. Kobayashi, M.; Terayama, Y.; Hosaka, N.; Kaido, M.; Suzuki, A.; Yamada, N.; Torikai, N.; Ishihara, K.; Takahara, A., Friction behavior of high-density poly(2-methacryloyloxyethyl phosphorylcholine) brush in aqueous media. *Soft Matter* 2007, 3 (6), 740-746.
19. Jiang, S. Y.; Cao, Z. Q., Ultralow-Fouling, Functionalizable, and Hydrolyzable Zwitterionic Materials and Their Derivatives for Biological Applications. *Adv. Mater.* 2010, 22 (9), 920-932.
20. Zhang, Z.; Chao, T.; Chen, S. F.; Jiang, S. Y., Superlow fouling sulfobetaine and carboxybetaine polymers on glass slides. *Langmuir* 2006, 22 (24), 10072-10077.
21. Yu, Y.; Vancso, G. J.; de Beer, S., Substantially enhanced stability against degrafting of zwitterionic PMPC brushes by utilizing PGMA-linked initiators. *Eur. Polym. J.* 2017, 89, 221-229.
22. Zoppe, J. O.; Ataman, N. C.; Mocny, P.; Wang, J.; Moraes, J.; Klok, H. A., Surface-Initiated Controlled Radical Polymerization: State-of-the-Art, Opportunities, and Challenges in Surface and Interface Engineering with Polymer Brushes (vol 117, pg 1105, 2017). *Chem. Rev.* 2017, 117 (5), 4667-4667.
23. Kobayashi, M.; Terayama, Y.; Kikuchi, M.; Takahara, A., Chain dimensions and surface characterization of superhydrophilic polymer brushes with zwitterion side groups. *Soft Matter* 2013, 9 (21), 5138-5148.

24. Kobayashi, M.; Terayama, Y.; Yamaguchi, H.; Terada, M.; Murakami, D.; Ishihara, K.; Takahara, A., Wettability and Antifouling Behavior on the Surfaces of Superhydrophilic Polymer Brushes. *Langmuir* 2012, 28 (18), 7212-7222.
25. Feng, W.; Brash, J.; Zhu, S. P., Atom-transfer radical grafting polymerization of 2-methacryloyloxyethyl phosphorylcholine from silicon wafer surfaces. *J Polym Sci Pol Chem* 2004, 42 (12), 2931-2942.
26. Feng, W.; Zhu, S. P.; Ishihara, K.; Brash, J. L., Adsorption of fibrinogen and lysozyme on silicon grafted with poly(2-methacryloyloxyethyl phosphorylcholine) via surface-initiated atom transfer radical polymerization. *Langmuir* 2005, 21 (13), 5980-5987.
27. Feng, W.; Brash, J. L.; Zhu, S. P., Non-biofouling materials prepared by atom transfer radical polymerization grafting of 2-methacryloyloxyethyl phosphorylcholine: Separate effects of graft density and chain length on protein repulsion. *Biomaterials* 2006, 27 (6), 847-855.
28. Kang, T.; Banquy, X.; Heo, J. H.; Lim, C. N.; Lynd, N. A.; Lundberg, P.; Oh, D. X.; Lee, H. K.; Hong, Y. K.; Hwang, D. S.; Waite, J. H.; Israelachvili, J. N.; Hawker, C. J., Mussel-Inspired Anchoring of Polymer Loops That Provide Superior Surface Lubrication and Antifouling Properties. *ACS Nano* 2016, 10 (1), 930-937.
29. Banquy, X.; Burdyska, J.; Lee, D. W.; Matyjaszewski, K.; Israelachvili, J., Bioinspired Bottle-Brush Polymer Exhibits Low Friction and Amontons-like Behavior. *J. Am. Chem. Soc.* 2014, 136 (17), 6199-6202.
30. Seror, J.; Merkher, Y.; Kampf, N.; Collinson, L.; Day, A. J.; Maroudas, A.; Klein, J., Articular Cartilage Proteoglycans As Boundary Lubricants: Structure and Frictional Interaction of Surface-Attached Hyaluronan and Hyaluronan-Aggregan Complexes. *Biomacromolecules* 2011, 12 (10), 3432-3443.
31. Seror, J.; Merkher, Y.; Kampf, N.; Collinson, L.; Day, A. J.; Maroudas, A.; Klein, J., Normal and Shear Interactions between Hyaluronan-Aggregan Complexes Mimicking Possible Boundary Lubricants in Articular Cartilage in Synovial Joints. *Biomacromolecules* 2012, 13 (11), 3823-3832.
32. Schmidt, T. A.; Gastelum, N. S.; Nguyen, Q. T.; Schumacher, B. L.; Sah, R. L., Boundary lubrication of articular cartilage - Role of synovial fluid constituents. *Arthritis Rheum.* 2007, 56 (3), 882-891.
33. Bonnevie, E. D.; Galesso, D.; Secchieri, C.; Cohen, I.; Bonassar, L. J., Elastoviscous Transitions of Articular Cartilage Reveal a Mechanism of Synergy between Lubricin and Hyaluronic Acid. *Plos One* 2015, 10 (11).

34. Greene, G. W.; Banquy, X.; Lee, D. W.; Lowrey, D. D.; Yu, J.; Israelachvili, J. N., Adaptive mechanically controlled lubrication mechanism found in articular joints. *Proc. Natl. Acad. Sci. USA* 2011, 108 (13), 5255-5259.
35. Abubacker, S.; Ham, H. O.; Messersmith, P. B.; Schmidt, T. A., Cartilage boundary lubricating ability of aldehyde modified proteoglycan 4 (PRG4-CHO). *Osteoarthr. Cartilage* 2013, 21 (1), 186-189.
36. Matyjaszewski, K.; Miller, P. J.; Shukla, N.; Immaraporn, B.; Gelman, A.; Luokala, B. B.; Siclovan, T. M.; Kickelbick, G.; Vallant, T.; Hoffmann, H.; Pakula, T., Polymers at interfaces: Using atom transfer radical polymerization in the controlled growth of homopolymers and block copolymers from silicon surfaces in the absence of untethered sacrificial initiator. *Macromolecules* 1999, 32 (26), 8716-8724.
37. Matyjaszewski, K.; Xia, J. H., Atom transfer radical polymerization. *Chem. Rev.* 2001, 101 (9), 2921-2990.
38. Pyun, J.; Kowalewski, T.; Matyjaszewski, K., Synthesis of Polymer Brushes Using Atom Transfer Radical Polymerization. *Macromol. Rapid Commun.* 2003, 24, 1043-1059.
39. Lobb, E. J.; Ma, I.; Billingham, N. C.; Armes, S. P.; Lewis, A. L., Facile synthesis of well-defined, biocompatible phosphorylcholine-based methacrylate copolymers via atom transfer radical polymerization at 20 degrees C. *J. Am. Chem. Soc.* 2001, 123 (32), 7913-7914.
40. Marti, A.; Hahner, G.; Spencer, N. D., Sensitivity of frictional forces to pH on a nanometer scale: A lateral force microscopy study. *Langmuir* 1995, 11 (12), 4632-4635.
41. Gunnewiek, M. K.; Ramakrishna, S. N.; di Luca, A.; Vancso, G. J.; Moroni, L.; Benetti, E. M., Stem-Cell Clinging by a Thread: AFM Measure of Polymer-Brush Lateral Deformation. *Adv. Mater. Interfaces* 2016, 3 (3), 1500456.
42. Jones, D. M.; Brown, A. A.; Huck, W. T. S., Surface-initiated polymerizations in aqueous media: Effect of initiator density. *Langmuir* 2002, 18 (4), 1265-1269.
43. Sui, X. F.; Zapotoczny, S.; Benetti, E. M.; Memesa, M.; Hempenius, M. A.; Vancso, G. J., Grafting mixed responsive brushes of poly(N-isopropylacrylamide) and poly(methacrylic acid) from gold by selective initiation. *Polym. Chem.* 2011, 2 (4), 879-884.
44. Sui, X. F.; Chen, Q.; Hempenius, M. A.; Vancso, G. J., Probing the Collapse Dynamics of Poly(N-isopropylacrylamide) Brushes by AFM: Effects of Co-nonsolvency and Grafting Densities. *Small* 2011, 7 (10), 1440-1447.
45. Gillich, T.; Benetti, E. M.; Rakhmatullina, E.; Konradi, R.; Li, W.; Zhang, A.; Schluter, A. D.; Textor, M., Self-Assembly of Focal Point Oligo-catechol Ethylene Glycol Dendrons on

Titanium Oxide Surfaces: Adsorption Kinetics, Surface Characterization, and Nonfouling Properties. *J. Am. Chem. Soc.* 2011, 133 (28), 10940-10950.

46. Assuming a comparable reactivity of the acyl bromide groups in PB and BiBB towards the amino functions exposed at the APTES monolayer, the relative concentration of ATRP initiator moieties generated at the surface is comparable to that of BiBB within the applied PB/BiBB mixtures. Further surface characterization of the obtained mixed monolayers is provided in the Supporting Information.

47. Fantin, M.; Ramakrishna, S. N.; Yan, J. J.; Yan, W. Q.; Divandari, M.; Spencer, N. D.; Matyjaszewski, K.; Benetti, E. M., The Role of Cu(0) in Surface-Initiated Atom Transfer Radical Polymerization: Tuning Catalyst Dissolution for Tailoring Polymer Interfaces. *Macromolecules* 2018, 51 (17), 6825-6835.

48. Dehghani, E. S.; Du, Y. H.; Zhang, T.; Ramakrishna, S. N.; Spencer, N. D.; Jordan, R.; Benetti, E. M., Fabrication and Interfacial Properties of Polymer Brush Gradients by Surface-Initiated Cu(0)-Mediated Controlled Radical Polymerization. *Macromolecules* 2017, 50 (6), 2436-2446.

49. Divandari, M.; Dehghani, E. S.; Spencer, N. D.; Ramakrishna, S. N.; Benetti, E. M., Understanding the effect of hydrophobic protecting blocks on the stability and biopassivity of polymer brushes in aqueous environments: A Tiramisù for cell-culture applications. *Polymer* 2016, 98, 470-480.

50. Morgese, G.; Ramakrishna, S. N.; Simic, R.; Zenobi-Wong, M.; Benetti, E. M., Hairy and Slippery Polyoxazoline-Based Copolymers on Model and Cartilage Surfaces. *Biomacromolecules* 2018, 19 (2), 680-690.

51. Huang, N. P.; Michel, R.; Voros, J.; Textor, M.; Hofer, R.; Rossi, A.; Elbert, D. L.; Hubbell, J. A.; Spencer, N. D., Poly(L-lysine)-g-poly(ethylene glycol) layers on metal oxide surfaces: Surface-analytical characterization and resistance to serum and fibrinogen adsorption. *Langmuir* 2001, 17 (2), 489-498.

52. Kenausis, G. L.; Vörös, J.; Elbert, D. L.; Huang, N.; Hofer, R.; Ruiz-Taylor, L.; Textor, M.; Hubbell, J. A.; Spencer, N. D., Poly(L-lysine)-g-Poly(ethylene glycol) Layers on Metal Oxide Surfaces: Attachment Mechanism and Effects of Polymer Architecture on Resistance to Protein Adsorption†. *J. Phys. Chem. B* 2000, 104 (14), 3298-3309.

53. Bijelic, G.; Shovsky, A.; Varga, I.; Makuska, R.; Claesson, P. M., Adsorption characteristics of brush polyelectrolytes on silicon oxynitride revealed by dual polarization interferometry. *J. Colloid Interf. Sci.* 2010, 348 (1), 189-197.

54. Furusawa, H.; Sekine, T.; Ozeki, T., Hydration and Viscoelastic Properties of High- and Low-Density Polymer Brushes Using a Quartz-Crystal Microbalance Based on Admittance Analysis (QCM-A). *Macromolecules* 2016, 49 (9), 3463-3470.
55. Yan, X.; Perry, S. S.; Spencer, N. D.; Pasche, S.; De Paul, S. M.; Textor, M.; Lim, M. S., Reduction of Friction at Oxide Interfaces upon Polymer Adsorption from Aqueous Solutions. *Langmuir* 2004, 20 (2), 423-428.
56. Morgese, G.; Gombert, Y.; Ramakrishna, S. N.; Benetti, E. M., Mixing Poly(ethylene glycol) and Poly(2-alkyl-2-oxazoline)s Enhances Hydration and Viscoelasticity of Polymer Brushes and Determines Their Nanotribological and Antifouling Properties. *ACS Appl. Mater. Interfaces* 2018, 10 (48), 41839-41848.
57. Morgese, G.; Cavalli, E.; Rosenboom, J. G.; Zenobi-Wong, M.; Benetti, E. M., Cyclic Polymer Grafts That Lubricate and Protect Damaged Cartilage. *Angew. Chem. Int. Edit.* 2018, 57 (6), 1621-1626.
58. Inverarity, I. A.; Hulme, A. N. *Org. Biomol. Chem* 2007, 5 (4), 636-643.
59. Napolitano, A.; Dischia, M.; Costantini, C.; Prota, G. *Tetrahedron* 1992, 48 (39), 8515-8522.
60. Hutter, J. L.; Bechhoefer, J. *Rev. Sci. Instrum.* 1993, 64 (7), 1868-1873.
61. Green, C. P.; Lioe, H.; Cleveland, J. P.; Proksch, R.; Mulvaney, P.; Sader, J. E. *Rev. Sci. Instrum.* 2004, 75 (6), 1988-1996.
62. Cannara, R. J.; Eglin, M.; Carpick, R. W. *Rev. Sci. Instrum.* 2006, 77 (5).

Chapter 5

Translating Surface-Initiated Atom Transfer Radical Polymerization into Technology: The Mechanism of Cu⁰-Mediated SI-ATRP under Environmental Conditions*

The exceptional features of Cu⁰-mediated surface-initiated, atom-transfer radical polymerization (Cu⁰ SI-ATRP), and its potential for implementation in technologically relevant surface functionalizations are clearly demonstrated thanks to a comprehensive understanding of its mechanism. Cu⁰ SI-ATRP enables the synthesis of multifunctional polymer brushes with a remarkable degree of control, over extremely large areas and without the need for inert atmosphere or deoxygenation of monomer solutions. When a polymerization mixture is placed between a flat copper plate and an ATRP-initiator-functionalized substrate, the vertical distance between these two overlaying surfaces determines the tolerance of the grafting process towards the oxygen, while the composition of the polymerization solution emerges as the critical parameter regulating polymer-grafting kinetics. At very small distances between the copper plate and the initiating surfaces, the oxygen dissolved in the solution is rapidly consumed via oxidation of the metallic substrate. In the presence of ligand, copper species diffuse to the surface-immobilized initiators and trigger a rapid growth of polymer brushes. Concurrently, the presence and concentration of added Cu^{II} regulates the generation of Cu^I-based activators through comproportionation with Cu⁰. Hence, under oxygen-tolerant conditions, the extent of comproportionation, together with the solvent-dependent rate constant of activation (k_{act}) of ATRP are the main determinants of the growth rate of polymer brushes.

* Edmondo M. Benetti., Krzysztof Matyjaszewski and Nicholas D. Spencer supervised this project. Wenqing Yan and Marco Fantin performed experimental work. All the authors wrote the paper. Part of this Chapter was published in ACS Macro Lett. 2019. 87865-870.

5.1 Introduction

Interest in setting up robust methods for the controlled synthesis of polymer brushes by surface-initiated “living” polymerization techniques under environmental conditions has been recently rising.¹⁻⁴

Focusing on the most widely applied of such methods, surface-initiated, atom-transfer radical polymerization (SI-ATRP),⁵ the reaction mixtures typically require careful degassing prior to incubation on initiator-bearing supports, while the polymerization vessels need to be either appropriately sealed, or under oxygen-free conditions during the entire duration of the grafting process. Moreover, the technical difficulties in performing SI-ATRP with large reaction volumes, while maintaining the system under fully inert conditions, hamper the fabrication of polymer brushes from large substrates. Hence, it is clear that an approach that could overcome these major drawbacks would tremendously broaden the applicability of SI-ATRP and, more generally, of “grafted-from” polymer brushes in technologically relevant fabrications.

Previously reported oxygen-tolerant SI-ATRP processes have involved the application of reducing agents, which simultaneously consume oxygen and generate catalytically active Cu^I-based species.⁶⁻¹² Photo-active compounds were also recently applied as oxygen scavengers and polymerization catalysts for metal-free SI-ATRP, enabling the synthesis of microstructured brushes under ambient conditions, with excellent temporal and spatial control.¹³

An alternative, highly efficient approach to circumventing the need for deoxygenation relies on the use of zerovalent copper, Cu⁰, which acts as a source of active catalyst,^{14, 15} simultaneously consuming dissolved oxygen when the polymerization mixture is not directly exposed to air.^{16, 17}

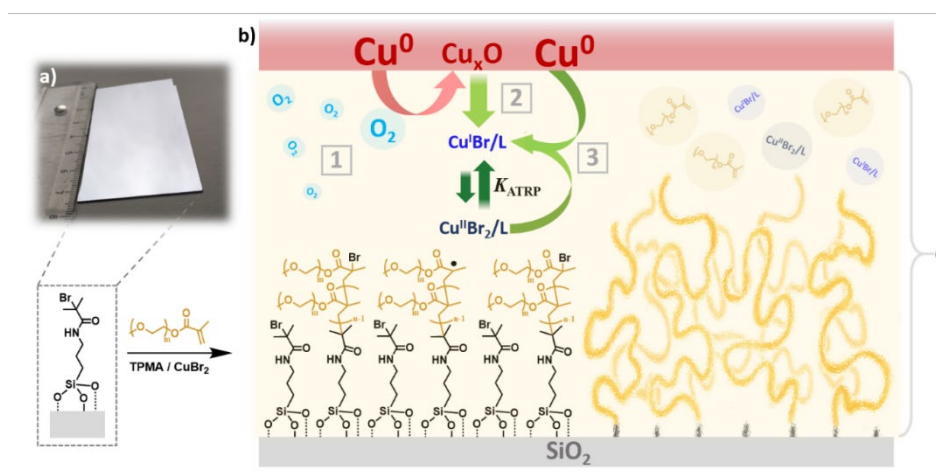
Although the robustness of Cu⁰-mediated SI-ATRP for the synthesis of multifunctional, gradient and microstructured polymer brushes has been already proven^{18-20, 21, 22} little has been revealed about the mechanism of this grafting process, and its tolerance to oxygen.

By gaining a comprehensive understanding of the Cu⁰ SI-ATRP mechanism, in this Chapter we demonstrate that the highly controlled growth of compositionally different brushes can be achieved from large substrates, without the need for deoxygenation of monomer mixtures or inert environments. In other words, a polymer grafting process through controlled/“living” radical polymerization can be readily performed on a benchtop, and translated into technology.

5.2 Results and Discussion

5.2.1 Cu⁰-mediated SI-ATRP and its oxygen tolerance

When a polymerization mixture is placed between a flat Cu⁰-coated plate and an ATRP initiator-functionalized substrate (Scheme 1 and Figure 1), the metallic surface first consumes oxygen within the polymerization mixture, generating an oxide layer that acts as source of both Cu^I activator and Cu^{II}-based deactivator species. In the presence of ligand (L), activators (CuBr/L) and deactivators (CuBr₂/L) diffuse through the reaction medium, reaching the initiator-bearing substrate and triggering polymerization, which proceeds according to the ATRP equilibrium. It is also significant that the exposed Cu⁰ surface further acts as a reducing agent for Cu^{II} species, generating Cu^I-based activators via comproportionation.¹⁴



Scheme 1. (a) A polymerization mixture comprising monomer (OEGMA), ligand (TPMA) and CuBr₂ is sandwiched between an ATRP-initiator-functionalized SiO₂ substrate, and a copper plate. (b) The copper surface consumes oxygen dissolved in the polymerization mixture (1), and acts as source of Cu^I-based activators and Cu^{II}-based deactivators (2), which in the presence of ligand diffuse to the initiator-bearing surface, regulating the polymerization. Moreover, Cu⁰ participates in the comproportionation equilibrium (3), providing additional activators.

The growth of poly(oligo(ethylene glycol) methacrylate) (POEGMA) and poly(methyl methacrylate) (PMMA) brushes, monitored *ex situ* by variable-angle spectroscopic ellipsometry (VASE), provide exemplary cases of Cu⁰ SI-ATRP performed under ambient conditions (Figure 2a and 2b). Significantly, neither the monomers nor the solvent were deoxygenated prior to polymerization, while the reaction mixture was simply poured onto a Cu⁰-coated silicon wafer and immediately covered with a 30 cm² initiator-functionalized SiO₂ substrate, onto which a pressure of 3 g cm⁻² was applied, by means of a weight (Figure 2c).

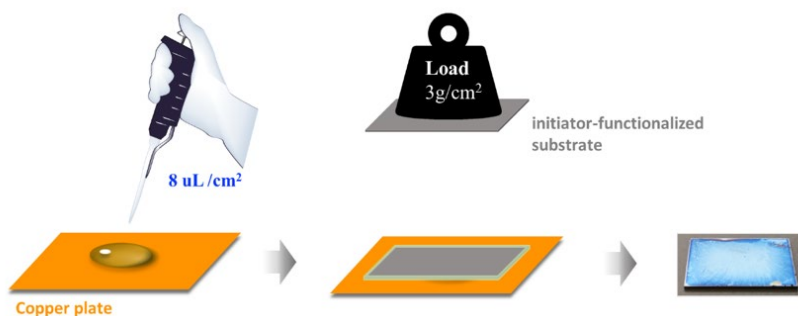


Figure 1. Schematic representation of the procedures followed during Cu⁰ SI-ATRP.

The vertical spacing (d) between the copper plate and ATRP initiator-bearing substrates (Scheme 1), and the presence and concentration of added Cu^{II} species, emerge as critical parameters regulating the synthesis of polymer brushes.

Under the experimental conditions applied, the reaction volume between the sandwiching surfaces corresponded to 1 $\mu\text{L cm}^{-2}$, and $d \sim 10 \mu\text{m}$. When the grafting process was performed in dimethyl sulfoxide (DMSO), and using tris(2-pyridylmethyl)amine (TPMA) as ligand, POEGMA and PMMA brushes reached 91 ± 3 and 36 ± 4 nm of dry thickness, respectively, after 60 minutes of polymerization. In both cases, no induction period was observed. This is consistent with the average diffusion path lengths calculated from the Einstein equation, which suggest that less than 1 second was necessary for activators to reach the initiator-bearing surface.

The diffusion rate by Cu species could be estimated applying Einstein's relation for average diffused path lengths (\bar{X}):

$$t = \frac{\bar{X}^2}{2D}$$

where \bar{X} is the diffusion path of 10 μm , and D is the diffusion coefficient of copper complexes in the presence of OEGMA ($6 \times 10^{-11} \text{ m}^2 \text{ s}^{-1}$).^[47]

Moreover, the virtually instantaneous polymer-brush growth indicates that the consumption of oxygen was rapid within the small reaction volumes existing between the two opposing surfaces.

5.2.2 Effect of ligand (L), activators (CuBr/L), and deactivators (CuBr₂/L)

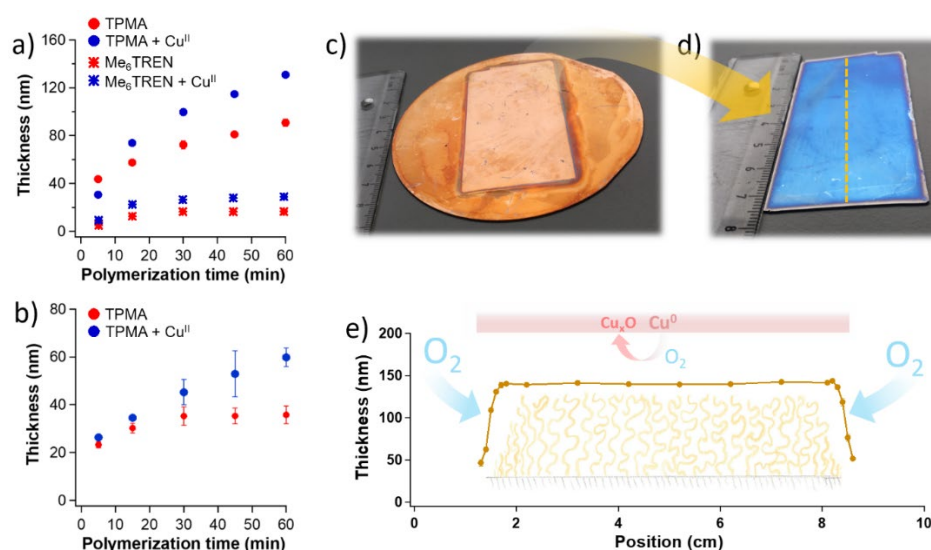


Figure 2. (a) POEGMA brush thickness measured by *ex situ* VASE during Cu⁰ SI-ATRP performed without deoxygenation. The polymerization mixtures included OEGMA (50% v/v) in DMSO, and 16 mM TPMA (red markers); OEGMA (50% v/v) in DMSO, 16 mM TPMA, and 11 mM CuBr₂ (blue markers). Similar polymerizations were conducted with Me₆TREN (16 mM) as ligand, with (blue markers) and without 11 mM CuBr₂ (red markers). (b) PMMA brush thickness measured by *ex-situ* VASE during Cu⁰ SI-ATRP. The polymerization mixtures included MMA (50% v/v) in DMSO, and 16 mM TPMA (red markers); MMA (50% v/v) in DMSO, 16 mM TPMA, and 11 mM CuBr₂ (blue markers). (c,d) Cu⁰ SI-ATRP of OEGMA was performed on ~ 30 cm² substrates generating relatively thick and uniform brush layers. (e) POEGMA brush dry thickness measured by VASE across the yellow dashed line highlighted in (d).

When 11 mM Cu^{II} was added to the polymerization mixture, the growth rates of POEGMA and PMMA brushes significantly increased, leading to the formation of 131 ± 2 and 60 ± 4 nm-thick brushes, respectively. The observed increment in brush-growth rates was clearly correlated to the dual functions of the externally added Cu^{II} species. An increase in the amount of deactivator, beyond the small concentration of Cu^{II} determined by the ATRP equilibrium, suppresses irreversible termination reactions between propagating grafts, leading to more efficient brush growth.²³ Under these conditions, and after just 5 minutes of reaction, Cu⁰ SI-ATRP provided PMMA brushes with a number-average molar mass of 38 kDa and Đ = 1.1 (Figure 3, corresponding to an average grafting density σ = 0.22 chains nm⁻²).

Furthermore, the addition of Cu^{II} species to the polymerization mixture influenced the concentration of Cu^I-based activators, which are continuously generated through comproportionation reactions with Cu⁰ from the copper surface (Scheme 1b).²⁴ This phenomenon could be monitored *in situ* by quartz crystal microbalance with dissipation (QCM-

D), subjecting a Cu^0 -coated sensor to the same reaction mixtures used during Cu^0 SI-ATRP, and simultaneously recording the mass variation of the metal layer with time (Figure 4a).

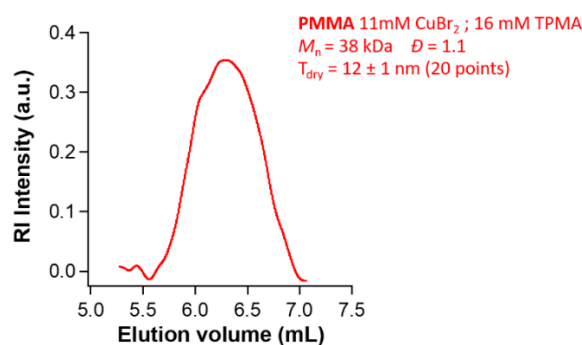


Figure 3. SEC elugram of PMMA brushes synthesized from a 10 cm diameter silicon wafer after 5 minutes of Cu^0 SI-ATRP and subsequently detached.

Increasing the concentration of externally added Cu^{II} within the range 0-35 mM, while maintaining a fixed concentration of TPMA (40 mM), led to a progressive increment in the amount of Cu species desorbed from the metallic plate (Figure 4b), which were presumably mainly constituted of Cu^{I} adducts generated by comproportionation.

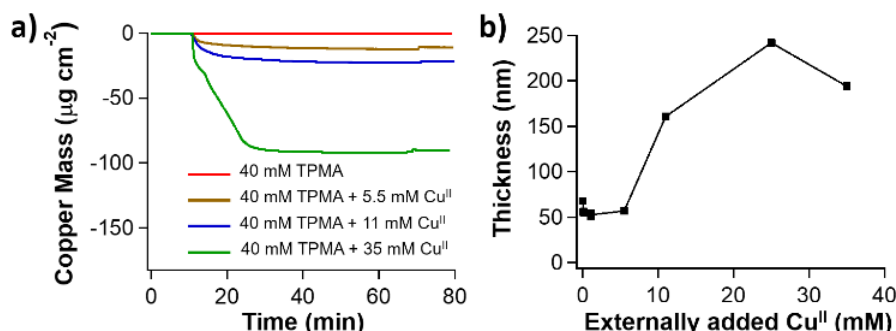


Figure 4. (a) Mass of copper species desorbed from a Cu^0 -coated QCM-D sensor subjected to different polymerization mixtures. (b) POEGMA brush thicknesses measured by VASE after 60 minutes of Cu^0 SI-ATRP performed with different initial concentrations of CuBr_2 and a fixed content of TPMA (40 mM).

In support of this hypothesis, the thickness of POEGMA brushes obtained after 60 minutes of polymerization progressively increased with the concentration of added Cu^{II} , reaching a maximum of 242 ± 2 nm for 25 mM of added Cu^{II} (Figure 4b). A further addition of Cu^{II} did not translate into an increment in brush thickness, which decreased by nearly 20% (194 ± 2 nm) when Cu^{II} concentration reached 35 mM (Figure 4b). Besides shifting the equilibrium of comproportionation towards the formation of Cu^{I} -based species, inducing an increment in both polymerization rate and brush thickness, Cu^{II} adducts intrinsically act as deactivators during Cu^0 SI-ATRP. The balance between these two roles, i.e. favouring the formation of activator,

as well as acting as deactivator, is highly dependent on the concentration of Cu^{II} initially added to the reaction mixture.²⁵

The central role of copper comproportionation in determining the polymerization kinetics was confirmed by comparing Cu^0 SI-ATRP of OEGMA employing TPMA and tris[2-(dimethylamino)ethyl]amine (Me_6TREN), the latter ligand providing higher ATRP activity but a slower rate of comproportionation in DMSO.²⁶ The growth of POEGMA brushes was remarkably slower when Me_6TREN was used (Figure 2a), and POEGMA-brush thicknesses could not exceed 30 nm even after 60 minutes of reaction.

5.2.3 Effect of alkyl halide initiator, the distance (d) and “polarity” of solvent

The consumption of oxygen appeared homogeneous even across extremely large substrates, with the exception of the areas close to their edges (Figure 2d-e and Figure 5a-b), where air diffused from the surrounding environment and locally terminated the polymerization. In this way, extremely uniform, 150 nm-thick POEGMA brushes could be synthesized from 10 cm diameter wafers on a lab bench, after just 1 hour of polymerization (Figure 5a).

The tolerance towards oxygen by Cu^0 SI-ATRP is reminiscent of that recently reported by Anastasaki and Haddleton, when ATRP in the presence of Cu^0 was performed in solution while removing the headspace of the reaction vessel.¹⁷ However, besides the presence of Cu^0 , an excess of alkyl halide initiator was previously identified as a prerequisite, in order to rapidly consume oxygen within the reaction medium. In contrast, the addition of 60 mM ethyl α -bromoisobutyrate (EBIB) during Cu^0 SI-ATRP significantly slowed down the growth of polymer brushes (Figure 5c-d). This was presumably due to the fast conversion of monomer within the small volume of solution overlying the initiator-bearing substrate, which limited the achievable molecular weight of the brushes, and simultaneously led a substantial increase in the viscosity of the reaction mixture. In addition, the presence of EBIB both consumed Cu^{I} and slowed down its diffusion from the Cu^0 plate due to the polymerization occurring in the interstitial solution.

In Cu^0 SI-ATRP, the distance between the initiator-bearing substrate and the copper plate (d) represents the main factor determining the oxygen tolerance of the grafting process. As displayed in Figure 5e, when $d \sim 10 \mu\text{m}$ the thickness of POEGMA brushes reached 110 ± 1 nm after 60 minutes of polymerization.

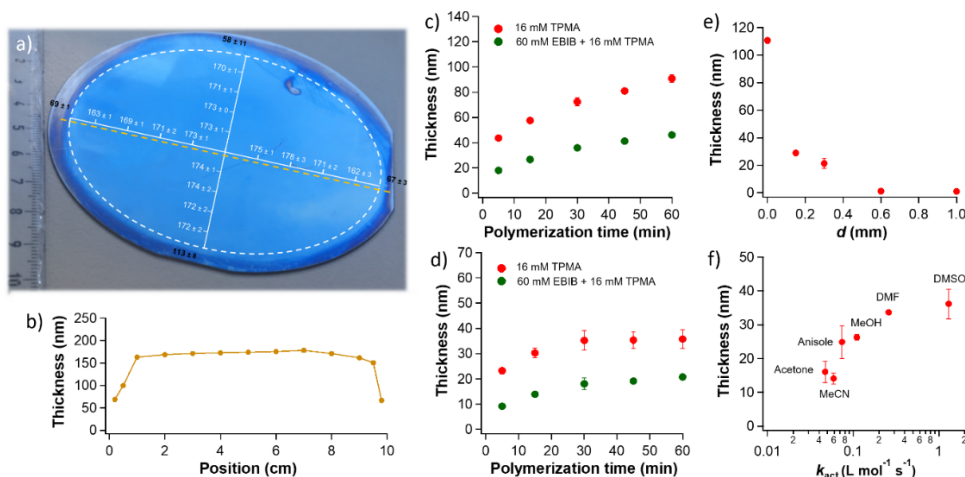


Figure 5. (a) POEGMA bushes synthesized by Cu^0 SI-ATRP under environmental conditions from a 10 cm diameter, ATRP-initiator-functionalized silicon wafer. The values of brush thickness (indicated in white) were measured across the whole wafer by VASE. The brush thickness at the edges was highlighted in black. (b) Brush thicknesses measured along the POEGMA-coated silicon wafer by VASE; the thickness values were measured along the dashed yellow line highlighted in (a). (c) POEGMA brush thickness measured by ex-situ VASE during Cu^0 SI-ATRP performed without deoxygenation. The polymerization mixtures included OEGMA (50% v/v) in DMSO, and 16 mM TPMA (red markers); OEGMA (50% v/v) in DMSO, 16 mM TPMA, and 60 mM EBIB (green markers). (d) PMMA brush thickness measured by ex-situ VASE during Cu^0 SI-ATRP. The polymerization mixtures included MMA (50% v/v) in DMSO, and 16 mM TPMA (red markers); MMA (50% v/v) in DMSO, 16 mM TPMA, and 60 mM EBIB (green markers). (e) POEGMA brush thickness measured by VASE after 60 minutes of Cu^0 SI-ATRP performed at different d values; the polymerization mixtures include OEGMA (50% v/v) in DMSO, 16 mM TPMA and 5.5 mM CuBr_2 . (f) PMMA brush thickness measured by VASE after 60 minutes of Cu^0 SI-ATRP performed in solvents showing a different rate constant of activation (k_{act} , measured for mixtures including CuBr , 1,1,4,7,10,10-hexamethyltriethylenetetramine, EBIB).²⁷ The polymerization mixtures included 16 mM TPMA, 11 mM CuBr_2 , and MMA (50% v/v) in acetonitrile (MeCN), acetone, anisole, methanol (MeOH), dimethylformamide (DMF) and DMSO.

An increase in d caused a concomitant increment in the area of the gas-liquid interface at the edges of oppositely facing surfaces, favouring the diffusion of oxygen from the surrounding environment. When $d > 0.6$ mm, no brush growth was recorded (brush thickness ≤ 1.5 nm), as the amount of oxygen diffusing into the polymerization medium from the atmosphere was likely exceeding that consumed by Cu^0 .

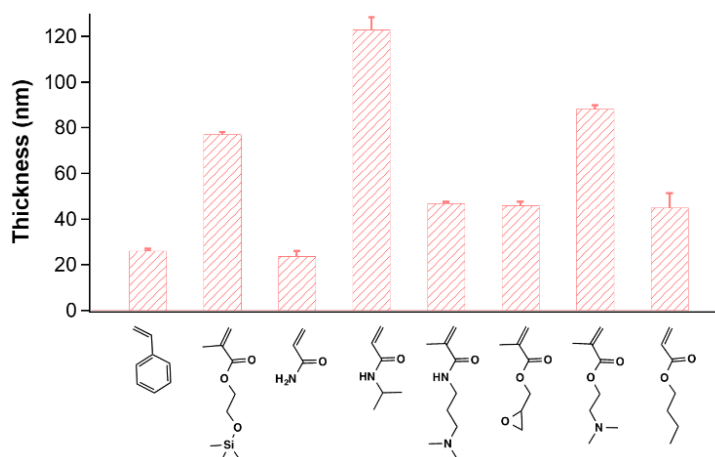


Figure 6. Brush thickness measured by VASE after 60 minutes of Cu^0 SI-ATRP performed with different monomers (using 16 mM TPMA, and 11 mM CuBr_2). These include styrene (50% v/v in anisole), 2-(trimethylsilyloxy)ethyl methacrylate (HEMATMS) (50% v/v in DMSO), acrylamide (3 M in DMSO), NIPAM (3 M in DMSO), 3-(dimethylamino)propyl methacrylamide (DMAPMA) (3 M in DMSO), glycidyl methacrylate (GMA) (50% v/v in DMSO), 2-(dimethylamino)ethyl methacrylate (DMAEMA) (50% v/v in DMSO), and butyl acrylate (BA) (50% v/v in DMSO).

Similarly to what was previously observed for homogeneous ATRP in solution,²⁸ the “polarity” of the solvent²⁹ additionally influenced the synthesis of brushes by Cu^0 SI-ATRP. In particular, the thickness of POEGMA brushes obtained after 60 minutes of polymerization in different media increased with the corresponding activation rate constant of ATRP (k_{act}), the thickest films could be synthesized in the most polar organic solvents amongst those studied, i.e. DMSO and dimethylformamide (DMF) (Figure 5f and Figure 7), while Cu^0 SI-ATRP in water showed an uncontrolled character (Figure 8).

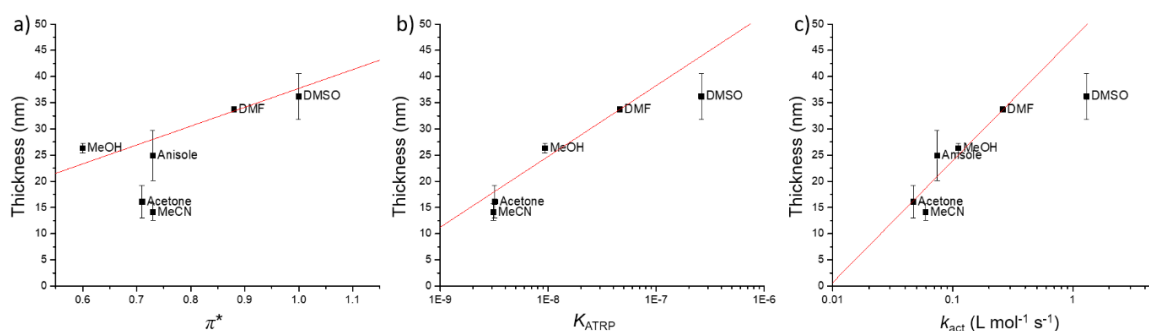


Figure 7. PMMA brush thickness measured by VASE after 60 minutes of Cu^0 SI-ATRP performed in solvents showing a different π^* (a). The relationships between brush thickness and K_{ATRP} and k_{act} were reported in (b) and (c) (K_{ATRP} and k_{act} were measured for mixtures including CuBr and 1,1,4,7,10,10-hexamethyltriethylenetetramine, EBIB).^[51] The polymerization mixtures included 16 mM TPMA, 11 mM CuBr_2 , and MMA (50% v/v) in acetonitrile (MeCN), acetone, anisole, methanol (MeOH), dimethylformamide (DMF) and DMSO.

The growth rate of polymer brushes synthesized by Cu^0 SI-ATRP was determined by the “polarity” of the solvent, which was expressed as the ability of the medium to stabilize solutes via nonspecific interactions, or dipolarity/polarizability of the solvent according to Kamlet and Taft (π^*).^[48] In particular, the thickness of PMMA brushes recorded after 60 min of polymerization in different solvents, and thus their grafting rate, increased with π^* , due to the simultaneous increment in the equilibrium rate constant (K_{ATRP}) and activation rate constant of ATRP (k_{act}) (Figure 7). Accordingly, the thickest films were obtained by using the most polar solvents amongst those studied, *i.e.* DMSO and dimethylformamide (DMF).

However, when Cu^0 SI-ATRP was performed with the same catalytic system (16 mM TPMA and 11 mM CuBr_2) in water, the large values of K_{ATRP} coupled to the dissociation of Cu^{II} -based species led to a high concentration of radicals and their inefficient deactivation (Figure 8).^[49] In the case of Cu^0 SI-ATRP of N-isopropylacrylamide (NIPAM), this phenomenon translated into an initial, markedly fast brush growth, which led to brush thicknesses > 200 nm, followed by a plateau in the brush-growth rate that suggested the occurrence of irreversible termination between propagating chains, in a way similar to a free radical polymerization process. In contrast, the use of DMSO as solvent provided a slower and more progressive PNIPAM-brush growth, following kinetics comparable to that observed for a highly controlled SI-ATRP process.^[50]

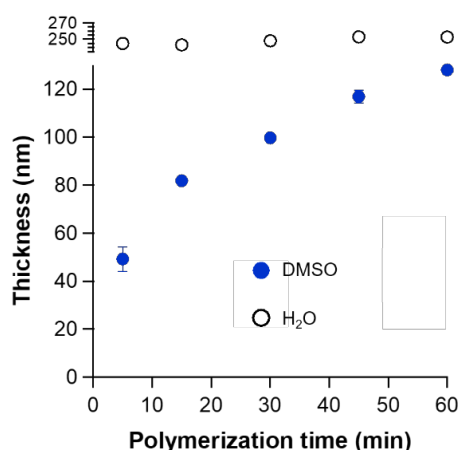


Figure 8. PNIPAM brush thickness measured by ex-situ VASE during Cu^0 SI-ATRP. The polymerization mixtures included NIPAM (3 M) in water, 16 mM TPMA and 11 mM CuBr_2 (black circles); NIPAM (3 M) in DMSO, 16 mM TPMA and 11 mM CuBr_2 (blue circles).

Using DMSO as solvent and TPMA as ligand, Cu^0 SI-ATRP could be thus applied to a large variety of monomers, enabling the polymerization of acrylates, methacrylates, acrylamides and styrene (Figure 6). Remarkably, in all these cases, relatively high brush thicknesses were

obtained in just 1 hour of polymerization, while applying the same ligand and Cu^{II} concentration.

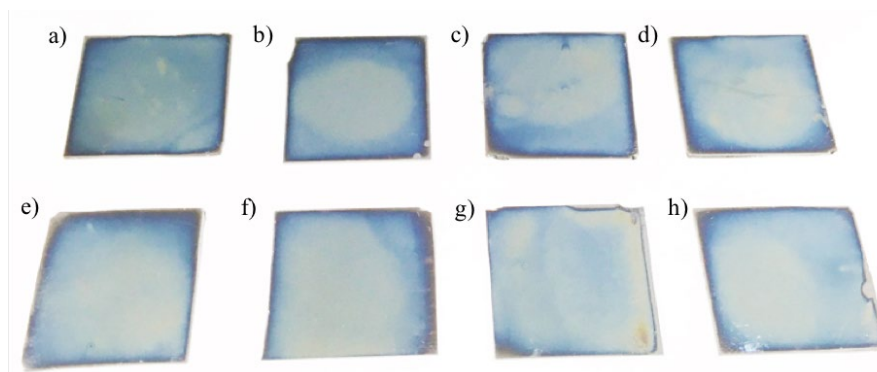


Figure 9. POEGMA brushes were grafted from 8 different ATRP-initiator-functionalized substrates by repeatedly employing the same Cu^0 surface as catalyst source. The average dry thickness of the films measured by VASE was: a) 171.7 ± 3.2 nm b) 174.7 ± 1.5 nm c) 176.3 ± 2.5 nm d) 181.7 ± 3.5 nm e) 173.3 ± 3.1 nm f) 171.2 ± 1.1 nm g) 160.3 ± 2.1 nm h) 176.3 ± 1.5 nm.

The same Cu^0 substrate was repeatedly used as catalyst source for the synthesis of 8 different samples of POEGMA brushes. Each film was subsequently analyzed by VASE, resulting in very reproducible grafting processes (Figure 9).

5.3 Conclusions

Overall, these results demonstrate that, under optimized reaction conditions, Cu^0 SI-ATRP enables the highly controlled synthesis of compositionally different, thick brushes in short reaction times, over extremely large areas and without the need for degassing the monomer mixtures or carrying out the reaction in the presence of an inert atmosphere. These highly attractive features, revealed through a comprehensive understanding of its mechanism, make oxygen-tolerant Cu^0 SI-ATRP a very promising method for translating surface-initiated polymerization from fundamental, academic studies, to technologically relevant applications, including the fabrication of hybrid coatings,³⁰⁻³² biosensors,³³⁻³⁵ cell-culture platforms³⁶⁻⁴¹ and lubricating films.^{42,43}

5.4 Materials and Methods

Materials

Methyl methacrylate (MMA, Sigma-Aldrich), oligo(ethylene glycol) methyl ether methacrylate (OEGMA, $M_n \sim 300$ g mol⁻¹, Sigma-Aldrich), styrene (99.5%, Acros), 2-

(Trimethylsilyloxy)ethyl methacrylate (HEMATMS, 96%, Sigma-Aldrich), acrylamide (\geq 99%, Sigma-Fine Chemicals), 2-(dimethylamino)ethyl methacrylate (DMAEMA, 98%, Aldrich-Fine Chemicals), glycidyl methacrylate (GMA, Sigma-Aldrich), N-[3-(Dimethylamino)propyl]methacrylamide (DMAPMA, 99%, Sigma-Aldrich), butyl acrylate (99%, Acros) were purified by passing through a basic alumina column to remove the inhibitor before use. N-Isopropylacrylamide (NIPAAM, > 98% GC, Tokyo Chemical Industry) was purified by re-crystallization from n-hexane and dried in an oven prior to use.

Dimethyl sulfoxide (DMSO, > 99.5%, VWR Chemicals), dimethylformamide (DMF, extrapure, Fisher Chemical), methanol (> 99%, VWR Chemicals), anisole (99.7%, Sigma-Aldrich), acetonitrile (> 99.5%, Sigma-Aldrich), acetone (> 99.8%, VWR Chemicals), tetrahydrofuran (THF, > 99.5%, VWR Chemicals), dichloromethane (DCM, dry, \geq 99.8%, Acros), triethylamine (TEA, \geq 99%, Merck), 2-bromoisobutryl bromide (BiBB, 98%, Sigma-Aldrich), ethyl 2-bromoisobutyrate (EBiB, 98%, Aldrich-Fine chemicals), 3-(aminopropyl)triethoxysilane (APTES, 99%, Acros), copper(II) bromide (CuBr_2 , 99.99%, Aldrich), tris(2-pyridylmethyl)amine (TPMA, 98%, Sigma-Aldrich), tris[2-(dimethylamino)ethyl]amine (Me_6TREN , 99%, abcr GmbH), tetrabutylammonium fluoride (TBAF, 1M in THF, Aldrich) were all used as received. Copper(I) Bromide (CuBr , 99.99%, Aldrich) was purified by stirring in glacial acetic acid overnight, followed by washing with diethyl ether and methanol, vacuum filtration and drying under high vacuum. The water used in all the experiments was Millipore Milli-Q grade. Silicon wafers were purchased from Si-Mat (Landsberg, Germany). Cu^0 -coated wafers were obtained by reactive magnetron sputtering (Paul Scherrer Institute, Villigen, Switzerland) obtaining 200 nm-thick layer of Cu^0 .

Surface Characterization Methods

A variable-angle spectroscopic ellipsometer (VASE, SENTECH Instruments GmbH) equipped with a He-Ne laser source ($\lambda = 633$ nm, J.A. Woollam Co., Lincoln, NE) was used to measure the dry thickness of polymer brushes. Amplitude (Ψ) and phase (Δ) components were recorded at a fixed angle of 70° as a function of wavelength (300–800 nm). Fitting of the raw data was performed based on a three-layers model (software WVASE32, LOT Oriel GmbH, Darmstadt, Germany), using bulk dielectric functions for Si and SiO_2 . The polymer brush layers were analyzed on the basis of the Cauchy model: $n = A + B \lambda^{-2}$, where n is the refractive index, λ is the wavelength and A and B were assumed to be 1.45 and 0.01, respectively, as values for transparent organic films.

Quartz-crystal microbalance with dissipation (QCM-D) was used to monitor the dissolution of copper species from Cu^0 -coated crystals in the presence of different polymerization mixtures,

using a Q-Sense E4 instrument (Q-Sense AB, Göteborg, Sweden) equipped with dedicated Q-Sense AB software. Before the experiment, Cu⁰-coated crystals were washed by sonication in toluene (2x30 min) and isopropanol (2x30 min), followed by UV-ozone treatment for 30 min. After cleaning, the crystals were dried under a stream of N₂. Just before placing them within the QCM-D cells, the Cu⁰-coated crystals were treated for few seconds with a 2:1 (v/v) HCl:methanol solution, in order to remove the CuO_x layer.

DMSO was first injected into the QCM-D cells, in order to record a stable baseline. After ~ 10 minutes, DMSO was replaced with different mixtures of solvent, ligand, MMA and CuBr₂. All the different solutions were not degassed prior to injection. The recorded frequency shifts (Δf) were translated into mass variation by applying Sauerbrey equation,^[44] using the sensitivity factor $C_f = -17.7 \text{ ng Hz}^{-1} \text{ cm}^{-2}$.

Preparation of ATRP initiator-bearing SiO_x substrates

SiO_x substrates of different size (Si-Mat, Landsberg, Germany) were cleaned for 15 minutes in piranha solution (3:1 mixture of 99.9% H₂SO₄ and H₂O₂), subsequently rinsed with ultrapure water thoroughly and finally dried under a stream of N₂. ATRP initiator-layers were subsequently deposited following the already reported two-step protocol.^[45] Namely, APTES was first deposited by vapour deposition for 3 hours. After this, APTES-functionalized substrates were incubated under Ar in a solution of α -bromoisobutryl bromide (BiBB) and triethylamine in dry DCM. After 2 hours the samples were washed with chloroform and dried under a stream of N₂.

Cu⁰-Mediated Surface Initiated Atom Transfer Radical Polymerization (Cu⁰ SI-ATRP)

Experimental Setup

Cu⁰-coated surfaces were sonicated in isopropanol for 5 min, followed by activation in 2:1 (v/v) methanol:HCl mixture for 5 minutes.^[46] Later on, the polymerization mixture (1 $\mu\text{L cm}^{-2}$) was poured on the Cu⁰-coated surface (Figure 1), and immediately covered with an ATRP initiator-bearing substrate, on which a weight of 3 g cm⁻² was applied during the whole reaction time.

Grafting of PMMA Brushes on Silicon Wafers for SEC Analysis

A 10 cm diameter silicon wafer functionalized with ATRP initiator was covered with a polymerization mixture comprising MMA (50% v/v) in DMSO, 16 mM TPMA and 11 mM CuBr₂ (the volume of the polymerization mixture poured on the substrate corresponded to 1 $\mu\text{L cm}^{-2}$), and immediately covered with a similar wafer coated with 200 nm-thick Cu⁰ layer, on which a weight of 3 g cm⁻² was subsequently applied. After 5 minutes of reaction, the PMMA brush-covered substrate was extensively rinsed with DMSO and acetone, and finally

dried under a stream of N₂. VASE was used to measure the average dry thickness of PMMA brushes, which was 12.1 ± 0.5 nm, as recorded over 20 positions across the entire wafer.

PMMA brushes were subsequently detached from the underlying SiO_x surface by incubating the wafer in a 0.05 M THF solution of TBAF at 60 °C overnight.^[52] After the reaction, the solvent was removed by rotary evaporation and the solid was filtered and re-dissolved in the SEC eluent.

Size exclusion chromatography (SEC) was performed on a Viskotek GPC-Max system (Malvern) equipped with 2 × PL-Gel Mix-B columns set (Malvern). The detached PMMA chains together were eluted in DMF containing 0.1 % w/v LiBr, and 0.1 % v/v toluene as a flow marker. The values of M_n and M_w of PMMA were obtained using the refractive index (RI) detector. Results were evaluated according to a conventional calibration employing narrowly dispersed PMMA standards.

References

1. Yeow, J.; Chapman, R.; Gormley, A. J.; Boyer, C., Up in the air: oxygen tolerance in controlled/living radical polymerisation. *Chem. Soc. Rev.* 2018, 47, 4357-4387.
2. Li, M.; Fromel, M.; Ranaweera, D.; Rocha, S.; Boyer, C.; Pester, C. W., SI-PET-RAFT: Surface-Initiated Photoinduced Electron Transfer-Reversible Addition–Fragmentation Chain Transfer Polymerization. *ACS Macro Lett.* 2019, 8, 374-380.
3. Barbey, R.; Lavanant, L.; Paripovic, D.; Schuwer, N.; Sugnaux, C.; Tugulu, S.; Klok, H. A., Polymer Brushes via Surface-Initiated Controlled Radical Polymerization: Synthesis, Characterization, Properties, and Applications. *Chem. Rev.* 2009, 109, 5437-5527.
4. Zoppe, J. O.; Ataman, N. C.; Mocny, P.; Wang, J.; Moraes, J.; Klok, H. A., Surface-Initiated Controlled Radical Polymerization: State-of-the-Art, Opportunities, and Challenges in Surface and Interface Engineering with Polymer Brushes *Chem. Rev.* 2017, 117, 4667-4667.
5. Matyjaszewski, K.; Miller, P. J.; Shukla, N.; Immaraporn, B.; Gelman, A.; Luokala, B. B.; Siclovan, T. M.; Kickelbick, G.; Vallant, T.; Hoffmann, H.; Pakula, T., Polymers at interfaces: Using atom transfer radical polymerization in the controlled growth of homopolymers and block copolymers from silicon surfaces in the absence of untethered sacrificial initiator. *Macromolecules* 1999, 32, 8716-8724.
6. Matyjaszewski, K.; Dong, H. C.; Jakubowski, W.; Pietrasik, J.; Kusumo, A., Grafting from surfaces for "Everyone": ARGET ATRP in the presence of air. *Langmuir* 2007, 23, 4528-4531.

7. Dunderdale, G. J.; Urata, C.; Miranda, D. F.; Hozumi, A., Large-Scale and Environmentally Friendly Synthesis of pH-Responsive Oil-Repellent Polymer Brush Surfaces under Ambient Conditions. *ACS Appl. Mater. Interfaces* 2014, 6, 11864-11868.
8. Dunderdale, G. J.; England, M. W.; Urata, C.; Hozumi, A., Polymer Brush Surfaces Showing Superhydrophobicity and Air-Bubble Repellency in a Variety of Organic Liquids. *ACS Appl. Mater. Interfaces* 2015, 7, 12220-12229.
9. Min, K.; Jakubowski, W.; Matyjaszewski, K., AGET ATRP in the presence of air in miniemulsion and in bulk. *Macromol. Rapid Commun.* 2006, 27, 594-598.
10. Sato, T.; Dunderdale, G. J.; Urata, C.; Hozumi, A., Sol-Gel Preparation of Initiator Layers for Surface-Initiated ATRP: Large-Scale Formation of Polymer Brushes Is Not a Dream. *Macromolecules* 2018, 51, 10065-10073.
11. Navarro, L. A.; Enciso, A. E.; Matyjaszewski, K.; Zauscher, S., Enzymatically Degassed Surface-Initiated Atom Transfer Radical Polymerization with Real-Time Monitoring. *J. Am. Chem. Soc.* 2019, 141, 3100-3109.
12. Enciso, A. E.; Fu, L. Y.; Russell, A. J.; Matyjaszewski, K., A Breathing Atom-Transfer Radical Polymerization: Fully Oxygen-Tolerant Polymerization Inspired by Aerobic Respiration of Cells. *Angew. Chem. Int. Edit.* 2018, 57, 933-936.
13. Narupai, B.; Page, Z. A.; Treat, N. J.; McGrath, A. J.; Pester, C. W.; Discekici, E. H.; Dolinski, N. D.; Meyers, G. F.; de Alaniz, J. R.; Hawker, C. J., Simultaneous Preparation of Multiple Polymer Brushes under Ambient Conditions using Microliter Volumes. *Angew. Chem. Int. Edit.* 2018, 57, 13433-13438.
14. Matyjaszewski, K.; Tsarevsky, N. V.; Braunecker, W. A.; Dong, H.; Huang, J.; Jakubowski, W.; Kwak, Y.; Nicolay, R.; Tang, W.; Yoon, J. A., Role of Cu⁰ in Controlled/"Living" Radical Polymerization. *Macromolecules* 2007, 40, 7795-7806.
15. Matyjaszewski, K.; Coca, S.; Gaynor, S. G.; Wei, M.; Woodworth, B. E., Zerovalent Metals in Controlled/"Living" Radical Polymerization. *Macromolecules* 1997, 30, 7348-7350.
16. Boyer, C.; Corrigan, N. A.; Jung, K.; Nguyen, D.; Nguyen, T. K.; Adnan, N. N. M.; Oliver, S.; Shanmugam, S.; Yeow, J., Copper-Mediated Living Radical Polymerization (Atom Transfer Radical Polymerization and Copper(0) Mediated Polymerization): From Fundamentals to Bioapplications. *Chem. Rev.* 2016, 116, 1803-1949.
17. Liarou, E.; Whitfield, R.; Anastasaki, A.; Engelis, N. G.; Jones, G. R.; Velonia, K.; Haddleton, D. M., Copper-Mediated Polymerization without External Deoxygenation or Oxygen Scavengers. *Angew. Chem. Int. Edit.* 2018, 57, 8998-9002.

18. Che, Y. J.; Zhang, T.; Du, Y. H.; Amin, I.; Marschelke, C.; Jordan, R., "On Water" Surface-initiated Polymerization of Hydrophobic Monomers. *Angew. Chem. Int. Edit.* 2018, 57, 16380-16384.
19. Zhang, T.; Du, Y. H.; Kalbacova, J.; Schubel, R.; Rodriguez, R. D.; Chen, T.; Zahn, D. R. T.; Jordan, R., Wafer-scale synthesis of defined polymer brushes under ambient conditions. *Polym. Chem.* 2015, 6, 8176-8183.
20. Zhang, T.; Du, Y.; Muller, F.; Amin, I.; Jordan, R., Surface-initiated Cu(0) mediated controlled radical polymerization (SI-CuCRP) using a copper plate. *Polym. Chem.* 2015, 6, 2726-2733.
21. Dehghani, E. S.; Du, Y.; Zhang, T.; Ramakrishna, S. N.; Spencer, N. D.; Jordan, R.; Benetti, E. M., Fabrication and Interfacial Properties of Polymer Brush Gradients by Surface-Initiated Cu(0)-Mediated Controlled Radical Polymerization. *Macromolecules* 2017, 50, 2436-2446.
22. Fantin, M.; Ramakrishna, S. N.; Yan, J. J.; Yan, W. Q.; Divandari, M.; Spencer, N. D.; Matyjaszewski, K.; Benetti, E. M., The Role of Cu⁰ in Surface-Initiated Atom Transfer Radical Polymerization: Tuning Catalyst Dissolution for Tailoring Polymer Interfaces. *Macromolecules* 2018, 51, 6825-6835.
23. Benetti, E. M.; Kang, C. J.; Mandal, J.; Divandari, M.; Spencer, N. D., Modulation of Surface-Initiated ATRP by Confinement: Mechanism and Applications. *Macromolecules* 2017, 50, 5711-5718.
24. Konkolewicz, D.; Wang, Y.; Zhong, M. J.; Krys, P.; Isse, A. A.; Gennaro, A.; Matyjaszewski, K., Reversible-Deactivation Radical Polymerization in the Presence of Metallic Copper. A Critical Assessment of the SARA ATRP and SET-LRP Mechanisms. *Macromolecules* 2013, 46, 8749-8772.
25. Zhang, Y. Z.; Wang, Y.; Peng, C. H.; Zhong, M. J.; Zhu, W. P.; Konkolewicz, D.; Matyjaszewski, K., Copper-Mediated CRP of Methyl Acrylate in the Presence of Metallic Copper: Effect of Ligand Structure on Reaction Kinetics. *Macromolecules* 2012, 45, 78-86.
26. Ribelli, T. G.; Krys, P.; Cong, Y.; Matyjaszewski, K., Model Studies of Alkyl Halide Activation and Comproportionation Relevant to RDRP in the Presence of Cu⁰. *Macromolecules* 2015, 48, 8428-8436.
27. Braunecker, W. A.; Tsarevsky, N. V.; Gennaro, A.; Matyjaszewski, K., Thermodynamic Components of the Atom Transfer Radical Polymerization Equilibrium: Quantifying Solvent Effects. *Macromolecules* 2009, 42, 6348-6360.

28. Horn, M.; Matyjaszewski, K., Solvent Effects on the Activation Rate Constant in Atom Transfer Radical Polymerization. *Macromolecules* 2013, 46, 3350-3357.
29. Kamlet, M. J.; Abboud, J. L. M.; Abraham, M. H.; Taft, R. W., Linear Solvation Energy Relationships .23. A Comprehensive Collection of the Solvatochromic Parameters, Pi-Star, Alpha and Beta, and Some Methods for Simplifying the Generalized Solvatochromic Equation. *J. Org. Chem.* 1983, 48, 2877-2887.
30. Christau, S.; Moller, T.; Yenice, Z.; Genzer, J.; von Klitzing, R., Brush/Gold Nanoparticle Hybrids: Effect of Grafting Density on the Particle Uptake and Distribution within Weak Polyelectrolyte Brushes. *Langmuir* 2014, 30, 13033-13041.
31. Christau, S.; Moller, T.; Brose, F.; Genzer, J.; Soltwedel, O.; von Klitzing, R., Effect of gold nanoparticle hydrophobicity on thermally induced color change of PNIPAM brush/gold nanoparticle hybrids. *Polymer* 2016, 98, 454-463.
32. Christau, S.; Moeller, T.; Genzer, J.; Koehler, R.; von Klitzing, R., Salt-Induced Aggregation of Negatively Charged Gold Nanoparticles Confined in a Polymer Brush Matrix. *Macromolecules* 2017, 50, 7333-7343.
33. Joh, D. Y.; Hucknall, A. M.; Wei, Q. S.; Mason, K. A.; Lund, M. L.; Fontes, C. M.; Hill, R. T.; Blair, R.; Zimmers, Z.; Achar, R. K.; Tseng, D.; Gordan, R.; Freemark, M.; Ozcan, A.; Chilkoti, A., Inkjet-printed point-of-care immunoassay on a nanoscale polymer brush enables subpicomolar detection of analytes in blood. *Proc. Natl. Acad. Sci. U.S.A.* 2017, 114, E7054-E7062.
34. Fortin, N.; Klok, H. A., Glucose Monitoring Using a Polymer Brush Modified Polypropylene Hollow Fiber-based Hydraulic Flow Sensor. *ACS Appl. Mater. Interfaces* 2015, 7, 4631-4640.
35. Badoux, M.; Billing, M.; Klok, H. A., Polymer brush interfaces for protein biosensing prepared by surface-initiated controlled radical polymerization. *Polym. Chem.* 2019, 10, 2925-2951
36. Paripovic, D.; Hall-Bozic, H.; Klok, H. A., Osteoconductive surfaces generated from peptide functionalized poly(2-hydroxyethyl methacrylate-co-2-(methacryloyloxy)ethyl phosphate) brushes. *J. Mater. Chem.* 2012, 22, 19570-19578.
37. Desseaux, S.; Klok, H. A., Temperature-Controlled Masking/Unmasking of Cell-Adhesive Cues with Poly(ethylene glycol) Methacrylate Based Brushes. *Biomacromolecules* 2014, 15, 3859-3865.

38. Bhat, R. R.; Chaney, B. N.; Rowley, J.; Liebmann-Vinson, A.; Genzer, J., Tailoring cell adhesion using surface-grafted polymer gradient assemblies. *Adv. Mater.* 2005, 17, 2802-2807.
39. Klein Gunnewiek, M.; Di Luca, A.; Bollemaat, H. Z.; van Blitterswijk, C. A.; Vancso, G. J.; Moroni, L.; Benetti, E. M., Creeping Proteins in Microporous Structures: Polymer Brush-Assisted Fabrication of 3D Gradients for Tissue Engineering. *Adv. Health. Mater.* 2015, 4, 1169–1174.
40. Lilge, I.; Schonherr, H., Block Copolymer Brushes for Completely Decoupled Control of Determinants of Cell-Surface Interactions. *Angew. Chem. Int. Edit.* 2016, 55, 13114-13117.
41. Dou, X. Q.; Li, P.; Jiang, S. Y.; Bayat, H.; Schonherr, H., Bioinspired Hierarchically Structured Surfaces for Efficient Capture and Release of Circulating Tumor Cells. *ACS Appl. Mater. Interfaces* 2017, 9, 8508-8518.
42. Chen, M.; Briscoe, W. H.; Armes, S. P.; Klein, J., Lubrication at Physiological Pressures by Polyzwitterionic Brushes. *Science* 2009, 323, 1698-1701.
43. Li, A.; Benetti, E. M.; Tranchida, D.; Clasohm, J. N.; Schonherr, H.; Spencer, N. D., Surface-Grafted, Covalently Cross-Linked Hydrogel Brushes with Tunable Interfacial and Bulk Properties. *Macromolecules* 2011, 44, 5344-5351.
44. Sauerbrey, G., Verwendung von Schwingquarzen zur Wägung dünner Schichten und zur Mikrowägung. *Z. Phys.* **1959**, 155, 206-222.
45. Zhou, T.; Qi, H.; Han, L.; Barbash, D.; Li, C. Y., Towards controlled polymer brushes via a self-assembly-assisted-grafting-to approach. *Nat. Commun.* **2016**, 7.
46. Yan, J. J.; Pan, X. C.; Wang, Z. Y.; Lu, Z.; Wang, Y.; Liu, L.; Zhang, J. N.; Ho, C. E.; Bockstaller, M. R.; Matyjaszewski, K., A Fatty Acid-Inspired Tetherable Initiator for Surface-Initiated Atom Transfer Radical Polymerization. *Chem. Mater.* **2017**, 29, 4963-4969.
47. Fantin, M.; Isse, A. A.; Matyjaszewski, K.; Gennaro, A., ATRP in Water: Kinetic Analysis of Active and Super-Active Catalysts for Enhanced Polymerization Control. *Macromolecules* **2017**, 50, 2696-2705.
48. Kamlet, M. J.; Abboud, J. L. M.; Abraham, M. H.; Taft, R. W., Linear Solvation Energy Relationships .23. A Comprehensive Collection of the Solvatochromic Parameters, Pi-Star, Alpha and Beta, and Some Methods for Simplifying the Generalized Solvatochromic Equation. *J. Org. Chem.* **1983**, 48, 2877-2887.
49. Tsarevsky, N. V.; Pintauer, T.; Matyjaszewski, K., Deactivation Efficiency and Degree of Control over Polymerization in ATRP in Protic Solvents. *Macromolecules* **2004**, 37, 9768-9778.

50. Gao, X.; Feng, W.; Zhu, S. P.; Sheardown, H.; Brash, J. L., Kinetic Modeling of Surface-Initiated Atom Transfer Radical Polymerization. *Macromol. React. Eng.* **2010**, *4*, 235-250.
51. Braunecker, W. A.; Tsarevsky, N. V.; Gennaro, A.; Matyjaszewski, K., Thermodynamic Components of the Atom Transfer Radical Polymerization Equilibrium: Quantifying Solvent Effects. *Macromolecules* **2009**, *42*, 6348-6360.
52. Patil, R.; Miles, J.; Ko, Y.; Datta, P.; Rao, B. M.; Kiserow, D.; Genzer, J., Kinetic Study of Degrafting Poly(methyl methacrylate) Brushes from Flat Substrates by Tetrabutylammonium Fluoride. *Macromolecules* **2018**, *51*, 10237-10245.

Chapter 6

Growing Polymer Brushes from a Variety of Substrates under Ambient Conditions by Cu⁰-Mediated Surface-Initiated ATRP*

As we demonstrated in Chapter 5, Cu⁰-mediated surface-initiated ATRP is a highly versatile, oxygen-tolerant, and extremely controlled polymer-grafting technique that enables the modification of flat inorganic surfaces, as well as porous organic and polymeric supports of different compositions. Exploiting the intimate contact between a copper plate, acting as source of catalyst and reducing agent, and an initiator-bearing support, Cu⁰ SI-ATRP enables the rapid growth of biopassive, lubricious brushes from large flat surfaces, as well as from various organic supports, including cellulose fibres and elastomers, by using microliter volumes of reaction mixtures, and without the need for deoxygenation of reaction mixtures or an inert atmosphere. Thanks to a detailed analysis of its mechanism and the parameters governing the polymerization process, polymer brush-growth by Cu⁰ SI-ATRP can be precisely modulated and adapted to be applied to morphologically and chemically different substrates, setting up the basis for translating SI-ATRP methods from academic studies into technologically relevant surface-modification approaches.

* Edmondo M. Benetti, Krzysztof Matyjaszewski and Nicholas D. Spencer supervised this project. Wenqing Yan, Marco Fantin and Shivaprakash Ramakrishna performed experimental work. All the authors wrote the paper. Part of this Chapter was published in *ACS Appl Mater Interfaces*. **2019**. 27470-27477.

6.1 Introduction

The synthesis of polymer brushes by surface-initiated reversible-deactivation radical polymerization (SI-RDRP), and their subsequent application in a variety of materials formulations have been the subjects of a significant number of academic studies over the last two decades.¹⁻⁴ Although “grafted-from” polymer brushes have proven to be extraordinarily versatile platforms for the design of sensors,⁵⁻¹⁰ the functionalization of biomaterials,¹¹⁻¹⁶ or the fabrication of lubricious surfaces¹⁷⁻¹⁸ and catalytic supports,¹⁹⁻²² the translation of SI-RDRP methods into technologically relevant surface-modification techniques still requires some intrinsic drawbacks to be overcome. These are mainly related to the low tolerance of SI-RDRP methods to oxygen,²³⁻²⁴ which limits the scaling up of such grafting processes for large substrates, or those of diverse composition.

Focusing in particular on the most widely applied version of SI-RDRP, namely surface-initiated atom transfer radical polymerization (SI-ATRP),²⁵ the need for deoxygenation of monomer solutions has been recently circumvented by the introduction of reducing agents²⁶⁻²⁸ or oxygen scavengers,²⁹ which consume oxygen that has diffused in from the surrounding environment, concomitantly regenerating the active catalyst or act as catalysts themselves,³⁰ ultimately enabling polymer grafting under ambient conditions.

Specifically, by exploiting activators regenerated by electron transfer (ARGET) ATRP, various waterborne monomers could be successfully polymerized from large polymeric films in the presence of oxygen,³¹ while the application of photocatalysts in light-mediated, metal-free SI-ATRP enabled the fabrication of micropatterned brushes over entire silicon wafers, with high resolution and without the need for deoxygenation of reaction mixtures.³⁰

Apart from the use of organic “additives” to improve the tolerance of SI-ATRP towards oxygen, Jordan et al. demonstrated that Cu⁰-coated plates placed upon initiator-bearing substrates within polymerization mixtures could efficiently act as sources of catalyst,³² simultaneously consuming oxygen³³ and triggering the rapid growth of a variety of compositionally different brushes.³⁴ Apart from these initial findings, little has been uncovered concerning the mechanism of Cu⁰-mediated SI-ATRP, and its tolerance towards oxygen, and its application has been limited to model, flat substrates.

While investigating the role played by the copper surface during Cu⁰-mediated SI-ATRP (Cu⁰ SI-ATRP), in Chapter 5 we demonstrated that the composition of the polymerization mixture and the separation between the Cu⁰ surface and the initiator-bearing substrate represent key parameters that determine polymer-brush growth and its kinetics.³⁵⁻³⁶

In this chapter, we show that Cu⁰ SI-ATRP enables the highly controlled synthesis of technologically relevant polymer brushes from large flat surfaces, as well as from different organic supports, including cellulose fibres and elastomers, by using microliter volumes of reaction mixtures—either under inert conditions or in the presence of oxygen. In particular, we systematically examine the parameters governing Cu⁰ SI-ATRP, while focusing on the synthesis of poly(2-methacryloyloxyethyl phosphorylcholine) (PMPC) brushes, which have been widely applied for the fabrication of highly lubricious coatings^{17-18, 37-39} and bio-repellent films.⁴⁰⁻⁴⁴

6.2 Results and Discussion

6.2.1 Mechanism of Cu⁰ SI-ATRP in Deoxygenated Media

The mechanism of Cu⁰ SI-ATRP of MPC can be exemplarily investigated by placing a copper plate at 1 mm distance from an ATRP initiator-functionalized silicon oxide surface (Scheme 1), in the presence of a 1 M methanol solution of MPC and 40 mM of 2,2'-bipyridine (bipy). The growth of PMPC brushes is firstly investigated within deoxygenated reaction mixtures, while surrounding the reaction system with an N₂ atmosphere during the entire polymerization process. In the presence of organic ligand (L), Cu^I/L and Cu^{II}/L complexes diffuse from the copper plate towards the initiator-bearing substrate, triggering the polymerization of MPC, which proceeds according to the ATRP equilibrium (Scheme 1).³⁶ The growth of PMPC brushes could be monitored *ex situ* by variable-angle spectroscopic ellipsometry (VASE), the dry brush thickness (T_{dry}) being determined for different polymerization times. As shown in Figure 3a, T_{dry} steadily increased during the first 40 minutes of polymerization, reaching ~ 20 nm, after which a plateau was attained, indicating that the grafting process irreversibly stopped. This phenomenon was likely due to radical termination between growing grafts, as the concentration of Cu^{II}-based deactivator solely generated through the ATRP equilibrium at the growing-brush front was presumably insufficient to guarantee a low concentration of surface-grafted radicals.³⁶

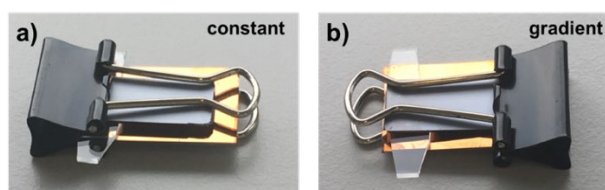
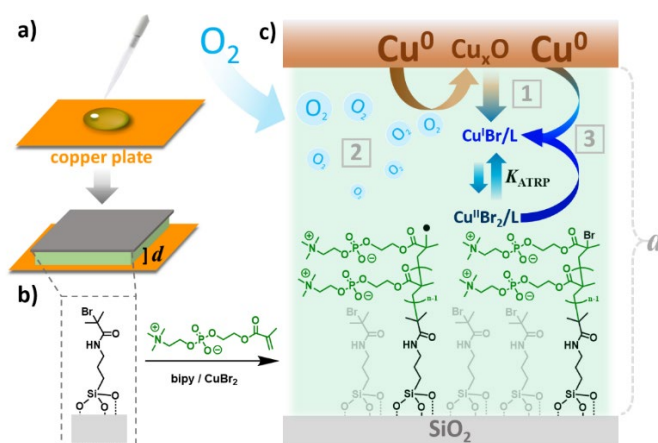


Figure 1. Setups used for Cu⁰ SI-ATRP of MPC to generate PMPC brushes with homogeneous thickness (a) and gradient brushes (b).

In order to fabricate PMPC brushes with homogeneous thickness ATRP-initiator-bearing substrates were clamped to Cu^0 -coated surfaces while maintaining a fixed distance (d) of 1 mm between the two surfaces, by means of a glass slide (Figure 1). PMPC brush gradients were prepared with a similar setup, but by tilting the ATRP-initiator-bearing surface with respect to the Cu^0 -coated substrate, as depicted in Figure 1b. The clamped substrates were laid in a sealed flask and degassed with Ar for 30 min. A degassed methanol mixture of MPC (1M) and bipy (40 mM), with and without CuBr_2 (0.2mM), was transferred into the flask containing the substrates, and left standing for the desired time. After this, the samples were rinsed extensively with water and ethanol and finally dried in a stream of N_2 .



Figure 2. PMPC brush gradients synthesized by Cu^0 SI-ATRP.



Scheme 1. Mechanism of Cu^0 SI-ATRP of MPC from ATRP-initiator-functionalized silicon oxide surfaces. (a,b) A polymerization solution (comprising 1 M methanol solution of MPC and 40 mM bipy, or 40 mM bipy and 0.2 mM CuBr_2) is sandwiched between a copper plate and an initiator-bearing substrate (c) When the solution has been previously degassed and the grafting process is carried out within an inert atmosphere, Cu^I/L and Cu^{II}/L species diffuse from the copper plate (1) and trigger MPC polymerization from the initiator-functionalized substrate, which proceeds according to the ATRP equilibrium. However, under ambient conditions and without previous deoxygenation of the reaction mixture, the dissolved oxygen is consumed by oxidation of Cu^0 (2), generating an oxide layer that acts as source of catalyst. Either in the presence or the absence of oxygen, the addition of Cu^{II} -based species stimulates the formation of Cu^I/L activators through comproportionation with the Cu^0 surface (3).

The addition of 0.2 mM CuBr₂ to the reaction mixture substantially altered the growth kinetics of PMPC brushes. In the presence of added deactivator, the PMPC brush thickness continuously increased with reaction time, following a nearly linear trend, T_{dry} reaching nearly 70 nm after 75 minutes of polymerization (Figure 3a). On the one hand, the presence of additional Cu^{II}-based deactivator suppressed irreversible termination by radical recombination, ensuring the controlled growth of PMPC grafts. On the other hand, following a similar mechanism to that previously described for supplemental activator and reducing agent (SARA) ATRP,⁴⁵⁻⁴⁷ Cu^{II} species comproportionated with the Cu⁰ surface, constantly (re)generating Cu^I-based adducts capable of activating both dormant PMPC grafts and unreacted initiator functions at the surface (Scheme 1). The combination of these two cooperative effects led to the observed, highly controlled grafting of PMPC brushes.

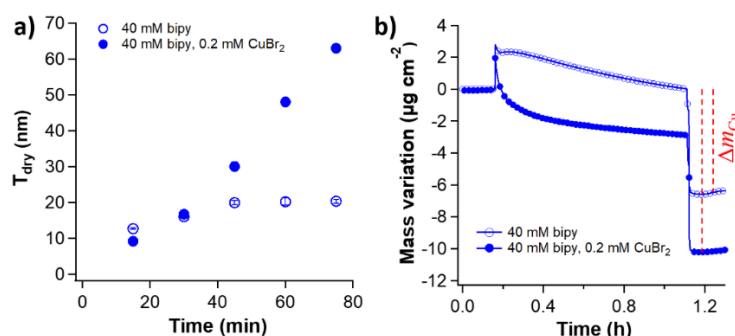


Figure 3. (a) PMPC brush dry thickness (T_{dry}) measured by VASE at different polymerization times, using a reaction mixture comprising either 1 M methanol solution of MPC and 40 mM bipy (empty markers), or 1 M MPC, 40 mM bipy and 0.2 mM CuBr₂ (filled markers). (b) Mass variation (Δm_{Cu}) of Cu⁰-coated QCM-D sensors obtained from fitting of the corresponding frequency shifts (Δf) with the Sauerbrey equation. The QCM-D sensors were subjected to different polymerization solutions: 1 M MPC and 40 mM bipy (empty markers), and 1 M MPC, 40 mM bipy and 0.2 mM CuBr₂ (filled markers).

Comproportionation between added Cu^{II} and the Cu⁰ surface could be precisely monitored by means of a quartz crystal microbalance with dissipation (QCM-D), subjecting a Cu⁰-coated QCM-D sensor to the same polymerization mixtures employed during Cu⁰ SI-ATRP of MPC, while simultaneously monitoring the dissolution of copper species from the metal surface as a mass change in the copper-coated sensor (Δm_{Cu}). As highlighted in Figure 3b, the addition of 0.2 mM CuBr₂ caused a more marked desorption of Cu species from the metal-coated sensor, presumably mainly comprising Cu^I complexes generated by comproportionation, when compared to the mass loss measured when the sensor was in contact with a solution containing only ligand and monomer.

6.2.2 Structure and Properties of PMPC Brushes Synthesized by Cu⁰ SI-ATRP

It is important to emphasize that the progressive brush thickening recorded by VASE was not simply due to an increase in the molar mass of PMPC grafts, but also to a simultaneous increment in their grafting density (σ). As Cu^I-based activators progressively diffuse from the Cu⁰ surface towards and through the growing brush layer, an increasing number of initiators become activated, subsequently generating PMPC chains that propagate from the surface.

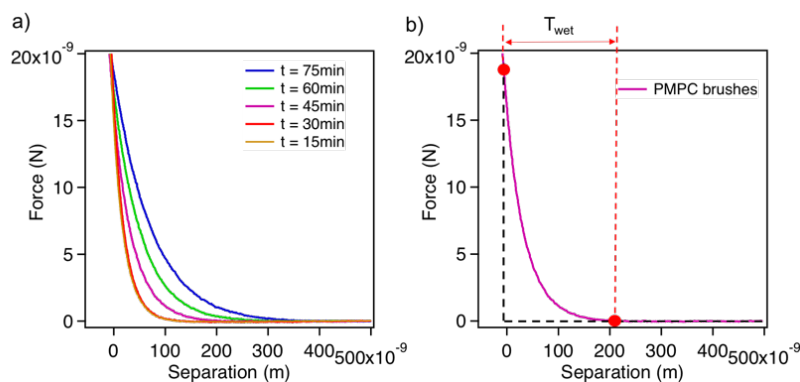


Figure 4. (a) FS profiles recorded on PMPC brushes in HEPES solution (pH = 7.4). (b) The swollen thickness (T_{wet}) of PMPC brushes was estimated from FS profiles. T_{wet} could be estimated as the separation between the brush-AFM probe contact point and the point of full brush compression, i.e. when the approaching FS curve approximates a vertical line.

Friction values were obtained by averaging 10 “friction loops” recorded on each brush surface over three different positions for each sample. The friction loops were acquired by laterally scanning over a line on each brush film at a given applied normal load. A scanning distance of 5 μ m and a scanning rate of 1 Hz were applied during the measurements. The values of coefficient of friction (μ) were obtained from the slope of the recorded friction force-vs-applied load (F_fL) profiles, assuming Amontons’ law of friction: $F_f = \mu L$.

Approximately 20 FS profiles were recorded on each PMPC brush by applying a Z-piezo distance of 500 nm and a ramping rate of 1 Hz (Figure 4). The swollen thickness of the brushes (T_{wet}) was obtained by estimating the separation included between the contact point at the brush interface (in correspondence of which the measured force deviates by more than 5% from the horizontal line corresponding to $F = 0$ nN) and the complete brush compression (Figure 4).

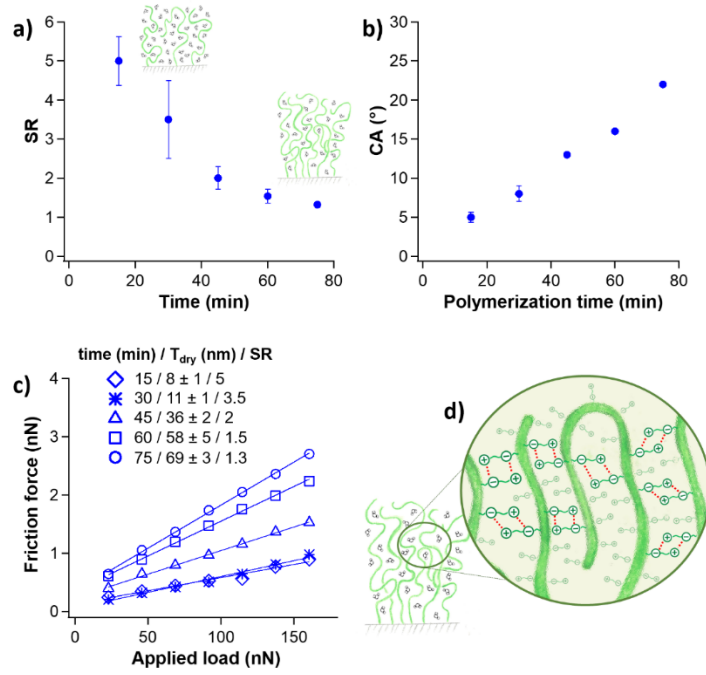


Figure 5. (a) Values of swelling ratio (SR) measured by a combination of VASE and AFM on PMPC brushes synthesized by Cu^0 SI-ATRP after different polymerization times under inert atmosphere ($\text{SR} = T_{\text{wet}}/T_{\text{dry}}$), using a reaction mixture comprising 1 M MPC, 40 mM bipy and 0.2 mM CuBr_2 . (b) Static water contact angle (CA) measured on PMPC brushes synthesized after different polymerization times, using the conditions reported in (a). (c) F_L profiles recorded by LFM on PMPC brushes, using an AFM colloidal probe with a normal spring constant (K_N) of 0.3 N m^{-1} , a lateral spring constant (K_L) of 5.1 E-9 N m^{-1} , and an $18 \mu\text{m}$ diameter silica colloid. The coefficients of friction (μ) were 0.005, 0.005, 0.008, 0.012, and 0.015, measured on PMPC brushes synthesized after 15, 30, 45, 60, and 75 minutes, respectively. (d) Schematic representation of densely grafted PMPC brushes forming inter- and intrachain ionic associations.

From the values of T_{dry} , obtained by VASE, and those of T_{wet} , the brush swelling ratio (SR) could be calculated as $T_{\text{wet}}/T_{\text{dry}}$. The grafting density (σ) of PMPC brushes was estimated according to the previously reported method, using Equation 1.^{36, 48-50}

$$\sigma = \rho_0 T_{\text{dry}} N_A \left((0.227 (T_{\text{wet}})^{1.5} (T_{\text{dry}} (\text{\AA}^2))^{-0.5}) M_0 \right)^{-1} \quad (1)$$

where ρ_0 is the dry density of PMPC (1.30 g cm^{-3}), N_A is Avogadro's number, M_0 is the monomer molecular weight (295 g mol^{-1}), 0.227 is a constant related to the excluded-volume parameter ($\omega = 7 \text{ \AA}^3$), a constant $\nu = (a^2/3)^{-1}$, where a represents the Kuhn length of the monomer unit (15 \AA for methyl methacrylate).

In order to support this hypothesis, we estimated the swelling ratio (SR) of PMPC brushes synthesized after different polymerization times by comparing the values of T_{dry} with the corresponding swollen brush thicknesses (T_{wet}), which could be measured by atomic force microscopy (AFM) nanoindentation (Figure 4). Since the SR of brushes in a good solvent is inversely proportional to σ ,⁴⁸⁻⁵⁰ its gradual decrease with the polymerization time from 5 to 1

(Figure 5a), indicated a simultaneous increment in brush surface coverage, which shifted from ~ 0.2 to ~ 0.7 chains nm^{-2} , between 15 and 75 minutes of polymerization.

This gradual change in brush structure was mirrored by a significant shift in other interfacial physicochemical properties. Besides the amount of swelling solvent, wettability progressively decreased due to the rising of inter- and intrachain ionic associations between zwitterions—a phenomenon that was previously reported for relatively thick and densely grafted sulfobetaine-based polyzwitterionic brushes, and which determined their more “hydrophobic” character with respect to thinner and less crowded brushes of identical composition (Figure 5a).⁵¹ The formation of ionic “bridges” between PMPC brushes and the concomitant decrease in SR further influenced their lubrication properties, which were characterized by lateral force microscopy (LFM) (Experimental Methods).⁵²⁻⁵³

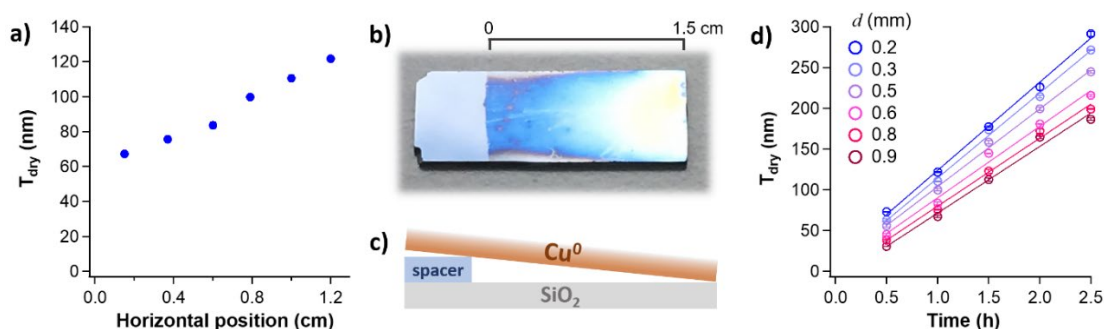


Figure 6. (a) Variation of T_{dry} across a PMPC brush gradient (b) synthesized by continuously varying the distance between a copper plate and an ATRP initiator-bearing substrate (c), in the presence of a polymerization mixture including a 1 M methanol solution of MPC, 40 mM bipy and 0.2 mM CuBr_2 . The reaction mixture was deoxygenated by N_2 bubbling prior to Cu^0 SI-ATRP, while the brush gradient was fabricated over 1 hour of polymerization under a N_2 atmosphere. The rate of Cu^0 SI-ATRP, which correlated with the slope of the T_{dry} vs polymerization time profiles reported in (d), could be tuned by varying d between the copper plates and ATRP initiator-substrates.

As highlighted by comparing the friction-force-vs-applied-load (F_fL) profiles measured on PMPC brushes featuring different values of thickness (Figure 5b), friction was generally low, with coefficients of friction (μ) lying between 0.015 and 0.005, for 69 ± 3 and 8 ± 1 nm-thick brushes, respectively. However, a clear increase in the slope of F_fL profiles—and thus a consequent increment in μ —was observed with increasing the polymerization time, suggesting that the progressive structural transition taking place within PMPC brushes affected mechanical energy dissipation when these were sheared by an AFM colloidal probe.

The distance (d) between the copper plate and the initiator-bearing substrate represented an additional parameter governing the growth of PMPC brushes by Cu^0 SI-ATRP. When a continuous variation of d was applied across a single, initiator-functionalized substrate, by

“tilting” the copper plate (Figure 6a-c), the diffusion time for activator species gradually changed along the surface, and a PMPC brush-gradient was obtained.³⁵⁻³⁶ In particular, in the presence of 0.2 mM CuBr₂ and after 1 hour of polymerization, the PMPC brush thickness progressively varied between 70 and 120 nm across a 1.5 cm-long substrate.

Alternatively, when the copper plate and the initiating surface were maintained parallel to each other, the rate of polymerization could be subsequently tuned by varying d , while keeping the other polymerization conditions constant. As reported in Figure 6d, polymer-brush-thickening rates increased with decreasing d , and the thickness of PMPC brushes synthesized after 2,5 hours of Cu⁰ SI-ATRP could be varied from ~ 180 to almost 300 nm by reducing the distance to the copper plate from 0.9 to 0.2 mm (Figure 6d).

6.2.3 Functionalization of Large and Compositionally Different Substrates by Cu⁰ SI-ATRP under Ambient Conditions

Cu⁰ SI-ATRP of MPC performed without deoxygenation of monomer mixtures and under ambient conditions followed a very similar mechanism to that observed for oxygen-free polymerizations carried out within an inert atmosphere.

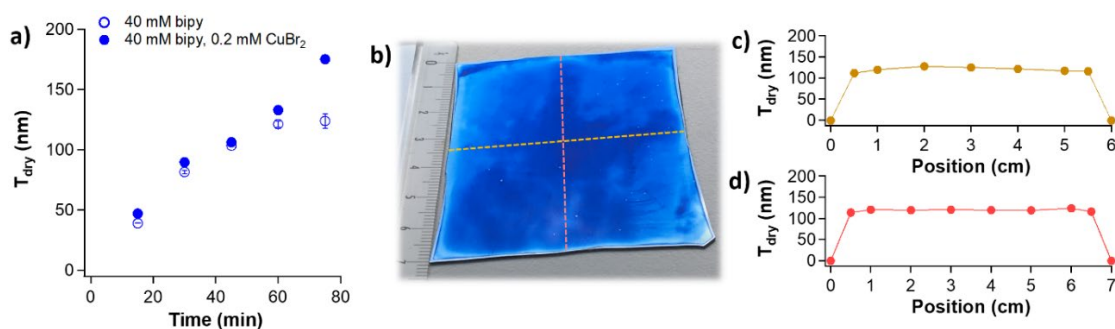


Figure 7. (a) Cu⁰ SI-ATRP of MPC performed without deoxygenation of monomer mixtures and under ambient conditions, using 1 M methanol solution of MPC and 40 mM bipy (empty markers), or 40 mM bipy and 0.2 mM CuBr₂ (filled markers). During these experiments, d was kept at 10 μm by applying a constant pressure of 3 g cm⁻² on the sandwiched assembly. (b) PMPC brushes synthesized by Cu⁰ SI-ATRP in the presence of oxygen from ~ 50 cm² silicon oxide substrate previously functionalized with ATRP initiator and covered by a copper plate with $d = 10 \mu\text{m}$. By using a polymerization mixture comprising 1 M MPC, 40 mM bipy and 0.2 mM CuBr₂ uniform PMPC brushes with a dry thickness of ~ 120 nm were synthesized after 60 minutes of reaction. (c,d) Brush-thickness profiles recorded by VASE across the large substrate reported in (b).

When the reaction mixture is sandwiched between the copper plate and the initiator-functionalized substrate, while a constant pressure of 3 g cm⁻² is applied, the distance between the two surfaces corresponds to ~ 10 μm . Under these conditions, the area of air-liquid interface

at the edges of the overlying substrates is small enough to guarantee limited diffusion of oxygen from the surrounding atmosphere (Scheme 1c). The Cu^0 surface consumes the oxygen dissolved in the reaction mixture, generating a CuO_x layer that acts as source of catalyst. In the presence of L, $\text{Cu}^{\text{I}}/\text{L}$ and $\text{Cu}^{\text{II}}/\text{L}$ species diffuse to the initiating surface and trigger the grafting of PMPC brushes, which proceeds according to the ATRP process.

Similarly to what was previously observed while using deoxygenated mixtures and an inert atmosphere, the addition of Cu^{II} strongly influenced the growth kinetics of PMPC brushes by Cu^0 SI-ATRP in the presence of oxygen. As shown in Figure 7a, in the absence of externally added Cu^{II} , PMPC brush growth proceeded steadily during the first 60 minutes of polymerization until ~ 100 nm of film thickness was reached. After this time, the brush-thickening rate slowed down and reached a plateau, presumably due to irreversible termination by radical combination/disproportionation.

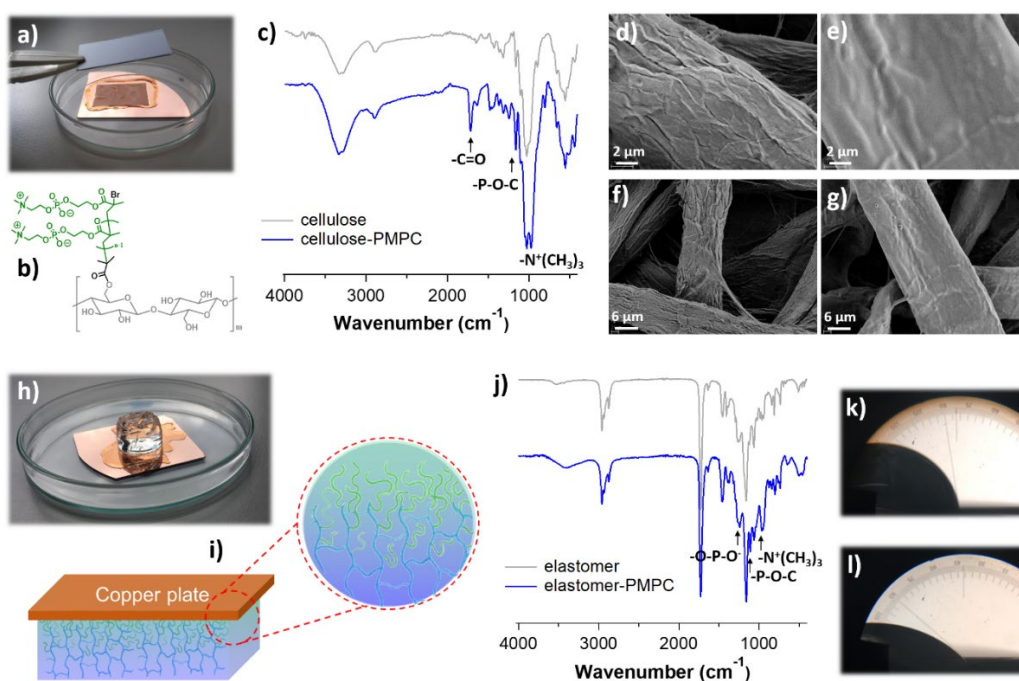


Figure 8. (a, b) Uniform PMPC brush-films can be successfully grown from cellulose sheets previously functionalized with ATRP initiator functions by Cu^0 SI-ATRP in the presence of oxygen. The reaction mixture comprised 1 M methanol solution of MPC, 40 mM bipy and 0.2 mM CuBr_2 and the polymerization time was set to 1 hour. (c) Attenuated total reflectance Fourier-transform infrared spectroscopy (ATR FTIR) confirmed the successful grafting of PMPC brushes, SEM further demonstrated the formation of a uniform PMPC brush film on cellulose fibres (d-g). Cu^0 SI-ATRP can be further applied for the modification of the outer surface of a PBA-based elastomer, by placing the stamp in contact with a copper plate previously covered by few drops of reaction mixture (h,i). The formation of PMPC brushes was confirmed by ATR FTIR spectroscopy (j) and wettability measurements (k, l).

In contrast, the addition of 0.2 mM CuBr₂ enabled a progressive brush growth, which followed a *quasi*-linear trend and indicated rapid and highly controlled polymerization. Under these conditions, ~ 130 nm-thick PMPC brushes could be synthesized in just 60 minutes of polymerization, while no sign of termination was observed.

Following this procedure, homogeneously thick PMPC brushes could be grown from large substrates, after just 1 hour of polymerization, without the need for degassing monomer mixtures, and by employing just 8 $\mu\text{L cm}^{-2}$ of polymerization solution.

An example of the applicability of Cu⁰ SI-ATRP for the functionalization of large substrates under full ambient conditions is provided in Figure 7b, which shows 120-nm-thick PMPC brushes grafted from a 50 cm² silicon substrate. PMPC brush thickness was homogenous across the entire surface (Figure 7c and 7d), with the exception of its edges, where unavoidable oxygen diffusion terminated the polymerization, resulting in a localized reduction in film thickness.

In order to further demonstrate the suitability of Cu⁰ SI-ATRP for the rapid and efficient modification of a variety of materials, beyond flat, model substrates, similar PMPC brushes were subsequently grafted from micro- and nanoporous supports, including cellulose sheets and poly(butyl acrylate) (PBA)-based elastomers (Figure 8 and Figure 9). It is noteworthy that structurally similar supports are widely applied for the fabrication of medical devices, such as wound dressings and catheters, where the highly hydrophilic, biopassive and lubricious properties of PMPC brushes^{18, 41, 43-44, 54-55} could substantially improve their performance when placed in contact with tissues and/or body fluids.

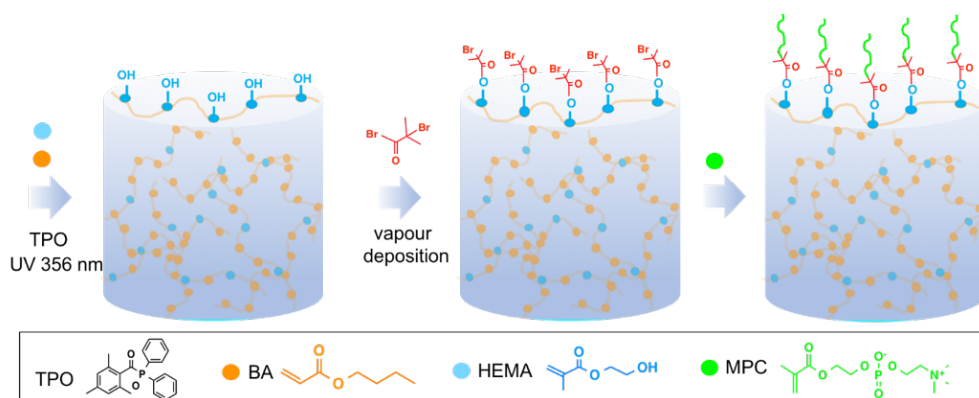


Figure 9. Preparation of PBA-based elastomers and subsequent growth of PMPC brushes by Cu⁰ SI-ATRP.

When microporous cellulose sheets previously derivatised by ATRP initiator functions (Experimental Methods) and soaked with few tens of μL of monomer mixture were sandwiched between an inert silicon substrate and a copper plate, thick PMPC brushes were successfully

grown in 60 minutes of reaction (Figure 8a and 8b), as evidenced by a combination of attenuated total reflectance Fourier-transform infrared spectroscopy (ATR FTIR) and scanning electron microscopy (SEM). In particular, ATR FTIR confirmed the successful grafting of PMPC brushes, through the appearance of the signal at 1730 cm^{-1} , corresponding to C=O stretching in the polymer repeating unit, the band centered at 1240 cm^{-1} , corresponding to -O-P-O-, and that at 970 cm^{-1} referring to $-\text{N}^+(\text{CH}_3)_3$ (Figure 8c). SEM further demonstrated the formation of a uniform PMPC brush film on cellulose fibres, by comparing the micrographs recorded on pristine sheets (Figure 8d and 8f) with those obtained after Cu^0 SI-ATRP of MPC (Figure 8e and 8g).

Alternatively, Cu^0 SI-ATRP could be applied for the modification of the exposed surface of a PBA-based elastomer, where uniform PMPC brushes were grafted by simply placing the elastomeric stamp in contact with a copper plate, which was previously covered by few drops of polymerization solution. Also in this case, the reaction mixture was not deoxygenated, and the modification of the elastomer was performed without the presence an inert atmosphere, but simply on a petri dish exposed to air. After 1 hour of polymerization, the growth of PMPC brushes was confirmed by ATR FTIR spectroscopy (Figure 8j), through the appearance of the signals at 1240 cm^{-1} (-O-P-O-), 1080 cm^{-1} (-P-O-C), and 970 cm^{-1} ($-\text{N}^+(\text{CH}_3)_3$), characteristic of the PMPC repeating unit. Wettability measurements further demonstrated the formation of a hydrophilic PMPC film on the elastomer, the static water contact angle (CA) shifting from $83 \pm 2^\circ$ (Figure 8k) to $40 \pm 1^\circ$ (Figure 8l).

6.3 Conclusions

Cu^0 SI-ATRP has been demonstrated to be an efficient, highly versatile and extremely controlled grafting technique, which is compatible with flat inorganic surfaces, as well as with porous organic supports of different compositions. The intrinsically confined nature of Cu^0 SI-ATRP, which exploits the intimate contact between a copper plate, acting as source of catalyst and reducing agent, and an initiator-bearing support, determines its many attractive features. This process enables the rapid growth of technologically relevant polymer brushes, over very large and morphologically different substrates, using microliter volumes of reaction mixtures, and without the need for their deoxygenation or an inert atmosphere. These unique characteristics, which were highlighted here for the case of the synthesis of PMPC brushes, demonstrate that the application of Cu^0 SI-ATRP for surface modification can translate SI-RDRP methods from academic studies into technology, opening a plethora of possible applications in materials science.

6.4 Materials and Methods

Materials

Silicon wafers were purchased from Si-Mat (P/B <100>, Si-Mat Silicon Wafers, Landsberg, Germany). Copper plates were obtained by coating silicon wafers with 200 nm of Cu⁰ by magnetron sputtering (Paul Scherrer Institute, Villigen, Switzerland).

3-(Aminopropyl)triethoxysilane (APTES, 99%, Acros), 2-bromoisobutryl bromide (BiBB, 98%, Sigma-Aldrich), triethylamine (TEA, ≥99%, Merck), dichloromethane (DCM, dry, ≥99.8%, Acros), 2-methacryloyloxyethyl phosphorylcholine (MPC, 97%, Sigma-Aldrich), methanol (> 99%, VWR Chemicals), 2,2'-bipyridine (≥99%, Sigma-Aldrich), diphenyl(2,4,6-trimethylbenzoyl)phosphine oxide (TPO, Sigma-Aldrich, 97%), 2-methacryloyloxyethyl phosphorylcholine (MPC, Sigma-Aldrich, 97%), and copper(II) bromide (CuBr₂, 99.99%, Aldrich) were used as received. Butyl acrylate (BA, 99%, Acros Organics), hydroxyethylmethacrylate (HEMA, 98%, Sigma-Aldrich) and poly(ethylene glycol) dimethacrylate (PEGDMA, *M_n* ~ 550) were purified from inhibitors by filtration through a basic alumina column. All the other chemicals were purchased from Sigma-Aldrich. Water used in all the experiments was Millipore Milli-Q grade.

Quartz Crystal Microbalance with Dissipation (QCM-D)

QCM-D was used to monitor the dissolution of Cu species from Cu⁰-coated sensors, when immersed in different polymerization mixtures, using an E4 instrument (Q-Sense AB, Göteborg, Sweden) equipped with dedicated Q-Sense AB software. Cu-coated crystals (LOT-Oriel AG) with a fundamental resonance frequency of 5 MHz were used as substrates. Before the experiment, the sensors were cleaned by 15 minutes sonication in toluene and 2-propanol, and finally immersed in a 2:1 v/v mixture of methanol and 37% HCl, in order to remove Cu_xO layer. After cleaning, the crystals were dried under a stream of N₂. In order to measure the desorption of Cu species, Cu⁰-coated sensors were mounted in the QCM-D chamber and subsequently subjected to different polymerization mixtures. The recorded frequency shift (Δf) was correlated to the decrease of mass of the Cu layer on the sensor, by applying the Sauerbrey relation,⁵⁶ using the sensitivity factor $C_f = -17.7 \text{ ng Hz}^{-1} \text{ cm}^{-2}$.

Variable-Angle Spectroscopic Ellipsometer (VASE)

The values of dry thickness of the different brush films (*T_{dry}*) were measured using a M-2000F Woollam variable angle spectroscopic ellipsometer (J.A. Woollam Co. U.S.). The values of Ψ and Δ were acquired as a function of wavelength (275–827 nm) using focusing lenses at 70 ° from the surface normal. Fitting of the raw data was performed based on a three-

layer model, using bulk dielectric functions for Si, and SiO₂. The polymer brush layers were analyzed on the basis of the Cauchy model: $n = A + B \lambda^{-2}$, where n is the refractive index, λ is the wavelength and A and B were assumed to be 1.45 and 0.01, respectively, as values for transparent organic films.⁵⁷

Atom Force Microscopy (AFM)

Force-vs-separation (FS) analysis and lateral force microscopy (LFM) on PMPC brushes was performed using a MFP3D AFM (Asylum Research, Oxford Instruments, Santa Barbara, USA) under 10 mM of 4-(2-hydroxyethyl)-1-piperazine-1-ethane- sulfonic acid (HEPES) buffer (pH = 7.4). The normal (K_N) and torsional spring (K_T) constants of tipless cantilevers were measured by the thermal-noise⁵⁸ and Sader's method,⁵⁹ respectively, resulting $K_N = 0.296 \text{ N m}^{-1}$ and $K_T = 5.1 \text{ E}^{-9} \text{ N m}$. The "wall method" reported by Cannara et al.,⁶⁰ was used for calibration of friction force.

Silica microspheres (EKA Chemicals AM, Kormasil) having a diameter of 18 μm were glued to the end of the calibrated cantilevers by a home-built micromanipulator, using an epoxy glue (Araldite® Standard). The cantilevers were cleaned by UV-ozone treatment for 30 min prior to the measurements.

Water-Contact-Angle Measurements

A Ramé-Hart goniometer (model-100, Netcong, NJ) was used to measure the static water contact angle (CA) on the different PMPC brush surfaces. Three individual measurements were performed with a drop-shape analysis system at room temperature. The contact-angle values were obtained by using the tangent-fitting method.

ATRP Initiator-Functionalized Silicon Oxide Substrates

Silicon wafers used as substrates for Cu⁰ SI-ATRP were cleaned for 30 minutes in "piranha" solution (3:1 v/v mixture of 99.9% H₂SO₄ and H₂O₂, CAUTION: piranha solutions react violently with organic compounds, and may result in explosion or skin burns if not handled with extreme caution), and subsequently rinsed with ultrapure water and ethanol. ATRP initiator layers were subsequently deposited using a two-steps protocol. APTES was first immobilized through vapour deposition during 3 hours. After this, the substrates were incubated for 2 hours in a dichloromethane solution of BiBB and TEA, subsequently washed with chloroform and dried under a stream of N₂.

Cu⁰ SI-ATRP of MPC under Ambient Conditions

Cu⁰-coated substrates were washed with isopropanol under sonication (5 min), followed by activation protocol in a 2:1 v/v mixture of methanol and 37% HCl. A polymerization mixture including MPC (1 M), bipy (40 mM), with or without CuBr₂ (0.2 mM) was dropped on the

activated Cu⁰ surface, and immediately covered with ATRP initiator-functionalized substrate, while a constant pressure of 3 g cm⁻² was applied between the sandwiched substrates. The volume of the polymerization mixture applied was 8 μL cm⁻². After the desired polymerization time, the substrates were thoroughly washed with water and ethanol and dried in a stream of N₂.

Functionalization of Cellulose Sheets with ATRP Initiator

Cellulose sheets were functionalized with ATRP initiator using the already reported method.⁶¹ Cellulose sheets were washed with acetone and tetrahydrofuran (THF) and subsequently immersed in a mixture containing BiBB (230 mg, 1.0 mmol, 50 mM), TEA (111 mg, 1.1 mmol, 55 mM), and a catalytic amount of DMAP in THF (20 mL). The reaction was conducted for 2 hours, after which the cellulose substrates were washed with dichloromethane and methanol thoroughly, and dried under N₂ stream.

Cu⁰ SI-ATRP from Cellulose Sheets.

50 μL of a solution of MPC (1M), bipy (40 mM), and CuBr₂ (0.2 mM) was poured on a cellulose sheet previously placed on a Cu⁰-coated substrate, and immediately covered by a freshly cleaned silicon substrate. After the desired polymerization time, the reaction was terminated by rinsing the filter paper with water and methanol and dried under a stream of N₂. The modified cellulose sheet was subsequently analyzed by attenuated total reflectance Fourier-transform infrared spectroscopy (ATR-FTIR) and SEM.

Synthesis of PBA-Based Elastomers.

PBA-based elastomers were synthesized via photo-initiated radical polymerization (Figure 9). Mixtures including butyl acrylate (0.153 mol, 4.78 M), HEMA (0.016 mol, 0.5 M) and PEGDMA (1.69 mmol, 52.8 mM) were degassed in 10 ml toluene for 20 min, after that, TPO (0.2 mM in toluene) was added. The polymerization was conducted under UV light ($\lambda = 365$ nm, 1.2 mW cm⁻²) using a Stratalinker UV crosslinker 2400 (Stratagene, La Jolla, CA, USA) at room temperature for 60 min. PBA elastomers were de-moulded from reaction vials, followed by washing thoroughly with toluene. ATRP initiators were generated on PBA-based elastomers by vapour deposition of BiBB (Figure 9), followed by rinsing with chloroform and toluene.

Cu⁰ SI-ATRP from PBA-Based Elastomers.

0.5 mL of a polymerization solution including MPC (1M), bipy (40 mM), and CuBr₂ (0.2 mM) were poured on a previously activated Cu⁰-coated substrate and immediately covered with an ATRP-initiator functionalized PBA-based elastomer. After the desired polymerization

time, the sample was rinsed with methanol and water, and finally dried under a stream of N₂. Elastomers presenting PMPC brushes were subsequently analyzed by ATR-FTIR and CA.

Scanning Electron Microscope (SEM).

PMPC brush-functionalized cellulose sheets were sputter coated (CCU-010 Compact coating unit; Safematic) with 3 nm of platinum, in order to avoid surface charging during imaging. A scanning electron microscope (SEM, Thermo scientific, ultradry) equipped with a LEO 1530 operating instrument (Zeiss GmbH, Germany), was used to record the micrographs.

References

1. Zoppe, J. O.; Ataman, N. C.; Mocny, P.; Wang, J.; Moraes, J.; Klok, H. A., Surface-Initiated Controlled Radical Polymerization: State-of-the-Art, Opportunities, and Challenges in Surface and Interface Engineering with Polymer Brushes (vol 117, pg 1105, 2017). *Chem. Rev.* **2017**, *117* (5), 4667-4667.
2. Barbey, R.; Lavanant, L.; Paripovic, D.; Schuwer, N.; Sugnaux, C.; Tugulu, S.; Klok, H. A., Polymer Brushes via Surface-Initiated Controlled Radical Polymerization: Synthesis, Characterization, Properties, and Applications. *Chem. Rev.* **2009**, *109* (11), 5437-5527.
3. Omar, A., Polymer Brushes Here, There, and Everywhere: Recent Advances in Their Practical Applications and Emerging Opportunities in Multiple Research Fields. *J. Polym. Sci. A* **2012**, *50* (16), 3225-3258.
4. Chen, W.-L.; Cordero, R.; Tran, H.; Ober, C. K., 50th Anniversary Perspective: Polymer Brushes: Novel Surfaces for Future Materials. *Macromolecules* **2017**, *50* (11), 4089-4113.
5. Zhou, F.; Shu, W. M.; Welland, M. E.; Huck, W. T. S., Highly Reversible and Multi-Stage Cantilever Actuation Driven by Polyelectrolyte Brushes. *J. Am. Chem. Soc.* **2006**, *128* (16), 5326-5327.
6. Joh, D. Y.; Hucknall, A. M.; Wei, Q. S.; Mason, K. A.; Lund, M. L.; Fontes, C. M.; Hill, R. T.; Blair, R.; Zimmers, Z.; Achar, R. K.; Tseng, D.; Gordan, R.; Freemark, M.; Ozcan, A.; Chilkoti, A., Inkjet-Printed Point-of-Care Immunoassay on a Nanoscale Polymer Brush Enables Subpicomolar Detection of Analytes in Blood. *Proc. Natl. Acad. Sci. U.S.A.* **2017**, *114* (34), E7054-E7062.
7. Badoux, M.; Billing, M.; Klok, H. A., Polymer Brush Interfaces for Protein Biosensing Prepared by Surface-Initiated Controlled Radical Polymerization. *Polym. Chem.* **2019**, *10*, 2925-2951

8. Fortin, N.; Klok, H. A., Glucose Monitoring Using a Polymer Brush Modified Polypropylene Hollow Fiber-based Hydraulic Flow Sensor. *ACS Appl. Mater. Interfaces* **2015**, *7* (8), 4631-4640.
9. Benetti, E. M.; Acikgoz, C.; Sui, X. F.; Vratzov, B.; Hempenius, M. A.; Huskens, J.; Vancso, G. J., Nanostructured Polymer Brushes by UV-Assisted Imprint Lithography and Surface-Initiated Polymerization for Biological Functions. *Adv. Funct. Mater.* **2011**, *21* (11), 2088-2095.
10. Christau, S.; Genzer, J.; von Klitzing, R., Polymer Brush/Metal Nanoparticle Hybrids for Optical Sensor Applications: from Self-Assembly to Tailored Functions and Nanoengineering. *Z. Phys. Chem.* **2015**, *229* (7-8), 1089-1117.
11. Gautrot, J. E.; Wang, C.; Liu, X.; Goldie, S. J.; Trappmann, B.; Huck, W. T.; Watt, F. M., Mimicking Normal Tissue Architecture and Perturbation in Cancer with Engineered Micro-Epidermis. *Biomaterials* **2012**, *33* (21), 5221-5229.
12. Desseaux, S.; Klok, H. A., Fibroblast adhesion on ECM-Derived Peptide Modified Poly(2-hydroxyethyl methacrylate) Brushes: Ligand Co-Presentation and 3D-Localization. *Biomaterials* **2015**, *44*, 24-35.
13. Desseaux, S.; Klok, H.-A., Temperature-Controlled Masking/Unmasking of Cell-Adhesive Cues with Poly(ethylene glycol) Methacrylate Based Brushes. *Biomacromolecules* **2014**, *15*, 3859-65.
14. Paripovic, D.; Hall-Bozic, H.; Klok, H. A., Osteoconductive Surfaces Generated from Peptide Functionalized Poly(2-hydroxyethyl methacrylate-co-2-(methacryloyloxy)ethyl phosphate) Brushes. *J. Mater. Chem.* **2012**, *22* (37), 19570-19578.
15. Raynor, J. E.; Petrie, T. A.; Garcia, A. J.; Collard, D. M., Controlling Cell Adhesion to Titanium: Functionalization of Poly[oligo(ethylene glycol)methacrylate] Brushes with Cell-Adhesive Peptides. *Adv. Mater.* **2007**, *19* (13), 1724-1728.
16. Klein Gunnewiek, M.; Di Luca, A.; Bollemaat, H. Z.; van Blitterswijk, C. A.; Vancso, G. J.; Moroni, L.; Benetti, E. M., Creeping Proteins in Microporous Structures: Polymer Brush-Assisted Fabrication of 3D Gradients for Tissue Engineering. *Adv. Health. Mater.* **2015**, *4* (8), 1169-1174.
17. Zhang, Z. Y.; Morse, A. J.; Armes, S. P.; Lewis, A. L.; Geoghegan, M.; Leggett, G. J., Effect of Brush Thickness and Solvent Composition on the Friction Force Response of Poly(2-(methacryloyloxy)ethylphosphorylcholine) Brushes. *Langmuir* **2011**, *27* (6), 2514-2521.
18. Kobayashi, M.; Terayama, Y.; Hosaka, N.; Kaido, M.; Suzuki, A.; Yamada, N.; Torikai, N.; Ishihara, K.; Takahara, A., Friction Behavior of High-Density Poly(2-

methacryloyloxyethyl phosphorylcholine) Brush in Aqueous Media. *Soft Matter* **2007**, *3* (6), 740-746.

19. Rafti, M.; Brunsen, A.; Fuertes, M. C.; Azzaroni, O.; Soler-Illia, G. J. A. A., Heterogeneous Catalytic Activity of Platinum Nanoparticles Hosted in Mesoporous Silica Thin Films Modified with Polyelectrolyte Brushes. *ACS Appl. Mater. Interfaces* **2013**, *5* (18), 8833-8840.

20. Benetti, E. M., Quasi-3D-Structured Interfaces by Polymer Brushes. *Macromol. Rapid Commun.* **2018**, *39* (14).

21. Costantini, F.; Benetti, E. M.; Tiggelaar, R. M.; Gardeniers, H. J. G. E.; Reinhoudt, D. N.; Huskens, J.; Vancso, G. J.; Verboom, W., A Brush-Gel/Metal-Nanoparticle Hybrid Film as an Efficient Supported Catalyst in Glass Microreactors. *Chem. Eur. J.* **2010**, *16* (41), 12406-12411.

22. Costantini, F.; Benetti, E. M.; Reinhoudt, D. N.; Huskens, J.; Vancso, G. J.; Verboom, W., Enzyme-Functionalized Polymer Brush Films on the Inner Wall of Silicon-Glass Microreactors with Tunable Biocatalytic Activity. *Lab. Chip* **2010**, *10* (24), 3407-3412.

23. Yeow, J.; Chapman, R.; Gormley, A. J.; Boyer, C., Up in the Air: Oxygen Tolerance in Controlled/Living Radical Polymerisation. *Chem. Soc. Rev.* **2018**, *47* (12), 4357-4387.

24. Li, M.; Fromel, M.; Ranaweera, D.; Rocha, S.; Boyer, C.; Pester, C. W., SI-PET-RAFT: Surface-Initiated Photoinduced Electron Transfer-Reversible Addition-Fragmentation Chain Transfer Polymerization. *ACS Macro Lett.* **2019**, *8*, 374-380.

25. Matyjaszewski, K.; Miller, P. J.; Shukla, N.; Immaraporn, B.; Gelman, A.; Luokala, B. B.; Siclovan, T. M.; Kickelbick, G.; Vallant, T.; Hoffmann, H.; Pakula, T., Polymers at Interfaces: Using Atom Transfer Radical Polymerization in the Controlled Growth of Homopolymers and Block Copolymers from Silicon Surfaces in the Absence of Untethered Sacrificial Initiator. *Macromolecules* **1999**, *32* (26), 8716-8724.

26. Matyjaszewski, K.; Dong, H. C.; Jakubowski, W.; Pietrasik, J.; Kusumo, A., Grafting from Surfaces for "Everyone": ARGET ATRP in the Presence of Air. *Langmuir* **2007**, *23* (8), 4528-4531.

27. Dunderdale, G. J.; England, M. W.; Urata, C.; Hozumi, A., Polymer Brush Surfaces Showing Superhydrophobicity and Air-Bubble Repellency in a Variety of Organic Liquids. *ACS Appl. Mater. Interfaces* **2015**, *7* (22), 12220-12229.

28. Dunderdale, G. J.; Urata, C.; Miranda, D. F.; Hozumi, A., Large-Scale and Environmentally Friendly Synthesis of pH-Responsive Oil-Repellent Polymer Brush Surfaces under Ambient Conditions. *ACS Appl. Mater. Interfaces* **2014**, *6* (15), 11864-11868.

29. Navarro, L. A.; Enciso, A. E.; Matyjaszewski, K.; Zauscher, S., Enzymatically Degassed Surface-Initiated Atom Transfer Radical Polymerization with Real-Time Monitoring. *J. Am. Chem. Soc.* **2019**, *141* (7), 3100-3109.
30. Narupai, B.; Page, Z. A.; Treat, N. J.; McGrath, A. J.; Pester, C. W.; Discekici, E. H.; Dolinski, N. D.; Meyers, G. F.; de Alaniz, J. R.; Hawker, C. J., Simultaneous Preparation of Multiple Polymer Brushes under Ambient Conditions using Microliter Volumes. *Angew. Chem. Int. Edit.* **2018**, *57* (41), 13433-13438.
31. Sato, T.; Dunderdale, G. J.; Urata, C.; Hozumi, A., Sol-Gel Preparation of Initiator Layers for Surface-Initiated ATRP: Large-Scale Formation of Polymer Brushes Is Not a Dream. *Macromolecules* **2018**, *51* (24), 10065-10073.
32. Zhang, T.; Du, Y. H.; Muller, F.; Amin, I.; Jordan, R., Surface-Initiated Cu(0) Mediated Controlled Radical Polymerization (SI-CuCRP) Using a Copper Plate. *Polym. Chem.* **2015**, *6* (14), 2726-2733.
33. Zhang, T.; Du, Y. H.; Kalbacova, J.; Schubel, R.; Rodriguez, R. D.; Chen, T.; Zahn, D. R. T.; Jordan, R., Wafer-Scale Synthesis of Defined Polymer Brushes under Ambient Conditions. *Polym. Chem.* **2015**, *6* (47), 8176-8183.
34. Zhang, T.; Benetti, E. M.; Jordan, R., Surface-Initiated Cu(0)-Mediated CRP for the Rapid and Controlled Synthesis of Quasi-3D Structured Polymer Brushes. *ACS Macro Lett.* **2019**, *8* (2), 145-153.
35. Dehghani, E. S.; Du, Y.; Zhang, T.; Ramakrishna, S. N.; Spencer, N. D.; Jordan, R.; Benetti, E. M., Fabrication and Interfacial Properties of Polymer Brush Gradients by Surface-Initiated Cu(0)-Mediated Controlled Radical Polymerization. *Macromolecules* **2017**, *50* (6), 2436-2446.
36. Fantin, M.; Ramakrishna, S. N.; Yan, J. J.; Yan, W. Q.; Divandari, M.; Spencer, N. D.; Matyjaszewski, K.; Benetti, E. M., The Role of Cu⁰ in Surface-Initiated Atom Transfer Radical Polymerization: Tuning Catalyst Dissolution for Tailoring Polymer Interfaces. *Macromolecules* **2018**, *51* (17), 6825-6835.
37. Zhang, Z. Y.; Morse, A. J.; Armes, S. P.; Lewis, A. L.; Geoghegan, M.; Leggett, G. J., Nanoscale Contact Mechanics of Biocompatible Polyzwitterionic Brushes. *Langmuir* **2013**, *29* (34), 10684-10692.
38. Tairy, O.; Kampf, N.; Driver, M. J.; Armes, S. P.; Klein, J., Dense, Highly Hydrated Polymer Brushes via Modified Atom-Transfer-Radical-Polymerization: Structure, Surface Interactions, and Frictional Dissipation. *Macromolecules* **2015**, *48* (1), 140-151.

39. Chen, M.; Briscoe, W. H.; Armes, S. P.; Klein, J., Lubrication at Physiological Pressures by Polyzwitterionic Brushes. *Science* **2009**, *323* (5922), 1698-1701.
40. Chang, Y.; Shih, Y. J.; Lai, C. J.; Kung, H. H.; Jiang, S. Y., Blood-Inert Surfaces via Ion-Pair Anchoring of Zwitterionic Copolymer Brushes in Human Whole Blood. *Adv. Funct. Mater.* **2013**, *23* (9), 1100-1110.
41. Zhang, Z.; Chao, T.; Chen, S. F.; Jiang, S. Y., Superlow Fouling Sulfobetaine and Carboxybetaine Polymers on Glass Slides. *Langmuir* **2006**, *22* (24), 10072-10077.
42. Kobayashi, M.; Terayama, Y.; Kikuchi, M.; Takahara, A., Chain Dimensions and Surface Characterization of Superhydrophilic Polymer Brushes with Zwitterion Side Groups. *Soft Matter* **2013**, *9* (21), 5138-5148.
43. Kobayashi, M.; Terayama, Y.; Yamaguchi, H.; Terada, M.; Murakami, D.; Ishihara, K.; Takahara, A., Wettability and Antifouling Behavior on the Surfaces of Superhydrophilic Polymer Brushes. *Langmuir* **2012**, *28* (18), 7212-7222.
44. Yu, Y.; Vancso, G. J.; de Beer, S., Substantially Enhanced Stability Against Degrafting of Zwitterionic PMPC Brushes by Utilizing PGMA-Linked Initiators. *Eur. Polym. J.* **2017**, *89*, 221-229.
45. Konkolewicz, D.; Wang, Y.; Krys, P.; Zhong, M.; Isse, A. A.; Gennaro, A.; Matyjaszewski, K., SARA ATRP or SET-LRP. End of Controversy? *Polym. Chem.* **2014**, *5* (15), 4396-4417.
46. Konkolewicz, D.; Krys, P.; Góis, J. R.; Mendonça, P. V.; Zhong, M.; Wang, Y.; Gennaro, A.; Isse, A. A.; Fantin, M.; Matyjaszewski, K., Aqueous RDRP in the Presence of Cu⁰: The Exceptional Activity of Cu^I Confirms the SARA ATRP Mechanism. *Macromolecules* **2014**, *47* (2), 560-570.
47. Konkolewicz, D.; Wang, Y.; Zhong, M.; Krys, P.; Isse, A. A.; Gennaro, A.; Matyjaszewski, K., Reversible-Deactivation Radical Polymerization in the Presence of Metallic Copper. A Critical Assessment of the SARA ATRP and SET-LRP Mechanisms. *Macromolecules* **2013**, *46* (22), 8749-8772.
48. Jordan, R.; Ulman, A.; Kang, J. F.; Rafailovich, M. H.; Sokolov, J., Surface-Initiated Anionic Polymerization of Styrene by Means of Self-Assembled Monolayers. *J. Am. Chem. Soc.* **1999**, *121* (5), 1016-1022.
49. Singh, N.; Cui, X. F.; Boland, T.; Husson, S. M., The Role of Independently Variable Grafting Density and Layer Thickness of Polymer Nanolayers on Peptide Adsorption and Cell Adhesion. *Biomaterials* **2007**, *28* (5), 763-771.

50. Ramakrishna, S. N.; Cirelli, M.; Kooij, E. S.; Klein Gunnewiek, M.; Benetti, E. M., Amplified Responsiveness of Multilayered Polymer Grafts: Synergy between Brushes and Hydrogels. *Macromolecules* **2015**, *48*, 7106-7116.
51. Cheng, N.; Brown, A. A.; Azzaroni, O.; Huck, W. T. S., Thickness-Dependent Properties of Polyzwitterionic Brushes. *Macromolecules* **2008**, *41* (17), 6317-6321.
52. Busutil, K.; Geoghegan, M.; Hunter, C. A.; Leggett, G. J., Contact Mechanics of Nanometer-Scale Molecular Contacts: Correlation between Adhesion, Friction, and Hydrogen Bond Thermodynamics. *J. Am. Chem. Soc.* **2011**, *133* (22), 8625-8632.
53. Hurley, C. R.; Leggett, G. J., Influence of the Solvent Environment on the Contact Mechanics of Tip-Sample Interactions in Friction Force Microscopy of Poly(ethylene terephthalate) Films. *Langmuir* **2006**, *22* (9), 4179-4183.
54. Jiang, S. Y.; Cao, Z. Q., Ultralow-Fouling, Functionalizable, and Hydrolyzable Zwitterionic Materials and Their Derivatives for Biological Applications. *Adv. Mater.* **2010**, *22* (9), 920-932.
55. Shivapooja, P.; Yu, Q.; Orihuela, B.; Mays, R.; Rittschof, D.; Genzer, J.; Lopez, G. P., Modification of Silicone Elastomer Surfaces with Zwitterionic Polymers: Short-Term Fouling Resistance and Triggered Biofouling Release. *ACS Appl. Mater. Interfaces* **2015**, *7* (46), 25586-25591.
56. Sauerbrey, G. Verwendung von Schwingquarzen zur Wägung dünner Schichten und zur Mikrowägung. *Z. Phys.* **1959**, *155*, 206-222.
57. Hilfiker, J. N.; Synowicki, R. A.; Bungay, C. L.; Carpio, R., Spectroscopic Ellipsometry for Polymer Thin Films. *Solid State Tech.* **1998**, *41* (10), 101.
58. Hutter, J. L.; Bechhoefer, J., Calibration of Atomic-Force Microscope Tips. *Rev. Sci. Instrum.* **1993**, *64* (7), 1868-1873.
59. Green, C. P.; Lioe, H.; Cleveland, J. P.; Proksch, R.; Mulvaney, P.; Sader, J. E., Normal and Torsional Spring Constants of Atomic Force Microscope Cantilevers. *Rev. Sci. Instrum.* **2004**, *75* (6), 1988-1996.
60. Cannara, R. J.; Eglin, M.; Carpick, R. W., Lateral Force Calibration in Atomic Force Microscopy: A New Lateral Force Calibration Method and General Guidelines for Optimization. *Rev. Sci. Instrum.* **2006**, *77* (5).
61. Carlmark, A.; Malmstrom, E. E., ATRP Grafting from Cellulose Fibers to Create Block-Copolymer Grafts. *Biomacromolecules* **2003**, *4* (6), 1740-1745.

Chapter 7

Oxygen Tolerant and Cytocompatible Fe⁰-Mediated ATRP Enables the Controlled Growth of Polymer Brushes from Mammalian Cell Cultures*

The use of zerovalent iron (Fe⁰)-coated plates, which act both as a source of catalyst and as a reducing agent during surface-initiated atom transfer radical polymerization (SI-ATRP), enables the controlled growth of a wide range of polymer brushes under ambient conditions, and utilizing either organic or aqueous reaction media. Thanks to its cytocompatibility, Fe⁰ SI-ATRP can be applied within cell cultures, providing a tool that can broadly and dynamically modify the substrate's affinity towards cells, without influencing their viability. Upon systematically assessing the application of Fe-based catalytic systems in the controlled grafting of polymers, Fe⁰ SI-ATRP emerges as an extremely versatile technique that could be applied to tune the physicochemical properties of cell's microenvironments on biomaterials or within tissue engineering constructs.

* Edmondo M. Benetti supervised this project. Amine Layadi, Benjamin Kesse and Wenqing Yan performed experimental work. Edmondo M. Benetti, Amine Layadi, Benjamin Kessel, Wenqing Yan, Matteo Romio, Nicholas D. Spencer, Marcy Zenobi-Wong and Krzysztof Matyjaszewski discussed the results and wrote the paper. Part of this Chapter was published in *J. Am. Chem. Soc.* **2020**, 3158-3164.

7.1 Introduction

While the evolution of oxygen-tolerant, surface-initiated reversible deactivation radical polymerizations (SI-RDRP) is paving the way for the translation of “grafted-from” polymers from fundamental studies into technology, the development of controlled polymerizations that are additionally compatible with physiological environments would substantially broaden the applicability of SI-RDRP in materials design. In particular, an RDRP process capable of modifying the physicochemical properties of cellular microenvironments through polymer grafting, without altering cell viability, would allow one to adjust the biological affinity of scaffolds towards a particular cell type during culturing, or alternatively to tune the presentation of biochemical cues triggering a defined cell behavior. More generally, the controlled growth of polymer brushes from cell-loaded supports would enable the fabrication of active biomaterials, capable of re-shaping themselves in a dynamic fashion following biocompatible processes.

Focusing on surface-initiated atom transfer radical polymerization (SI-ATRP), the most widely applied SI-RDRP method, we demonstrate in this Chapter that the application of Fe^0 plates, acting as a source of both biocompatible catalyst and reducing agent, can enable the controlled, rapid growth of polymer brushes within organic as well as in aqueous and cell-culture media.

While introducing and systematically assessing the use of Fe-based catalytic systems in the fabrication of polymer brushes,¹⁴ we show that Fe^0 -mediated SI-ATRP (Fe^0 SI-ATRP) can be performed in the presence of primary articular chondrocytes (ACs) that had been previously cultured on initiator-bearing substrates, generating in situ polymer brushes that substantially alter the settlement of cells without affecting their viability.

7.2 Results and Discussion

7.2.1 Mechanism and kinetics of Fe^0 SI-ATRP

When a monomer and ligand (L) mixture is sandwiched between a Fe^0 -coated plate and an ATRP-bearing substrate, the metallic surface rapidly consumes oxygen through the formation of Fe_xO_y species, which act as a source of $\text{Fe}^{\text{II}}/\text{Fe}^{\text{III}}$ catalysts, diffusing towards the initiating sites (Figure 1). The growth of polymer brushes then proceeds according to the ATRP equilibrium, and can be efficiently performed without the need for prior deoxygenation of monomer mixtures, or an inert atmosphere.

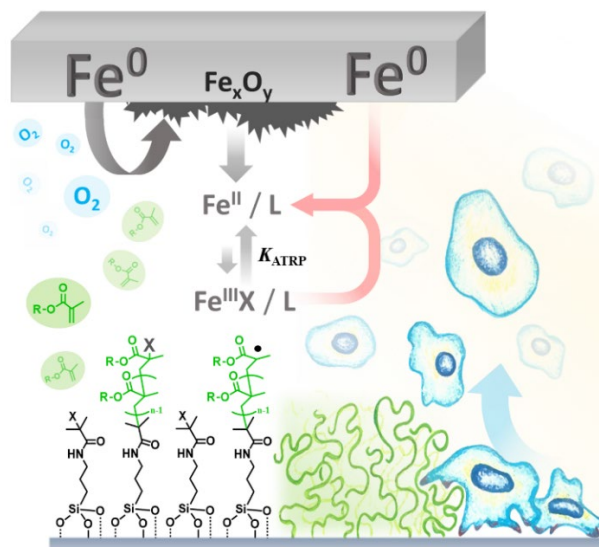


Figure 1. Schematic depicting the mechanism of Fe⁰ SI-ATRP.

To illustrate the mechanism of Fe⁰ SI-ATRP and its main features, the synthesis of polymer brushes in organic solvents was first examined. Similarly to what was previously reported in the case of Cu⁰-mediated SI-ATRP,¹⁰ in the absence of externally added deactivator (Fe^{III}Br₃) the growth of poly(methyl methacrylate) (PMMA) brushes using anisole as solvent and 20 mM of weakly coordinating halide ligands (in the form of tetra-*n*-butylammonium bromide, TBABr)¹⁵⁻¹⁷ proceeded slowly, reaching just a few nm of dry thickness in several hours of reaction (Figure 2a), as measured ex situ by variable-angle spectroscopic ellipsometry (VASE). In contrast, when 10 mM Fe^{III}Br₃ was added to the mixture, the polymerization proceeded rapidly, leading to a progressive growth of PMMA brushes, which reached ~ 20 nm after 5 hours of reaction. It is important to emphasize that an excess of TBABr with respect to Fe^{III}Br₃ was necessary to guarantee the complete dissolution of Fe species, especially in 50:50 anisole:MMA mixtures (v/v), where their solubility in the absence of ligand would be limited.¹⁵

In both these cases, an induction time necessary to oxygen consumption was never observed, suggesting that oxidation of Fe⁰ surface quickly takes place just at the very early stages of the reaction.

An analogous result was obtained in the case of Fe⁰ SI-ATRP of oligo(ethylene glycol) methacrylate (OEGMA) performed in *N,N*-dimethylformamide (DMF), where a comparable amount of Fe^{III}Br₃ was required to attain a significant growth of POEGMA brushes, reaching nearly 30 nm of thickness in 5 hours (Figure 2b).

The role played by added Fe^{III}Br₃ was elucidated while monitoring the variation of POEGMA-brush thickness as a function of Fe^{III}Br₃ concentration for fixed polymerization times (Figure 2c). The thickness of POEGMA brushes increased with [Fe^{III}Br₃], reaching a

maximum between 5 and 10 mM. Under these conditions, Fe^{III} species acted both as a deactivator, suppressing irreversible termination by radical recombination between growing chains, and contributed to generating Fe^{II} -based activators through comproportionation with Fe^0 (Figure 1), in this way accelerating the grafting process.¹⁵

A further addition of $\text{Fe}^{\text{III}}\text{Br}_3$ beyond 10 mM led to a decrease in brush thickness, suggesting a significant deactivation and a simultaneous slowing down of the polymerization.

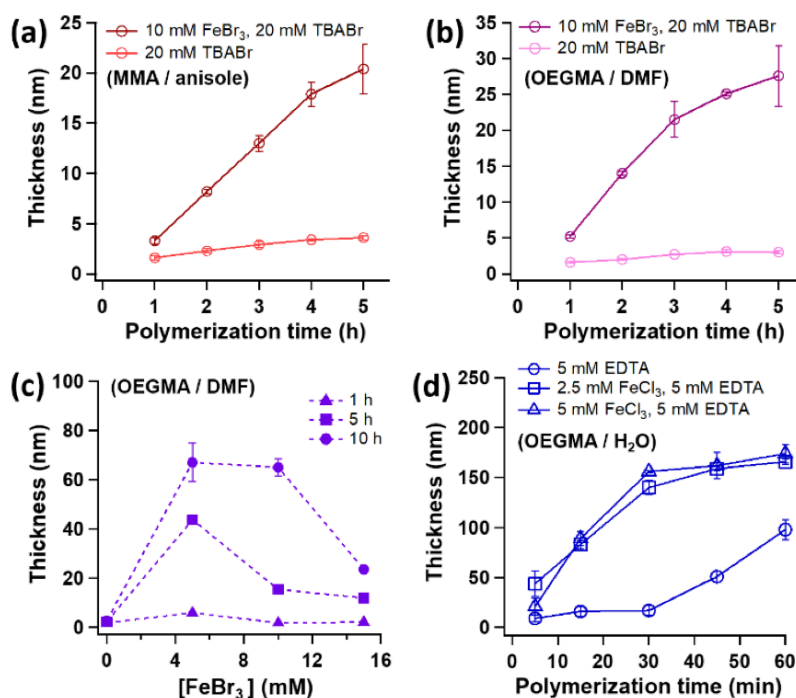


Figure 2. (a) Dry thickness of PMMA brushes measured *ex situ* by VASE during Fe^0 SI-ATRP of MMA performed in 50% (v/v) anisole solutions with 20 mM TBABr and with or without 10 mM $\text{Fe}^{\text{III}}\text{Br}_3$. (b) Fe^0 SI-ATRP of OEGMA performed in 50% (v/v) DMF solutions with 20 mM TBABr and with or without 10 mM $\text{Fe}^{\text{III}}\text{Br}_3$. (c) Variation of POEGMA-brush thickness measured by VASE, as a function of $\text{Fe}^{\text{III}}\text{Br}_3$ concentration, while keeping the concentration of TBABr fixed at 20 mM. (d) Dry thickness of POEGMA brushes measured by VASE during Fe^0 SI-ATRP of OEGMA performed in 50% (v/v) water solutions containing 5 mM EDTA, 10 mM NaCl and variable concentrations of $\text{Fe}^{\text{III}}\text{Cl}_3$.

It is important to emphasize that the balance between the above-mentioned effects determined the position of the maximum of polymer-brush thickness as a function of $[\text{Fe}^{\text{III}}\text{Br}_3]$, which might shift during the progression of the grafting process. An increment in the content of activators through comproportionation led to an increase in brush-growth rate, especially during the early stages of polymerization. Simultaneously, an increase in deactivation by added Fe^{III} species slowed down the grafting process, although it additionally suppressed irreversible termination by radical recombination between propagating grafts, which is especially relevant after relatively long reaction times (for more flexible, high-molecular-weight grafted chains).¹⁸

Fe⁰ SI-ATRP was subsequently investigated in aqueous environments, and using ethylenediaminetetraacetic acid (EDTA) as a ligand. EDTA strongly binds Fe species to form cytocompatible complexes¹⁹ to efficiently catalyze Fe-based ATRP in solution and heterogeneous systems, as previously demonstrated.^{20,21}

In the exemplary case of Fe⁰ SI-ATRP of OEGMA performed in 50% water mixtures (v/v), the growth of brushes followed much faster kinetics compared to those recorded in organic media, as expected from the significantly larger ATRP equilibrium constant (K_{ATRP}) that is characteristic for aqueous systems.²²⁻²⁴ More than 150 nm-thick POEGMA brushes could be grown in just one hour of polymerization when 2.5-5 mM Fe^{III}Cl₃-EDTA were added to the aqueous reaction mixture (Figure 2d and Figure 3), whereas just ~ 5 nm-thick brushes were grafted after the same time using DMF as solvent, and no appreciable brush growth could be recorded in anisole.

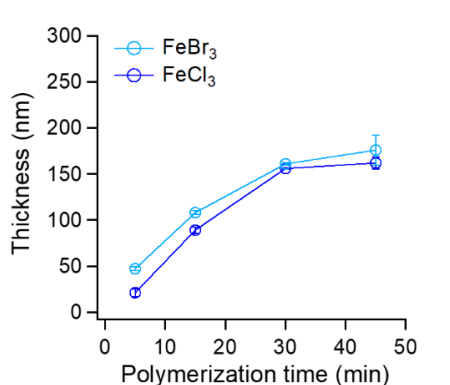


Figure 3. Dry thickness of OEGMA brushes measured ex situ by VASE during Fe⁰ SI-ATRP. Two different catalytic systems were used, either including EDTA (5 mM), FeBr₃ (5 mM), and NaBr (10 mM), or EDTA (5 mM), FeCl₃ (5 mM), and NaCl (10 mM). In both cases, the catalysts were dissolved in a 50:50 H₂O:OEGMA mixture (v/v). No significant differences were observed between the growth rates of POEGMA during Fe⁰ SI-ATRP using FeBr₃ and FeCl₃.

The presence of 5 mM EDTA alone enabled the synthesis of significantly thinner films, which initially grew following relatively slow kinetics. This was presumably due to the time required by Fe^{II}/Fe^{III}-EDTA adducts to diffuse from the Fe plate to the initiator-bearing substrate.¹⁰

As displayed in Figure 4, an increment in the distance between Fe⁰ and ATRP initiator-bearing substrates translated into a progressive decrease of POEGMA-brush thickness, as a result of the slow diffusion of Fe^{II}-based activator species from the Fe⁰ surface to the initiating surfaces.

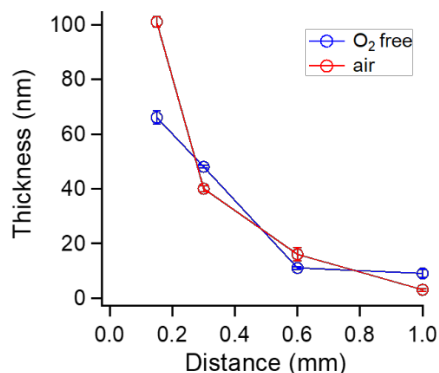


Figure 4. Dry thickness of POEGMA brushes measured *ex situ* by VASE following 45 min of Fe^0 SI-ATRP performed by applying different distances between Fe^0 and ATRP initiator-bearing surfaces.

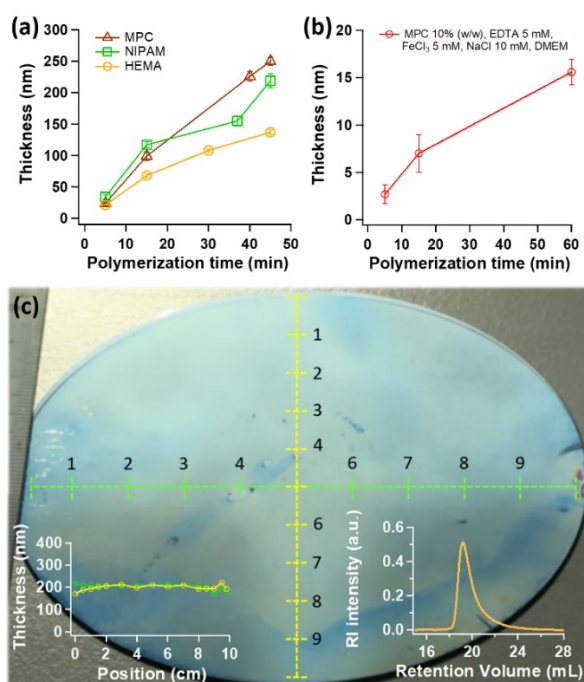


Figure 5. (a) Evolution of brush thickness measured by VASE during Fe^0 SI-ATRP of MPC, NIPAM and HEMA. (b) PMPC-brush thickness measured by VASE during Fe^0 SI-ATRP performed in 0.3 M MPC DMEM solutions. (c) PMPC brushes grafted from an entire, 4-inch silicon wafer by Fe^0 SI-ATRP. The brush thickness measured by VASE across the surface is reported in the inset. A SEC trace from detached PMPC brushes is also shown.

Using 5 mM $Fe^{III}Cl_3$ -EDTA, a range of bio-relevant polymer brushes could be grafted by polymerizing 2-methacryloyloxyethyl phosphorylcholine (MPC, 3 M), N-isopropylacrylamide (NIPAM, 2 M) and 2-hydroxyethyl methacrylate (HEMA, 4 M), obtaining extremely thick PMPC (250 ± 7 nm), PNIPAM (219 ± 12 nm) and PHEMA (137 ± 5 nm) films just after 45 min of reaction (Figure 5a).

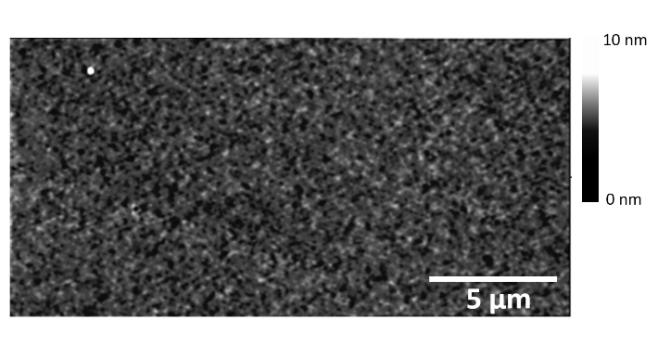


Figure 6. AFM tapping-mode height micrograph recorded in air on 200 nm-thick PMPC brushes synthesized by Fe^0 SI-ATRP from 8-inch silicon wafer.

Aqueous Fe^0 SI-ATRP could be further applied for growing similar brush films from large substrates, as demonstrated in the case of PMPC brushes, which could be grown from 4-inch silicon wafers, forming ~ 200 nm-thick films with homogeneous thickness and morphology after 30 min of polymerization (Figure 5c and Figure 6). Detachment of PMPC grafts²⁵⁻²⁷ enabled their characterization by size-exclusion chromatography (SEC), yielding a M_n of 600 kDa and a \bar{D} of 1.34 (corresponding to a surface coverage of 0.23 chains nm^{-2}),²⁸ and suggesting a well-controlled polymerization process (inset in Figure 5c).

7.2.2 Cytocompatibility toward mammalian cells

In order to test the applicability of Fe^0 SI-ATRP within cell cultures, we subsequently analyzed the growth of PMPC brushes using Dulbecco's modified Eagle's medium (DMEM) as a solvent, and simultaneously tested the cytocompatibility of the polymerization conditions employed towards ACs.

PMPC brushes are especially relevant in the design of biointerfaces due to their biocompatibility and inertness towards unspecific protein and cell contamination.²⁹⁻³¹ As a result of their pronounced hydration, the growth of PMPC grafts from substrates previously cultured with cells would directly translate into an evident variation in the strength of cell attachment, leading to the progressive detachment of ACs when the thickness and density of the underlying brushes reached sufficiently high values.³²

Fe^0 SI-ATRP of a diluted, 0.3 M MPC solution in DMEM using 5 mM $Fe^{III}Cl_3$ -EDTA resulted in a slow but notable growth of brushes, which reached ~ 15 nm after 60 min of reaction (Figure 5b). Relevantly, the slower polymer-brush thickening rate compared to those recorded using pure water as solvent (Figure 5a) was mainly due to the relatively low monomer concentration employed (Figure 7). When ACs were cultured for 24 h on tissue culture

polystyrene wells (TCPS), and subsequently exposed for 1 hour to a 0.3 M DMEM solution of MPC, the cell density did not significantly vary (from 45000 ± 12700 to 43200 ± 7500 cells cm^{-2} , $p = 0.99$) (Figure 8a), while cell viability was higher than 90% just after exposure to monomer solution, and increased to 98% after 48 h of additional culture in standard DMEM-based medium (Figure 8b). Incubation for 1 h in 5 mM DMEM solution of $\text{Fe}^{\text{III}}\text{Cl}_3$ -EDTA resulted in a significant reduction in cell density (17500 ± 5300 cells cm^{-2}) both with respect to the control ($p = 0.03$), and compared to the substrates treated with just 0.3 M MPC ($p = 0.05$) (Figure 8a).

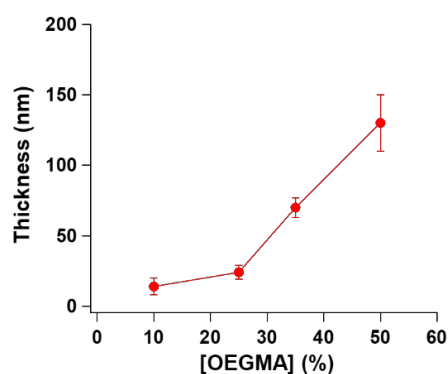


Figure 7. Dry thickness of POEGMA brushes measured *ex situ* by VASE following 60 min of Fe^0 SI-ATRP using DMEM as solvent, 5 mM EDTA- $\text{Fe}^{\text{III}}\text{Cl}_3$, 10 mM NaCl and different concentrations of OEGMA.

Partial cell detachment after treatment with $\text{Fe}^{\text{III}}\text{Cl}_3$ -EDTA was presumably due to complexation of Ca^{II} within membrane proteins by residual amounts of unbound ligand, which influenced integrin-mediated ACs adhesion.^{33,34} A comparable result was observed when ACs were incubated in the complete polymerization mixture (0.3 M MPC + 5 mM $\text{Fe}^{\text{III}}\text{Cl}_3$ -EDTA), while a slight increment in cell density was recorded when Fe^0 -coated plates were additionally placed in contact with the cultures, reproducing the reaction setup typically employed during Fe^0 SI-ATRP of MPC ($p = 0.35$, Figure 8a). In these samples, additional $\text{Fe}^{\text{II}}/\text{Fe}^{\text{III}}$ species leaking from the iron plates were probably complexed by the residual, unbound EDTA, finally preventing complexation of Ca^{II} from cell proteins.

It is important to emphasize that, despite the observed variations in cell density after exposure to the different monomer/ligand mixtures, AC viability was in all cases higher than 90%, and comparable to that measured for the controls. Even when the oxygen dissolved in the culture media was rapidly consumed by exposure to Fe^0 , the tolerance of chondrocytes towards anaerobic conditions³⁵ guaranteed their remarkably high viability, while AC densities were similar to those recorded for the control samples (39000 ± 6000 and 45000 ± 12700 cells cm^{-2} , respectively, in Figure 8a, $p = 0.94$).

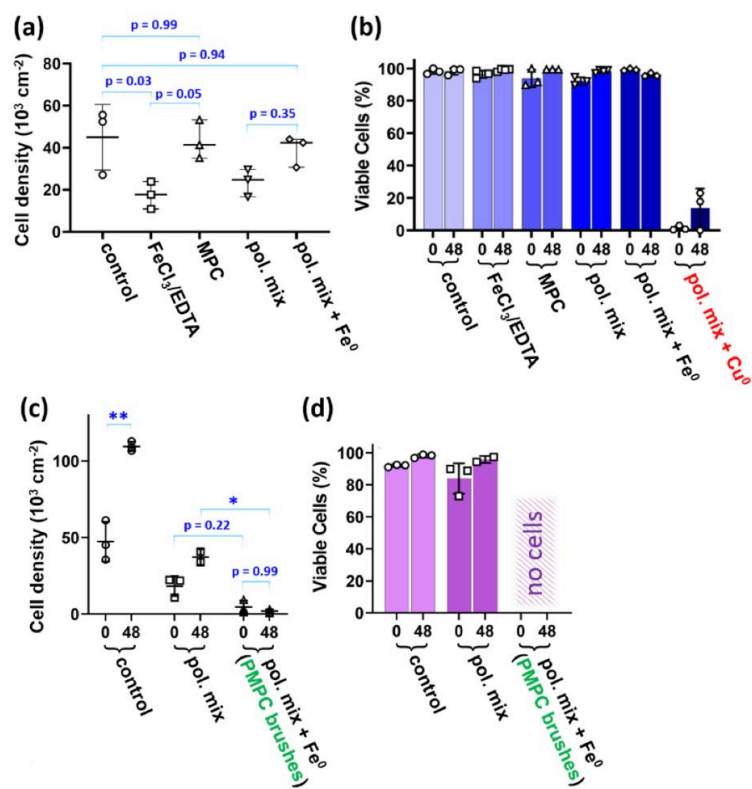


Figure 8. (a) Density of ACs estimated after 24 h of culture on TCPS, followed by exposure for 1 h to different media, including DMEM (indicated as control), 5 mM EDTA with 5 mM Fe^{III}Cl₃ in DMEM (indicated as EDTA/FeCl₃), 0.3 M MPC in DMEM (indicated as MPC), 0.3 M MPC with 5 mM Fe^{III}Cl₃-EDTA and 10 mM NaCl (indicated as pol. mix), and the latter mixture covered by a Fe⁰ plate (indicated as pol. mix + Fe⁰). Statistical analysis was conducted by one-way analysis of variance (ANOVA) with a Dunnett's post-hoc-Test; * indicates $p < 0.05$. (b) Cell viability estimated by live-dead staining on AC cultures subjected for 1 h to the solutions indicated above, and a polymerization mixture including 0.3 M MPC, 5 mM CuBr₂-tris(2-pyridylmethyl)amine (TPMA), 10 mM NaBr, and covered with a Cu⁰ plate.¹² (c) Density of ACs estimated after 24 h of culture on ATRP initiator-functionalized SiO_x substrates and subjected to 1 h of exposure to different mixtures, and after the growth of PMPC brushes (pol. mix + Fe⁰). Statistical analysis was conducted by two-way ANOVA with Tukey's multiple comparisons test; * indicates $p < 0.05$, ** indicates $p < 0.001$. (d) Cell viability estimated by live-dead staining for AC cultures on ATRP initiator-bearing SiO_x surfaces subjected for 1 h to different mixtures.

The cytocompatibility of the polymerization mixtures employed during Fe⁰ SI-ATRP was further highlighted by comparing the viability of ACs exposed to a corresponding Cu-based catalytic system, which was previously reported to enable the rapid growth of polymer brushes by Cu⁰ SI-ATRP.⁶⁻¹³ In this latter case, AC viability was nearly 0% after 1 h of exposure, and increased just to ~ 10% following 48 h of further culture in standard medium (Figure 8b and 11), confirming the toxicity towards mammalian cells of mixtures typically employed during Cu-based ATRP.

When TCPS substrates were replaced by ATRP-initiator-bearing SiO_x surfaces, the effect of PMPC brush growth on AC adhesion was analyzed.

Also in these experiments, ACs were initially cultured on the substrates for 24 h, followed by exposure to different mixtures for 1 h, followed by additional 48 h of culture.

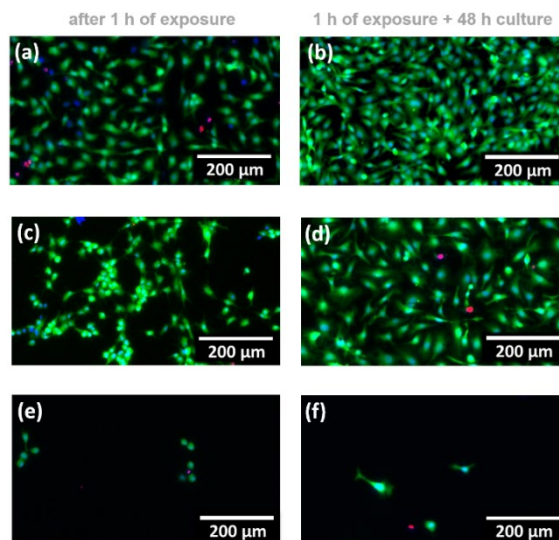


Figure 9. Immunofluorescence micrographs displaying ACs stained with calcein AM (green), Hoechst 33342 (blue), and propidium iodide (red) after 1 h of exposure to the different polymerization mixtures (a, c, e) and following 48 h of further culture (b, d, f).

Cell density significantly decreased after 1 h of exposure to the polymerization mixture (0.3 M MPC, 5 mM Fe^{III}Cl₃-EDTA) compared to that measured when ACs were simply incubated in DMEM-based medium, from 47400 ± 11000 to 18300 ± 12700 cells cm⁻² ($p < 0.05$). Nevertheless, cell viability remained relatively high ($83 \pm 15\%$). As highlighted in the immunofluorescence micrographs reported in Figure 9c, ACs exhibited a more rounded morphology as a result of partial inhibition of cell-cell and cell-substrate adhesion through Ca^{II} complexation by EDTA. However, it is remarkable that following a further 48 h of culture in standard medium an increment in cell density from 18300 ± 12700 to 37300 ± 6900 cells cm⁻² ($p = 0.08$) was observed, due to AC proliferation, basically attaining cell densities similar to those recorded before exposure to the polymerization medium. This result confirmed the cytocompatibility of the polymerization conditions applied during Fe⁰ SI-ATRP. In addition, a well-spread cell morphology was completely recovered (Figure 9d), indicating that ACs strongly adhered to the substrate after an additional 48 h of culture.

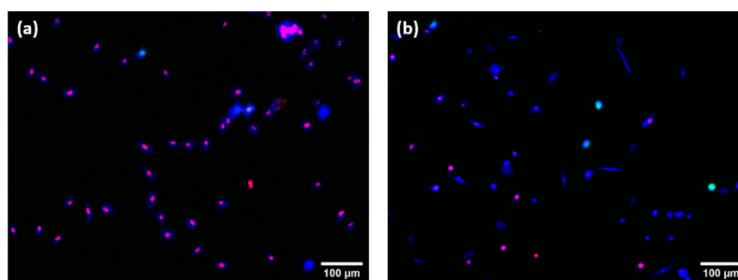


Figure 10. Immunofluorescence micrographs displaying ACs stained with calcein AM (green), Hoechst 33342 (blue), and propidium iodide (red), (a) following 1 h of exposure to a polymerization mixture including 0.3 M MPC, 5 mM CuBr_2 -tris(2-pyridylmethyl)amine (TPMA), 10 mM NaBr, and covered with a Cu^0 plate, and (b) after 48h of further culture in DMEM.

When Fe^0 -coated plates were applied together with the polymerization mixtures on AC cultures, the rapid growth of PMPC brushes led to the formation of a highly hydrated, and cell-repellent interface, which substantially weakened AC attachment and lead to a nearly complete detachment of cells (4700 ± 4300 cells cm^{-2} , after 1 h of exposure). Relatively few, rounded cells remained on the substrates, adhering to surface defects where polymer grafting did not occur due to the adventitious, mechanical removal of ATRP initiator, and were surrounded by a uniform film of PMPC brushes, as evidenced by atomic force microscopy (AFM) (Figure 12).

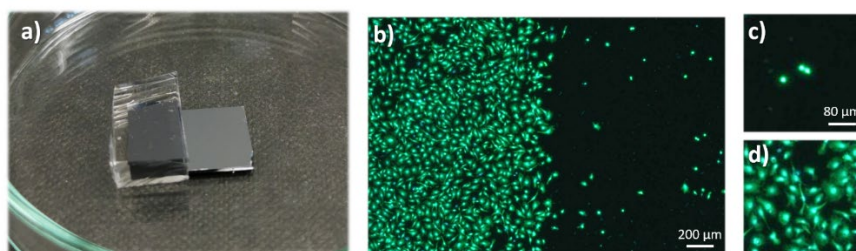


Figure 11. (a) ATRP-initiator deposition was spatially confined to half the surface of a silicon substrate, by applying a smooth polydimethylsiloxane (PDMS) stamp partially covering the surface during the vapour functionalization process. (b) Immunofluorescence micrograph displaying ACs following exposure to Fe^0 SI-ATRP mixture and additional 48 h of culture. Cells selectively adhere on the area of the substrate where PMPC grafting was hindered due to absence of ATRP initiator functions. (c,d) Few ACs showing a rounded morphology remained in the areas where PMPC brushes were synthesized by Fe^0 SI-ATRP, while cells spread and densely adhered on the unfunctionalized SiO_x surface.

Selective deposition of ATRP initiator on just one side of a silicon substrate additionally proved that Fe^0 SI-ATRP could be easily applied to spatially control the growth of biopassive polymer brushes, and trigger cell detachment specifically on the areas of the substrate where polymer grafting could be initiated (Figure 11).

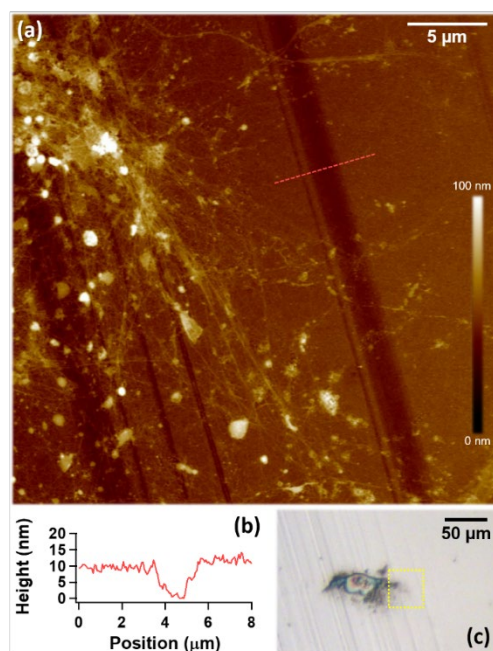


Figure 12. (a) AFM tapping mode micrographs displaying cellular components of ACs extending on surface defects where PMPC brushes did not grow following Fe^0 SI-ATRP, due to mechanical removal of ATRP initiator layer. In (b) a cross section highlighting the height of PMPC brushes around a mechanically scratched area on the substrate is provided. The optical micrograph (c) displays how ACs remained attached on areas where PMPC brushes could not be grown due to the removal of ATRP initiator layer by mechanical scratching.

These results collectively indicated that PMPC-brush growth by Fe^0 SI-ATRP could be performed from AC cultures, substantially altering the interfacial physicochemical properties of the supporting substrates, and thus strongly influencing cell attachment. The observed release of cells was clearly not due to the polymerization conditions applied during culturing, as confirmed by the tolerance of ACs towards the reaction mixtures, their markedly high viability and tendency to proliferate in such media.

The growth of bio-repellent brushes, mediated by Fe^0 , emerges as the main phenomenon leading to a critical shift in the characteristics of the surrounding environment, to which ACs respond by weakening their affinity towards the substrates, ultimately being released from a surface that is no longer bio-adhesive.

It is noteworthy to mention that ATRP methods were already demonstrated to be applicable within cell cultures while maintaining viable cells.³⁶ However, polymer growth was tested in the presence of yeast cells, which are known to be extremely resilient, and which, similarly to bacteria, are protected by strong cell walls and can survive greater stresses than mammalian cells.³⁷

7.3 Conclusions

Due to its tolerance to ambient conditions and scalability, Fe⁰ SI-ATRP emerges as a versatile method to synthesize chemically diverse polymer brushes for a variety of materials formulations. Its highly confined nature enables the generation of uniform brush films over very large areas, without the need of previous deoxygenation of the reaction mixtures or the presence of an inert atmosphere, and by employing just few microliters of monomer/catalyst solutions. These unique features, which are highlighted through a comprehensive analysis of its mechanistic aspects, make Fe⁰ SI-ATRP a very promising technique for translating SI-RDRP processes into technologically relevant surface fabrications.

Thanks to its cytocompatibility towards mammalian cells, Fe⁰ SI-ATRP could be easily applied to biomaterials and within tissue engineering constructs, dynamically tuning the physicochemical properties of cell microenvironments.

7.4 Materials and Methods

Materials

Methyl methacrylate (MMA, Sigma-Aldrich), oligo(ethylene glycol) methyl ether methacrylate (OEGMA, Mn ~ 500 g mol⁻¹, Sigma-Aldrich), styrene (99.5%, Acros), hydroxyethyl methacrylate (HEMA, Sigma-Aldrich) were purified by passing through a basic alumina column to remove the inhibitor before use. N-Isopropylacrylamide (NIPAM, > 98% GC, Tokyo Chemical Industry) was purified by re-crystallization from n-hexane and dried in an oven prior to use.

N,N-dimethylformamide (DMF, extrapure, Fisher Chemical), anisole (99.7%, Sigma-Aldrich), dichloromethane (DCM, dry, ≥ 99.8%, Acros), triethylamine (TEA, ≥ 99%, Merck), 2-bromoisobutryl bromide (BiBB, 98%, Sigma-Aldrich), 3-(aminopropyl)triethoxysilane (APTES, 99%, Acros), iron(III) bromide (FeBr₃, 98%, Aldrich), iron(III) chloride (FeCl₃, 97%, Aldrich), tetrabutylammonium bromide (TBABr, 98%, Aldrich), tetrabutylammonium fluoride (TBAF, 1M in THF, Aldrich) were all used as received. The water used in all the experiments was Millipore Milli-Q grade. Silicon wafers were purchased from Si-Mat (Landsberg, Germany). Fe⁰-coated wafers were obtained by reactive magnetron sputtering (Paul Scherrer Institute, Villigen, Switzerland) obtaining 200 nm-thick layer of Fe⁰.

Functionalization of SiO_x Surfaces with ATRP Initiator

Silicon substrates were cut in 15x15 mm² and cleaned with piranha solution (H₂O₂:H₂SO₄ 1:3 v/v) at room temperature for 30 min (*caution: piranha solution reacts violently with*

organic matter). The substrates were subsequently washed extensively with Milli-Q water, and dried under a N₂ stream. Freshly cleaned substrates were functionalized with APTES by vapour deposition for 2 h inside a desiccator that was kept under vacuum. After the formation of an APTES monolayer, the substrates were washed with ethanol and chloroform and dried under a N₂ stream. APTES-bearing SiO_x surfaces were then placed in an Erlenmeyer flask sealed with a septum and flushed with N₂ for 15 min. After that, 20 mL of dry DCM were added under N₂ followed by 0.2 mL of TEA. Then 0.2 mL of BiBB were slowly. The mixture was let to react for 1.5 h. Subsequently, the substrates were rinsed with ethanol and chloroform, and finally dried under a N₂ stream.

Fe⁰ SI-ATRP

Fe⁰-coated wafers were cut into 20 x 20 mm² pieces, and sonicated for 20 min in isopropanol and 20 min in toluene. In the exemplary case of POEGMA brushes grafted from aqueous mixtures, the polymerization solution was prepared by dissolving EDTA (5 mM), FeCl₃ (5 mM), and NaCl (10 mM) in a 50:50 H₂O:OEGMA mixture (v/v). The Fe⁰-coated substrates were placed on an open petri dish with the Fe⁰-coated surface facing upwards. 16 μL of the polymerization solution were poured on each Fe⁰-coated substrate, and ATRP initiator-functionalized SiO_x samples were placed in contact with the Fe⁰-coated substrates covered by the polymerization mixture. A pressure of 3 g cm⁻² was applied on each substrate, in order to maintain a distance between the surfaces ~ 10 μm.

After the desired time, the substrates were extensively washed with Milli-Q water and ethanol, and finally dried under a N₂ stream.

Similar polymerization procedures were applied for the synthesis of PNIPAM, PMPC and PHEMA in aqueous media, using 2 M NIPAM, 3 M MPC and 4 M HEMA mixtures including EDTA (5 mM), FeCl₃ (5 mM) and NaCl (10 mM). Fe⁰ SI-ATRP of diluted (0.3 M) MPC solution in DMEM was performed by using 5 mM EDTA, 5 mM FeCl₃ and 10 mM NaCl.

Fe⁰ SI-ATRP of MMA was performed in anisole, using 20 mM TBABr and different concentrations of FeBr₃. In an analogous way, Fe⁰ SI-ATRP of OEGMA was additionally performed in DMF, using 20 mM TBABr and different concentrations of FeBr₃.

Variable-Angle Spectroscopic Ellipsometry (VASE)

A Woolam ellipsometer (J.A. Woolam Co. U.S.) was used to measure the dry thickness of the polymer films (T_{dry}). Ψ and Δ were acquired as a function of wavelength (350-800 nm) and analyzed employing the Complete EASE package (Woollam). Fitting of the raw data was performed based on a layered model using bulk dielectric functions for Si, SiO₂. The polymer-brush layers were analyzed on the basis of the Cauchy model: $n = A + B \lambda^{-2}$, where n is the

refractive index, λ is the wavelength and A and B were assumed to be 1.45 and 0.01, respectively, as values for transparent organic films.

Degrading of Polymer Brushes

4-inches wafers with PMPC brushes grafted by Fe⁰ SI-ATRP from were cut into 20x20 mm² and placed in a 50 mL Erlenmeyer, which was sealed and degassed for 15 min. 14 mL of dry tetrahydrofuran (THF) and 0,6 mL of TBAF were added. The solution was stirred at 60°C for 72 h. The solution was later on transferred to a 100 mL round bottom flask. The solvent was evaporated with a rotary evaporator and the remaining solid was dissolved in hexafluoroisopropanol (HFIP) with 0.02 M potassium trifluoroacetate (K-TFAC) and analyzed by size exclusion chromatography.

Size Exclusion Chromatography

Number- and weight-average absolute molecular weights, M_n and M_w , of degrafted PMPC samples were determined using an Agilent 1100 GPC/SEC unit equipped with two PFG linear M columns (PSS) connected in series with an Agilent 1100 VWD/UV detector operated at 290 nm, a DAWN HELEOS 8 multi-angle laser light scattering (MALS) detector (Wyatt Technology Europe) followed by an Optilab T-rEX RI detector from Wyatt. Samples were eluted in HFIP with 0.02 M K-TFAC at 1 mL min⁻¹ at room temperature.

Effect of Distance between Fe⁰ and ATRP Initiator-Bearing Substrates

Fe⁰-coated silicon wafers were cut into 20x20 mm² pieces, sonicated for 20 min in isopropanol and 20 min in toluene and then dried under a N₂ stream. Fe⁰-coated surfaces were covered with by 50:50 H₂O:OEGMA mixtures (v/v) containing EDTA (5 mM), FeCl₃ (5 mM), and NaCl (10 mM), and sandwiched with ATRP initiator-functionalized substrates, placing glass wedges with different thicknesses at one side of the two facing surfaces. The polymerization was performed for 45 min, after which the thickness of POEGMA brushes obtained under ambient conditions was measured by VASE (Figure 4). Oxygen-free Fe⁰ SI-ATRP was performed using similar reaction setups placed within sealed Erlenmeyer flasks kept under N₂, and using reaction mixtures previously deoxygenated by N₂ bubbling (30 min).

Cell Culture

In order to assess the cytotoxicity of the polymerization mixture, solutions of EDTA/FeCl₃ (5 mM), MPC (0.3 M), EDTA-FeCl₃ (5 mM), NaCl (10 mM) and MPC (0.3 M) in high glucose Dulbecco's modified Eagle's medium (DMEM) (Thermo Fisher Scientific) were prepared and the pH was adjusted to 7,4 using 1 M NaOH. Primary articular chondrocytes (ACs) were isolated from the femoral cartilage of 6 months-old calves obtained from the local slaughterhouse. Cartilage from the medial and lateral condyle was harvested, minced and

digested by collagenase solution. ACs were cultured in a humidified atmosphere with 5% CO₂ at 37°C. Cells were passaged at 90% confluence by detachment with trypsin/EDTA. ACs at passage 2 (30000 cells/cm²) were seeded in 48-wells plates and expanded for 24 h in DMEM, 10% Fetal Bovine Serum (FBS), 50 µg mL⁻¹ L-ascorbic acid, and gentamicin sulfate (50 µg ml⁻¹), following standard cell-culture procedures. The wells were subsequently washed twice with PBS, and the supernatant was replaced by mixtures of EDTA/FeCl₃, MPC, EDTA/FeCl₃ + MPC in DMEM, which were previously sterile filtered.

ACs were incubated for 1 h at 37 °C in the different solutions and cell viability was assessed immediately after, and after 48 hours of additional culture in DMEM.

Cell viability was analyzed by fluorescent live/dead staining. Namely, the wells were washed three times with PBS and ACs were subsequently stained with propidium iodide (0.5 µg ml⁻¹), calcein AM (0.008 mM) and Hoechst 33342 (5 µg ml⁻¹) for 30 minutes and imaged with a fluorescence microscope (ZEISS, Axio Observer Z1).

Statistical Analysis

All statistical analyses were conducted with GraphPad Prism 8.2.0. A one-way analysis of variance (ANOVA) was conducted to compare density of cells cultured on tissue culture plastic between groups. All groups were tested against the control group with a Dunnett's post hoc test. Density of cells on silicon wafers was analyzed with a two-way ANOVA with the factors group and time. All groups and times were compared between each other with Tukey's multiple comparisons test.

Cell Culture during Fe⁰ SI-ATRP of MPC

Silicon wafers functionalized with ATRP initiator were immersed in ethanol for 20 min for sterilization. The substrates were placed in 6-well plates and passage 2 ACs (30000 cells/cm²) were seeded on top and left to adhere for 24 hours. The polymerization solution (5 mM FeCl₃, 5 mM EDTA, 10 mM NaCl, 0.3 M MPC in DMEM) was freshly prepared and the pH was adjusted to 7,4 using 1 M NaOH solution. The polymerization solution was sterile filtered before use. The cell-seeded substrates were washed with PBS twice and the polymerization solution was added in the wells. The substrates were then covered with Fe⁰-coated plates and incubated for 1 h at 37 °C. Chondrocyte viability and density were assessed directly after and 48 hours after treatment via fluorescent live/dead staining. Three images per substrate were acquired and analysed with ImageJ software (<https://imagej.net/Citing>).

Atomic Force Microscopy

The morphology of PMPC brush-coated substrates cultured with ACs was investigated in the dry state by using a Dimension Icon AFM (Bruker Corporation) in tapping mode, selecting a cantilever having a nominal spring constant of 26 N m^{-1} (OMCL-AC240TS-R3, Olympus).

References

1. Yeow, J.; Chapman, R.; Gormley, A. J.; Boyer, C., Up in the air: oxygen tolerance in controlled/living radical polymerisation. *Chem. Soc. Rev.* **2018**, *47* (12), 4357-4387.
2. Narupai, B.; Page, Z. A.; Treat, N. J.; McGrath, A. J.; Pester, C. W.; Discekici, E. H.; Dolinski, N. D.; Meyers, G. F.; de Alaniz, J. R.; Hawker, C. J., Simultaneous Preparation of Multiple Polymer Brushes under Ambient Conditions using Microliter Volumes. *Angew. Chem. Int. Edit.* **2018**, *57* (41), 13433-13438.
3. Li, M.; Fromel, M.; Ranaweera, D.; Rocha, S.; Boyer, C.; Pester, C. W., SI-PET-RAFT: Surface-Initiated Photoinduced Electron Transfer-Reversible Addition-Fragmentation Chain Transfer Polymerization. *ACS Macro Lett.* **2019**, *8*, 374-380.
4. Matyjaszewski, K.; Dong, H. C.; Jakubowski, W.; Pietrasik, J.; Kusumo, A., Grafting from surfaces for "Everyone": ARGET ATRP in the presence of air. *Langmuir* **2007**, *23* (8), 4528-4531.
5. Navarro, L. A.; Enciso, A. E.; Matyjaszewski, K.; Zauscher, S., Enzymatically Degassed Surface-Initiated Atom Transfer Radical Polymerization with Real-Time Monitoring. *J. Am. Chem. Soc.* **2019**, *141* (7), 3100-3109.
6. Zhang, T.; Du, Y.; Muller, F.; Amin, I.; Jordan, R., Surface-initiated Cu(0) mediated controlled radical polymerization (SI-CuCRP) using a copper plate. *Polym. Chem.* **2015**, *6* (14), 2726-2733.
7. Zhang, T.; Du, Y. H.; Kalbacova, J.; Schubel, R.; Rodriguez, R. D.; Chen, T.; Zahn, D. R. T.; Jordan, R., Wafer-scale synthesis of defined polymer brushes under ambient conditions. *Polym. Chem.* **2015**, *6* (47), 8176-8183.
8. Dehghani, E. S.; Du, Y.; Zhang, T.; Ramakrishna, S. N.; Spencer, N. D.; Jordan, R.; Benetti, E. M., Fabrication and Interfacial Properties of Polymer Brush Gradients by Surface-Initiated Cu(0)-Mediated Controlled Radical Polymerization. *Macromolecules* **2017**, *50* (6), 2436-2446.

9. Che, Y. J.; Zhang, T.; Du, Y. H.; Amin, I.; Marschelke, C.; Jordan, R., "On Water" Surface-initiated Polymerization of Hydrophobic Monomers. *Angew. Chem. Int. Edit.* **2018**, *57* (50), 16380-16384.
10. Fantin, M.; Ramakrishna, S. N.; Yan, J. J.; Yan, W. Q.; Divandari, M.; Spencer, N. D.; Matyjaszewski, K.; Benetti, E. M., The Role of Cu⁰ in Surface-Initiated Atom Transfer Radical Polymerization: Tuning Catalyst Dissolution for Tailoring Polymer Interfaces. *Macromolecules* **2018**, *51* (17), 6825-6835.
11. Zhang, T.; Benetti, E. M.; Jordan, R., Surface-Initiated Cu(0)-Mediated CRP for the Rapid and Controlled Synthesis of Quasi-3D Structured Polymer Brushes. *ACS Macro Lett.* **2019**, *8* (2), 145-153.
12. Yan, W. Q.; Fantin, M.; Spencer, N. D.; Matyjaszewski, K.; Benetti, E. M., Translating Surface-Initiated Atom Transfer Radical Polymerization into Technology: The Mechanism of Cu⁰-Mediated SI-ATRP under Environmental Conditions. *ACS Macro Lett.* **2019**, *8*, 865-870.
13. Yan, W. Q.; Fantin, M.; Ramakrishna, S.; Spencer, N. D.; Matyjaszewski, K.; Benetti, E. M., Growing Polymer Brushes from a Variety of Substrates under Ambient Conditions by Cu⁰-Mediated Surface-Initiated ATRP. *ACS Appl. Mater. Interfaces* **2019**, *11* (30), 27470-27477.
14. Divandari, M.; Pollard, J.; Dehghani, E.; Bruns, N.; Benetti, E. M., Controlling Enzymatic Polymerization from Surfaces with Switchable Bioaffinity. *Biomacromolecules* **2017**, *18* (12), 4261-4270.
15. Wang, Y.; Zhang, Y. Z.; Parker, B.; Matyjaszewski, K., ATRP of MMA with ppm Levels of Iron Catalyst. *Macromolecules* **2011**, *44* (11), 4022-4025.
16. Wang, Y.; Matyjaszewski, K., ATRP of MMA Catalyzed by Fe^{II}Br₂ in the Presence of Triflate Anions. *Macromolecules* **2011**, *44* (6), 1226-1228.
17. Teodorescu, M.; Gaynor, S. G.; Matyjaszewski, K., Halide anions as ligands in iron-mediated atom transfer radical polymerization. *Macromolecules* **2000**, *33* (7), 2335-2339.
18. Zhou, D. P.; Gao, X.; Wang, W. J.; Zhu, S. P., Termination of Surface Radicals and Kinetic Modeling of ATRP Grafting from Flat Surfaces by Addition of Deactivator. *Macromolecules* **2012**, *45* (3), 1198-1207.
19. Lanigan, R. S.; Yamarik, T. A., Final report on the safety assessment of EDTA, Calcium Disodium EDTA, diammonium EDTA, Dipotassium EDTA, Disodium EDTA, TEA-EDTA, Tetrasodium EDTA, Tripotassium EDTA, Trisodium EDTA, HEDTA, and Trisodium HEDTA. *Int. J. Toxicol.* **2002**, *21* (5), 95-142.

20. Bergenudd, H.; Jonsson, M.; Nystrom, D.; Malmstrom, E., Heterogeneous iron(II)-chloride mediated radical polymerization of styrene. *J. Mol. Catal. A-Chem.* **2009**, *306* (1-2), 69-76.
21. Wang, G. X.; Lu, M.; Wu, H., SET LRP of MMA mediated by Fe(0)/EDTA in the presence of air. *Polym. Bull.* **2012**, *69* (4), 417-427.
22. Coullerez, G.; Carlmark, A.; Malmström, E.; Jonsson, M., Understanding Copper-Based Atom-Transfer Radical Polymerization in Aqueous Media. *J. Phys. Chem. A* **2004**, *108*, 7129-7131.
23. Jones, D. M.; Huck, W. T. S., Controlled surface-initiated polymerizations in aqueous media. *Adv. Mater.* **2001**, *13* (16), 1256-1259.
24. Konkolewicz, D.; Kryszewski, P.; Gois, J. R.; Mendonca, P. V.; Zhong, M. J.; Wang, Y.; Gennaro, A.; Isse, A. A.; Fantin, M.; Matyjaszewski, K., Aqueous RDRP in the Presence of Cu-0: The Exceptional Activity of Cu-I Confirms the SARA ATRP Mechanism. *Macromolecules* **2014**, *47* (2), 560-570.
25. Patil, R. R.; Turgman-Cohen, S.; Srogl, J.; Kiserow, D.; Genzer, J., Direct Measurement of Molecular Weight and Grafting Density by Controlled and Quantitative Degrafting of Surface-Anchored Poly(methyl methacrylate). *ACS Macro Lett.* **2015**, *4* (2), 251-254.
26. Benetti, E. M.; Kang, C. J.; Mandal, J.; Divandari, M.; Spencer, N. D., Modulation of Surface-Initiated ATRP by Confinement: Mechanism and Applications. *Macromolecules* **2017**, *50* (15), 5711-5718.
27. Kang, C. J.; Ramakrishna, S. N.; Nelson, A.; Cremmel, C. V. M.; Stein, H. V.; Spencer, N. D.; Isa, L.; Benetti, E. M., Ultrathin, freestanding, stimuli-responsive, porous membranes from polymer hydrogel-brushes. *Nanoscale* **2015**, *7* (30), 13017-13025.
28. Milner, S. T.; Witten, T. A.; Cates, M. E., Theory of the Grafted Polymer Brush. *Macromolecules* **1988**, *21* (8), 2610-2619.
29. Chang, Y.; Shih, Y. J.; Lai, C. J.; Kung, H. H.; Jiang, S. Y., Blood-Inert Surfaces via Ion-Pair Anchoring of Zwitterionic Copolymer Brushes in Human Whole Blood. *Adv. Funct. Mater.* **2013**, *23* (9), 1100-1110.
30. Zhang, Z.; Chao, T.; Chen, S. F.; Jiang, S. Y., Superlow fouling sulfobetaine and carboxybetaine polymers on glass slides. *Langmuir* **2006**, *22* (24), 10072-10077.
31. Jiang, S. Y.; Cao, Z. Q., Ultralow-Fouling, Functionalizable, and Hydrolyzable Zwitterionic Materials and Their Derivatives for Biological Applications. *Adv. Mater.* **2010**, *22* (9), 920-932.

32. Feng, W.; Brash, J. L.; Zhu, S. P., Non-biofouling materials prepared by atom transfer radical polymerization grafting of 2-methacryloxyethyl phosphorylcholine: Separate effects of graft density and chain length on protein repulsion. *Biomaterials* **2006**, *27* (6), 847-855.
33. Luo, B. H.; Carman, C. V.; Springer, T. A., Structural basis of integrin regulation and signaling. *Annu. Rev. Immunol.* **2007**, *25*, 619-647.
34. Gumbiner, B. M., Regulation of cadherin-mediated adhesion in morphogenesis. *Nat. Rev. Mol. Cell Bio.* **2005**, *6* (8), 622-634.
35. Marcus, R. E., Effect of Low Oxygen Concentration on Growth, Glycolysis, and Sulfate Incorporation by Articular Chondrocytes in Monolayer Culture. *Arthritis Rheum.* **1973**, *16* (5), 646-656.
36. Kim, J. Y.; Lee, B. S.; Choi, J.; Kim, B. J.; Choi, J. Y.; Kang, S. M.; Yang, S. H.; Choi, I. S., Cytocompatible Polymer Grafting from Individual Living Cells by Atom-Transfer Radical Polymerization. *Angew. Chem. Int. Edit.* **2016**, *55* (49), 15306-15309.
37. Broach, J. R.; Jones, E. W.; Pringle, J. R., *The Molecular and Cellular Biology of the Yeast Saccharomyces*, Cold Spring Harbor Laboratory Press, Cold Spring Harbor, NY, **1991**.

Chapter 8

Surface-Initiated Photoinduced ATRP: Mechanism, Oxygen Tolerance and Temporal Control during the Synthesis of Polymer Brushes*

Surface-initiated, photoinduced atom transfer radical polymerization (SI-photoATRP) enables the controlled and rapid synthesis of compositionally diverse polymer brushes over large areas, by employing very small reaction volumes, under ambient conditions and without the need for prior deoxygenation of monomer mixtures. The concentration of copper species, and the type and content of amine-based ligands determine the mechanism of SI-photoATRP, regulate the kinetics of polymer-brush growth, and govern the tolerance of this polymer-grafting method toward oxygen. Despite mechanistic analogies with the corresponding solution processes, the intrinsic, highly confined nature of SI-photoATRP leads to significant differences from polymerizations within homogeneous systems. This is especially important to attain controlled/living polymerization and temporal control over polymer-brush growth using UV light as a trigger.

* Edmondo M. Benetti, Krzysztof Matyjaszewski and Nicholas D. Spencer supervised this project. Wenqing Yan conducted the experiment. Sajjad Dadashi-Silab did the UV-vis spectroscopy. All the authors wrote the paper. It is in large part published in *Macromolecules*. **2020**. 53, 8, 2801–2810.

8.1 Introduction

Over the past decade, there have been significant advancements in photochemically stimulated reversible deactivation radical polymerization (RDRP) methods. These have involved the application of light for inducing and/or catalyzing controlled polymer growth.¹⁻⁴ Prominent examples include photoinduced electron transfer reversible-addition fragmentation radical polymerization (PET-RAFT),⁵⁻⁷ photoinduced atom transfer radical polymerization (photoATRP)⁸⁻¹¹ and photocatalyzed metal-free ATRP.¹²⁻¹⁶

Focusing on photoATRP, this polymerization technique presents several advantages with respect to other ATRP processes. These include the possibility of temporal control over polymer chain growth, which is regulated by illumination time, enhanced tolerance of photoATRP toward oxygen,¹⁷⁻²¹ and the reduction in the amount of catalyst necessary to attain a controlled polymerization.⁹

All these unique features rely on the intrinsic mechanism of photoATRP, which mainly involves the (re)generation of Cu^IX/L-based activators under light irradiation. Upon excitation of initially present Cu^{II}X₂/L ([Cu^{II}X₂/L]* in Scheme 1a), a single-electron transfer with an electron donor, typically a free ligand (L), generates Cu^IX/L activators. Thus, in photoATRP, electron donors act as reducing agents similar to activator regenerated by electron transfer (ARGET) ATRP. To a lesser extent, alkyl halide initiators (RX) can additionally undergo homolytic cleavage upon irradiation, generating a halide radical (X·) and a carbon-centered radical (R·) that can initiate/propagate chains in the presence of monomer.^{10, 22}

Mechanistic studies of photoATRP reveal that in the presence of oxygen, Cu^IX/L generates Cu^{II}X(O₂)/L species, which in the excited state can recombine with L (or an electron donor), yielding oxidized species (L_{ox}), as well as regenerating Cu^IX/L activators.¹⁷⁻¹⁹ In a closed, non-deoxygenated reaction system, and with a limited amount of dissolved oxygen, this process continues until essentially all oxygen has been consumed.^{17, 23} Thus, the presence of excess ligand (or other electron donors) guarantees the efficient regeneration of an activator, and imparts to photoATRP a degree of tolerance towards environmental conditions, circumventing the need for tedious deoxygenation procedures prior to polymerization.

The translation of these features into the controlled synthesis of polymer brushes, via surface-initiated photoATRP (SI-photoATRP), would substantially broaden the applicability of RDRP methods for the creation of functional surfaces, and the modification of a variety of materials.

The tolerance of SI-photoATRP to environmental conditions is of special relevance for polymer grafting from large substrates.²⁴⁻²⁶ These include sensors,²⁷⁻³⁰ cell-sensitive and tissue-engineering platforms³¹⁻³⁷ or catalytic supports.³⁸⁻⁴⁰ Scaling up polymer-brush synthesis using classical ATRP processes from such substrates would require the use of extremely large reaction volumes, with the necessity for maintaining inert conditions for relatively long reaction times. Such processes would additionally require the use of large quantities of catalyst. All these factors hamper the translation of commonly applied surface-initiated ATRP (SI-ATRP) methods into technologically relevant processes.

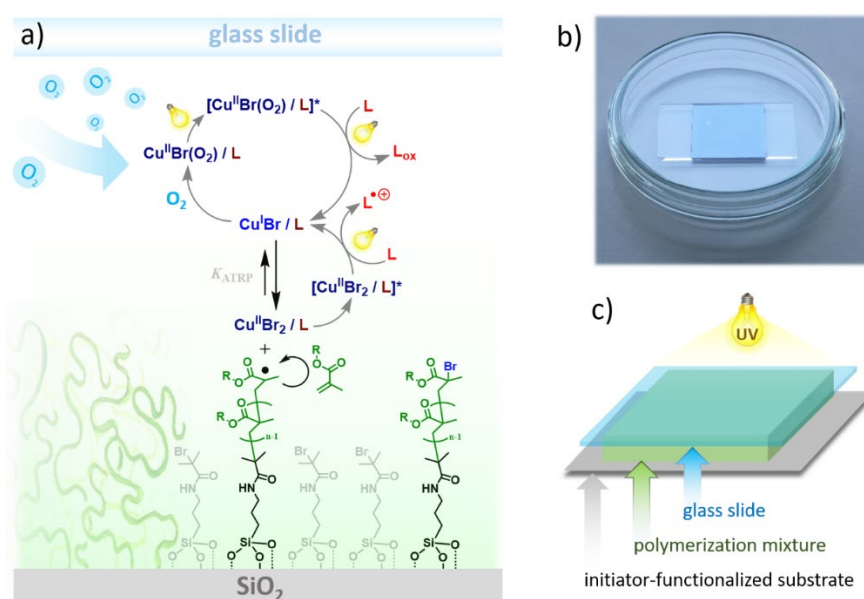
With the aim of investigating the mechanism of SI-photoATRP, in this study we focus on exploring how the presence of a grafting surface affects those parameters that have already been identified as crucial for photoATRP in solution. During SI-photoATRP, the concentration of Cu^{II} species initially added to the reaction mixture as well as the type and amount of ligand determine polymer-brush growth rate, and the degree of control over the polymerization. These parameters additionally regulate the tolerance of the polymerization toward oxygen.

8.2 Results and Discussion

We employed a reaction setup in which initiator-functionalized substrates were uniformly covered with a few microliters of monomer/catalyst solutions (Scheme 1). We demonstrated that under constant UV illumination, SI-photoATRP enables the generation of extremely uniform polymethacrylate brush films over very large areas, without the need for prior deoxygenation of the reaction mixtures or the presence of an inert atmosphere.

Due to the minimal reaction volumes employed, coupled to the intrinsically confined nature of SI-photoATRP, only a brief period of UV irradiation was sufficient to consume dissolved oxygen in the system, and trigger a progressive, controlled brush-growth over several hours in complete darkness. This unique feature redefines the concept of temporal control during photoinduced RDRP, which is typically regulated by switching on/off the light source, in the particular case of systems where polymer growth takes place under highly confined environments. Attaining polymer growth without the need for continuous UV irradiation thus highlights SI-photoATRP as an extremely energetically efficient polymerization technique. This is particularly well-suited for the generation of coatings on substrates where limited light penetration can be achieved, as is the case for the in situ modification of implants, or the fabrication of adhesive films.

The mechanism of SI-photoATRP was initially explored by analyzing the parameters that had been previously identified as the principal determinants for the controlled growth of polymers in the corresponding solution processes.^{9-11, 22-23} In particular, the effects of catalyst concentration (expressed as the amount of CuII species initially added), and the content and type of ligand (L) on the synthesis of polymer brushes by SI-photoATRP were investigated. As illustrated in Scheme 1a, the amine-based L substantially contributes to the generation of Cu^IX/L species, and prevents accumulation of Cu^{II}X₂/L deactivators throughout the grafting process, following an overall mechanism that is reminiscent ofARGET ATRP.⁴¹⁻⁴²



Scheme 1. (a) Proposed mechanism of SI-photoATRP; (b, c) reaction setup employed for the synthesis of polymethacrylate brushes by SI-photoATRP, including an ATRP initiator-functionalized SiO_x substrate covered with a polymerization mixture and sandwiched with a glass slide.

In the presence of UV irradiation Cu^{II}X₂/L can be photo-excited to [Cu^{II}X₂/L]*, which is subsequently quenched by L in solution, generating Cu^IX/L and a radical cation (L^{•+}). Hence, a concentration of L beyond the stoichiometric amount necessary to form Cu^{II} complexes is typically required to efficiently generate activators and enable a steady initiation and propagation.

Besides the type and amount of L, the concentration of Cu^{II} species present in solution determines the degree of control over the polymerization process. This is especially relevant in the case of polymer-brush synthesis from macroscopic surfaces, where the concentration of catalyst at the brush-growing front regulates deactivation efficiency, and the extent of irreversible termination reactions between propagating grafts.⁴³⁻⁴⁶ This latter phenomenon becomes important in determining the growth of brush films via SI-ATRP processes. On the

one hand, a relatively high local concentration of radicals is generated, since they are virtually all confined to the surface. On the other hand, just a limited amount of Cu^{II} species is produced in the medium through the ATRP equilibrium, and as a result of termination processes, owing to the overall extremely low concentration of initiating/propagating sites.⁴⁷

8.2.1 Effect of Ligand

Table 1. SI-photoATRP Of OEGMA Performed By Varying L, [CuBr₂], and [CuBr₂]:[L].

| Monomer and Ligand | [CuBr ₂] | [CuBr ₂]:[L] | Time (h) | T _{dry} (nm) |
|-------------------------------|----------------------|--------------------------|----------|-----------------------|
| OEGMA Me ₆ TREN | 100 ppm | 1: 2 | 1 | 36.8 ± 0.4 |
| | 100 ppm | 1: 4 | 1 | 39.4 ± 1.5 |
| | 100 ppm | 1: 6 | 1 | 40.5 ± 2.3 |
| OEGMA Me ₆ TREN | 5 mM | 1: 2 | 1 | 51.6 ± 0.1 |
| | 5 mM | 1: 4 | 1 | 44.1 ± 0.9 |
| | 5 mM | 1: 6 | 1 | 47.7 ± 0.2 |
| OEGMA TPMA | 100 ppm | 1: 2 | 1 | 45.6 ± 0.2 |
| | 100 ppm | 1: 4 | 1 | 48.5 ± 2.3 |
| | 100 ppm | 1: 6 | 1 | 49.3 ± 0.2 |
| OEGMA TPMA | 5 mM | 1: 2 | 1 | 23.4 ± 1.1 |
| | 5 mM | 1: 4 | 1 | 26.3 ± 1.2 |
| | 5 mM | 1: 6 | 1 | 28.4 ± 0.1 |
| OEGMA PMDETA | 100 ppm | 1: 2 | 3 | 0.8 ± 0.1 |
| | 100 ppm | 1: 4 | 3 | 0.9 ± 0.1 |
| | 100 ppm | 1: 6 | 3 | 1.2 ± 0.1 |
| OEGMA PMDETA | 5 mM | 1: 2 | 3 | 8.7 ± 0.2 |
| | 5 mM | 1: 4 | 3 | 41.5 ± 0.4 |
| | 5 mM | 1: 6 | 3 | 42.2 ± 0.3 |
| OEGMA HMTETA | 100 ppm | 1: 2 | 3 | 0.8 ± 0.1 |
| | 100 ppm | 1: 4 | 3 | 0.9 ± 0.1 |
| | 100 ppm | 1: 6 | 3 | 0.9 ± 0.1 |
| OEGMA HMTETA | 5 mM | 1: 2 | 3 | 1.9 ± 0.3 |
| | 5 mM | 1: 4 | 3 | 6.1 ± 0.1 |
| | 5 mM | 1: 6 | 3 | 20.5 ± 0.7 |

The synthesis of poly[oligo(ethylene glycol) methacrylate] (POEGMA) and poly(methyl methacrylate) (PMMA) brushes by SI-photoATRP was investigated. In both cases, polymer grafting was performed from ATRP-initiator-functionalized SiO_x surfaces, onto which 1 μL

cm⁻² 1:1 (v/v) monomer:dimethylformamide (DMF) mixtures were applied, without deoxygenation. The samples were subsequently covered with a glass slide, and irradiated under environmental conditions (no inert atmosphere) by a UV light source with $\lambda_{\text{max}} = 365$ nm, and an intensity of 1.5 mW cm⁻². Four different ligands, yielding Cu-based catalysts with a broad range of activities were tested, namely tris[2-(dimethylamino)ethyl]amine (Me₆TREN), tris(2-pyridylmethyl)amine (TPMA), N,N,N',N'',N''-pentamethyldiethylenetriamine (PMDETA) and 1,1,4,7,10,10-hexamethyltriethylenetetramine (HMTETA). Two concentrations of CuBr₂ were used for each ligand type, 0.44 mM (100 ppm) and 5 mM (~1100 ppm), and different relative amounts of L were tested, generating mixtures with [CuBr₂]:[L] of 1:2, 1:4 and 1:6.

Table 2. SI-photoATRP Of MMA Performed By Varying L, [CuBr₂], and [CuBr₂]:[L].

| Monomer and Ligand | [CuBr ₂] | [CuBr ₂]:[L] | Time (h) | T _{dry} (nm) |
|-----------------------------|----------------------|--------------------------|----------|-----------------------|
| MMA Me ₆ TREN | 100 ppm | 1: 2 | 1 | 34.8 ± 0.2 |
| | 100 ppm | 1: 4 | 1 | 41.0 ± 0.3 |
| | 100 ppm | 1: 6 | 1 | 42.1 ± 0.8 |
| MMA Me ₆ TREN | 5 mM | 1: 2 | 1 | 28.2 ± 0.2 |
| | 5 mM | 1: 4 | 1 | 24.0 ± 0.3 |
| | 5 mM | 1: 6 | 1 | 26.5 ± 0.4 |
| MMA TPMA | 100 ppm | 1: 2 | 1 | 5.8 ± 0.2 |
| | 100 ppm | 1: 4 | 1 | 9.4 ± 0.1 |
| | 100 ppm | 1: 6 | 1 | 6.4 ± 0.2 |
| MMA TPMA | 5 mM | 1: 2 | 1 | 5.7 ± 0.3 |
| | 5 mM | 1: 4 | 1 | 4.7 ± 0.1 |
| | 5 mM | 1: 6 | 1 | 5.6 ± 0.1 |
| MMA PMDETA | 100 ppm | 1: 2 | 3 | 0.7 ± 0.1 |
| | 100 ppm | 1: 4 | 3 | 0.9 ± 0.2 |
| | 100 ppm | 1: 6 | 3 | 1.0 ± 0.3 |
| MMA PMDETA | 5 mM | 1: 2 | 3 | 6.1 ± 0.3 |
| | 5 mM | 1: 4 | 3 | 6.3 ± 0.1 |
| | 5 mM | 1: 6 | 3 | 9.6 ± 0.1 |
| MMA HMTETA | 100 ppm | 1: 2 | 3 | 0.7 ± 0.1 |
| | 100 ppm | 1: 4 | 3 | 0.7 ± 0.1 |
| | 100 ppm | 1: 6 | 3 | 0.8 ± 0.1 |
| MMA HMTETA | 5 mM | 1: 2 | 3 | 1.3 ± 0.1 |
| | 5 mM | 1: 4 | 3 | 4.9 ± 0.2 |
| | 5 mM | 1: 6 | 3 | 10.5 ± 0.1 |

As summarized in Table 1 and 2, when Me₆TREN and TPMA were used as ligands, relatively thick POEGMA and PMMA brushes were obtained after just one hour of UV

irradiation, in all cases exceeding 20-30 nm of dry thickness (T_{dry}), as measured by variable angle spectroscopic ellipsometry (VASE). It is important to emphasize that, in contrast to previously reported data focusing on photoATRP of acrylates in solution,^{10-11, 18-19} when Me₆TREN and TPMA were used as ligands a decrease in [CuBr₂]:[L] did not translate into a faster polymerization from the surface, as similar values of T_{dry} for different brush films typically indicate a comparable molar mass of the corresponding grafted polymers.⁴⁸⁻⁵⁴ This result agrees well with the data reported by Mosnàček et al.¹⁷, who suggested that the rate of photoATRP of methacrylates might be independent of the excess of ligand present in the reaction.

Significantly different results were obtained when PMDETA and HMTETA were used as L. Both ligands generated much less active Cu catalysts, characterized by markedly lower values of ATRP equilibrium constant (K_{ATRP}).⁵⁵ In both these cases, 100 ppm of CuBr₂ was not sufficient to enable the grafting of POEGMA and PMMA brushes, even after 3 hours of irradiation, while films with a measurable thickness were obtained by increasing [CuBr₂] to 5 mM. At higher concentration of Cu, a clear dependency of T_{dry} on the relative content of L was recorded. In particular, the thickness of POEGMA brushes increased from 8.7 ± 0.2 nm when [CuBr₂]:[PMDETA] was 1:2, to 42.2 ± 0.3 nm when four fold excess of PMDETA with respect to CuBr₂ was applied. Similarly, T_{dry} of POEGMA increased from 1.9 ± 0.3 to 20.5 ± 0.7 nm when [CuBr₂]:[HMTETA] was shifted from 1:2 to 1:6, while analogous trends, although with overall lower values of thickness, were recorded for SI-photoATRP of MMA (Table 2).

8.2.2 Effect of Catalyst Concentration

Kinetic studies of polymer-brush growth shed further light on the mechanism of SI-photoATRP. To analyze the thickening rates of POEGMA brushes, and assess their dependency on the variation of reaction parameters, we focused on catalytic systems involving Me₆TREN and TPMA, which provided the fastest polymerizations according to the results reported in Tables 1 and 2.

As highlighted by comparing the growth profiles reported in Figure 1a and 1b, when POEGMA was grafted by using Me₆TREN as a ligand, brush thickness steadily increased during the early stages of UV irradiation, reaching values of T_{dry} between 40 and 50 nm after 1 h of polymerization (Figure 1a). In contrast, for catalytic systems involving TPMA as a ligand, a discontinuity in the slope of brush-growth profiles was recorded after 1 h of exposure to UV, for all values of [CuBr₂] and [CuBr₂]:[L] tested (Figure 1b). The differences observed along

the brush-thickening profiles at the beginning of the polymerization were due to the different rates of photoinduced reduction of $\text{Cu}^{\text{II}}\text{X}/\text{L}$ species between the two ligands. Since Me_6TREN contains four reactive aliphatic amine moieties, the rate of photoreduction of Cu^{II} -based species was significantly higher than that with TPMA, which has one alkyl-amine moiety and three pyridinic groups (Figure 5).¹¹

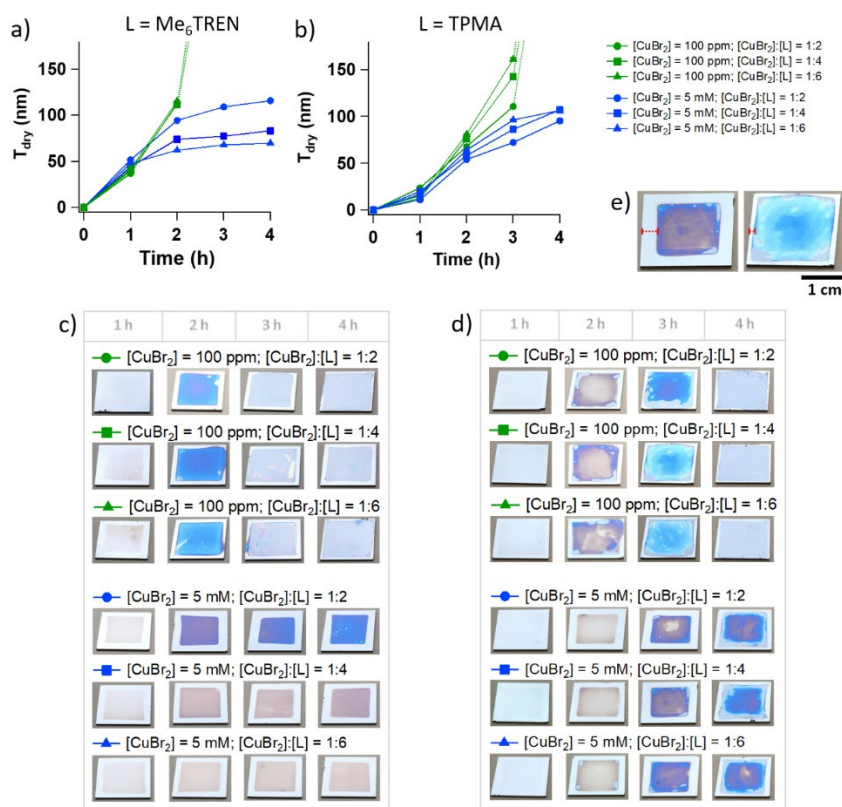


Figure 1. (a, b) POEGMA brush-growth rates recorded by measuring T_{dry} of polymer brushes following different UV irradiation times during SI-photoATRP. The polymerization mixtures comprised 1:1 (v/v) DMF:OEGMA, 100 ppm (green traces) and 5 mM (blue traces) CuBr_2 , and different contents of L, corresponding to $[\text{CuBr}_2]:[\text{L}]$ of 1:2, 1:4 and 1:6. (a) $\text{L} = \text{Me}_6\text{TREN}$; (b) $\text{L} = \text{TPMA}$. (c, d) Pictures of representative substrates following POEGMA brush synthesis using Me_6TREN and TPMA as ligands, respectively, are reported. The brush films show different colours due to thickness-dependent light interference, while inhomogeneous layers are highlighted by areas presenting patches of different colours. (e) Pictures depicting POEGMA brushes synthesized after 4 h of SI-photoATRP using TPMA as ligand, 5 mM (left side) and 100 ppm of CuBr_2 (right side), while maintaining in both cases $[\text{CuBr}_2]:[\text{L}]$ of 1:4.

Hence, oxygen consumption at the early stages of reaction through complexation with photogenerated $\text{Cu}^{\text{I}}\text{X}/\text{L}$ (Scheme 1a) was slower with TPMA, and a certain induction period was observed before a progressive POEGMA brush growth could be attained.

As expected from the initial polymerizations summarized in Table 1 and 2, an evident increment in polymerization rate with increase in ligand concentration was not observed, in the case of either Me₆TREN or TPMA. In contrast, significantly faster brush-thickening rates were recorded for relatively low initial contents of CuBr₂. In particular, the growth of POEGMA brushes assumed a rather uncontrolled behavior after a few hours of UV irradiation when [CuBr₂] was set to 100 ppm, and the entire reaction completely gelled after 2 and 3 h, with Me₆TREN and TPMA ligands, respectively. Under these conditions, T_{dry} of POEGMA films reached values > 1 μm, and the films were generally inhomogeneous. In addition, the fitting of VASE data when [CuBr₂] = 100 ppm often provided unreliable results both during the synthesis of PMMA and POEGMA brushes.

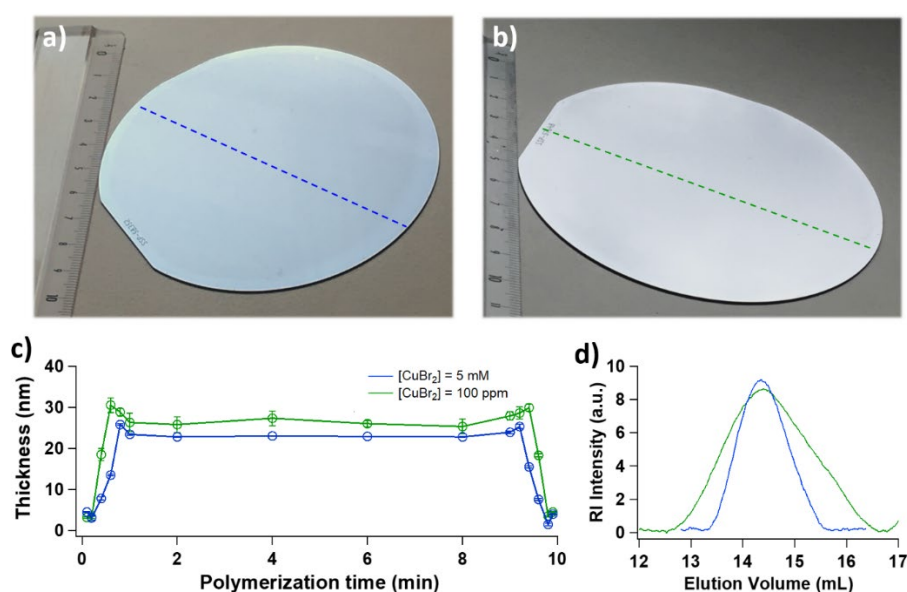


Figure 2. PMMA brushes synthesized by SI-photoATRP from ATRP initiator-functionalized, 4-inch silicon wafers, and using different polymerization mixtures. (a) 1:1 (v/v) MMA:DMF, 5 mM CuBr₂, [CuBr₂]:[L] = 1:4. (b) 1:1 (v/v) MMA:DMF, 100 ppm CuBr₂, [CuBr₂]:[L] = 1:4. (c) After 3 h of UV irradiation T_{dry} of PMMA brushes lay between 20 and 30 nm, as measured by VASE. (d) SEC analysis of detached PMMA brushes provided M_n of 75 kDa and Đ of 2.5 when 100 ppm of CuBr₂ were used, while an M_n of 101 kDa and Đ of 1.3 were obtained when 5 mM CuBr₂ were applied.

The uncontrolled nature of SI-photoATRP at relatively low values of [CuBr₂] was further confirmed by synthesizing PMMA brushes over large areas, and subsequently analyzing chemically detached chains by size-exclusion chromatography (SEC). As reported in Figure 2, after 3 h of UV irradiation, PMMA brushes with T_{dry} between 20 and 30 nm were obtained from 4-inch silicon wafers, with [CuBr₂] = 5 mM (Figure 2a) or 100 ppm (Figure 2b). Although applying the two different formulations resulted in similar thicknesses of PMMA brushes, at

lower catalyst concentration (100 ppm) polymers with a significantly larger dispersity (\mathcal{D}) = 2.5 was obtained, whereas increasing $[\text{CuBr}_2]$ to 5 mM decreased \mathcal{D} to 1.3.

Hence, at relatively low concentration of Cu species, SI-photoATRP was very fast, as previously reported by Laun *et al.* for SI-photoATRP of various acrylates.⁵⁶ However, in the case of polymethacrylate brushes, the grafting process was less controlled, showing features reminiscent of surface-initiated conventional free radical polymerization (SI-FRP).

A similar result was recently reported by Wang *et al.*,⁴⁷ when reduction of catalyst concentration in the synthesis of PMMA brushes by SI-ARGET ATRP from initiator-functionalized SiO_2 nanoparticles (NPs) resulted in a loss of control over the grafting process. This was ascribed to inefficient deactivation and inhomogeneous initiation, leading to the concomitant generation of sparsely grafted polymer-brush shells. Interestingly, during grafting from NPs, a value of $[\text{CuBr}_2] > 10$ ppm was the threshold above which the growth of brushes became controlled. In contrast, when PMMA was grafted from macroscopic surfaces through SI-photoATRP, a relatively higher concentration of catalyst was needed to attain a progressive and controlled growth of narrowly dispersed polymer chains. We believe that the observed differences were mainly due to the geometry of the reaction setup used to generate brushes from large, macroscopic surfaces, and the absence of stirring within the extremely small reaction volumes (layer thickness). Both these factors determined a relatively low concentration of Cu^{II} species at the brush-growing front.

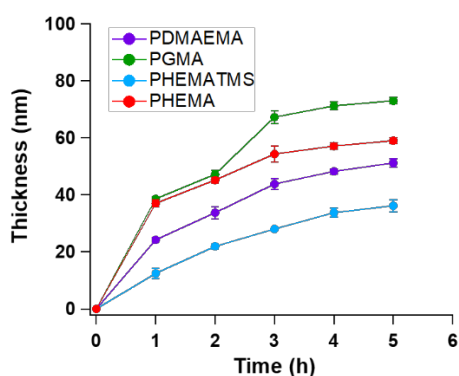


Figure 3. Growth rates of chemically different polymer brushes recorded by measuring T_{dry} following different UV irradiation times by VASE. The polymerization mixtures comprised 1:1 (v/v) DMF:monomer, 5 mM CuBr_2 , and 20 mM TPMA.

The interface between the propagating chains and the surrounding medium, where the deactivation by $\text{Cu}^{\text{II}}\text{X/L}$ species takes place, is in fact limited to the area of the substrate (significantly lower than the interfacial area between NPs and the surrounding medium).

Additionally, the absence of stirring reduced the local concentration of deactivator. Hence, as a result of the intrinsic design of SI-photoATRP applied from flat substrates, a relatively high concentration of catalyst is necessary to guarantee an efficient deactivation of radicals, and thus a controlled progressive polymer growth.

The application of a catalytic system consisting of 5 mM CuBr₂ and TPMA as ligand thus enabled the synthesis from extremely large substrates of thick and compositionally different brushes, including poly(hydroxyethyl methacrylate) (PHEMA), poly[2-(dimethylamino)ethyl methacrylate] (PDMAEMA), poly(glycidyl methacrylate) (PGMA) and polystyrene (PS) brushes (Figure 3).

The different behavior of SI-photoATRP when relatively “low” and “high” catalyst concentrations were applied, additionally influenced the effect plaid by diffusing oxygen on the grafting process. Considering the polymerization setup designed for these experiments (Schemes 1b and 1c), with an initiator-bearing substrate and a glass slide sandwiching a thin liquid film with an average thickness of ~ 10 μm, the constant dissolution of oxygen through the open sides of this setup substantially hampered polymer growth in the areas of the substrate close to the edges. In these regions, T_{dry} was < 5 nm, regardless of the polymerization time or other reaction parameters. In contrast, in areas further away from the edges oxygen could be consumed through complexation by Cu^I/L, followed by reaction with excess of ligand to yield oxidized species (Scheme 1a).¹⁷⁻¹⁸

It is important to emphasize that, while the edges could be clearly distinguished when SI-photoATRP was performed with 5 mM CuBr₂ (typically ~ 5 mm on a 2×2 cm² substrate), a significant reduction in the areas where polymer grafting did not occur was evident for [CuBr₂] = 100 ppm (Figure 1e). Under these conditions, the growth of polymer brushes was accompanied by an increase in viscosity of the reaction mixture, which is typical of SI-FRP. Hence, this phenomenon presumably decreased the rate of oxygen diffusion through the edges of the sandwiched substrates, leading to a reduction in the non-grafted areas.

8.2.3 Temporal Control of SI-photoATRP

Having established the critical parameters for the mechanism of SI-photoATRP, and its tolerance toward ambient conditions, we subsequently investigated how polymer grafting could be temporally regulated by modulating the UV illumination.

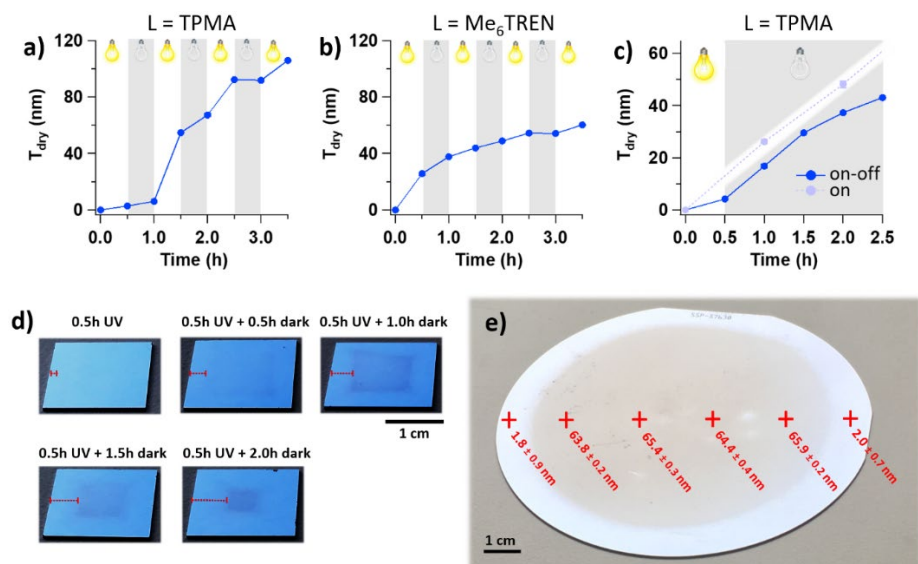


Figure 4. POEGMA brush growth by SI-photoATRP was monitored by VASE, alternating periods of UV illumination with intervals in the dark, using polymerization mixtures including 1:1 (v/v) OEGMA:DMF, 5 mM CuBr₂, and CuBr₂:[L] of 1:4. (a) L = TPMA. (b) L = Me₆TREN. (c) POEGMA brush growth was monitored by VASE, subjecting ATRP-initiator-functionalized substrates covered with a polymerization mixture to UV irradiation for 30 min, followed by 2 h in the dark. The growth of POEGMA brushes during SI-photoATRP under constant UV irradiation is also reported as a pale-blue, dashed profile. (d) Digital photographs of PEOGMA brushes synthesized by SI-photoATRP from 2×2 cm² ATRP initiator-functionalized substrates after 0.5 h of UV illumination, followed by different periods during which the substrates were kept in the dark. The size of the edge where brush growth is hindered due to oxygen diffusion is highlighted with a red marker. (e) POEGMA brushes grafted by SI-photoATRP from an ATRP-initiator-functionalized, 4 inch silicon wafer covered by polymerization mixture and subsequently subjected to 30 min of UV irradiation and 2 h of darkness.

Control over polymer chain growth by switching on and off the light source that triggers the generation of active catalyst was extensively studied for homogeneous photoATRP in solution.^{9, 11, 17, 57-59} Under certain conditions, polymerization in the absence of light could also continue.⁶⁰⁻⁶¹

Temporal control over SI-photoATRP was studied for OEGMA (1:1 v/v in DMF), using 5 mM CuBr₂ and 30 mM TPMA, by alternating periods of 30 min of UV illumination and darkness.

As shown in Figure 4a, the first irradiation step resulted in a moderate thickening of the films, presumably due to initial oxygen consumption, as observed in the brush-growth rates recorded under continuous UV illumination (Figure 1b). A subsequent period of darkness did not stop the brush growth. In contrast, POEGMA brushes showed a slight but significant thickening, analogous to that recorded during the first 30 min under UV irradiation.

The second UV illumination step was mirrored by a significant increment in brush thickness, which reached a T_{dry} of almost 50 nm. During the subsequent 30 min of darkness, the brush growth continued without a sharp response to the absence of UV light by a rapid termination.

When Me_6TREN was used as ligand within otherwise analogous polymerization mixtures, temporal control over POEGMA brush growth by switching UV light alternatively on and off was not attained. In fact, brush-thickening rates recorded during UV illumination were similar to those observed in the darkness (Figure 4b).

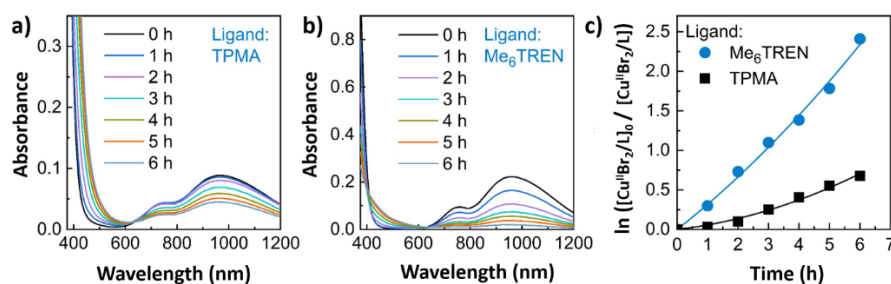


Figure 5. Evolution of the UV-Vis spectra of CuBr_2 in the presence of (a) TPMA or (b) Me_6TREN ligands under UV light irradiation. (c) Kinetics of photoreduction of CuBr_2 demonstrating a faster rate of reduction in the presence of Me_6TREN compared to TPMA. Conditions: $[\text{CuBr}_2] = 5 \text{ mM}$, $[\text{L}]:[\text{CuBr}_2] = 4$, in DMF. A cuvette with a path length of 1 mm was used without deoxygenation of the solution. Irradiated under a UV light (365 nm , 2 mW cm^{-2}).

These results indicated that achieving excellent temporal control over SI-photoATRP by modulating UV irradiation is a more challenging task than for solution polymerizations. This could be due to the large excess of Cu catalysts over alkyl halides during SI-photoATRP. In homogeneous systems, the content of Cu catalyst is typically much lower than that of alkyl halides, and radical termination in the dark can consume all available activators, halting the chain growth.^{60,61} Therefore, in the absence of UV light, photo(re)generation of Cu^{I} -based activators does not occur and polymer growth stops. In contrast, in SI-photoATRP the amount of Cu catalysts is much larger than that of alkyl halides.⁶² Thus, a small fraction of terminated chains cannot significantly affect the concentration of Cu^{I} species and polymerization continues also in the dark periods. Interestingly, more efficient temporal control over brush growth was observed with TPMA as ligand. The relatively lower observed rate of photoreduction of $\text{Cu}^{\text{II}}\text{Br}_2/\text{TPMA}$ (Figure 5) produces lower concentration of Cu^{I} -based activators that can be comparable to a fraction of terminated chains growing from the surface.

Despite the observed limitations in gaining precise temporal control over the grafting process, the unavoidable brush growth taking place in the absence of light, and following a relatively short period of UV illumination, emerged as an appealing feature of SI-photoATRP.

This could be especially convenient, if this surface functionalization method was applied for generating coatings or adhesive layers from spatially confined or light-sensitive supports, where continuous illumination over long periods of time is undesirable or cannot be easily achieved.

POEGMA brush growth under “dark conditions” could be monitored by initially irradiating an initiator-bearing substrate covered with the same polymerization mixture used for the “on-off” experiments for 30 min, and subsequently measuring the brush-thickening rate by VASE while the reaction setup was kept in the dark for several hours (Figure 4c).

As illustrated in Figure 4c, when UV light was applied, increase of T_{dry} showed a slight initial induction period, due to oxygen consumption in the mixture. In contrast, during the subsequent period in the dark, a progressive film thickening was recorded over ~ 1.5 h, following a kinetics similar to that recorded during continuous UV illumination. After this relatively long stage, film thickening slowed down, significantly deviating from the growth rates observed when the UV light was continuously applied.

In the absence of UV light that (re)generates Cu^{I} species, the diffusion of oxygen from the sides of the sample led to a progressive increment in the size of the edges where polymerization was retarded, which increased from ~ 0.1 cm, after 0.5 h, to ~ 0.7 cm, after 2.5 h in the dark. Due to this phenomenon, the areas covered with propagating brushes gradually decreased in size, with the POEGMA films covering just the center of the substrates after several hours without UV illumination (Figure 4d). This drawback could be easily overcome by increasing the size of the entire substrate, thus minimizing the observed edge-effect caused by oxygen diffusion and catalyst deactivation. As shown in Figure 4e, when POEGMA brushes were grafted from a 4-inch silicon wafer following a similar sequence of UV illumination and darkness, an extremely large area (many tens of cm^2) covered with a uniformly thick brush were obtained.

8.3 Conclusions

The mechanistic analysis of SI-photoATRP highlights the parameters determining its controlled character, the kinetics of polymer-brush growth, and the tolerance of this surface modification method toward ambient conditions.

A relatively high concentration of catalyst was required to attain the synthesis of narrowly dispersed polymer brushes. In contrast, when just 100 ppm of CuBr_2 was used, inefficient

deactivation of radicals caused an extremely fast polymer-brush growth, which followed a behavior typical of free radical polymerization.

Contrary to what was previously observed in the case of the corresponding solution processes, polymer-brush growth rates were independent of the content of free ligand, especially for ligands generating catalysts with relatively high K_{ATRP} , such as TPMA and Me₆TREN. In the cases of less ATRP-active catalysts with HMTETA and PMDETA ligands, brush thickness increased with the excess of ligand, confirming the central role of alkyl amines as reducing agents for Cu^{II} species in the presence of UV irradiation.

The extremely low amount of alkyl halide functions compared to Cu-based catalyst during SI-photoATRP strongly influenced the possibility of controlling the grafting process temporally, by modulating the exposure to UV light. Following a relatively short period of illumination, a non-negligible film growth was always recorded, suggesting that polymer grafts were continuously activated by the excess of Cu^I species. Hence, a progressive and controlled growth of polymer brushes can be attained in the dark, just following a short, initial stage of UV illumination, during which oxygen was consumed and Cu^I-based activators were generated. Uniformly thick brush films could be generated over large areas, suggesting an extremely efficient method to fabricate functional coatings from light-sensitive substrates, or from spatially confined supports where just a limited dose of UV light can be applied.

8.4 Materials and Methods

Materials

Dimethylformamide (DMF, extra pure, Fisher Chemical), acetone (> 99.8%, VWR Chemicals), tetrahydrofuran (THF, > 99.5%, VWR Chemicals), triethylamine (TEA, ≥99%, Merck), 2-bromoisobutryl bromide (BiBB, 98%, Sigma-Aldrich), 3-(aminopropyl)triethoxysilane (APTES, 99%, Acros), copper(II) bromide (CuBr₂, 99.99%, Aldrich), tris(2-pyridylmethyl)amine (TPMA, 98%, Sigma-Aldrich), tris[2-(dimethylamino)ethyl]amine (Me₆TREN, 99%, abcr GmbH), tetrabutylammonium fluoride (TBAF, 1M in THF, Aldrich), iron(III) bromide (FeBr₃, 98%, Sigma-Aldrich), tetrabutylammonium bromide (TBABr, >99%, Fluka), 1,1,4,7,7-pentamethyldiethylenetriamine (PMDETA, 99%, Aldrich-Fine Chemicals), 1,1,4,7,10,10-hexamethyltriethylenetetramine (HMTETA, 97%, Aldrich-Fine Chemicals), 2,2'-bipyridyl (bpy, ≥99%, Sigma-Aldrich), ethylenediaminetetraacetic acid (EDTA, 99.995%, Sigma-

Aldrich), and sodium bromide (NaBr, >=99.0%, Sigma-Aldrich) were used as received. Silicon wafers were purchased from Si-Mat (Landsberg, Germany).

Methyl methacrylate (MMA, Sigma-Aldrich), oligo[(ethylene glycol) methyl ether methacrylate] (OEGMA, $M_n \sim 480 \text{ g mol}^{-1}$, Sigma-Aldrich), 2-(trimethylsilyloxy)ethyl methacrylate (HEMATMS, 96%, Sigma-Aldrich), 2-(dimethylamino)ethyl methacrylate (DMAEMA, 98%, Aldrich-Fine Chemicals), 2-hydroxyethyl methacrylate (HEMA, 97%, aber GmbH), and glycidyl methacrylate (GMA, Sigma-Aldrich) were purified by passing through a basic alumina column to remove the inhibitor before use.

Variable-Angle Spectroscopic Ellipsometry (VASE)

The values of dry thickness of polymer brushes (T_{dry}) were measured using a M-2000F John Woollam variable angle spectroscopic ellipsometer (VASE, SENTECH Instruments GmbH) equipped with a He-Ne laser source ($\lambda = 633 \text{ nm}$, J.A. Woollam Co., Lincoln, NE). Amplitude (Ψ) and phase (Δ) components were recorded using focusing lenses at 70° from the surface normal as a function of wavelength (350–800 nm). Fitting of the raw data was performed based on a layered model using bulk dielectric functions for Si and SiO₂ (software WVASE32, LOT Oriel GmbH, Darmstadt, Germany). The polymer-brush layers were analyzed on the basis of a Cauchy model: $n = A + B \lambda^{-2}$, where n is the refractive index, λ is the wavelength and A and B were assumed to be 1.45 and 0.01, respectively, as values for transparent organic films.⁶³

Size Exclusion Chromatography (SEC)

Polymer brushes grafted from 8-inch silicon wafer by SI-photoATRP were detached after overnight treatment in a 0.05 M THF solution of TBAF at 60°C . After the reaction, the solvent was removed in rotary evaporator and the solid was filtered and re-dissolved in THF.

SEC was performed on a Viskotek GPCMax system (Malvern) equipped with two PFG linear M columns (PSS), eluting the samples in THF at a rate of 1 mL min^{-1} at room temperature. The values of M_n and PDI of de-grafted polymer brushes were obtained using the signal originating from a refractive index (RI) detector, and a conventional calibration employing narrowly dispersed PMMA standards.

Preparation of ATRP Initiator Layer on SiO_x Substrates

Silicon substrates with an area of 4 cm^2 were cleaned for 20 minutes in *piranha* solution (3:1 mixture (v/v) of H₂SO₄ and H₂O₂), and subsequently rinsed with ultrapure water (Millipore Milli-Q grade) and ethanol. APTES was subsequently deposited on SiO_x surfaces by vapour deposition, in a desiccator that was kept under vacuum for 3 hours. After this, ATRP-initiator layers were obtained by incubating APTES-bearing substrates in a 0.12 M DCM solution of BiBB, containing 0.12 M TEA. The reaction was carried out for 2 hours at room

temperature, and the samples were subsequently washed with DCM, and finally dried under a stream of N₂.

Surface-Initiated Photoinduced ATRP

Surface-initiated photoinduced ATRP was conducted in a Stratalinker UV Crosslinker 2400 (Stratagene, La Jolla, CA, USA) equipped with 6 UV lamps having $\lambda_{\text{max}} = 365$ nm, and generating a power of 1.5 mW cm⁻². The reactions were carried out at room temperature and in the presence of oxygen. SiO_x substrates previously functionalized with ATRP initiator were placed in a glass petri dish, covered with 10 $\mu\text{L cm}^{-2}$ of polymerization mixture and a glass slide. The sandwiched substrates were irradiated for the desired time, rinsed with solvent and finally dried under a stream of N₂.

Ligand Effect on Photoreduction of Cu^{II}X/L Species

The kinetics of photoreduction of Cu^{II}X/L species in the presence of TPMA and Me₆TREN ligands were analyzed by UV-vis spectroscopy (Cary 60 UV-vis spectrometer, Agilent Technologies), subjecting 5 mM CuBr₂/L solutions with [CuBr₂]:[L] = 1:4 to UV irradiation ($\lambda_{\text{max}} = 365$ nm, 2 mW cm⁻²) for different times, and subsequently recording UV-vis spectra in the range 400-1200 nm. The concentration of Cu^{II}-based species was estimated by measuring the absorbance at 960 nm, and applying extinction coefficients (ϵ) of 443.5 and 177.1 M⁻¹cm⁻¹ for CuBr₂/Me₆TREN and CuBr₂/TPMA, respectively.

References

1. Dadashi-Silab, S.; Doran, S.; Yagci, Y., Photoinduced Electron Transfer Reactions for Macromolecular Syntheses. *Chem. Rev.* **2016**, *116* (17), 10212-10275.
2. Shanmugam, S.; Xu, J. T.; Boyer, C., Photocontrolled Living Polymerization Systems with Reversible Deactivations through Electron and Energy Transfer. *Macromol. Rapid Commun.* **2017**, *38* (13).
3. Ribelli, T. G.; Lorandi, F.; Fantin, M.; Matyjaszewski, K., Atom Transfer Radical Polymerization: Billion Times More Active Catalysts and New Initiation Systems. *Macromol. Rapid Commun.* **2019**, *40* (1).
4. Pan, X. C.; Tasdelen, M. A.; Laun, J.; Junkers, T.; Yagci, Y.; Matyjaszewski, K., Photomediated controlled radical polymerization. *Prog. Polym. Sci.* **2016**, *62*, 73-125.
5. Jung, K.; Xu, J. T.; Zetterlund, P. B.; Boyer, C., Visible-Light-Regulated Controlled/Living Radical Polymerization in Miniemulsion. *ACS Macro Lett.* **2015**, *4* (10), 1139-1143.

6. Shanmugam, S.; Xu, J. T.; Boyer, C., Exploiting Metalloporphyrins for Selective Living Radical Polymerization Tunable over Visible Wavelengths. *J. Am. Chem. Soc.* **2015**, *137* (28), 9174-9185.
7. Shanmugam, S.; Xu, J. T.; Boyer, C., Light-Regulated Polymerization under Near-Infrared/Far-Red Irradiation Catalyzed by Bacteriochlorophyll a. *Angew. Chem. Int. Ed.* **2016**, *55* (3), 1036-1040.
8. Tasdelen, M. A.; Uygun, M.; Yagci, Y., Photoinduced Controlled Radical Polymerization. *Macromol. Rapid Commun.* **2011**, *32* (1), 58-62.
9. Konkolewicz, D.; Schröder, K.; Buback, J.; Bernhard, S.; Matyjaszewski, K., Visible Light and Sunlight Photoinduced ATRP with ppm of Cu Catalyst. *ACS Macro Lett.* **2012**, *1* (10), 1219-1223.
10. Ribelli, T. G.; Konkolewicz, D.; Bernhard, S.; Matyjaszewski, K., How are Radicals (Re)Generated in Photochemical ATRP? *J. Am. Chem. Soc.* **2014**, *136* (38), 13303-13312.
11. Anastasaki, A.; Nikolaou, V.; Zhang, Q.; Burns, J.; Samanta, S. R.; Waldron, C.; Haddleton, A. J.; McHale, R.; Fox, D.; Percec, V.; Wilson, P.; Haddleton, D. M., Copper(II)/Tertiary Amine Synergy in Photoinduced Living Radical Polymerization: Accelerated Synthesis of ω -Functional and α,ω -Heterofunctional Poly(acrylates). *J. Am. Chem. Soc.* **2014**, *136* (3), 1141-1149.
12. Treat, N. J.; Sprafke, H.; Kramer, J. W.; Clark, P. G.; Barton, B. E.; de Alaniz, J. R.; Fors, B. P.; Hawker, C. J., Metal-Free Atom Transfer Radical Polymerization. *J. Am. Chem. Soc.* **2014**, *136* (45), 16096-16101.
13. Miyake, G. M.; Theriot, J. C., Perylene as an Organic Photocatalyst for the Radical Polymerization of Functionalized Vinyl Monomers through Oxidative Quenching with Alkyl Bromides and Visible Light. *Macromolecules* **2014**, *47* (23), 8255-8261.
14. Allushi, A.; Jockusch, S.; Yilmaz, G.; Yagci, Y., Photoinitiated Metal-Free Controlled/Living Radical Polymerization Using Polynuclear Aromatic Hydrocarbons. *Macromolecules* **2016**, *49* (20), 7785-7792.
15. Theriot, J. C.; Lim, C. H.; Yang, H.; Ryan, M. D.; Musgrave, C. B.; Miyake, G. M., Organocatalyzed Atom Transfer Radical Polymerization Driven by Visible Light. *Science* **2016**, *352* (6289), 1082-1086.
16. Pan, X. C.; Fang, C.; Fantin, M.; Malhotra, N.; So, W. Y.; Peteanu, L. A.; Isse, A. A.; Gennaro, A.; Liu, P.; Matyjaszewski, K., Mechanism of Photoinduced Metal-Free Atom Transfer Radical Polymerization: Experimental and Computational Studies. *J. Am. Chem. Soc.* **2016**, *138* (7), 2411-2425.

17. Mosnacek, J.; Eckstein-Andicsova, A.; Borska, K., Ligand effect and oxygen tolerance studies in photochemically induced copper mediated reversible deactivation radical polymerization of methyl methacrylate in dimethyl sulfoxide. *Polym. Chem.* **2015**, *6* (13), 2523-2530.
18. Borska, K.; Moravcikova, D.; Mosnacek, J., Photochemically Induced ATRP of (Meth)Acrylates in the Presence of Air: The Effect of Light Intensity, Ligand, and Oxygen Concentration. *Macromol. Rapid Commun.* **2017**, *38* (13).
19. Bondarev, D.; Borska, K.; Soral, M.; Moravcikova, D.; Mosnacek, J., Simple Tertiary Amines as Promoters in Oxygen Tolerant Photochemically Induced ATRP of Acrylates. *Polymer* **2019**, *161*, 122-127.
20. Yang, Q. Z.; Lalevee, J.; Poly, J., Development of a Robust Photocatalyzed ATRP Mechanism Exhibiting Good Tolerance to Oxygen and Inhibitors. *Macromolecules* **2016**, *49* (20), 7653-7666.
21. Pan, X. C.; Fantin, M.; Yuan, F.; Matyjaszewski, K., Externally Ccontrolled Atom Transfer Radical Polymerization. *Chem. Soc. Rev.* **2018**, *47* (14), 5457-5490.
22. Frick, E.; Anastasaki, A.; Haddleton, D. M.; Barner-Kowollik, C., Enlightening the Mechanism of Copper Mediated PhotoRDRP via High-Resolution Mass Spectrometry. *J. Am. Chem. Soc.* **2015**, *137* (21), 6889-6896.
23. Liarou, E.; Anastasaki, A.; Whitfield, R.; Iacono, C. E.; Patias, G.; Engelis, N. G.; Marathianos, A.; Jones, G. R.; Haddleton, D. M., Ultra-low volume oxygen tolerant photoinduced Cu-RDRP. *Polym. Chem.* **2019**, *10* (8), 963-971.
24. Dunderdale, G. J.; Urata, C.; Miranda, D. F.; Hozumi, A., Large-Scale and Environmentally Friendly Synthesis of pH-Responsive Oil-Repellent Polymer Brush Surfaces under Ambient Conditions. *ACS Appl. Mater. Interfaces* **2014**, *6* (15), 11864-11868.
25. Dunderdale, G. J.; England, M. W.; Urata, C.; Hozumi, A., Polymer Brush Surfaces Showing Superhydrophobicity and Air-Bubble Repellency in a Variety of Organic Liquids. *ACS Appl. Mater. Interfaces* **2015**, *7* (22), 12220-12229.
26. Sato, T.; Dunderdale, G. J.; Urata, C.; Hozumi, A., Sol-Gel Preparation of Initiator Layers for Surface-Initiated ATRP: Large-Scale Formation of Polymer Brushes Is Not a Dream. *Macromolecules* **2018**, *51* (24), 10065-10073.
27. Schuwer, N.; Tercier-Waeber, M. L.; Danial, M.; Klok, H. A., Voltammetric Detection of Hg²⁺ Using Peptide-Functionalized Polymer Brushes. *Austr. J. Chem.* **2012**, *65* (8), 1104-1109.

28. Fortin, N.; Klok, H. A., Glucose Monitoring Using a Polymer Brush Modified Polypropylene Hollow Fiber-based Hydraulic Flow Sensor. *ACS Appl. Mater. Interfaces* **2015**, *7* (8), 4631-4640.
29. Badoux, M.; Billing, M.; Klok, H. A., Polymer Brush Interfaces for Protein Biosensing Prepared by Surface-Initiated Controlled Radical Polymerization. *Polym. Chem.* **2019**, *10* (23), 2925-2951.
30. Christau, S.; Genzer, J.; von Klitzing, R., Polymer Brush/Metal Nanoparticle Hybrids for Optical Sensor Applications: from Self-Assembly to Tailored Functions and Nanoengineering. *Z. Phys. Chem.* **2015**, *229* (7-8), 1089-1117.
31. Krishnamoorthy, M.; Hakobyan, S.; Ramstedt, M.; Gautrot, J. E., Surface-Initiated Polymer Brushes in the Biomedical Field: Applications in Membrane Science, Biosensing, Cell Culture, Regenerative Medicine and Antibacterial Coatings. *Chem. Rev.* **2014**, *114* (21), 10976-11026.
32. Moroni, L.; Gunnewiek, M. K.; Benetti, E. M., Polymer Brush Coatings Regulating Cell Behavior: Passive Interfaces Turn into Active. *Acta Biomater.* **2014**, *10* (6), 2367-2378.
33. Klein Gunnewiek, M.; Di Luca, A.; Bollemaat, H. Z.; van Blitterswijk, C. A.; Vancso, G. J.; Moroni, L.; Benetti, E. M., Creeping Proteins in Microporous Structures: Polymer Brush-Assisted Fabrication of 3D Gradients for Tissue Engineering. *Adv. Health. Mater.* **2015**, *4* (8), 1169–1174.
34. Benetti, E. M.; Gunnewiek, M. K.; van Blitterswijk, C. A.; Vancso, G. J.; Moroni, L., Mimicking Natural Cell Environments: Design, Fabrication and Application of Bio-Chemical Gradients on Polymeric Biomaterial Substrates. *J. Mater. Chem. B* **2016**, *4* (24), 4244-4257.
35. Gunnewiek, M. K.; Ramakrishna, S. N.; di Luca, A.; Vancso, G. J.; Moroni, L.; Benetti, E. M., Stem-Cell Clinging by a Thread: AFM Measure of Polymer-Brush Lateral Deformation. *Adv. Mater. Interfaces* **2016**, *3* (3), 1500456.
36. Nagase, K.; Hatakeyama, Y.; Shimizu, T.; Matsuura, K.; Yamato, M.; Takeda, N.; Okano, T., Thermoresponsive Cationic Copolymer Brushes for Mesenchymal Stem Cell Separation. *Biomacromolecules* **2015**, *16* (2), 532-540.
37. Morgese, G.; Cavalli, E.; Rosenboom, J. G.; Zenobi-Wong, M.; Benetti, E. M. Cyclic Polymer Grafts That Lubricate and Protect Damaged Cartilage. *Angew. Chem. Int. Edit.* **2018**, *57* (6), 1621-1626.
38. Costantini, F.; Benetti, E. M.; Reinhoudt, D. N.; Huskens, J.; Vancso, G. J.; Verboom, W., Enzyme-Functionalized Polymer Brush Films on the Inner Wall of Silicon-Glass Microreactors with Tunable Biocatalytic activity. *Lab Chip* **2010**, *10* (24), 3407-3412.

39. Costantini, F.; Benetti, E. M.; Tiggelaar, R. M.; Gardeniers, H. J. G. E.; Reinhoudt, D. N.; Huskens, J.; Vancso, G. J.; Verboom, W., A Brush-Gel/Metal-Nanoparticle Hybrid Film as an Efficient Supported Catalyst in Glass Microreactors. *Chem. Eur. J.* **2010**, *16* (41), 12406-12411.
40. Rafti, M.; Brunsen, A.; Fuertes, M. C.; Azzaroni, O.; Soler-Illia, G. J. A. A., Heterogeneous Catalytic Activity of Platinum Nanoparticles Hosted in Mesoporous Silica Thin Films Modified with Polyelectrolyte Brushes. *ACS Appl. Mater. Interfaces* **2013**, *5* (18), 8833-8840.
41. Jakubowski, W.; Min, K.; Matyjaszewski, K., Activators Regenerated by Electron Transfer for Atom Transfer Radical Polymerization of Styrene. *Macromolecules* **2006**, *39* (1), 39-45.
42. Jakubowski, W.; Matyjaszewski, K., Activators Regenerated by Electron Transfer for Atom-Transfer Radical Polymerization of (Meth)acrylates and Related Block Copolymers. *Angew. Chem. Int. Ed.* **2006**, *45* (27), 4482-4486.
43. Cheng, N.; Azzaroni, O.; Moya, S.; Huck, W. T. S., The Effect of $[Cu^I]/[Cu^{II}]$ Ratio on the Kinetics and Conformation of Polyelectrolyte Brushes by Atom Transfer Radical Polymerization. *Macromol. Rapid Commun.* **2006**, *27* (19), 1632-1636.
44. Matyjaszewski, K.; Miller, P. J.; Shukla, N.; Immaraporn, B.; Gelman, A.; Luokala, B. B.; Siclovan, T. M.; Kickelbick, G.; Vallant, T.; Hoffmann, H.; Pakula, T., Polymers at Interfaces: Using Atom Transfer Radical Polymerization in the Controlled Growth of Homopolymers and Block Copolymers from Silicon Surfaces in the Absence of Untethered Sacrificial Initiator. *Macromolecules* **1999**, *32* (26), 8716-8724.
45. Dehghani, E. S.; Du, Y. H.; Zhang, T.; Ramakrishna, S. N.; Spencer, N. D.; Jordan, R.; Benetti, E. M., Fabrication and Interfacial Properties of Polymer Brush Gradients by Surface-Initiated Cu(0)-Mediated Controlled Radical Polymerization. *Macromolecules* **2017**, *50* (6), 2436-2446.
46. Zhou, D. P.; Gao, X.; Wang, W. J.; Zhu, S. P., Termination of Surface Radicals and Kinetic Modeling of ATRP Grafting from Flat Surfaces by Addition of Deactivator. *Macromolecules* **2012**, *45* (3), 1198-1207.
47. Wang, Z. Y.; Yan, J. J.; Liu, T.; Wei, Q. B.; Li, S. P.; Olszewski, M.; Wu, J. N.; Sobieski, J. L.; Fantin, M.; Bockstaller, M. R.; Matyjaszewski, K., Control of Dispersity and Grafting Density of Particle Brushes by Variation of ATRP Catalyst Concentration. *ACS Macro Lett.* **2019**, *8* (7), 859-864.

48. Milner, S. T.; Witten, T. A.; Cates, M. E., A Parabolic Density Profile for Grafted Polymers. *Europhys. Lett.* **1988**, *5* (5), 413-418.
49. Milner, S. T.; Witten, T. A.; Cates, M. E., Theory of the Grafted Polymer Brush. *Macromolecules* **1988**, *21* (8), 2610-2619.
50. Benetti, E. M.; Kang, C. J.; Mandal, J.; Divandari, M.; Spencer, N. D., Modulation of Surface-Initiated ATRP by Confinement: Mechanism and Applications. *Macromolecules* **2017**, *50* (15), 5711-5718.
51. Kang, C.; Crockett, R. M.; Spencer, N. D., Molecular-Weight Determination of Polymer Brushes Generated by SI-ATRP on Flat Surfaces. *Macromolecules* **2014**, *47*, 269-275.
52. Kang, C. J.; Ramakrishna, S. N.; Nelson, A.; Cremmel, C. V. M.; Stein, H. V.; Spencer, N. D.; Isa, L.; Benetti, E. M., Ultrathin, Freestanding, Stimuli-Responsive, Porous Membranes from Polymer Hydrogel-Brushes. *Nanoscale* **2015**, *7* (30), 13017-13025.
53. Patil, R. R.; Turgman-Cohen, S.; Srogl, J.; Kiserow, D.; Genzer, J., Direct Measurement of Molecular Weight and Grafting Density by Controlled and Quantitative Degrafting of Surface-Anchored Poly(methyl methacrylate). *ACS Macro Lett.* **2015**, *4* (2), 251-254.
54. Patil, R. R.; Turgman-Cohen, S.; Srogl, J.; Kiserow, D.; Genzer, J., On-Demand Degrafting and the Study of Molecular Weight and Grafting Density of Poly(methyl methacrylate) Brushes on Flat Silica Substrates. *Langmuir* **2015**, *31* (8), 2372-2381.
55. Wang, Y.; Kwak, Y.; Buback, J.; Buback, M.; Matyjaszewski, K., Determination of ATRP Equilibrium Constants under Polymerization Conditions. *ACS Macro Lett.* **2012**, *1* (12), 1367-1370.
56. Laun, J.; Vorobii, M.; de los Santos Pereira, A.; Pop-Georgievski, O.; Trouillet, V.; Welle, A.; Barner-Kowollik, C.; Rodriguez-Emmenegger, C.; Junkers, T., Surface Grafting via Photo-Induced Copper-Mediated Radical Polymerization at Extremely Low Catalyst Concentrations. *Macromol. Rapid Commun.* **2015**, *36* (18), 1681-1686.
57. Zhang, T.; Chen, T.; Amin, I.; Jordan, R., ATRP with a Light Switch: Photoinduced ATRP Using a Household Fluorescent Lamp. *Polym. Chem.* **2014**, *5* (16), 4790-4796.
58. Pan, X. C.; Malhotra, N.; Simakova, A.; Wang, Z. Y.; Konkolewicz, D.; Matyjaszewski, K., Photoinduced Atom Transfer Radical Polymerization with ppm-Level Cu Catalyst by Visible Light in Aqueous Media. *J. Am. Chem. Soc.* **2015**, *137* (49), 15430-15433.

59. Jones, G. R.; Whitfield, R.; Anastasaki, A.; Haddleton, D. M., Aqueous Copper(II) Photoinduced Polymerization of Acrylates: Low Copper Concentration and the Importance of Sodium Halide Salts. *J. Am. Chem. Soc.* **2016**, *138* (23), 7346-7352.

60. Dolinski, N. D.; Page, Z. A.; Discekici, E. H.; Meis, D.; Lee, I. H.; Jones, G. R.; Whitfield, R.; Pan, X. C.; McCarthy, B. G.; Shanmugam, S.; Kottisch, V.; Fors, B. P.; Boyer, C.; Miyake, G. M.; Matyjaszewski, K.; Haddleton, D. M.; de Alaniz, J. R.; Anastasaki, A.; Hawker, C. J., What Happens in the Dark? Assessing the Temporal Control of Photo-Mediated Controlled Radical Polymerizations. *J. Polym. Sci. Pol. Chem.* **2019**, *57* (3), 268-273.

61. Dadashi-Silab, S.; Matyjaszewski, K., Temporal Control in Atom Transfer Radical Polymerization Using Zerovalent Metals. *Macromolecules* **2018**, *51* (11), 4250-4258.

62. Considering a typical grafting density (σ) of 0.3 chains nm^{-2} , at the lowest catalyst concentration applied of 0.44 M the content of photogenerated $\text{Cu}^{\text{I}}/\text{Me}_6\text{TREN}$ species after 1 hour of UV irradiation (Figure 5) is approximately an order of magnitude higher than the amount of alkyl halides in the system. However, for TPMA ligand, the reduction is much slower and the content of $\text{Cu}^{\text{I}}/\text{TPMA}$ could be comparable or lower than the amount of alkyl halides, as reflected by decrease of the polymerization rate during the off-periods.

63. Hilfiker, J. N.; Synowicki, R. A.; Bungay, C. L.; Carpio, R., Spectroscopic ellipsometry for polymer thin films. *Solid State Technology* **1998**, *41* (10), 101-+.

Chapter 9

Conclusions

In this thesis, surface-confined polymerization methods that are tolerant toward environmental conditions were developed and applied to fabricate compositionally and structurally diverse polymer-brush films, on an array of different substrates. A special focus was given to the characterization of technologically relevant interfacial properties, including biopassivity and lubrication.

A variety of branched-brush architectures have been synthesized by SI-ATRP, including linear, graft-copolymer and bottlebrush brushes featuring PMPC side chains. Their morphological, nanomechanical and nanotribological characteristics have been investigated and compared. For surface grafting densities (σ) > 0.1 chains nm^{-2} , the effect of branched-polymer-brush architecture on the nanotribological properties of the films was evidenced, demonstrating that increasing the content of hydrophilic polymer grafts results in an increment in lubricity.

The mechanism of Cu^0 SI-ATRP was systematically investigated, posing particular attention to the parameters determining brush-growth kinetics, and those enabling the formation of structured polymer-brush films. Exploiting Cu^0 SI-ATRP the rapid and controlled grafting of PMPC brushes from flat inorganic surfaces as well as porous organic supports of different compositions was demonstrated.

Similarly to Cu^0 SI-ATRP, Fe^0 SI-ATRP enables the generation of uniform brush films over very large areas by employing just a few microliters of monomer/catalyst solutions without the presence of an inert atmosphere. The reaction kinetics in different solvent and monomer/catalyst systems were investigated. In addition, its cytocompatibility was demonstrated for substrates used for cell culture.

Finally, the mechanism and application of SI-photoATRP were presented. Besides being tolerant toward environmental conditions, this process enabled polymer growth from flat substrates without the need for continuous UV irradiation. This unique feature makes SI-photoATRP an extremely energetically efficient polymerization technique, particularly suited to the generation of coatings on substrates where limited light penetration can be achieved, as is the case for the in situ modification of implants, or the fabrication of adhesive films between materials.

Acknowledgements

It has been almost four years since I came to Zurich and joined in the Laboratory for Surface Science and Technology (LSST). From Master thesis to Doctoral thesis, I feel so lucky to work and study here. It will be one of the most important and joyful parts in my life.

First of all, I would like to thank Prof. Nicholas D. Spencer and Dr. Edmondo M. Benetti. Nic, thank you for providing me with the opportunity to carry out my doctoral studies at LSST. At work, you always guide us to do things independently, I have learned a lot at each meeting with you. In life, you teach us how to be gentle and elegant in behavior. Eddy, I still remember the first time we talked over Skype, you invited me to do a master thesis project. Through the phone call, you gave a very detailed and professional description regarding the project. When I look back to these past four years, you encourage me to think deeply and do research systematically. You are strict but tolerant. I appreciate to be your student and friend.

I would like to thank my four-year officemate Moh, the chemistry lab members, and LSST members. Moh, I could not have carried out many experiments so smoothly without your help and suggestions. We see each other almost every day, you are a real gentleman. Shiva, thank you for training me to do AFM. Kaihuan (and his wife Sijia Xie), I would like to thank you for your support and useful suggestions at all times. Josephine, you always make things easier. Yvonne, I enjoyed our lunch breaks and appreciate for your kind reminding for many things. Joydeb, thanks for some useful handy hints you suggested. Rok, thank you for helping me with FTIR spectroscopy and the tribometer. Amine, Matteo and Toby, I enjoy the lab time with you. I would like to thank Giovanni, Antonella, Cristiana, Daichi, some LSST alumnus, Giulia, Matthias, Ella, Andrea, and some people in the SMI group.

I am grateful to my friends in China, Wangyang Ma, Yuwei Wang, Ziyu Zhao, Wen Jin, Xiuge Cao, and supervisor for my Bachelor's thesis, Prof. Bin Cui. I would also like to thank my friends in Zurich, Tian Liu, Yaru Wang, Liqing Zheng et al.

It would not have been possible to write this thesis without the help and support of the kind people around me, even to only some of them it is possible to give a particular mention here. The moments we spent together will always be my cherished experiences and I will always remember you in distance.

Last but not least, many thanks to my parents and boyfriend, Yanrui Ju, for their support and encouragement.

List of Publications

Journal Articles

1. **W Yan**, S Dadashi-Silab, K Matyjaszewski, N D Spencer, E M Benetti. Surface-Initiated Photoinduced ATRP: Mechanism, Oxygen Tolerance, and Temporal Control during the Synthesis of Polymer Brushes. *Macromolecules*. **2020**, 53, 8, 2801-2810.
2. **W Yan**, M Fantin, S Ramakrishna, N D Spencer, K Matyjaszewski, E M Benetti. Growing Polymer Brushes from a Variety of Substrates under Ambient Conditions by Cu⁰-Mediated Surface-Initiated ATRP. *ACS Appl Mater Interfaces*. **2019**, 11, 30, 27470-27477.
3. **W Yan**, M Fantin, N D Spencer, K Matyjaszewski, E M Benetti. Translating Surface-Initiated Atom Transfer Radical Polymerization into Technology: The Mechanism of Cu⁰-Mediated SI-ATRP under Environmental Conditions. *ACS Macro Lett*. **2019**. 8, 7, 865-870.
4. **W Yan**, S Ramakrishna, N D Spencer, E M Benetti. Brushes, Graft-Copolymers or Bottlebrushes? The Effect of Polymer Architecture on the Nanotribological Properties of Grafted-From Assemblies. *Langmuir*. **2019**. 35, 35, 11255-11264.
5. **W Yan**, S Ramakrishna, M Romio, E M Benetti. Bioinert and Lubricious Surfaces by Macromolecular Design. *Langmuir*. **2019**. 35, 42, 13521–13535.
6. **W Yan**, M Divandari, J G Rosenboom, S N Ramakrishna, L Trachsel, N D Spencer, G Morgese, E M Benetti. Design and characterization of ultra-stable, bio-passive and lubricious cyclic poly(2-alkyl-2-oxazoline) brushes. *Polym. Chem*. **2018**. 9, 2580–2589.
7. K Zhang, **W Yan**, R Simic, E M Benetti, N D Spencer. Versatile Surface Modification of Hydrogels by Surface-Initiated, Cu⁰-Mediated Controlled Radical Polymerization. *ACS Appl. Mater. Interfaces*. **2020**. 12, 5, 6761–6767.
8. Y Wang , **W Yan**, M Frey, M V Blanco, M Schubert, M Adobes-Vidal, E Cabane. Liquid-Like SiO₂-g-PDMS Coatings on Wood Surfaces with Underwater Durability, Antifouling, Anti-smudge, and Self-Healing Properties. *Adv. Sustain. Syst*. **2019**. 3, 1, 1800070.
9. A R Faggion, **W Yan**, M Romio, E R Leite, N D Spencer, K Matyjaszewski, E M Benetti. Mechanism and Application of Surface-Initiated Zn(0)-Mediated ATRP. *Polym. Chem*. **2020**. (accepted)
10. A Layadi, B Kessel, **W Yan**, M Romio, N D Spencer, M Zenobi-Wong, K Matyjaszewski, E M Benetti. Oxygen Tolerant and Cytocompatible Iron(0)-Mediated ATRP Enables the

- Controlled Growth of Polymer Brushes from Mammalian Cell Cultures. *J. Am. Chem. Soc.* **2020**. 142, 6, 3158–3164.
11. K Zhang, R Simic, **W Yan**, N D Spencer. Creating an Interface: Rendering a Double-Network Hydrogel Lubricious via Spontaneous Delamination. *ACS Appl. Mater. Interfaces.* **2019**, 11, 28, 25427-25435.
 12. M Divandari, L Trachsel, **W Yan**, J Rosenboom, N D Spencer, M Zenobi-Wong, G Morgese, S N Ramakrishna, E M Benetti. Surface Density Variation within Cyclic Polymer Brushes Reveals Topology Effects on Their Nanotribological and Biopassive Properties. *ACS Macro Lett.* **2018**. 7, 12, 1455-1460.
 13. J Mandal, R S Varunprasaath, **W Yan**, N D Spencer, M Dübner. In situ monitoring of SI-ATRP throughout multiple re-initiations under flow by means of a quartz crystal microbalance. *RSC Adv.*, **2018**, 8, 36, 20048–20055.
 14. M Fantin, S N Ramakrishna, J Yan, **W Yan**, M Divandari, N D Spencer, K Matyjaszewski, E M Benetti. The Role of Cu⁰ in Surface-Initiated Atom Transfer Radical Polymerization: Tuning Catalyst Dissolution for Tailoring Polymer Interfaces. *Macromolecules.* **2018**. 51, 17, 6825-6835.
 15. E M Benetti, M Divandari, S N Ramakrishna, G Morgese, **W Yan**, L Trachsel. Loops and Cycles at Surfaces: The Unique Properties of Topological Polymer Brushes. *Chem. Eur. J.* **2017**. 23, 51, 12433–12442.

Other publications and patents

1. Y Liu, S Jing, **W Yan**, Q Zhang, H Zhan, Bin Cui. Synthesis and Characterization of CaCu₃Ti₄O₁₂ Nano-Powders and Their Ceramics. *Hans Journal of Nanotechnology.* **2011**. 1, 1-5.
2. M Li, B Cui, Z Hu, Y Wang, **W Yan**. Barium titanate-based X8R ceramics with high dielectric constant by adding Zn-B-Si-O nanocomposites. *International Journal of Nanomanufacturing.* **2014**. 10, 1/2, 152 - 159.
3. L Zhang, B Cui, R Ma, L Li, Y Wang, **W Yan**, Z Chang. High permittivity of Ba(Ti_{1-x}Zrx)O₃-based Y5V-type nano-powders and ceramics synthesized using a one-step sol-gel method. *Journal of Advanced Dielectrics.* **2013**. 03, 04, 1350018.
4. B Cui, M Li, **W Yan**. High-dielectric-property X8R-type ceramic capacitor dielectric materials and the preparation method. 2013. China. Patent. CN103204677A.
5. B Cui, Q Zhang, Zhuguo Chang, **W Yan**, et al. Synthetic method for giant dielectric constant material copper-calcium titanate. 2011. China. Patent. CN102351241A.

Curriculum Vitae

Personal data

Name: Wenqing Yan

Date of Birth: 13.07.1991

Place of Birth: Xi'an (China)

Nationality: China

E-mail: steffi_yan@hotmail.de; wenqing.yan@mat.ethz.ch

Education

04/2017 – 06/2020

Doctoral Student in the Laboratory for Surface Science and Technology (LSST), Department of Materials, ETH Zürich, Switzerland.

04/2014 – 04/2017

Master of Science in Polymer Science at the University of Freiburg, Germany

Master's Thesis at LSST, ETH Zürich

09/2009 – 07/2013

Bachelor in Chemistry at Northwest University, China

Research Experiences

04/2016 – 09/2016

Research Assistant at CPI, IMTEK, University of Freiburg, Germany

Polymer Brush Project, funded by the Deutsche Forschungsgesellschaft (DFG) (Ru 498/28-1)

03/2010 – 03/2013

Project participant funded by Chinese National Innovation Fund for College Students (101069703)